Titre: Title:	Modeling of Wind Parks for Steady State Short Circuit Studies
Auteur: Author:	Thomas Kauffmann
Date:	2018
Type:	Mémoire ou thèse / Dissertation or Thesis
Référence: Citation:	Kauffmann, T. (2018). Modeling of Wind Parks for Steady State Short Circuit Studies [Thèse de doctorat, École Polytechnique de Montréal]. PolyPublie. https://publications.polymtl.ca/3256/

URL de PolyPublie: PolyPublie URL:	https://publications.polymtl.ca/3256/
Directeurs de recherche: Advisors:	Ilhan Kocar, & Ulas Karaagac
Programme: Program:	génie électrique

UNIVERSITÉ DE MONTRÉAL

MODELING OF WIND PARKS FOR STEADY STATE SHORT CIRCUIT STUDIES

THOMAS KAUFFMANN

DÉPARTEMENT DE GÉNIE ÉLECTRIQUE

ÉCOLE POLYTECHNIQUE DE MONTRÉAL

THÈSE PRÉSENTÉE EN VUE DE L'OBTENTION

DU DIPLÔME DE PHILOSOPHIAE DOCTOR

(GÉNIE ÉLECTRIQUE)

AOÛT 2018

UNIVERSITÉ DE MONTRÉAL

ÉCOLE POLYTECHNIQUE DE MONTRÉAL

Cette thèse intitulée :

MODELING OF WIND PARKS FOR STEADY STATE SHORT CIRCUIT STUDIES

présentée par : KAUFFMANN Thomas

en vue de l'obtention du diplôme de : Philosophiae Doctor

a été dûment acceptée par le jury d'examen constitué de :

M. MAHSEREDJIAN Jean, Ph. D., président

M. KOCAR Ilhan, Ph. D., membre et directeur de recherche

M. KARAAGAC Ulas, Ph. D., membre et codirecteur de recherche

M. EMIN Zia, Ph. D., membre

M. TÖR Osman Bülent, Ph. D., membre externe

DEDICATION

A mes parents et à mon frère.

ACKNOWLEDGEMENTS

I would like to thank my main supervisor Dr. Ilhan Koçar for giving me his trust for this project, for being available and guiding me all along the PhD. And another thanks for letting me the chance to teach one 3rd year bachelor course in Polytechnique Montreal.

I also thank a lot Dr. Ulas Karaagac for his huge support all along this research project, for his advice and corrections for the publications.

A sincere and great thank to Baki and Isabel for the nice atmosphere in the office, and all the ideas and funny moments we shared inside and outside the office, but also for listening during the harder moments.

Another thank to Baki for his help at the beginning of this project.

Another sincere thank to Isabel for her support, encouragements and advices, all the time we shared, and for showing me the richness of the Portuguese culture.

A thank to all other officemates with whom I shared nice time inside and outside Polytechnique: Ming, Haoyan, Aramis, Jesus, Miguel, Anton, Reza, Aboutaleb, Fidji and Pr. Ametani. And again Anton, Reza and Aboutaleb for their help for my project.

All my other international friends of Polytechnique for sharing their culture, for opening my eyes on the cultural richness of the world: Alexis, Leticia, Kim, Sampada, Jesus, Sandra, Rodrigo, Nazli, Xin, and Celso.

To Lingnan who supported me a lot during the last months of the project.

Finally, I thank a lot my parents and my brother for supporting and encouraging me already long time before this project but who have allowed me to reach it.

RÉSUMÉ

La part croissante des énergies renouvelables dans la production d'électricité impose une adaptation des systèmes de protection des réseaux électriques. Ceci est dû au fait que ces énergies renouvelables utilisent majoritairement l'électronique de puissance, et que leurs comportements en conditions transitoires sont différents de ceux des centrales électriques fonctionnant avec des génératrices synchrones. Le comportement de ces énergies renouvelables est dicté par le contrôleur des convertisseurs, et en principe, ce comportement en conditions de court-circuit peut être reproduit de manière précise avec des logiciels de simulation dynamique ou transitoire. Cependant les progiciels de protection et de court-circuit utilisés par les ingénieurs fonctionnent avec des outils d'analyse en régime permanent dans le domaine phaseur.

L'objectif principal de cette thèse est de développer un modèle phaseur de parc photovoltaïque ou éolien qui donne la contribution de courant en conditions permanentes de court-circuit. Le modèle phaseur est développé pour les éoliennes de type-III et type-IV. La répresentation de la séquence inverse et d'un contrôleur de parc sont aussi développés. Le modèle de type-IV peut aussi représenter un parc photovoltaïque comme tous deux transmettent l'ensemble de leur puissance via un onduleur.

Les modèles phaseur sont validés avec des modèles temporels détaillés, construits dans le logiciel EMTP-RV. Ces modèles temporels ont été construits et améliorés grâce à des retours d'un des leaders européens de la fabrication d'éoliennes. Les modèles phaseur prennent en compte le comportement des contrôleurs de convertisseurs et différentes stratégies de contrôle associées. Pour les grands parcs éoliens connectés au réseau haute tension, le point de contrôle est situé au point d'interconnection du parc. Les différentes stratégies de contrôle agissent sur la tension, la puissance réactive ou le facteur de puissance. En plus de ces 3 modes de contrôle, un mode d'alimentation sans panne (Fault Ride Through en anglais) est aussi disponible pour relever la tension pendant les court-circuits. Un limiteur de courant protège les convertisseurs contre les surintensités, et fonctionne en donnant la priorité à la composante active ou réactive du courant. Ce limiteur est indispensable mais ajoute un comportement non linéaire au contrôleur.

Les modèles phaseur présentés donnent le comportement de séquence inverse avec 2 niveaux de precision : simple et détaillé. Ces deux niveaux ne s'appliquent qu'aux contrôleurs qui ne régulent pas directement leur courant de séquence inverse. Une meilleure précision demande plus

de détails des contrôleurs, comme les gains des régulateurs proportionnel-intégral de la boucle de contrôle interne. Ces modèles phaseur représentent les éoliennes avec des sources de courant contrôlées, dont le courant est calculé en fonction des paramètres du contrôleur et de la tension aux bornes de l'éolienne. A cause du comportement non linéaire de ces contrôleurs, les modèles phaseur proposés sont construits avec une structure itérative.

Les modèles d'éolienne sont implémentés dans un solveur phaseur basé sur l'analyse nodale modifiée augmentée. L'étude de court-circuit est initialisée par un écoulement de puissance. Après l'application du court-circuit au réseau initial, le courant produit par les éoliennes est mis à jour selon l'état du réseau et les paramètres des contrôleurs. Le courant produit par les éoliennes dépend des conditions de tension du réseau, mais avec une relation non-linéaire. En retour, les conditions de tension du réseau dépendent des courants des éoliennes. Ainsi, une solution itérative est proposée. La convergence de cette solution se base sur la variation de tension sur le réseau. Les résultats sont validés par comparaison avec des simulations temporelles. Plusieurs conditions de court-circuit, avec différents modes de contrôle sont appliquées à des éoliennes de type-III et -IV, et démontrent la précision des modèles phaseur développés.

Pour certains phénomènes qui touchent les réseaux, la représentation phaseur a des limites comparées au domaine temporel. Ces limites sont aussi brièvement décrites.

ABSTRACT

The increasing share of renewable energy resources in electricity generation requires reassessment of protection systems. This is due to the fact that renewables are often electronically coupled to the grid and their behavior under transient conditions is different from the behavior of power plants generating power using classical synchronous generators. The behavior of electronically coupled generators depends on the controllers of their converters, and in principle, their precise simulation under short-circuit conditions is possible using dynamic or transient tools which allow detailed modeling of controllers. However, protection and short-circuit software packages used by practicing engineers depend on steady-state solution engines built in phasor domain.

The main objective of this thesis is to develop steady-state phasor models of wind and solar parks that provide their current contribution under steady-state short-circuit conditions. The steady-state models are developed for type-III and type-IV wind turbine generators. Negative sequence control and park controller options are also considered. The Type-IV model can also be used for modeling solar plants since both sources are connected via full converters.

The steady-state models are validated using a detailed time-domain model that is developed in EMTP-RV software with the feedback of a leading European manufacturer of wind turbines. The phasor models take into account the behavior of converter conrollers and various control strategies associated with it. For large-scale wind parks connected to high voltage networks, the point of control is located at the point of interconnection of the park. The control strategies act on voltage, reactive power or power factor. In addition to these three control modes, a fault ride through mode is also available to support voltage during fault conditions. A current limiter protects the converters against overcurrent, and operates with P- or Q-priority. This limiter is indispensable but introduces a non-linear behavior.

The phasor models take into account the natural negative sequence response of the wind turbine generator with two levels of precision if the controllers are not set to regulate negative sequence: simplified and detailed. Higher precision requires more details about the controller, such as the gains of the inner loop proportional-integral controller. The proposed steady-state models represent a wind turbine generator with a control-based equivalent current source of which the current is specified according to the response of controller and the three-phase voltages at the

terminals of the wind turbine generator. The models need to be hosted in an iterative short-circuit solver because of the non-linear behavior of controllers.

The models are integrated with a steady-state solver that builds the network equations using modified-augmented-nodal-analysis. The short-circuit analysis is initialized from load flow solution. Following the application of a short-circuit condition to the initial network, the contribution of a wind turbine generator is updated using network conditions and controller settings. The contribution of a wind turbine generator depends on the network voltage conditions but with a nonlinear relation. In return, the network voltage conditions depend on the contribution of wind turbine generators. Therefore, an iterative solution is proposed, of which the convergence is tested based on a tolerance on the variation of network voltages. Final results are validated by comparing them with time-domain simulation results. Various fault conditions with different control strategies are applied to type-III and -IV wind parks, and the accuracy of the proposed phasor models is demonstrated.

Besides comparing steady-state models to time-domain models, their limitations as opposed to time domain models in terms of studying power systems for various phenomena, are also briefly discussed.

TABLE OF CONTENTS

LIST OF TABLES

LIST OF FIGURES

LIST OF SYMBOLS AND ABBREVIATIONS

AC	Alternative Current
AVM	Average Value Model
BtB	Back-to-Back
CP	Constant Parameters
DC	Direct Current
DFIG	Doubly Fed Induction Generator
DSRF	Double Synchronous Reference Frame
ECG	Electronically Coupled Generator
EMT	Electromagnetic Transients
EMTP-RV	Electromagnetic Transients Program, Revised Version
FRT	Fault Ride Through
FSC	Full-scale Converter
GSC	Grid-side Converter
LF	Load-Flow
LG	Line-to-Ground (fault)
LL	Line-to-Line (fault)
LLG	Line-to-Line-to-Ground (fault)
LOS	Loss Of Synchronism
LPF	Low-Pass Filter
MANA	Modified Augmented Nodal Analysis
MPPT	Maximum Power Point Tracking
MSC	PMSG stator side converter
MV	Medium Voltage

PGC	Point of Generator Connection
PF	Power Factor
PI	Proportional Integral
PLL	Phase Lock Loop
PMSG	Permanent Magnet Synchronous Generator
POI	Point of Interconnection
PQ	active and reactive power (constraint for load-flow)
PWM	Pulse Width Modulation
pu	per-unit
RSC	Rotor Side Converter
SC	Short Circuit
SFR	Stator Flux Reference
SS	Steady-State
SSR	Sub-Synchronous Resonance
SVR	Stator Volate Reference
TD	Time-Domain
VSC	Voltage Source Converter
WTG	Wind Turbine Generator
WP	Wind Park
WPC	Wind Park Controller
WTC	Wind Turbine Controller
WTG	Wind Turbine Generator

LIST OF APPENDICES

CHAPTER 1 INTRODUCTION

1.1 Motivation

There have been important technological developments in the field of renewable power plants mainly due to environmental concerns, public support and both state- and private-level initiatives. Accordingly, the integration of renewable power plants into the grid at all voltage levels has increased considerably over the years after 2001 (Figure 1.1). In 2017, the global installed wind power capacity was 539 GW. Figure 1.2 suggests that this growth will continue in the years to come, and it may reach 840 GW by 2022, i.e. an increase of more than 55%.

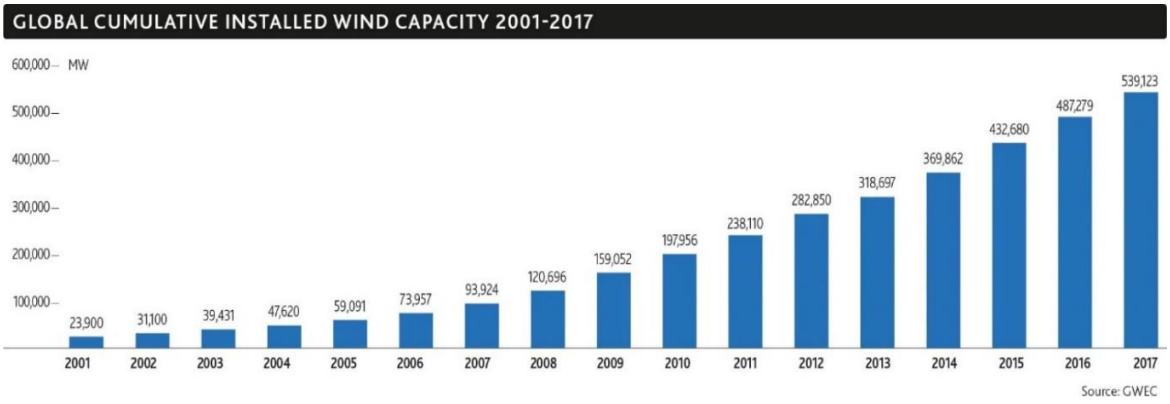

Figure 1.1 Growth of installed wind power since the year 2001 [1].

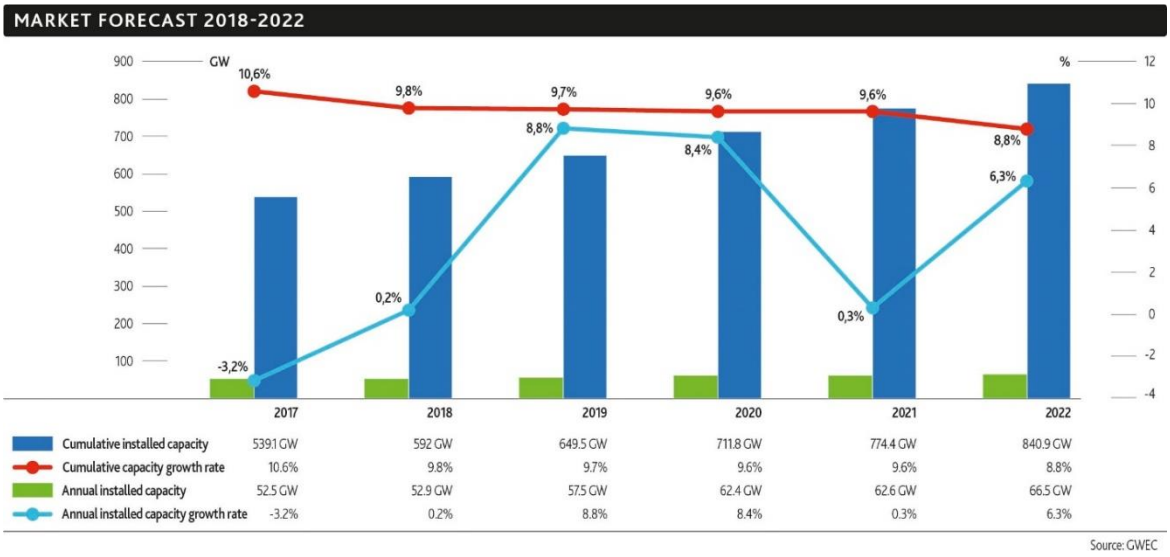

Figure 1.2 Predicted growth of installed wind power until 2022 [2].

As another indication of the level of integration of wind energy, we may consider the example of Denmark where 37.6% of its annual electricity consumption in 2016 was generated by wind [3].

Electronic converters are needed for most if not all renewable energy sources to be safely connected to the electrical power network or even to be connected to local loads. There are several reasons why electronic converters are needed. The first reason is the nature of the renewable enery source itself. For example, photovoltaic panels produce only DC power. As another example, when permanent magnet synchronous generators are used in wind turbines, the generated output power is dirty, and its quality needs to be improved in terms of voltage and frequency. In addition to the above reasons, converters allow wind turbines to operate within a wider range of wind conditions, thus enhancing the overall efficiency of the system. A converter-interfaced source is also called an electronically-coupled generator (ECG). Although this terminology is more common in distribution level applications, in this work it will refer to all generators connected to the grid by means of one or several converters.

The electrical behavior of an ECG depends on the type of the converter controller used. This is one of the differences between ECGs and traditional electromechanical rotating machines.

The behavior of interest here is what happens when there is a fault in the network. For short-circuit (SC) studies, a synchronous generator (SG) is represented as a voltage source behind an impedance (subtransient, transient or synchronous). It generates a high SC current and provides a low impedance path for the negative sequence current, because of the low subtransient and transient impedance. This is the typical generator model in most SC packages, and it is considered to be precise within the requirements of SC studies.

Following the introduction of ECGs into the grid, one of the first methods to model ECGs in SC studies was to treat them as SGs. Considering the small share of the ECGs in total production in the past, the impact of modeling, no matter how inaccurate, did not seem significant. However, in view of the high integration levels of renewable sources today and considering the projection for the trend in the future (Figure 1.2), accurate models are required.

The goal of this thesis is to develop SC models in phasor frame which accurately represent the behavior of certain types of ECGs, namely, type-III and type-IV Wind Turbine Generators (WTGs) during steady-state (SS) SC conditions. These models will improve the protection analysis of networks containing ECGs.

This research project was developed in collaboration with the Electrical Power Research Institute (EPRI) and in partnership with companies manufacturing simulation tools for protection studies in phasor frame.

1.2 Literature review

The behavior and widespread integration of ECGs throughout power networks have affected the detection of faults and the operation of protection devices [4], [5].

There exist well developed standards and commonly accepted models to describe the operation under fault conditions of rotating machines directly connected to the grid [6]–[8]. However, there are no well-established standards or commonly accepted models for the ECGs. Concerning the criteria and the requirements on ECGs interconnected to distribution systems, IEEE 1547 is an evolving standard. In its initial forms, IEEE 1547 stipulated that converters should disconnect when the voltage across their interconnection terminals drops below 0.88 pu [9]. However, amendment 1 allows ECGs to support grid voltage regulation and provide voltage ride through. The distribution grid operators and ECG owners are required to specify voltage and frequency ride through, and coordinate the participation of the ECGs in voltage regulation, which is done by adjusting real and reactive power outputs of the ECGs.

Regarding the interconnection of ECGs at the transmission level, the voltage ride through is stipulated by grid codes specific to grid operators. The ECGs connected to the grid must stay connected until the graph of voltage versus time crosses a certain boundary curve set by the grid operator (see references [10] and [11] for examples in Europe and in Quebec, respectively). Figure 1.3 presents the voltage-time boundary curves used by the German grid operator E.ON. In Figure 1.3, U_N is the nominal voltage. Above limit line 1, all non-synchronous generators must stay connected; between limit line 1 and 2, the non-synchronous generators can trip only under conditions set by the grid operator. A brief disconnection (less than 2 seconds) from the grid is always allowed below limit line 2.

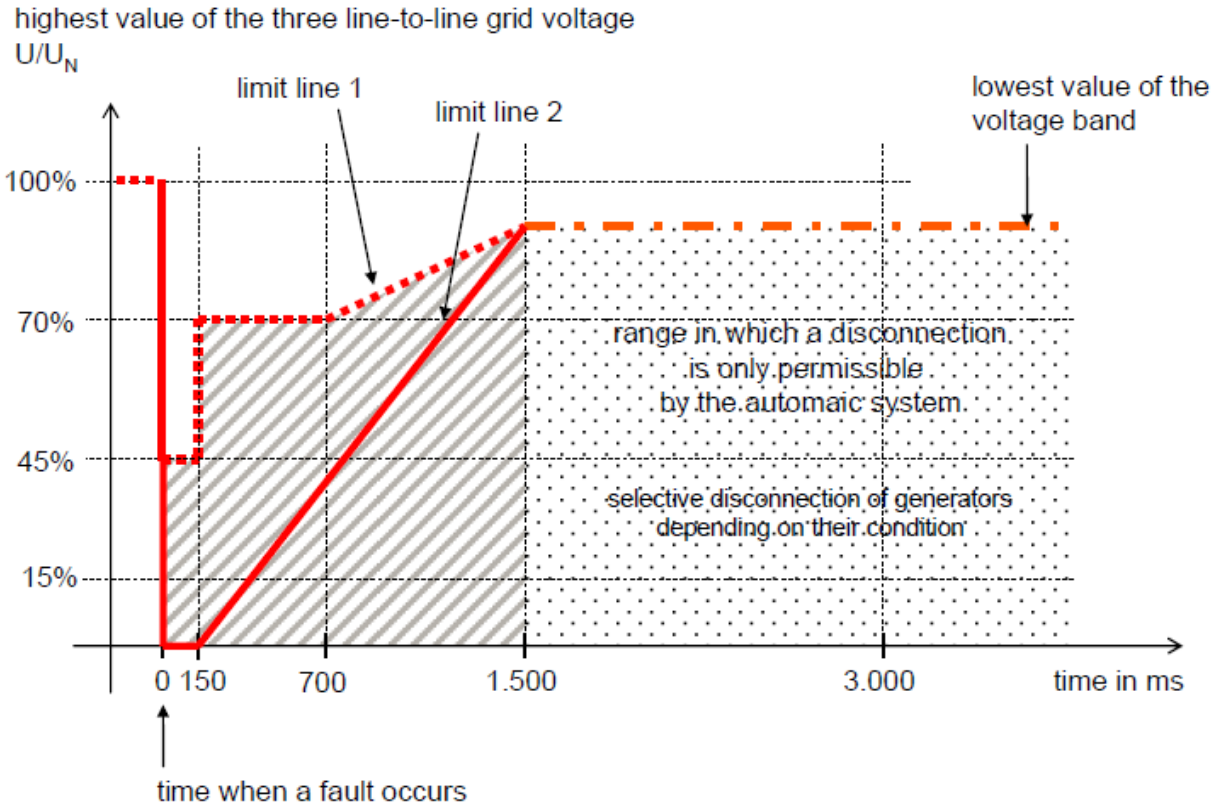

Figure 1.3 Limit curves for the voltage pattern at the grid connection for non-synchronous generator [12].

Although voltage ride through is often well characterised in grid codes, the exact behavior of ECGs during low voltage (LV) conditions is not always detailed. For example, Hydro-Québec imposes a power factor higher than 0.95 in normal conditions for ECGs connected to the transmission level, but has no requirements for reactive current during LV conditions [13].

The German [12] and Spanish [10] grid codes give a curve of reactive current injection as a function of the positive sequence voltage. It becomes necessary in this case to introduce accurate models for the ECGs by considering the grid code requirements.

The Electromagnetic Transient Program (EMTP-RV) or Electromagnetic Transient-Type (EMT-type) programs in general provide a modeling and simulation environment that allows reproducing the behavior of power electronics-based devices with high levels of precision. Detailed models of ECGs in EMTP-RV have already been used to demonstrate that the SC behavior of a converter cannot be approximated by a rotating machine model (synchronous or asynchronous) [14].

In [15], a time-domain (TD) model for converters during SC conditions is proposed. The model involves two control loops: one outer loop and one inner loop. The outer loop calculates the current that should be supplied by the converter. The inner loop calculates the output AC voltage of the converter which allows supplying the current defined in the outer loop. Such a two-loop control system is still in use today. Various control types to be used for single converter applications are discussed in [15]. Reference [16] proposes controllers for systems involving several converters; such systems are encountered in, for example, wind parks.

The control of converters can be done in several coordinate systems (dq0, αβ0, phase), however, the dq0 coordinate system is standard [17]. It has the advantage of transforming the three-phase sine-wave signals into two DC signals which are easier to handle. Early models of converters with DC-link assumed the DC-link voltage to be constant, whereas this voltage depends on the power balance on the DC-link [18]. A control system for the DC-link voltage is given in [19]. In [20] and [21], the TD response during SC periods for several control schemes is further improved, and an iterative method is proposed to calculate the non-linear current contribution of converters in a network having several converters. References [19] to [21] present TD models; they discuss problems associated with protection systems that need to be adapted to renewable sources of energy.

Protection engineers working at utilities and independent system operators are still accustomed to SS tools that perform SC analysis in phasor domain [22]. It is emphasized in [14] that there is a lack of phasor models for the SC behavior of converters. In an effort to develop such phasor models, a first suggestion was to define upper and lower limits for the current contribution of an ECG [23] for balanced faults. Of course, the lower limit would be zero because the wind speed can be zero.

There are simple equivalent circuits that can model the complex behavior of a converter under certain special conditions (voltage close to nominal, fixed amount of reactive power, no negative sequence current). These equivalent circuits are usually current sources in parallel with impedances or voltage sources in series with impedances. Such equivalent circuits can be easily included in a multiphase load-flow (LF) solver using modified augmented nodal analysis (MANA) [24]. However, a converter can be represented in this fashion only for certain special cases and not for a wide spectrum of conditions. LF sequence models are developed in [25] for

type-III WTGs, and in [26] for full-scale converter (FSC) type generators. These models maintain the LF constraints while respecting the limits of ECGs and correct the constraints if the limits are violated. The models also perform under unbalanced conditions, by considering the regulation of negative sequence components provided by the converter controller. This type of control, i.e., the regulation of negative and positive sequence components separately, is called decoupled sequence control. The LF models, however, cannot produce the behavior of ECGs accurately under LV conditions, and hence cannot be used for SC studies.

A SC model of FSC generators is developed in [27] under the assumption that only active power is injected by the converter. This is a reasonable assumption for operation under normal conditions. However, for operation under fault conditions, the reactive power injection that can be stipulated to support the system voltage must also be considered.

In [28], the SC current contribution of a converter is fixed at its maximum current value. This current is purely reactive (injection of reactive power), i.e, the current phase angle is 90° lagging relative to the voltage phase angle. The equivalent circuit consists of a voltage source in series with an impedance: the voltage is fixed, and the impedance is modified iteratively to maintain the specified maximum reactive current. Reference [29] uses the same method of adaptive impedance as in [28], but also considers varying the phase angle of the voltage source in the Thevenin equivalent circuit. In addition, [29] retains an active component of the current while giving priority to the reactive component. In MANA, the impedances are in the coefficient matrix $\mathbf{A}$ whereas the voltage and current sources are in the right-hand side vector $\mathbf{b}$ in the system $\mathbf{Ax} = \mathbf{b}$ where $\mathbf{x}$ is the unknown. From the standpoint of the speed of computation, it is more efficient to keep $\mathbf{A}$ fixed. Therefore, methods such as those in [28] and [29] may not be the fastest. Besides, reference [29] does not deal with unbalanced conditions, and the controller in [28] is set to prevent any negative sequence current from flowing through the converter.

Reference [30] presents a SS phasor models reproducing the behavior of a TD model of type-III and type-IV WTGs. These models employ the outer and inner control loops and the current limiter of the converters. For type-IV WTGs, the active part of the current is increased to maintain the active power output, while respecting a maximum, and the reactive part of the current is adjusted to increase the reactive power injection in order to support the voltage. This is the only control mode presented in [30], where priority is given to the active power. This implies

that the reactive current is increased until the total current limit is reached, and that the active current cannot be decreased to give further support to voltage. As in [28], the model in [30] assumes that no negative sequence current flows through the converter. The reason is that the feedforward term in the inner loop makes the output negative sequence voltage of the grid-side converter (GSC) equal to the measured voltage at the PGC (converter side of the turbine transformer).

For the type-III WTG model in [30], the balanced and unbalanced conditions are treated seperately. For balanced fault (presented also in [31]), the GSC and the rotor side converter (RSC) are represented by current sources with their prefault currents. Magnetizing reactance adaptation is employed in the model. Under unbalanced conditions, the GSC has the same behavior (prefault current) and does not allow any negative sequence current to flow. The RSC is represented by a positive sequence current source, and the magnetizing reactance is adapted again. The reactance deals with the saturation of the iron core, and the current source considers the limitation of the RSC voltage. In [30], the crowbar activation during fault conditions is also considered. The crowbar, short-circuiting the rotor, used to be an easy means to protect the two converters. However, a crowbarred type-III WTG will behave as an induction machine [32], and will consequently consume reactive power. The crowbar prevents the turbine from satisfying the reactive current injection requirements imposed by grid codes [10].

The FSC-type generator SC model in [33] works with a voltage controlled current source, updated iteratively because of the non-linear behavior of the limiter of the GSC. The limiter, however, is not based on current quantities. Rather, it uses the reactive and active powers as boundaries. Furthermore, this model has a decoupled sequence controller to act on the negative sequence response or the power quality of the GSC. The concept of an iterative solution process as existing in [33] is also present in [34]. It has been used in this thesis as well.

The algorithm to calculate the current contributions of type-IV WTGs in [34] is closer to the one used in this thesis. Reference [34] presents only the FRT control, however, it does mention that other control modes are implementable.

In addition to implementing different control modes, the present thesis also considers the presence of a WPC in the calculation of current contributions and more importantly applies the

procedure to type-III based WPs which have a significantly more complex controller structure compared to type-IV based WPs.

The SS models built in this thesis are validated using detailed TD models available in the EMTP-RV software [35]. The EMTP-RV models are based on [36]; they are fully described in [37].

1.3 General technical aspects regarding modeling of WPs

Wind Parc Controller (WPC)

A wind park consists of several WTGs, each connected through a step-up turbine transformer to the medium voltage (MV) collector grid composed of underground cables (Figure 1.4). The collector grid connects all the WTGs to the park transformer (or plant transformer) which connects the collector bus to the high voltage (HV) transmission grid. The HV side of the park transformer is called the point of interconnection (POI) (Figure 1.4).

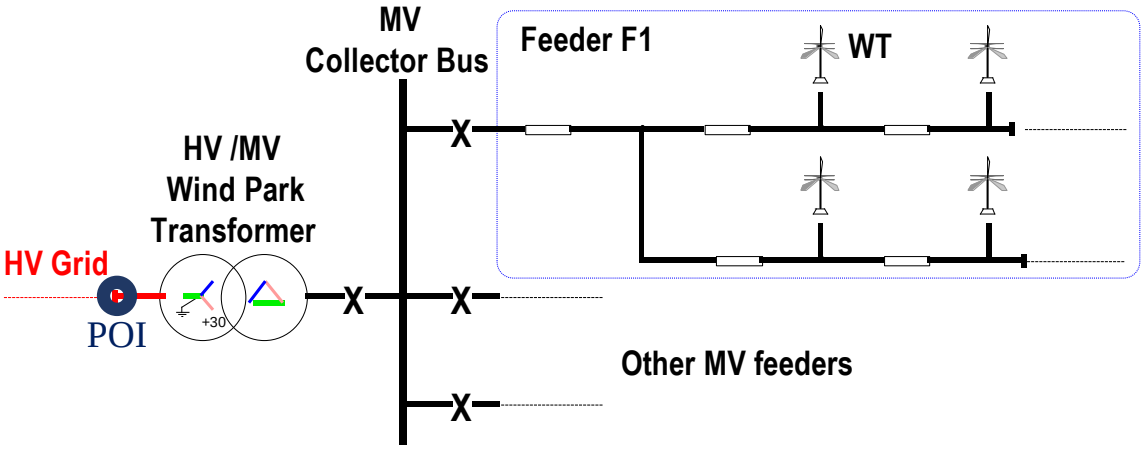

Figure 1.4 Single-line diagram of a typical wind park.

The active power at the POI depends on the wind conditions at each WTG inside the WP. However, according to customary grid code requirements, the WP should have a central WPC to control the reactive power at POI.

The control mode refers to the specific electrical parameter being regulated: the positive sequence voltage magnitude, positive sequence reactive power or positive sequence power factor (V-

control, Q-control and PF-control, respectively). To simplify the notation, "positive sequence" will not be repeated each time the control mode is mentioned.

In the EMT model used in this thesis, the WP reactive power control is based on the concept of secondary voltage control [38]. At the primary level (turbine level), the wind turbine controller (WTC) monitors and controls its own positive sequence terminal voltage (V_{wt}^{+}) with a proportional voltage regulator. At the secondary level, the WPC monitors the reactive power at the POI (Q_{POI}) and controls it by modifying the WTC reference voltage values ($V' = 1 + \Delta V'$) via a proportional-integral (PI) reactive power regulator as shown in Figure 1.5. The output of the PI is a voltage correction $\Delta U'$ which is distributed over all the turbines. As the turbines are distant from the POI, a communication delay Tcom is introduced. In Figure 1.5 and thereafter, all variables are in pu (per-unit) unless explicitly stated otherwise, and the apostrophe (or the prime) sign is used to indicate the reference values.

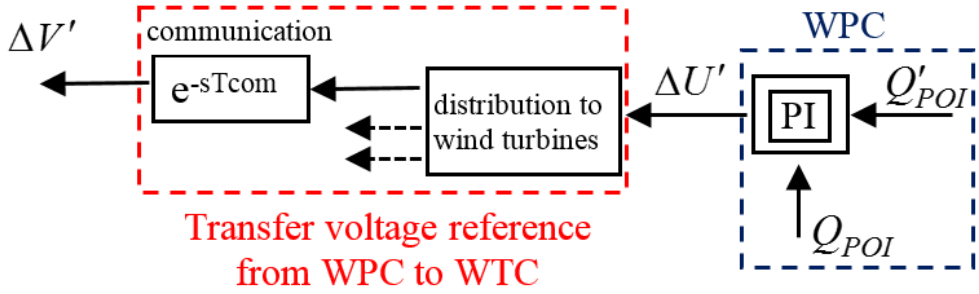

Figure 1.5 Reactive power control at the POI (Q-control).

Although not shown in Figure 1.5, the WPC may also contain voltage control (V-control) and power factor control (PF-control) functions. When the WPC is working under the V-control function, the reactive power reference in Figure 1.5 (Q'_{POI}) is calculated by an outer proportional voltage control:

$$Q'_{POI} = K_{Vpoi}\left(V'_{POI} - \left|\bar{V}^{+}_{POI}\right|\right) \tag{1.1}$$

where $\left|\bar{V}^{+}_{POI}\right|$ is the magnitude of the positive sequence voltage at the POI and K_{Vpoi} is the WPC voltage regulator gain.

When the WPC is working under the PF-control function, Q'_{POI} is calculated using the active power at the POI (P_{POI}) and the desired power factor at POI (PF'_{POI}):

$$Q'_{POI} = sign\left(PF'_{POI}\right) P_{POI} \sqrt{\frac{1}{\left(PF'_{POI}\right)^2} - 1} \tag{1.2}$$

The "sign" function gives 1 if its argument is positive and –1 if its argument is negative. The condition for zero argument is not considered as it corresponds to an unrealistic situation. When PF'_{POI} is positive, the WP injects reactive power into the grid.

As the response of the PI regulator is very slow, its output ($\Delta U'$) may be assumed to be constant during faults.

Wind and mechanical model

The active power production of the WTG is calculated by means of an aerodynamical and mechanical model, and a maximum power point tracking (MPPT) controller. The aerodynamical model calculates the mechanical power generated by the wind according to the wind speed, the picth angle and the rotation speed of the blades. The mechanical model is a two-mass system which represents the hub with the blades and the rotor of the machine. A pitch controller ensures that the maximum power point tracking is achieved and prevents excessive rotation speeds. Details about these models are given in [37].

The machine, the converters and their controllers are developed in the next chapters for the type-IV-based and type-III-based WPs.

To reduce the computational burden of representing each WTG of a WP separately, the complete WP is represented by a single aggregated WTG and an equivalent collector grid. In other words, a single WTG generates the power of the complete WP, and an equivalent pi-line model represents the active and reactive losses of the collector grid [39].

Converter model

The EMT models used in this thesis were built with 2-level VSC. The relatively high switching frequencies used in this topology require time steps as low as 10 µs or less. As harmonics are not essential for fundamental phasor representation, average value models (AVM) can be used to represent the 2-level converters. The AVM reproduces the average response of the switching

devices thanks to controlled sources [40] (Figure 1.6). The AVMs were validated for the converters of WTGs [41] [42], and also for HVDC systems [43].

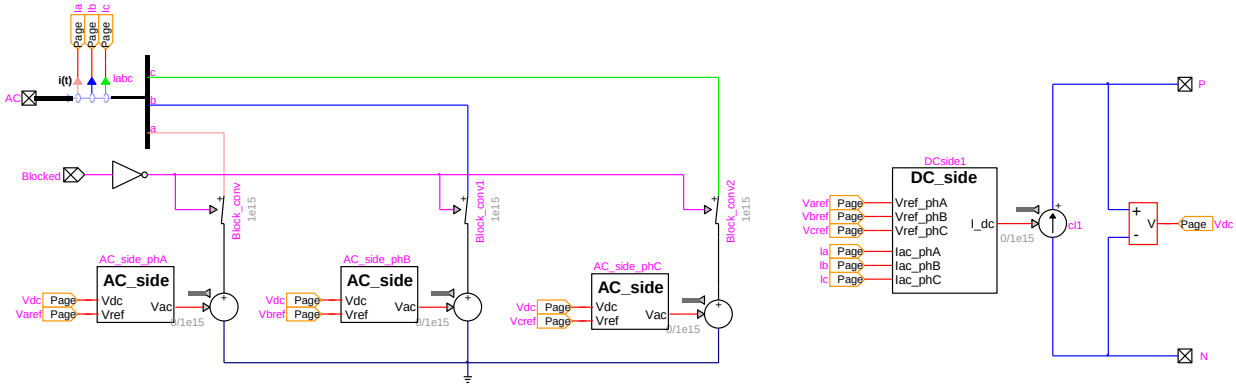

Figure 1.6 AVM representation of the VSC.

Converter's shunt filters

The type-III and type-IV WTGs have a GSC which produces harmonics that propagate into the grid. At the AC terminals of the GSC, those harmonics are filtered by means of a series inductance (choke) and two shunt filters. The shunt filters have a high impedance at nominal grid frequency and a very low impedance at the desired cut-off frequency. One shunt filter has a cut-off frequency that is equal to the switching frequency of the converter, and the cut-off frequency of the other filter is twice this switching frequency.

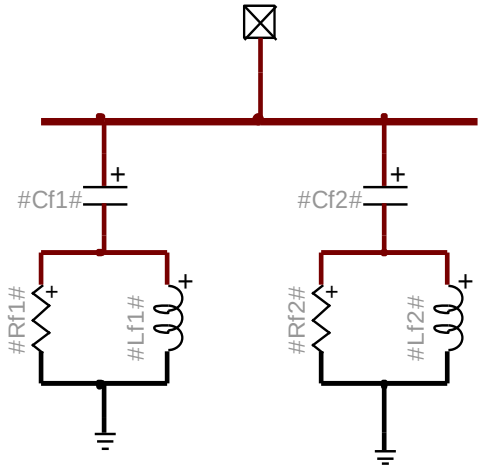

Figure 1.7 Electrical circuit of the two shunt filters.

The structure of the two shunt filters is shown in Figure 1.7. For one filter, C_{filter} is the capacity in Farad of the capacitor, L_{filter} is the inductance in Henry of the inductor, R_{filter} is the resistance in Ohm of the resistor. Those three parameters are calculated as follows:

$$\begin{aligned} C_{filter} &= \frac{Q_{filter}}{\omega_s \left(V_{LL-RMS}^{base}\right)^2} \\ L_{filter} &= \frac{1}{C_{filter}\left(2\pi f_c\right)^2} \\ R_{filter} &= 2\pi f_c L_{filter} Q_f \end{aligned} \tag{1.3}$$

where f_c is the cut-off frequency in Hz, Q_{filter} is the reactive power in var produced by one filter, V_{LL-RMS}^{base} is the RMS line-to-line voltage base at the GSC's terminal, and Q_f is the quality factor of the filter.

The reactive power Q_{filter} and the quality factor Q_f are the same for both filters.

Measurement filter

The input electrical parameters of the controllers are filtered by the measurement filter before being conveyed. The goal of this filter is to remove the harmonics generated by the converter. In this thesis, the measurement filters are either second-order Butterworth low-pass filters with transfer function $H_{mf}^{Butt}(p)$, or a second-order Bessel low-pass filter with transfer function $H_{mf}^{Bessel}(p)$. Equation (1.4) shows their transfer functions.

$$H_{mf}^{Butt}(p) = \frac{1}{1+\frac{\sqrt{2}p}{\omega_{c,m}}+\frac{p^2}{\omega_{c,m}{}^2}} \qquad H_{mf}^{Bessel}(p) = \frac{1}{1+\frac{1.3601p}{\omega_{c,m}}+\frac{0.6165p^2}{\omega_{c,m}{}^2}} \tag{1.4}$$

where $\omega_{c,m}$ is the cut-off angular frequency of the measurement filter.

The complex gain at the nominal frequency is obtained by replacing p in (1.4) by $j\omega_s$ where ω_s is the nominal angular frequency of the grid.

1.4 Thesis objective and outline

The goal of this thesis is to develop flexible, fast and easy to integrate SS phasor models reproducing the SC behavior of type-III and type-IV wind WTGs and WPs. The models are validated using the detailed models available in EMTP-RV. The ECG TD models in EMTP-RV evolved in parallel during the realization of this project in collaboration with different stakeholders including a major European wind turbine manufacturer. The TD models were also validated against field tests on several occasions during this project [44].

This thesis contains 6 chapters and 3 appendices:

- CHAPTER 1 – INTRODUCTION. It explains the motivation of this PhD project, highlights its objectives and contributions, and summarizes the contents of the thesis.
- CHAPTER 2 – FULL-SCALE CONVERTER SHORT-CIRCUIT STEADY-STATE MODEL. It contains the description of the FSC-type generator with its different control strategies. It presents the procedure to calculate the positive and negative sequence current contributions of FSC-type generators depending on the terminal voltage and controller.
- CHAPTER 3 – TYPE-III WTG SHORT-CIRCUIT STEADY-STATE MODEL. It follows the same structure as in CHAPTER 2 but for type-III WTGs (DFIGs). It presents the procedure to calculate the positive and negative sequence current contribution of the DFIGs depending on the terminal voltage and controller.
- CHAPTER 4 – STEADY-STATE SOLVER, SIMULATIONS AND VALIDATIONS. It presents the proposed solver to calculate the current contributions from the WPs based on type-III and type-IV WTGs. It presents comparisons with TD simulations in order to validate the proposed SS models.
- CHAPTER 5 – ACCURACY LIMITATIONS OF THE STEADY-STATE MODELS. It describes the limitations of the proposed SS models. The limitations are related to the accuracy of the WTG models, solver and phasor representation.
- CHAPTER 6 – CONCLUSION AND RECOMMENDATIONS. It gives a summary of this thesis as well as suggested future work related to the SC phasor representation of ECGs.

1.5 Contributions

The main contribution of this thesis is the development of SS phasor models giving the current contribution of type-III-based and type-IV-based WPs in faulted networks. These models consider different control strategies for the positive sequence parameters (voltage, reactive power, power-factor control and fault-ride-through). The SS phasor models also give the negative sequence behavior of the WPs. For the type-IV, the current contribution depends only on the GSC controller, and for the type-III, the model considers the impacts of both converters (grid and rotor ones) and of the machine itself. These models are presented in the form of algorithms, which can be integrated into various software platforms in phasor frame (protection and SC).

The more detailed a system model is, the more articulated its controller dynamics and parameters are. Both simplified models and detailed models have been developed. Simplified models don't require detailed controller parameters and allow quick estimates of fault currents.

The type-III and type-IV WTG phasor models have been transferred to the software industry and are being implemented in well known protection packages [45], [46].

A further contribution of this work is the demonstration of the existence of a proportional relation between the negative sequence voltage and current for a type-IV WTG. For a type-III WTG, a similar relation exists if the negative sequence voltage at the terminals is low or if the inner loop limiter is ignored (to exclude the possibility of non-linear behavior). Relations representing various constraints regarding negative sequence quantities can also be included in a sequence or multiphase LF solver for the precise evaluation of the SS conditions under normal but unbalanced conditions. This LF application was tested for type-IV WTG [47].

The models attempt to reproduce the SS SC behavior using phasor domain relations; therefore, they have limitations in capturing the transient behavior accurately. The models also fall short in identifying certain power system phenomena associated with the dynamic behavior of controllers and power electronic converters such as power swing, ferroresonance, stability and subsynchronous resonance as discussed in [48].

1.6 List of publications

The research work associated with this thesis has led to several publications and has served many technical reports for prestigious organizations.

Journal papers

T. Kauffmann, U. Karaagac, I. Kocar, S. Jensen, J. Mahseredjian, E. Farantatos, "An Accurate Type III Wind Turbine Generator Short Circuit Model for Protection Applications," IEEE Trans. Power Delivery, vol. 32, no. 6, pp. 2370-2379, December 2017.

T. Kauffmann, U. Karaagac, I. Kocar, J. Mahseredjian, E. Farantatos, "Short-Circuit Model for Type IV Wind Turbine Generators with Decoupled Sequence Control," IEEE Trans. Power Delivery, **submitted, IEEE Trans. Power Delivery, July 2018.**

Conference papers

I. Kocar, **T. Kauffmann**, U. Karaagac, J. Mahseredjian and E. Farantatos, "Phasor Domain Modelling of Full Scale Frequency Converters for Protection Studies," *Proc. of 4th International Workshop on Integration of Solar Power into Power Systems*, Berlin, Germany, Nov. 2014.

T. Kauffmann, U. Karaagac, I. Kocar, H. Gras, J. Mahseredjian, and F. Farantatos, "Phasor domain modeling of Type III wind turbine generator for protection studies," Proc. IEEE Power Eng. Soc. Gen. Meeting, Denver, CO, USA, pp. 1-5, Jul. 2015.

U. Karaagac, **T. Kauffmann**, I. Kocar, H. Gras, J. Mahseredjian, and F. Farantatos, "Phasor domain modeling of Type IV wind turbine generator for protection studies," Proc. IEEE Power Eng. Soc. Gen.Meeting, Denver, CO, USA, pp. 1-5, Jul. 2015.

E. Farantatos, **T. Kauffmann**, U. Karaagac, I. Kocar, and J. Mahseredjian, "Phasor Domain Modelling of Electronically Coupled Generators for System Protection Studies," *Proc. of 5th International Workshop on Integration of Solar Power into Power Systems*, Brussels, Belgium, Oct. 2015.

B. Cetindag, **T. Kauffmann** and I. Kocar, "Modeling of wind parks in multiphase load flow solver with augmented Jacobian matrix formulation," Proc. IEEE Power Eng. Soc. Gen. Meeting, Boston, MA, USA, pp. 1-5, Jul. 2016.

Reports for the Electrical Power Research Institute (EPRI), Palo Alto, CA, USA

Impact of Renewables on System Protection: Frequency Domain Short-Circuit Models of Converter Interfaced Renewables and Guidelines for Protection Studies. EPRI, Palo Alto, CA, 3002002810, 2014.

Impact of Renewables on System Protection: Short-Circuit Phasor Models of Converter Interfaced Renewable Resources and Performance of Transmission Line Distance Protection, EPRI, Palo Alto, CA, USA, 3002005765, 2015.

Impact of Renewables on System Protection: Wind/PV Short-Circuit Phasor Model Library and Guidelines for System Protection Studies. EPRI, Palo Alto, CA, USA, 3002008367, 2016.

Short-Circuit Phasor Models of Converter Based Renewable Energy Resources for Fault Studies, EPRI, Palo Alto, CA, 3002010936, 2017.

System Protection Guidelines for Systems with High Levels of Renewables: Impact of Wind & Solar Generation on Negative Sequence and Power Swing Protection, EPRI, Palo Alto, CA, 3002010937, 2017.

CHAPTER 2 FULL-SCALE CONVERTER SHORT-CIRCUIT STEADY-STATE MODEL

This chapter presents the type-IV WTG and details a SS phasor model reproducing the behavior of this type of WTG during SCs in the grid. This model can also be used for other types of generators connected to the grid via full-scale converters. Examples of other types of generators include non-wind mechanical sources as well as DC power sources such as photovoltaic panels and fuel cells.

The first step is to describe in detail in section 2.1 the EMT model for type-IV WTG, and to give the basic elements of the structure of the GSC controller. The two different types of control, namely coupled sequence and the decoupled sequence are also described. The negative sequence behavior is not controllable under the coupled sequence control, whereas it is controllable under the decoupled sequence control. Section 2.2 presents the SC phasor model reproducing the SS behavior of the EMT model presented. The phasor model incorporates all of the control possibilities; it is given in the form of an algorithm in section 2.3.

2.1 Controller structure and time-domain model of full-scale converter generators

The type-IV, i.e. the full-scale converter (FSC) WTG uses a rotating machine connected to the grid through a back-to-back (BtB) DC link. In this thesis, the rotating machine is a permanent-magnet synchronous generator (PMSG). Depending on the size of the WTG, the machine-side converter (MSC) can be either a diode rectifier or a voltage-source converter (VSC). On the other hand, the grid-side converter (GSC) is typically a VSC. The BtB VSC topology is used in this study. Figure 2.1 presents the structure of a type-IV WTG.

The DC voltage part is called the DC-link. The chopper protects the DC-link against over-voltages, and the capacitor smooths the voltage. When activated, the chopper short-circuits the two DC terminals through a resistance to dissipate excessive power. At the AC terminals of the GSC, the harmonics are filtered and hence the power quality is improved by means of a series inductance (choke) and two shunt filters (Figure 1.7). The connection downstream of the filters is

called the PGC (Point of Generator Connection). The turbine transformer connects the PGC to the MV collector grid.

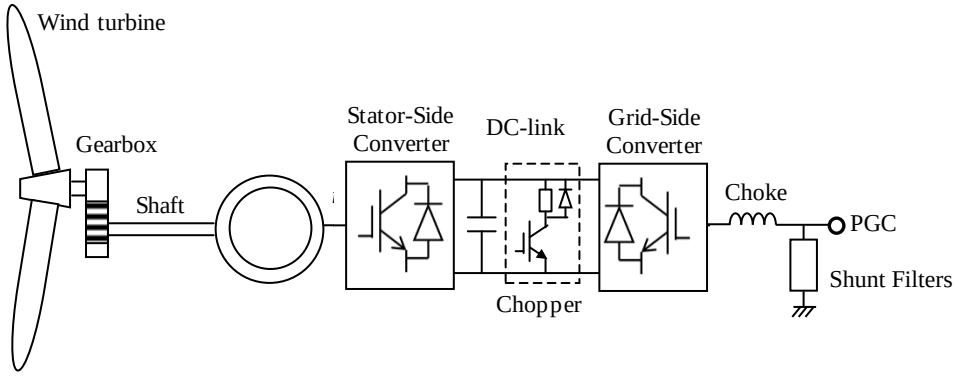

Figure 2.1 Structure of the type-IV WTG.

For such type of WTG, the GSC dictates the behavior of the generator during a fault on the grid. The GSC controller can function in different manners and for different purposes as explained below.

The GSC controller can either separate the positive and negative sequences of voltages and currents (decoupled control), or not (coupled control). A sequence decoupled controller controls both the positive and negative sequences. A sequence coupled controller only regulates the positive sequence.

Structure of converter controllers

The main elements of a converter controller can be seen in Figure 2.2.

The next sections provide more details on the blocks of Figure 2.2. All paramaters are meant to be in pu.

In this chapter, variables follow the following construction rules:

- the subscript “pgc” refers to the PGC,
- the subscript “g” refers to the AC current of the GSC, or to the PGC voltage in the dq coordinates,
- the superscript “+” (plus) and “-” (minus) refer to the positive and negative sequences, respectively,

- upper-case letters refer to the DC component of signals,
- the overbar refers to nominal frequency phasors,
- the subscript “d” and “q” refer, respectively, to the d- and q-components of a variable,
- hatted variables indicate the desired values,
- primes (apostrophes) indicate the reference values.

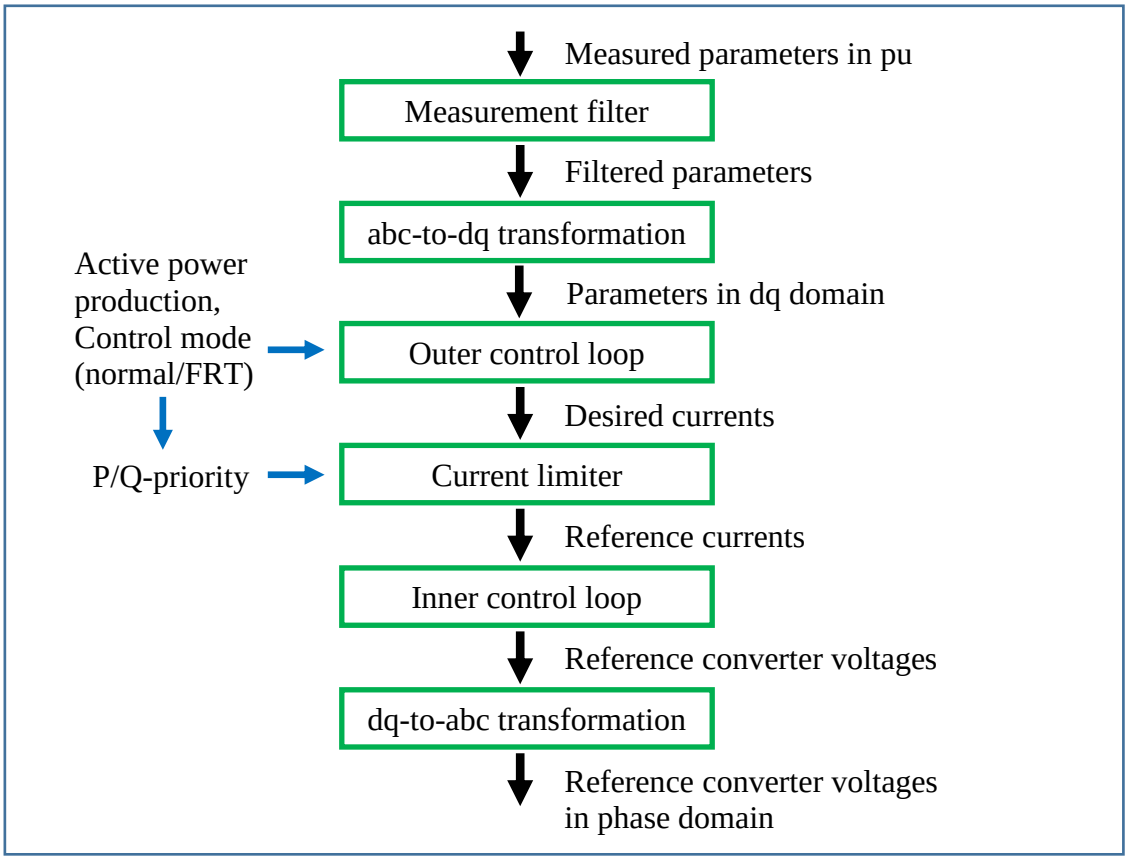

Figure 2.2 Basic structure of a converter controller.

Measurement filter

The first element is a measurement low-pass filter (see section 1.3). Its goal is to remove the harmonics generated by the converter. This filter has a gain of unity at the grid frequency. The type of filter and its parameters are detailed in section 4.4 including the simulation results.

2.1.1 abc-to-dq transformation

The goal of the abc-to-dq transformation (direct-quadrature transformation) is to convert a given set of three AC signals under steady, balanced conditions into a set of two DC signals. Most converter controllers use this technique because DC signals are easier to manipulate and regulate. Furthermore, the active and reactive components of the current are independently controllable. The zero sequence current does not exist as the GSC is connected with only 3 wires.

The dq transformation is realized using the transformation matrix **T**:

$$\begin{bmatrix} v_{dg} \\ v_{qg} \\ v_{0g} \end{bmatrix} = \mathbf{T}(\theta) \begin{bmatrix} v_a \\ v_b \\ v_c \end{bmatrix} \tag{2.1}$$

where

$$\mathbf{T}(\theta) = \frac{2}{3} \begin{bmatrix} \cos(\theta) & \cos(\theta - 2\pi/3) & \cos(\theta + 2\pi/3t) \\ -\sin(\theta) & -\sin(\theta - 2\pi/3) & -\sin(\theta + 2\pi/3) \\ 1/2 & 1/2 & 1/2 \end{bmatrix} \tag{2.2}$$

v_a, v_b, v_c are the instantaneous measured and filtered phase voltages at the PGC, and v_{dg}, v_{qg}, v_{0g} are the d, q and 0 components of the 3 previous voltages.

The phase angle θ of the rotating reference frame is derived by the double synchronous reference frame (DSRF) PLL [49] (Figure 2.3). A PI controller adjusts θ at the synchronous speed to have the q-component of the positive sequence voltage equal to zero, i.e., to have the direct axis aligned with the voltage.

In (2.1) and thereafter, variable names denoted by lower-case letters represent the TD variables.

After this block, all filtered voltages and currents are in dq domain. As the d-axis is aligned with the voltage, the d-axis current corresponds to the active current and q-axis current represents the reactive current.

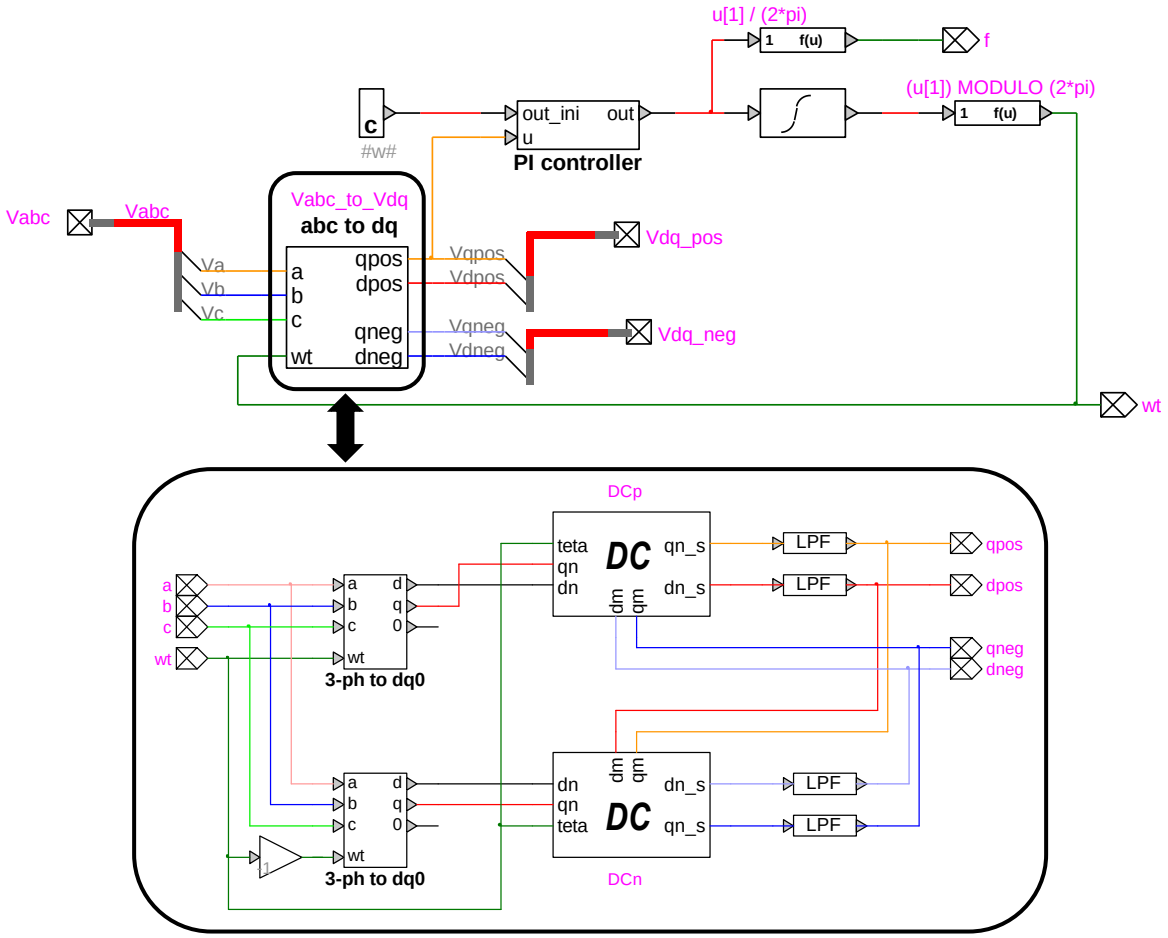

Figure 2.3 EMTP-RV diagram of the DSRF PLL.

2.1.2 Outer control loop

The third element is the outer control loop which calculates the desired active and reactive currents from the measurements. The reference direction for the currents is from the GSC to the PGC.

A PI controller on the DC-link voltage deviation from 1 pu provides the desired active current $\hat{i}_{dg}$. The active power coming from the MSC is determined by a MPPT system in the MSC controller.

For the reactive current, the outer loop is a proportional gain on the positive sequence voltage deviation, where the reference voltage depends on the WPC (Figure 1.5). As the WP is represented by an aggregated turbine and collector grid, the circuit becomes:

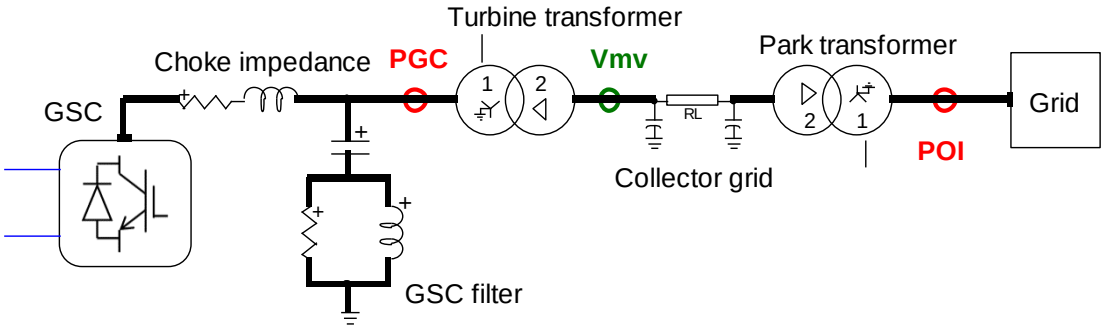

Figure 2.4 Circuit of the aggregated type-IV based WP.

To simplify the circuit, only one of the two shunt filters has been displayed in Figure 2.4 (instead of 2).

As the model is aggregated, the output of the park controller $\Delta U'$ is fed directly to the outer loop of the converter controller. Therefore, $\Delta V' = \Delta U'$. The outer loop equation for reactive current is:

$$\hat{i}_{qg} = -K_V \left(1 + \Delta U' - \left|\bar{V}_{ctrl}^{+}\right|\right) \tag{2.3}$$

where $\hat{i}_{qg}$ is the desired reactive current, K_V is the proportional gain ($K_V > 0$), and $\left|\bar{V}_{ctrl}^{+}\right|$ is the magnitude of the positive sequence controlled voltage. The controlled voltage is either the PGC voltage or the voltage at the MV side of the turbine transformer (Vmv in Figure 2.4). The MV is not measured, but calculated from the turbine transformer series impedance as well as the voltage and current at the PGC. This is the case also in practice, because of the cost of the voltage and current transformers on the MV side.

The controller also has an FRT mode during large voltage sags. In this thesis, this mode generates a reactive current component proportional to voltage deviation from 1pu (Figure 2.5). The FRT mode is essential if the grid code requires voltage support.

The FRT mode is activated only when the controlled positive sequence voltage is off the deadband. In Figure 2.5, the FRT mode is activated for a voltage deviation from 1 pu by at least 0.1 pu, and the FRT gain (the slope) is 2.

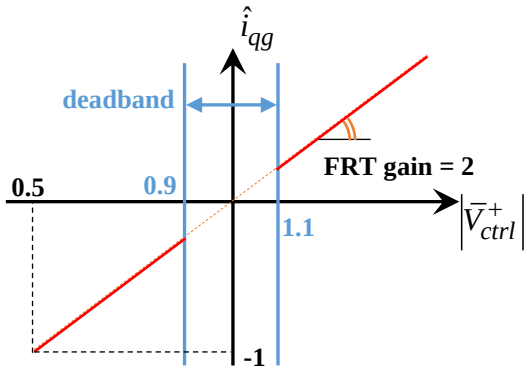

Figure 2.5 Example of an FRT curve [50].

The outer loop equation in FRT mode becomes:

$$\hat{i}_{qg} = -K_{FRT}\left(1-\left|\bar{V}^{+}_{ctrl}\right|\right) \tag{2.4}$$

where K_{FRT} is the proportional gain ($K_{FRT} > 0$).

When the controlled voltage falls slightly below the FRT activation limit, the FRT mode can push the voltage above this activation limit. In the TD, when the FRT mode is activated, the controller stays in this mode for a fixed duration to avoid repetitive mode changing.

The deadband represents the usual or normal conditions (positive sequence voltage between 0.9 and 1.1 pu). In this deadband, the park controller regulates the reactive power, voltage or power factor at the POI.

2.1.3 Current limiter

During voltage sags, $\hat{i}_{dg}$ and $\hat{i}_{qg}$ can be too large and damage the converter. A first bound is set on each component: $I_{dg}^{\lim}$ for the d-axis and $I_{qg}^{\lim}$ for the q-axis. According to those bounds, the total current magnitude can still be too large for the converter. Consequently, a maximum current magnitude $I_{g}^{\lim}$ that the converter can stand due to thermal constraints is set (usually between 1.1 and 1.4 pu). $I_{dg}^{\lim}$ and $I_{qg}^{\lim}$ are equal to or less than $I_{g}^{\lim}$. The total current magnitude is

maintained within its bound by chopping, if necessary, the active or the reactive component of the current. The component which is not chopped, is the one having the priority.

In normal conditions (no FRT), the priority can be given to the active or reactive component, but usually to the active one (P-priority). In the FRT mode where the goal is to maintain the voltage, priority is always given to the reactive current (Q-priority). The corrected currents are called reference currents and written with an apostrophe: i'_{dg} and i'_{qg}.

In P-priority, $\hat{i}_{dg}$ respects its own limit and becomes the reference value:

$$i_{dg}^{\max} = I_{dg}^{\lim} \tag{2.5}$$

$$i'_{dg} = \min\left(\hat{i}_{dg}, i_{dg}^{\max}\right) \tag{2.6}$$

and $\hat{i}_{qg}$ is limited:

$$i_{qg}^{\max} = \min\left(\sqrt{\left(I_g^{\lim}\right)^2 - \left(i'_{dg}\right)^2}, I_{qg}^{\lim}\right) \tag{2.7}$$

$$i'_{qg} = \operatorname{sign}\left(\hat{i}_{qg}\right) \cdot \min\left(\left|\hat{i}_{qg}\right|, i_{qg}^{\max}\right) \tag{2.8}$$

The "sign" function gives +1 if the input is positive and –1 if negative. This function is required because $\hat{i}_{qg}$ can be positive or negative.

In Q-priority, $\hat{i}_{qg}$ respects its own limit and becomes the reference value.

$$i_{qg}^{\max} = I_{qg}^{\lim} \tag{2.9}$$

$$i'_{qg} = \operatorname{sign}\left(\hat{i}_{qg}\right) \cdot \min\left(\left|\hat{i}_{qg}\right|, i_{qg}^{\max}\right) \tag{2.10}$$

and $\hat{i}_{dg}$ is limited:

$$i_{dg}^{\max} = \min\left(\sqrt{\left(I_g^{\lim}\right)^2 - \left(i'_{qg}\right)^2}, I_{dg}^{\lim}\right) \tag{2.11}$$

$$i'_{dg} = \min\left(\hat{i}_{dg}, i_{dg}^{\max}\right) \tag{2.12}$$

$i_{dg}^{\max}$ and $i_{qg}^{\max}$ are the maximum values for d and q currents. These maximum values depend on the three current limits ($I_g^{\lim}$, $I_{dg}^{\lim}$, $I_{qg}^{\lim}$) and on the prioritized component. $i_{dg}^{\max}$ and $i_{qg}^{\max}$ are consequently fault-dependent.

When the active power is limited by the action of the limiter, not all of the active power produced is transferred to the grid; the excessive active power in this case is consumed by the DC-link chopper.

The outputs of the limiter are the active and reactive current references i'_{dg} and i'_{qg}.

A description of the bounds and the action of the limiter along with an example is given graphically in Figure 2.6. The example involves balanced conditions and hence DC signals as the dq components of current. $\hat{i}$ is the desired current, i'_Q is the limited current with Q-priority, and i'_P is the limited current with P-priority.

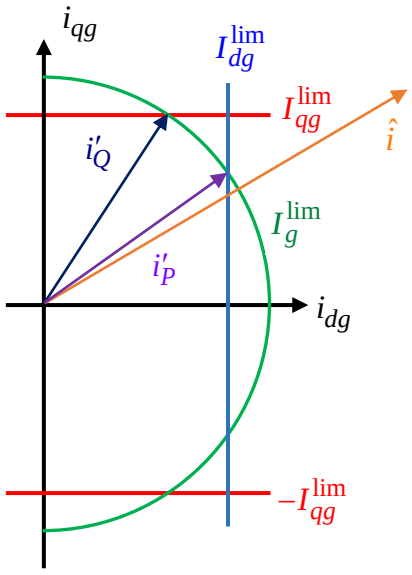

Figure 2.6 Geometrical representation of current limits.

2.1.4 Inner control loop with coupled control

The inner control loop contains PI controllers and calculates the converter reference voltages (in dq domain) to reach the desired currents.

The GSC regulates its transmitted power through its GSC output voltage and the choke impedance. The following equation gives the relation between the GSC output voltage, PGC voltage, GSC current, and choke resistance and inductance:

$$v_{pgc}^{j} = Ri_{g}^{j} + L\frac{di_{g}^{j}}{dt} + v_{cv}^{j} \tag{2.13}$$

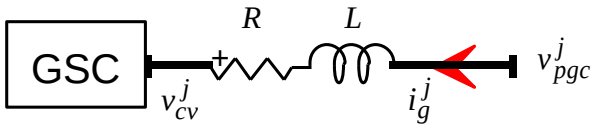

Figure 2.7 Current regulation through the choke impedance.

where v_{pgc}^{j} and v_{cv}^{j} are the AC voltages of, respectively, the PGC and the converter for phase j (*j=a,b,c)*. Moreover, i_{g}^{j} is the AC current through the choke impedance for phase j, and R is the choke resistance, and L is the choke inductance.

Note: the inner control loop is built with currents flowing from the grid to the converter.

Applying the abc-to-dq transformation matrix $\mathbf{T}$ to (2.13), we obtain:

$$v_{dcv} = -Ri_{dg} - L\frac{di_{dg}}{dt} + \omega_s Li_{qg} + v_{dg} \tag{2.14}$$

$$v_{qcv} = -Ri_{qg} - L\frac{di_{qg}}{dt} - \omega_s Li_{dg} + v_{qg} \tag{2.15}$$

where ω_s is the grid nominal angular frequency, v_{dcv} and v_{qcv} are, respectively, the d- and q-components of the converter voltage, and i_{dg} and i_{qg} are, respectively, the d- and q-components of the converter current.

On replacing the derivative term with a PI controller processing the error between the actual current and its reference, we get:

$$v'_{dcv} = -Ri_{dg} - \left[K_P\left(i'_{dg} - i_{dg}\right) + K_I\int\left(i'_{dg} - i_{dg}\right)dt\right] + \omega_s Li_{qg} + v_{dg} \tag{2.16}$$

$$v'_{qcv} = -Ri_{qg} - \left[K_P \left(i'_{qg} - i_{qg} \right) + K_I \int \left(i'_{qg} - i_{qg} \right) dt \right] - \omega_s L i_{dg} + v_{qg} \tag{2.17}$$

where K_P and K_I are the proportional and integral gains of the PI controller, and v'_{dcv} and v'_{qcv} are the dq components of the converter reference voltages.

The feedforward terms $-Ri_{dg} + \omega_s L i_{qg} + v_{dg}$ on the d-axis and $-Ri_{qg} - \omega_s L i_{dg} + v_{qg}$ on the q-axis make the output of the PI controller close to 0.

The output of the PI controller is limited to 1 pu to avoid over-correction, and an anti-windup system prevents the integral part from growing when the PI output is limited.

As the choke resistance is very small, it is generaly negligible. Equations (2.16) and (2.17) become:

$$v'_{dcv} = -\left[K_P \left(i'_{dg} - i_{dg} \right) + K_I \int \left(i'_{dg} - i_{dg} \right) dt \right] + \omega_s L i_{qg} + v_{dg} \tag{2.18}$$

$$v'_{qcv} = -\left[K_P \left(i'_{qg} - i_{qg} \right) + K_I \int \left(i'_{qg} - i_{qg} \right) dt \right] - \omega_s L i_{dg} + v_{qg} \tag{2.19}$$

Equations (2.18) and (2.19) represent the inner control loop equations.

This inner control loop is called coupled (or sequence coupled), because the measured parameters i_{dg}, i_{qg}, v_{dg} and v_{qg} contain the positive sequence (DC component of the signal) and the negative sequence (twice the grid frequency component of the signal) components. Figure 2.8 shows that the measured currents and voltages are not filtered in dq domain, unlike the decoupled sequence controller which use the same method as the PLL (see Figure 2.3).

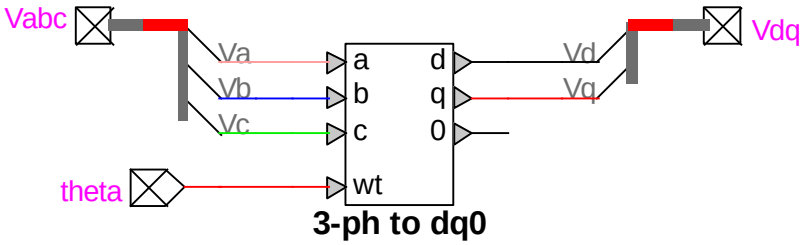

Figure 2.8 abc-to-dq transformation with coupled control.

With this coupled inner control loop, the negative sequence is not controlled, and the twice the grid frequency oscillations circulate in the control loop. The controller elements which impact these oscillations are detailed in the section 2.2.4.

Figure 2.9 shows the outer and inner control loops as well as the limiter associated with the coupled control. In that figure, v_{dc} is the measured and filtered DC-link voltage, V'_{dc} is the reference value for the DC voltage and equal to 1 pu, and m is the modulation pattern for the switches of the converter.

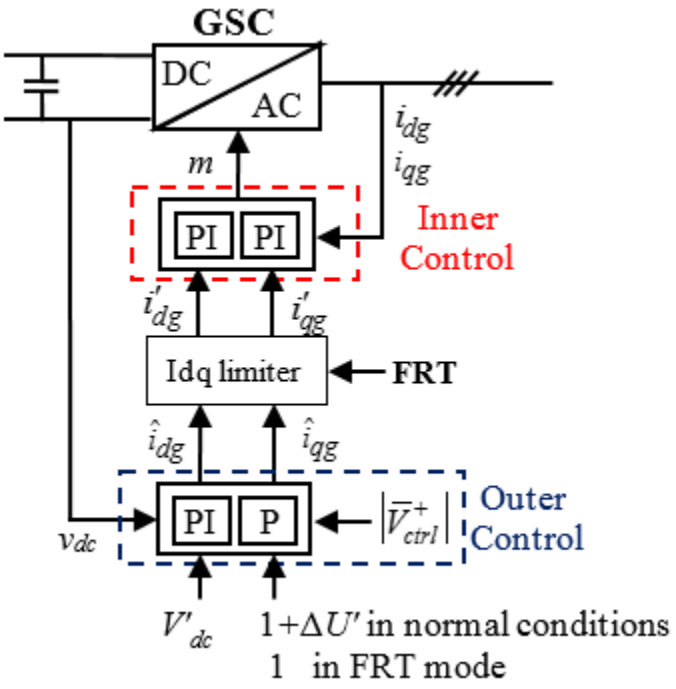

Figure 2.9 Schematic diagram of GSC coupled control.

2.1.5 Decoupled controller

With a decoupled controller, the positive and negative sequences are separated and both are represented by d- and q-components. The PGC voltages are decomposed into v^{+}_{dg}, v^{+}_{qg}, v^{-}_{dg} and v^{-}_{qg} (Figure 2.3) where the superscripts + (plus) and – (minus) stand, respectively, for positive and negative sequences. The same holds for converter currents: i^{+}_{dg}, i^{+}_{qg}, i^{-}_{dg} *and* i^{-}_{qg}.

The voltage and current components of the previous paragraph are filtered after their abc-to-dq transformation to reduce the variation rate (see the LPF block in Figure 2.3):

$$H_0(p) = \frac{\omega_0}{\omega_0 + p} \qquad with\ \omega_0 = 2\pi 1000 \tag{2.20}$$

where p is the complex Laplace variable.

The goal of this decoupled abc-to-dq transformation is to control the negative sequence response of the converter.

For FSC, one of the goals of the negative sequence controller is to reduce active power oscillations during unbalanced conditions. Negative sequence components induce oscillations of the active power, and the frequency of oscillations is twice the grid frequency. These power oscillations induce voltage oscillations of the same frequency on the DC-link. The power oscillations then appear on the AC side of the MSC and induce torque oscillations which are harmful to the PMSG.

To circumvent the problem of torque oscillations and its harmful consequences, the GSC injects a negative sequence current to suppress or reduce the power oscillations. But as before, the GSC must respect the thermal limitation on the injected current. In addition, due to FRT requirements, the negative sequence current injection is also limited by the reactive current injection imposed by the FRT curve.

Considering only the fundamental components of currents and voltages, the instantaneous active power at the PGC side of the choke impedance can be written as [51]:

$$p(t) = P_0 + P_{C2}\cos(2\omega_s t) + P_{S2}\sin(2\omega_s t) \tag{2.21}$$

where P_0 is the average value of $p(t)$, and P_{C2} and P_{S2} are the magnitudes of the second harmonic oscillating terms:

$$P_0 = v_{dg}^{+} i_{dg}^{+} + v_{qg}^{+} i_{qg}^{+} + v_{dg}^{-} i_{dg}^{-} + v_{qg}^{-} i_{qg}^{-} \tag{2.22}$$

$$P_{C2} = v_{dg}^{-} i_{dg}^{+} + v_{qg}^{-} i_{qg}^{+} + v_{dg}^{+} i_{dg}^{-} + v_{qg}^{+} i_{qg}^{-} \tag{2.23}$$

$$P_{S2} = v_{qg}^{-} i_{dg}^{+} - v_{dg}^{-} i_{qg}^{+} - v_{qg}^{+} i_{dg}^{-} + v_{dg}^{+} i_{qg}^{-} \tag{2.24}$$

The sum of the sine and cosine components in (2.21) results in a single sinewave with a phase shift:

$$P_{C2}\cos(2\omega_s t) + P_{S2}\sin(2\omega_s t) = P_2\sin(2\omega_s t + \alpha) \tag{2.25}$$

where:

$$P_2 = \sqrt{\left(P_{C2}\right)^2 + \left(P_{S2}\right)^2} \tag{2.26}$$

Equation (2.26) shows that the magnitude of active power oscillations is a nonlinear function of P_{C2} and P_{S2}, and consequenctly a nonlinear function of the dq components of currents and voltages. To maintain a linear equation, (2.21) is used.

To avoid active power oscillations, the GSC current references (d- and q-components of positive and negative sequences) are calculated so P_{C2} and P_{S2} vanish, i.e., $P_{C2} = P_{S2} = 0$.

P_0 is approximated by:

$$P_0 = \left|\bar{V}_{ctrl}^{+}\right| i'_{dg} \tag{2.27}$$

where $\left|\bar{V}_{ctrl}^{+}\right|$ is the magnitude of the positive sequence controlled voltage.

The FRT constraint on the reactive positive sequence current requires that: $i_{qg}^{+\prime} = i'_{qg}$.

These constraints are taken into account in a system of equations to calculate the four current references [37] :

$$\begin{bmatrix} i_{qg}^{+\prime} \\ i_{dg}^{+\prime} \\ i_{qg}^{-\prime} \\ i_{dg}^{-\prime} \end{bmatrix} = \begin{bmatrix} 1 & 0 & 0 & 0 \\ v_{qg}^{+} & v_{dg}^{+} & v_{qg}^{-} & v_{dg}^{-} \\ v_{qg}^{-} & v_{dg}^{-} & v_{qg}^{+} & v_{dg}^{+} \\ -v_{dg}^{-} & v_{qg}^{-} & v_{dg}^{+} & -v_{qg}^{+} \end{bmatrix}^{-1} \begin{bmatrix} i'_{qg} \\ P_0 \\ P_{C2} \\ P_{S2} \end{bmatrix} \tag{2.28}$$

The calculated current references $i_{dg}^{+\prime}, i_{qg}^{+\prime}, i_{dg}^{-\prime}, i_{qg}^{-\prime}$ in (2.28) are revised according to the converter limits $I_{dg}^{\lim}$ and $I_{qg}^{\lim}$:

$$
\begin{aligned}
i_{qg}^{+}{}'' &= \operatorname{sign}\left(i_{qg}^{+}{}'\right)\min\left(\left|i_{qg}^{+}{}'\right|, I_{qg}^{\lim}\right)\\
i_{dg}^{+}{}'' &= \operatorname{sign}\left(i_{dg}^{+}{}'\right)\min\left(\left|i_{dg}^{+}{}'\right|, I_{dg}^{\lim}\right)\\
i_{qg}^{-}{}'' &= \operatorname{sign}\left(i_{qg}^{-}{}'\right)\min\left(\left|i_{qg}^{-}{}'\right|, I_{qg}^{\lim}\right)\\
i_{dg}^{-}{}'' &= \operatorname{sign}\left(i_{dg}^{-}{}'\right)\min\left(\left|i_{dg}^{-}{}'\right|, I_{dg}^{\lim}\right)
\end{aligned}
\tag{2.29}
$$

where $i_{dg}^{+}{}''$, $i_{qg}^{+}{}''$, $i_{dg}^{-}{}''$, $i_{qg}^{-}{}''$ are the revised current references.

In addition to this first limitation, if $\left(i_{qg}^{+}{}'' + i_{qg}^{-}{}''\right) > i_{qg}^{\max}$ (for example), the q-axis current references must be corrected again. The same applies to the d-axis current references. Both positive and negative components are limited according to their proportion of the total:

$$
i_{dg}^{+}{}''' = i_{dg}^{+}{}''\ \min\left(\frac{i_{dg}^{\max}}{\left|i_{dg}^{+}{}''\right| + \left|i_{dg}^{-}{}''\right|}, 1\right) \qquad i_{dg}^{-}{}''' = i_{dg}^{-}{}''\ \min\left(\frac{i_{dg}^{\max}}{\left|i_{dg}^{+}{}''\right| + \left|i_{dg}^{-}{}''\right|}, 1\right) \tag{2.30}
$$

$$
i_{qg}^{+}{}''' = i_{qg}^{+}{}''\ \min\left(\frac{i_{qg}^{\max}}{\left|i_{qg}^{+}{}''\right| + \left|i_{qg}^{-}{}''\right|}, 1\right) \qquad i_{qg}^{-}{}''' = i_{qg}^{-}{}''\ \min\left(\frac{i_{qg}^{\max}}{\left|i_{qg}^{+}{}''\right| + \left|i_{qg}^{-}{}''\right|}, 1\right) \tag{2.31}
$$

where $i_{dg}^{+}{}'''$, $i_{dg}^{-}{}'''$, $i_{qg}^{+}{}'''$ and $i_{qg}^{-}{}'''$ are the corrected reference currents. $i_{dg}^{\max}$ and $i_{qg}^{\max}$ are obtained from the first current limiter (see section 2.1.3), and they consider the P- or Q-priority.

2.1.6 Inner control loop with decoupled control

The decoupled inner control loop has a structure similar to that of the coupled inner control loop. There is a PI controller for each one of the 4 current components.

For the positive sequence:

$$
v_{dcv}'^{+} = -K_P\left(i_{dg}^{+}{}''' - i_{dg}^{+}\right) - K_I\int\left(i_{dg}^{+}{}''' - i_{dg}^{+}\right)dt \tag{2.32}
$$

$$
v_{qcv}'^{+} = -K_P\left(i_{qg}^{+}{}''' - i_{qg}^{+}\right) - K_I\int\left(i_{qg}^{+}{}''' - i_{qg}^{+}\right)dt \tag{2.33}
$$

where v'^{+}_{dcv} and v'^{+}_{qcv} are the d- and q-components of the positive sequence converter reference voltages respectively.

For the negative sequence:

$$v'^{-}_{dcv} = -K_P\left(i^{-}_{dg}{}''' - i^{-}_{dg}\right) - K_I\int\left(i^{-}_{dg}{}''' - i^{-}_{dg}\right)dt \tag{2.34}$$

$$v'^{-}_{qcv} = -K_P\left(i^{-}_{qg}{}''' - i^{-}_{qg}\right) - K_I\int\left(i^{-}_{qg}{}''' - i^{-}_{qg}\right)dt \tag{2.35}$$

where v'^{-}_{dcv} and v'^{-}_{qcv} are the d- and q-components of the negative sequence converter reference voltages respectively.

As for the coupled inner control loop, the outputs of the PI controllers are limited to avoid over-correction, and an anti-windup system prevents the integral part from growing when the PI output is limited.

In addition to their similarity with respect to the use of PI controllers, the feedforward terms of the decoupled inner control loop are the same as the terms of the coupled inner control loop:

$$dv_{dcv} = \omega_s L i_{qg} + v_{dg} \tag{2.36}$$

$$dv_{qcv} = -\omega_s L i_{dg} + v_{qg} \tag{2.37}$$

where dv_{dcv} and dv_{qcv} are, respectively, the feedforward terms on the d- and q-axis for the converter voltage. These feedforward terms use coupled parameters. They have a DC component and an AC signal with twice the grid frequency under unbalanced conditions.

The combination of the PI controller and the feedforward terms will be dealt with in the αβ domain in the next section.

Figure 2.14 depicts in a graphical way the outer and the inner control loops with limiter for decoupled control.

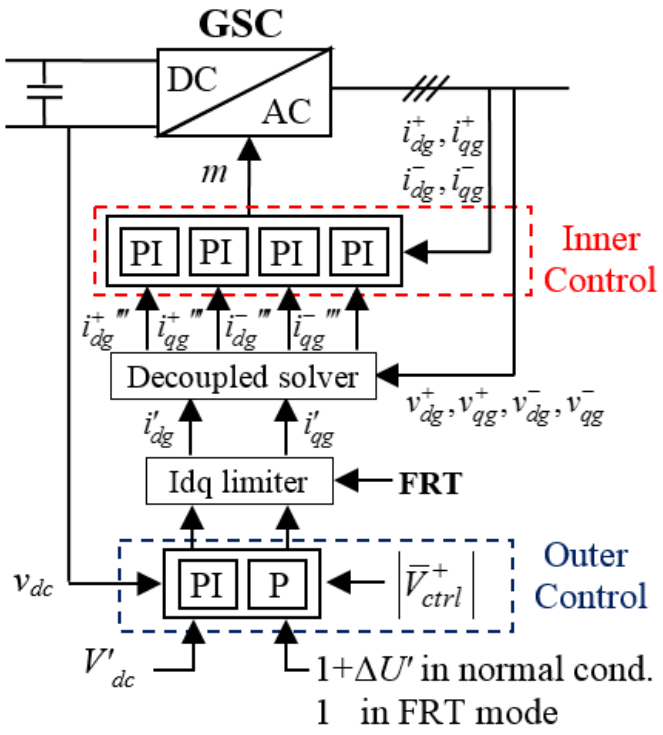

Figure 2.10 Schematic diagram of GSC decoupled control.

2.1.7 dq-to-abc transformation

The last block of the diagram in Figure 2.3 has to do with the transformation of the reference converter voltages in phase domain. Pulse width modulation (PWM) and the reference converter voltages are used to control the switching action of the semiconductor switches of the converter.

To avoid overvoltage of the converter, the reference converter voltages are limited in the $\alpha\beta$ domain or coordinate system.

The dq-to-αβ transformation for the coupled inner control loop is:

$$\begin{bmatrix} v'_{\alpha cv} \\ v'_{\beta cv} \end{bmatrix} = \begin{bmatrix} \cos(\theta) & -\sin(\theta) \\ \sin(\theta) & \cos(\theta) \end{bmatrix} \begin{bmatrix} v'_{dcv} \\ v'_{qcv} \end{bmatrix} \tag{2.38}$$

where $v'_{\alpha cv}$ and $v'_{\beta cv}$ are the α and β components of the converter voltage respectively, and θ is the same angle as that in the abc-to-dq transformation in (2.2).

The dq-to-αβ transformation associated with the decoupled inner control loop is as follows:

$$\begin{bmatrix} v'^{+}_{\alpha cv} \\ v'^{+}_{\beta cv} \end{bmatrix} = \begin{bmatrix} \cos(\theta) & -\sin(\theta) \\ \sin(\theta) & \cos(\theta) \end{bmatrix} \begin{bmatrix} v'^{+}_{dcv} + dv_{dcv} \\ v'^{+}_{qcv} + dv_{qcv} \end{bmatrix} \tag{2.39}$$

$$\begin{bmatrix} v'^{-}_{\alpha cv} \\ v'^{-}_{\beta cv} \end{bmatrix} = \begin{bmatrix} \cos(\theta) & \sin(\theta) \\ -\sin(\theta) & \cos(\theta) \end{bmatrix} \begin{bmatrix} v'^{-}_{dcv} \\ v'^{-}_{qcv} \end{bmatrix} \tag{2.40}$$

where $v'^{+}_{\alpha cv}$ and $v'^{+}_{\beta cv}$ are, respectively, the α and β components of the converter voltage corresponding to the positive sequence PI controllers and the feedforward terms. Similarly, $v'^{-}_{\alpha cv}$ and $v'^{-}_{\beta cv}$ are, respectively, the α and β components of the converter voltage corresponding to the negative sequence PI controllers.

$$\begin{aligned} v'_{\alpha cv} &= v'^{+}_{\alpha cv} + v'^{-}_{\alpha cv} \\ v'_{\beta cv} &= v'^{+}_{\beta cv} + v'^{-}_{\beta cv} \end{aligned} \tag{2.41}$$

The relations discussed in the rest of this section apply to both coupled and decoupled sequence controllers.

The magnitude of the converter voltage in αβ coordinates is limited to 1.5 times the DC-link voltage:

$$v''_{\alpha cv} + jv''_{\beta cv} = \frac{\left(v'_{\alpha cv} + jv'_{\beta cv}\right)}{v_{dc}\sqrt{2/3}} \min\left(\frac{1.5 v_{dc}\sqrt{2/3}}{\sqrt{\left(v'_{\alpha cv}\right)^2 + \left(v'_{\beta cv}\right)^2}}, 1 \right) \tag{2.42}$$

where $v''_{\alpha cv}$ and $v''_{\beta cv}$ are the corrected α and β components of the converter reference voltages, and v_{dc} is the measured and filtered DC-link voltage. The $\sqrt{2/3}$ in (2.42) comes from the relation between the DC voltage base V_{DC}^{base} and the line-to-line RMS voltage base on the AC side of the GSC $V_{LL,RMS}^{base}$:

$$V_{DC}^{base} = 2\sqrt{\frac{2}{3}} V_{LL,RMS}^{base} \tag{2.43}$$

In the end, the corrected converter voltages in the $\alpha\beta$ coordinates are transformed into *abc* coordinates through the Clarke transformation:

$$\begin{bmatrix} v'_{a,cv} \\ v'_{b,cv} \\ v'_{c,cv} \end{bmatrix} = \begin{bmatrix} 1 & 0 & 1 \\ -0.5 & 0.5\sqrt{3} & 1 \\ -0.5 & -0.5\sqrt{3} & 0.5 \end{bmatrix} \begin{bmatrix} v''_{\alpha cv} \\ v''_{\beta cv} \\ 0 \end{bmatrix} \quad (2.44)$$

where $v'_{a,cv}$, $v'_{b,cv}$ and $v'_{c,cv}$ are the voltage references for the abc phases of the PWM system. These values are multiplied by one-half of the DC-link voltage in volts (not in pu) to obtain the 3-phase instantaneous voltages of the AVM for the converter [43].

2.2 Phasor model of full-scale converter WTGs

The phasor model discussed in this section considers the control structure and the behavior of the TD model presented in the previous section. The difference compared to the TD model is that the inputs, outputs and controller parameters are based on, or in terms of, phasors of voltages and currents. This phasor model will provide the phasors of the converter currents. The limiter of converter voltages (see section 2.1.7) is not treated in this section because it has an impact only if the DC-link voltage prevents the converter from reaching its reference voltages. This happens when there are overvoltages at the PGC and the DC-link voltage stays at 1 pu, or the DC-link voltage drops because of a fault inside the turbine. During grid faults those situations cannot happen.

2.2.1 Outer control loop

In this section, the d- and q-components of currents represent currents flowing from the converter to the PGC.

Active power behavior

A common goal of all control modes is to transmit the active power coming from the DC-link. As the wind speed and direction do not change much for a time-interval in the order of 100 milliseconds, we assume that there is no active power variation between the fault condition and the prefault SS. Consequently, the active power production during the fault is the same as that before the fault.

In the case of a voltage sag, the outer loop will increase the active part of current to maintain the active power output at the PGC $\left(i.e.\ P_{pgc} = P'_{pgc}\right)$:

$$\hat{I}_{dg} = \frac{P'_{pgc}}{\left|\bar{V}^{+}_{pgc}\right|} + \text{real}\left(\frac{\left|\bar{V}^{+}_{pgc}\right|}{Z_{filter}}\right) \tag{2.45}$$

where Z_{filter} is the total impedance of GSC shunt filters at grid frequency. Its resistive part is usually negligible, but the general formula is given here for the sake of completeness. P'_{pgc} is the reference active power flowing at PGC to the grid, and is obtained from prefault conditions. Consequently, P'_{pgc} and $\hat{I}_{dg}$ are positive.

Reactive power behavior

Recall that control is performed at the POI, the point where the wind park is connected to the host grid. The WPC can have three control modes under normal conditions: V-control, Q-control and PF-control. For any control mode, the WPC provides the outer control loop of the GSC controller with a correction $\Delta U'$. As an aggregated turbine model is used, $\Delta U'$ is directly used in the GSC controller.

As the WPC has a very slow response (scale of seconds), its output variation during faults lasting for less than half a second is neglected. Consequently, the $\Delta U'$ during the fault is equal to the $\Delta U'$ before the fault, and it is calculated on the basis of prefault conditions which depend on the control mode and the reference value:

$$\Delta U' = \left|\bar{V}^{+(0)}_{ctrl}\right| - 1 - I^{(0)}_{qg} / K_V \tag{2.46}$$

where the superscript "(0)" refers to the prefault value, and K_V is the proportional gain of the outer loop ($K_V > 0$).

The controlled voltage $\bar{V}^{+}_{ctrl}$ can be either the PGC voltage or the voltage at the MV side of turbine transformer ("Vmv" in Figure 2.4). In the former case, $V^{+}_{ctrl} = \left|\bar{V}^{+}_{pgc}\right|$ and in the latter,

$V_{ctrl}^{+} = \left|\bar{V}_{mv}^{+}\right|$. $\bar{V}_{mv}^{+}$ is calculated from the turbine transformer series impedance and the voltage and current at the PGC:

$$\bar{V}_{mv}^{+} = \bar{V}_{pgc}^{+} - \bar{I}_{pgc}^{+} Z_{tt}^{+} \tag{2.47}$$

where Z_{tt}^{+} is the positive sequence series complex impedance of the turbine transformer at the nominal frequency.

During the fault, the desired reactive current $\hat{I}_{qg}$ is obtained for V-control, Q-control or PF-control through the following formula:

$$\hat{I}_{qg} = -K_V \left(1 - V_{ctrl}^{+} + \Delta U'\right) \tag{2.48}$$

The control mode does not directly affect the outer control loop, however, it does affect the prefault conditions which in turn determine $\Delta U'$. Consequently, the outer control loop responses will be identical for different control modes yielding the same prefault conditions.

All control modes associated with the normal conditions can have an FRT function. If the WP has a FRT function, this function is activated when V_{ctrl}^{+} leaves the deadband (see Figure 2.5). With FRT function, the desired reactive current $\hat{I}_{qg}$ becomes:

$$\hat{I}_{qg} = -K_{FRT} \left(1 - V_{ctrl}^{+}\right) \tag{2.49}$$

where K_{FRT} is the proportional voltage regulator gain defined by the FRT requirement ($K_{FRT} > 0$).

2.2.2 Current limiter

The current limiter protects the GSC against overcurrent by cutting the active and/or the reactive component of the desired current. This section uses the same equations as those of section 2.1.3, except that the variables are DC signals (uppercase letters instead of lowercase).

In P-priority, $\hat{I}_{dg}$ respects its own limit and becomes the reference value.

$$I_{dg}^{\max} = I_{dg}^{\lim} \tag{2.50}$$

$$I'_{dg} = \min\left(\hat{I}_{dg}, I_{dg}^{\max}\right) \tag{2.51}$$

and $\hat{I}_{qg}$ is reduced:

$$I_{qg}^{\max} = \min\left(\sqrt{\left(I_g^{\lim}\right)^2 - \left(I'_{dg}\right)^2}, I_{qg}^{\lim}\right) \tag{2.52}$$

$$I'_{qg} = \text{sign}\left(\hat{I}_{qg}\right) \cdot \min\left(\left|\hat{I}_{qg}\right|, I_{qg}^{\max}\right) \tag{2.53}$$

The "sign" function gives +1 if the input is positive and –1 if negative. This function is required because $\hat{I}_{qg}$ can be positive or negative.

In Q-priority, $\hat{I}_{qg}$ respects its own limit and becomes the reference value.

$$I_{qg}^{\max} = I_{qg}^{\lim} \tag{2.54}$$

$$I'_{qg} = \text{sign}\left(\hat{I}_{qg}\right) \cdot \min\left(\left|\hat{I}_{qg}\right|, I_{qg}^{\max}\right) \tag{2.55}$$

and $\hat{I}_{dg}$ is reduced:

$$I_{dg}^{\max} = \min\left(\sqrt{\left(I_g^{\lim}\right)^2 - \left(I'_{qg}\right)^2}, I_{dg}^{\lim}\right) \tag{2.56}$$

$$I'_{dg} = \min\left(\hat{I}_{dg}, I_{dg}^{\max}\right) \tag{2.57}$$

To illustrate the behaviors of I'_{dg} and I'_{qg} , an example is presented here for reference currents as functions of voltage levels.

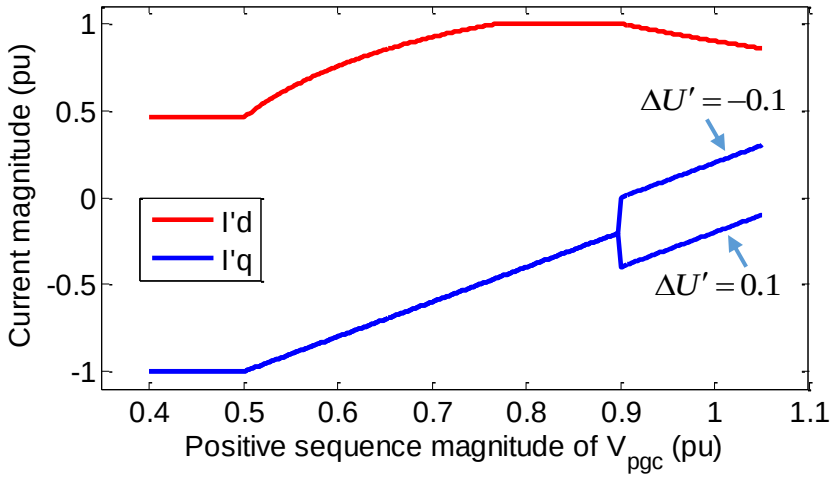

Figure 2.11 Difference between control at PGC and control at POI.

In Figure 2.11, the controlled variable is the PGC voltage, i.e., $V_{ctrl}^{+} = \left|\bar{V}_{pgc}^{+}\right|$, the WTG provides its nominal active power ($P'_{pgc} = 0.9\,pu$), and the following parameter values are used:

$$I_g^{\lim} = 1.1\,pu \qquad I_{dg}^{\lim} = I_{qg}^{\lim} = 1\,pu \qquad K_V = K_{FRT} = 2$$

2.2.3 Coupled control: positive sequence behavior

The inner loop only calculates the output voltage of the converter to reach the current references calculated in the previous section. The two PI controllers adjust their outputs so that the reference currents are reached.

Using the dq-to-abc transformation with the converter reference currents I'_{dg} and I'_{qg}, the phasor of the positive sequence current of the converter is obtained:

$$\bar{I}_g^{+} = \left(I'_{dg} + jI'_{qg}\right)\exp\left[\, j\,\text{angle}\left(\bar{V}_{pgc}^{+}\right)\right] \tag{2.58}$$

To unify the notation here with the notation for decoupled control, (2.58) is rewritten as:

$$\begin{aligned} I_{dg}^{+}{}''' &= I'_{dg} \\ I_{qg}^{+}{}''' &= I'_{qg} \end{aligned} \tag{2.59}$$

$$\bar{I}_g^+ = \left(I_{dg}^{+\,\prime\prime\prime} + jI_{qg}^{+\,\prime\prime\prime} \right) \exp\left[j \,\text{angle}\left(\bar{V}_{pgc}^+ \right) \right] \tag{2.60}$$

$\bar{I}_g^+$ is the phasor of the positive sequence current flowing from the converter to the PGC.

2.2.4 Coupled control: negative sequence behavior

In a GSC controller with coupled control, no specific behavior is imposed on or required of the negative sequence. The negative sequence exists in the dq components of the measured signals, and in the output of the controller. This section details how the negative sequence voltage and current impact the controller.

The first step is to define the negative sequence in dq domain. Below are the negative sequence components of a non-specific variable which may be either voltage or current:

$$\begin{aligned} x_a &= X_{mag} \sin\left(\omega_s t + \varphi_1 \right) \\ x_b &= X_{mag} \sin\left(\omega_s t + \varphi_1 + \frac{2\pi}{3} \right) \\ x_c &= X_{mag} \sin\left(\omega_s t + \varphi_1 - \frac{2\pi}{3} \right) \end{aligned} \tag{2.61}$$

where X_{mag} is the magnitude and φ_1 is the phase angle.

The abc-to-dq transformation results in components with the same magnitude but at twice the grid frequency:

$$\begin{aligned} x_d &= X_{mag} \sin\left(2\omega_s t + \varphi \right) \\ x_q &= X_{mag} \cos\left(2\omega_s t + \varphi \right) = X_{mag} \sin\left(2\omega_s t + \varphi + \pi / 2 \right) \end{aligned} \tag{2.62}$$

where φ depends on φ_1 and the transformation angle used by the abc-to-dq transformation. The oscillations on the d-axis are delayed by 90° with respect to the oscillations on the q-axis.

The negative sequence behavior of the GSC depends on how the oscillations defined in (2.62) flow in the inner control loop. The equations of the inner control loop with coupled control have been presented in section 2.1.4. Recall that for the inner loop, the reference direction of currents is from the grid to the converter. The equations in Laplace domain are:

$$\tilde{V}'_{dcv-c} = -\left(\tilde{I}'_{dg} - \tilde{I}_{dg}\right)\left(K_P + K_I / p\right) - R\tilde{I}_{dg} + X\tilde{I}_{qg} + \tilde{V}_{dg} \quad (2.63)$$

$$\tilde{V}'_{qcv-c} = -\left(\tilde{I}'_{qg} - \tilde{I}_{qg}\right)\left(K_P + K_I / p\right) - R\tilde{I}_{qg} - X\tilde{I}_{dg} + \tilde{V}_{qg} \quad (2.64)$$

where

- K_P and K_I are the proportional and integral constants of the inner loop PI controller,
- R and $X = \omega_s L$ are the choke resistance and reactance (at nominal frequency),
- $\tilde{I}'_{dg}$ and $\tilde{I}'_{qg}$ are the currents coming from the outer control loop via the current limiter,
- $\tilde{I}_{dg}$ and $\tilde{I}_{qg}$ are the measured converter currents,
- $\tilde{V}_{dg}$ and $\tilde{V}_{qg}$ are the measured PGC voltages,
- $\tilde{V}'_{dcv-c}$ and $\tilde{V}'_{qcv-c}$ are the calculated voltages of the voltage source,
- "~" indicates the signals in the Laplace domain,
- p is the complex Laplace variable.

The outputs of the inner loop PI controllers are equipped with a limiter. In the models used in this thesis, the bounds of this limiter are higher than the peak value of the oscillations. Consequently, this limiter has no impact on the negative sequence behavior of the turbine.

Under unbalanced conditions, oscillations at twice the network frequency appear in the measured voltage and current signals. The reference currents of the inner loop come from the outer loop through the current limiter. $\tilde{\tilde{I}}_{qg}$ is calculated in the outer loop on the basis of positive sequence parameters; consequently, it has no oscillations, i.e., it contains no AC part. This is the case under normal conditions and in the FRT mode.

$\tilde{\tilde{I}}_{dg}$ is calculated in the outer loop on the basis of the DC-link voltage which also contains an AC signal with twice the grid frequency. But as $\tilde{\tilde{I}}_{dg}$ is cut by the limiter under fault conditions (absolute limitation or limitation due to Q-priority), the oscillations are also cut.

However, for a remote fault (low drop of voltage), $\tilde{\tilde{I}}_{dg}$ is too small to be affected by the limiter. In such a case, the negative sequence current is also very small. Therefore, perturbations on the DC link can also be neglected for SC studies. In addition, the AC part of the DC-link signal is filtered out by the measurement blocks and processed by the PI controller of the outer loop.

These are the reasons for considering the reference currents used in the inner loop as DC signals even during unbalanced conditions.

There is no zero sequence current flowing from the converter due to its structure with 3 wires.

As seen in (2.62), the magnitude of oscillations with twice the grid frequency is equal to the magnitude of the negative sequence component. The oscillations on the d-axis are delayed by 90° with respect to the oscillations on the q-axis. From this observation, only one equation among (2.63) and (2.64) is required. In the following development, only (2.64) is used.

Equation (2.64) is solved with phasors at twice the grid frequency. In the following equations, the double bar indicates the second harmonic phasors in the dq reference frame.

$$\begin{aligned} \bar{\bar{I}}_{qg} &= \bar{I}_g^- \\ \bar{\bar{I}}_{dg} &= -j\,\bar{I}_g^- \\ \bar{\bar{V}}_{qg} &= \bar{V}_{pgc}^- \end{aligned} \tag{2.65}$$

Equation (2.64) becomes:

$$\bar{\bar{V}}'_{qcv-c} = \bar{V}_{pgc}^- + jX\,\bar{I}_g^- + \left(H_{PI}^g - R\right)\bar{I}_g^- \tag{2.66}$$

where H_{PI}^g is the complex gain of the PI controller at twice the grid frequency: $2\,f_{nom}$

$$H_{PI}^g = K_P + \frac{K_I}{j\,2\pi \cdot 2\,f_{nom}} \tag{2.67}$$

$\tilde{I}'_{qg}$ is not present in (2.66) because it has no oscillations.

The next step is the transformation of $\bar{\bar{V}}'_{qcv-c}$ in phase domain. The measured voltages and currents are filtered to remove harmonics due to switching. This filtering is essential but it induces a phase shift at network frequency.

The abc-to-dq transformation uses these shifted voltage and current signals. Therefore, the transformation angle θ in (2.1) does not follow the true voltage. As the voltages and the currents signals are shifted with the same angle, the shift does not affect the outer and the inner control loops. However, as the dq-to-abc transformation uses the incorrect angle, the converter voltages do not impose the correct GSC current.

The positive sequence current control is not affected by the phase shift of the measurement filter because the integral function of the inner loop PI controllers corrects the reference voltages sent to the converter. There is no such control for negative sequence current.

The impact of the measurement filter on the converter negative sequence voltage is written as:

$$\bar{\bar{V}}'^{-}_{qcv-c} = \frac{\bar{V}^{-}_{cv}}{H_{filter}} \tag{2.68}$$

where H_{filter} is the complex gain of the measurement filter at the network frequency.

Equation (2.68) is now substituted into equation (2.66):

$$\frac{\bar{V}^{-}_{cv}}{H_{filter}} = \bar{V}^{-}_{pgc} + jX\,\bar{I}^{-}_{g} + \left(H^{g}_{PI} - R\right)\bar{I}^{-}_{g} \tag{2.69}$$

$$\bar{V}^{-}_{cv} = H_{filter}\bar{V}^{-}_{pgc} + H_{filter}\left(H^{g}_{PI} - R + jX\right)\bar{I}^{-}_{g} \tag{2.70}$$

From the electrical circuit (Figure 2.7), we have:

$$\bar{V}^{-}_{cv} = \bar{V}^{-}_{pgc} - \left(R + jX\right)\bar{I}^{-}_{g} \tag{2.71}$$

Recall that the reference direction of current in the inner loop is from the grid side to the converter side.

Eliminating the converter voltage between equations (2.70) and (2.71) we find:

$$0 = H_{filter}\bar{V}^{-}_{pgc} + H_{filter}\left(H^{g}_{PI} - R + jX\right)\bar{I}^{-}_{g} - \bar{V}^{-}_{pgc} + \left(R + jX\right)\bar{I}^{-}_{g} \tag{2.72}$$

Now, it is possible to isolate the negative sequence current:

$$0 = \left(H_{filter} - 1\right)\bar{V}^{-}_{pgc} + \left[H_{filter}\left(H^{g}_{PI} - R + jX\right) + R + jX\right]\bar{I}^{-}_{g} \tag{2.73}$$

$$\bar{I}^{-}_{g} = \frac{\bar{V}^{-}_{pgc}\left(1 - H_{filter}\right)}{R + jX + H_{filter}\left(H^{g}_{PI} - R + jX\right)} \tag{2.74}$$

This expression gives the negative sequence current flowing from the grid to the converter. As all of the control parameters are constant, there is a proportional relation between the GSC negative sequence current and the negative sequence voltage at the PGC.

$$\bar{I}_g^- = Y_g^- \bar{V}_{pgc}^- \qquad \text{with } Y_g^- = \frac{\left(1 - H_{filter}\right)}{R + jX + H_{filter}\left(H_{PI}^g - R + jX\right)} \tag{2.75}$$

These results are based on the inner current control loop expressed by (2.63) and (2.64).

If the choke resistance is not considered in the inner control loop equations, the resistance term *R* is set to zero in equations (2.63), (2.64) and (2.70). Then Y_g^- becomes:

$$Y_g^- = \frac{1 - H_{filter}}{R + jX + H_{filter}\left(H_{PI}^g + jX\right)} \tag{2.76}$$

One resistance term is still present in equation (2.76) because of (2.71).

Table 2.1 below provides some numerical values for Y_g^- in terms of the cut-off frequency of the measurement filter and the choke impedance with resistance taken into account. The measurement filter is a second order Butterwoth one (see section 1.3). It is worth noting that the measurement filter's phase-shift at grid frequency in that table is calculated from the cut-off frequency of the filter and the filter's transfer function; hence that phase-shift is not an independent variable. Similarly, H_{PI}^g is calculated from the impedance seen from the GSC and depends on the choke impedance.

In Table 2.1, the grid frequency is 60Hz and Y_g^- is given in the polar form: magnitude (angle in degrees).

Table 2.1 Control parameters impact Y_g^-.

Cut-off frequency	*Phase shift at grid frequency*	$R + jX$ = 4.5 + 450j 10^{-3} pu	1.5 + 150j 10^{-3} pu	0.5 + 50j 10^{-3} pu
		H_{PI}^g = 0.387 – 0.015j	0.212 – 0.015j	0.154 – 0.014j
100 kHz	-0.05°	0.001 (-156.4)	0.002 (-143.4)	0.005 (-119.1)
10 kHz	-0.49°	0.009 (-156.3)	0.024 (-143.3)	0.048 (-118.9)
2.5 kHz	-1.95°	0.035 (-156.2)	0.096 (-143.1)	0.194 (-118.4)
1 kHz	-4.87°	0.089 (-156.0)	0.244 (-142.6)	0.492 (-117.3)

Lower cut-off frequency and lower choke impedance increase the magnitude of Y_g^-.

Y_g^- requires several specific details of the controller, like the PI gains. If those details are not available, a possible simplification is to assume $Y_g^- = 0$. Such an assumption would be equivalent to the GSC not allowing any negative sequence current. This simplification will be refered to the simple model for the type-IV WTG.

2.2.5 Decoupled control

In decoupled control, the abc-to-dq transformation separates the positive and negative sequence components of voltages and currents. The goal of this decoupled transformation in this thesis is to control the negative sequence response of the converter and to reduce the active power oscillations during unbalanced conditions, which are harmful for the PMSG.

This section reproduces the equations of section 2.1.5 but with phasor variables.

Equation (2.28) becomes:

$$\begin{bmatrix} I_{qg}^{+\prime} \\ I_{dg}^{+\prime} \\ I_{qg}^{-\prime} \\ I_{dg}^{-\prime} \end{bmatrix} = \begin{bmatrix} 1 & 0 & 0 & 0 \\ V_{qg}^{+} & V_{dg}^{+} & V_{qg}^{-} & V_{dg}^{-} \\ V_{qg}^{-} & V_{dg}^{-} & V_{qg}^{+} & V_{dg}^{+} \\ -V_{dg}^{-} & V_{qg}^{-} & V_{dg}^{+} & -V_{qg}^{+} \end{bmatrix}^{-1} \begin{bmatrix} I'_{qg} \\ P_0 \\ P_{C2} \\ P_{S2} \end{bmatrix} \tag{2.77}$$

where I'_{qg} comes from section 2.2.2, and:

$$P_0 = \left|\bar{V}_{ctrl}^{+}\right| I'_{dg} \tag{2.78}$$

In (2.77), the dq components of voltage are obtained from the positive and negative sequence voltage phasors at the PGC, and based on the PLL (section 2.1.1):

$$V_{dg}^{+} = \left|\bar{V}_{pgc}^{+}\right| \qquad V_{qg}^{+} = 0 \tag{2.79}$$

$$\begin{aligned} V_{dg}^{-} &= \mathrm{Re}\left[\bar{V}_{pgc}^{-} / \exp\left(j\,\mathrm{angle}\left(\bar{V}_{pgc}^{+}\right)\right)\right] \\ V_{qg}^{-} &= -\mathrm{Im}\left[\bar{V}_{pgc}^{-} / \exp\left(j\,\mathrm{angle}\left(\bar{V}_{pgc}^{+}\right)\right)\right] \end{aligned} \tag{2.80}$$

The calculated reference values in (2.77) are revised considering the converter limits $I_{dg}^{\lim}$ and $I_{qg}^{\lim}$:

$$\begin{aligned} I_{qg}^{+}{}'' &= \mathrm{sign}\left(I_{qg}^{+}{}'\right)\min\left(\left|I_{qg}^{+}{}'\right|, I_{qg}^{\lim}\right) \\ I_{dg}^{+}{}'' &= \mathrm{sign}\left(I_{dg}^{+}{}'\right)\min\left(\left|I_{dg}^{+}{}'\right|, I_{dg}^{\lim}\right) \\ I_{qg}^{-}{}'' &= \mathrm{sign}\left(I_{qg}^{-}{}'\right)\min\left(\left|I_{qg}^{-}{}'\right|, I_{qg}^{\lim}\right) \\ I_{dg}^{-}{}'' &= \mathrm{sign}\left(I_{dg}^{-}{}'\right)\min\left(\left|I_{dg}^{-}{}'\right|, I_{dg}^{\lim}\right) \end{aligned} \tag{2.81}$$

In addition to this first limitation, if, for example, $\left(I_{qg}^{+}{}'' + I_{qg}^{-}{}''\right) > I_{qg}^{\max}$, then the q-axis current references must be corrected again. The same applies to the d-axis. Both positive and negative component are trimmed based on their proportion to the total:

$$I_{dg}^{+}{}''' = I_{dg}^{+}{}''\ \min\left(\frac{I_{dg}^{\max}}{\left|I_{dg}^{+}{}''\right| + \left|I_{dg}^{-}{}''\right|}, 1\right) \qquad I_{dg}^{-}{}''' = I_{dg}^{-}{}''\ \min\left(\frac{I_{dg}^{\max}}{\left|I_{dg}^{+}{}''\right| + \left|I_{dg}^{-}{}''\right|}, 1\right) \tag{2.82}$$

$$I_{qg}^{+}{}''' = I_{qg}^{+}{}''\ \min\left(\frac{I_{qg}^{\max}}{\left|I_{qg}^{+}{}''\right| + \left|I_{qg}^{-}{}''\right|}, 1\right) \qquad I_{qg}^{-}{}''' = I_{qg}^{-}{}''\ \min\left(\frac{I_{qg}^{\max}}{\left|I_{qg}^{+}{}''\right| + \left|I_{qg}^{-}{}''\right|}, 1\right) \tag{2.83}$$

where $I_{dg}^{+}{}'''$, $I_{dg}^{-}{}'''$, $I_{qg}^{+}{}'''$ and $I_{qg}^{-}{}'''$ are the corrected reference currents. $I_{dg}^{\max}$ and $I_{qg}^{\max}$ are obtained with the first current limiter (see section 2.2.3), and they consider the P or Q-priority.

In phasor domain, the sequence phasors of the GSC currents (from the GSC to the PGC) are:

$$\bar{I}_{g}^{+} = \left(I_{dg}^{+}{}''' + jI_{qg}^{+}{}'''\right)\exp\left[\,j\,\mathrm{angle}\left(\bar{V}_{pgc}^{+}\right)\right] \tag{2.84}$$

$$\bar{I}_g^- = \left(I_{dg}^{-\prime\prime\prime} - jI_{qg}^{-\prime\prime\prime} \right) \exp\left[j \,\text{angle}\left(\bar{V}_{pgc}^+ \right) \right] \tag{2.85}$$

The minus sign in front of $jI_{qg}^{-\prime\prime\prime}$ in (2.85) is due to the properties of the dq-to-abc transformation for negative sequence.

2.2.6 Loss of synchronism

When a 3-phase fault occurs between an FSC-type generator and all other generators, then that FSC will continue to work under islanded condition. Under such circumstances, the PLL may fail to maintain the frequency.

If there are loads in the island, and the active power produced is below the consumption, the frequency will drop. In the opposite case where the active power produced is above the losses and the loads, the frequency increases. The rate of change of frequency depends on the PLL parameters.

As the frequency varies, the voltage reference angle for the abc-to-dq transformation varies too.

Here is an example of a TD simulation with EMTP-RV:

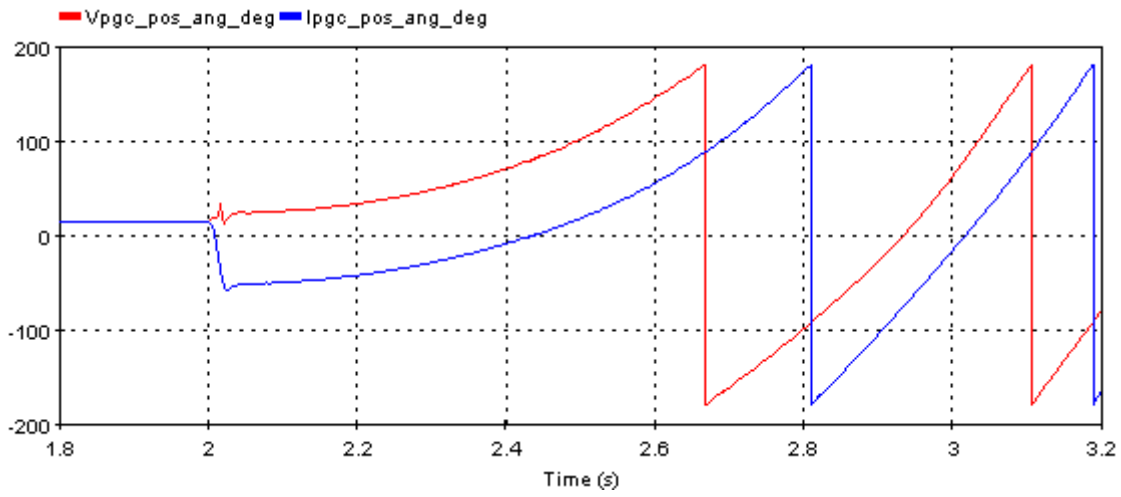

Figure 2.12 Phasor angles of positive sequence voltage (red) and current (blue) do not converge during a 3-phase fault at the POI.

Due to the variations of frequency, the PLL is unable to function properly. The controller measures currents which track their reference values, but this is due to the frequency variation.

As there is only one impedance between the converter and the ground, this impedance will determine the angle between the voltage and current (Figure 2.13).

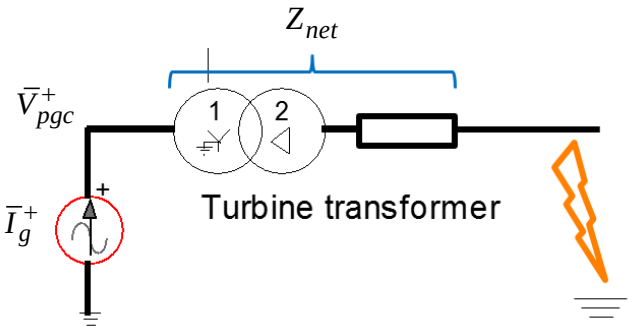

Figure 2.13 Equivalent phasor circuit during LOS conditions.

Under these conditions, the phasor solutions of $\bar{I}_g^+$ as in (2.58) or in (2.84) give a different angle at each iteration. Then the current contribution calculated by the model does not converge.

To avoid this angle fluctuation and to have a solution with a fixed angle, the prefault voltage condition is adopted. Obviously, this cannot represent the fault current contribution for a sustained fault, but it is valid for the first cycles of the fault. During the first 200ms of the fault (and after the fast transient part) the angle variation is relatively small (Figure 2.12). Under islanding conditions, the output current of the converter will depend on the prefault voltage and the fault response of the controller. That means, given the same set of prefault conditions, the current contribution of the turbine depends on active and reactive current references that the controller calculates (even if those references are not respected).

Under loss of synchronism (LOS) conditions, the converter's positive sequence current $\bar{I}_g^+$ becomes:

$$\bar{I}_g^+ = \left(I_{dg}^{+\prime\prime\prime} + jI_{qg}^{+\prime\prime\prime}\right)\exp\left[\, j\,\text{angle}\left(\bar{V}_{pgc}^{+(0)}\right)\right] \tag{2.86}$$

where $\bar{V}_{pgc}^{+(0)}$ is the prefault positive sequence voltage at the PGC.

The detection of LOS conditions is based on the positive sequence impedance seen from the PGC. If the magnitude of this impedance is below a certain threshold Z_{LOS}, the controller goes into a LOS mode. This threshold must be calculated through a 3-phase fault test in the most

distant electrical point where a 3-phase fault triggers a LOS. The positive sequence impedance seen from the PGC is calculated from the positive sequence voltage and positive sequence current at the PGC.

2.3 FSC phasor model algorithm

The following algorithm summarizes the calculations involved in finding the current contribution of an FSC-type WP for all of the control schemes presented in this chapter.

The algorithm is divided into two parts: the prefault calculations and the iterative algorithm. The prefault calculations provide the reference values and initialize the variables and the parameters for the iterative algorithm.

Due to the non-linear behavior of the current limiter, the solution requires an iterative algorithm. The iterative algorithm calculates the current contribution of the FSC based on the voltage at the PGC. The sub-algorithm below gives the procedure for a single iteration k. The iteration number is present as a superscript between a pair of parentheses. A 0 in brackets means prefault value, and $k-1$ means the previous iteration.

The complete solver which considers several WTGs for both type-III and type-IV WTG is given in CHAPTER 4.

Figure 2.14 presents in a visual way the main steps of the FSC algorithm. For the sake of clarity, each control mode, coupled and decoupled, is dealt with separately in the figure below.

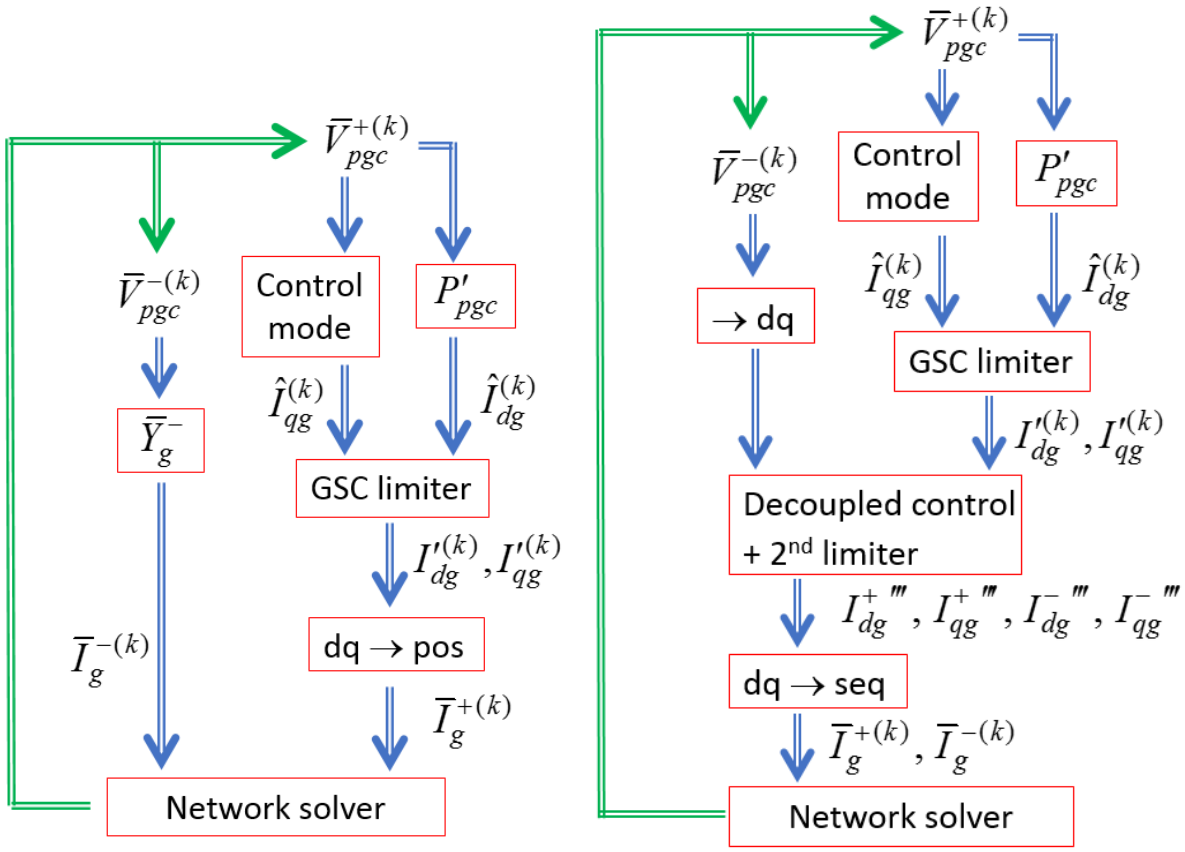

Figure 2.14 Block diagram of the FSC algorithm (left: coupled, right: decoupled).

Prefault calculations

It is assumed that the prefault PGC active power is at its SS value. This active power is then the reference value.

$$P'_{pgc} + j\,Q'_{pgc} = \bar{V}_{pgc}^{+(0)} \left(\bar{I}_{pgc}^{+(0)}\right)^* \tag{2.87}$$

$$\bar{I}_g^{+(0)} = \bar{I}_{pgc}^{+(0)} + \frac{\bar{V}_{pgc}^{+(0)}}{Z_{filter}} \tag{2.88}$$

$$I_{dg}^{(0)} + j\,I_{qg}^{(0)} = \frac{\bar{I}_g^{+(0)}}{\exp\left(j\,\text{angle}\left(\bar{V}_{pgc}^{+(0)}\right)\right)} \tag{2.89}$$

$$\bar{Y}_g^- = \frac{\left(1 - H_{filter}\right)}{R + jX + H_{filter}\left(H_{PI}^g - R + jX\right)} \tag{2.90}$$

IF {control at MV side of turbine transformer}

$$\bar{V}_{ctrl}^{+(0)} = \bar{V}_{mv}^{+(0)} = \bar{V}_{pgc}^{+(0)} - \bar{I}_{pgc}^{+(0)} \bar{Z}_{tt}^{+} \tag{2.91}$$

ELSE

$$\bar{V}_{ctrl}^{+(0)} = \bar{V}_{pgc}^{+(0)} \tag{2.92}$$

END

$$\Delta U' = -I_{qg}^{(0)} / K_V + \left|\bar{V}_{ctrl}^{+(0)}\right| - 1 \tag{2.93}$$

FSC iterative algorithm

$$\hat{I}_{dg}^{(k)} = \frac{P'_{pgc}}{\left|\bar{V}_{pgc}^{+(k)}\right|} + \text{real}\left(\frac{\left|\bar{V}_{pgc}^{+(k)}\right|}{Z_{filter}}\right) \qquad \textit{(Calculation of the active component of current)} \tag{2.94}$$

Calculations of the reactive component of current:

IF {controlled voltage is $\bar{V}_{mv}^{+}$}

$$\begin{aligned} \bar{V}_{mv}^{+(k)} &= \bar{V}_{pgc}^{+(k)} - \bar{I}_{pgc}^{+(k-1)} Z_{tt}^{+} \\ V_{ctrl}^{+(k)} &= \left|\bar{V}_{mv}^{+(k)}\right| \end{aligned} \tag{2.95}$$

ELSE

$$V_{ctrl}^{+(k)} = \left|\bar{V}_{pgc}^{+(k)}\right| \tag{2.96}$$

END

IF {Q-control **OR** PF-control **OR** V-control}

$$\hat{I}_{qg}^{(k)} = -K_V \left(1 - V_{ctrl}^{+(k)} + \Delta U'\right) \tag{2.97}$$

IF {FRT-function}

$$\hat{I}_{qg}^{(k)} = -K_{FRT}\left(1 - V_{ctrl}^{+(k)}\right) \tag{2.98}$$

END

$$\hat{I}_{qg}^{(k)} = 0.5\left(\hat{I}_{qg}^{(k)} + I_{qg}'^{(k-1)}\right) \tag{2.99}$$

Limitation according to the priority:

IF {P-priority}

$$\begin{aligned} I_{dg}'^{(k)} &= \min\left(\hat{I}_{dg}^{(k)}, I_{dg}^{\lim}\right) \\ I_{dg}^{\max} &= I_{dg}^{\lim} \end{aligned} \tag{2.100}$$

$$\begin{aligned} I_{qg}^{\max} &= \min\left(\sqrt{\left(I_g^{\lim}\right)^2 - \left(I_{dg}'^{(k)}\right)^2}, I_{qg}^{\lim}\right) \\ I_{qg}'^{(k)} &= \operatorname{sign}\left(\hat{I}_{qg}^{(k)}\right)\min\left(\left|\hat{I}_{qg}^{(k)}\right|, I_{qg}^{\max}\right) \end{aligned} \tag{2.101}$$

IF {Q-priority **OR** FRT-function}

$$\begin{aligned} I_{qg}'^{(k)} &= \operatorname{sign}\left(\hat{I}_{qg}^{(k)}\right)\min\left(\left|\hat{I}_{qg}^{(k)}\right|, I_{qg}^{\lim}\right) \\ I_{qg}^{\max} &= I_{qg}^{\lim} \end{aligned} \tag{2.102}$$

$$\begin{aligned} I_{dg}^{\max} &= \min\left(\sqrt{\left(I_g^{\lim}\right)^2 - \left(I_{qg}'^{(k)}\right)^2}, I_{dg}^{\lim}\right) \\ I_{dg}'^{(k)} &= \min\left(\hat{I}_{dg}^{(k)}, I_{dg}^{\max}\right) \end{aligned} \tag{2.103}$$

END

IF {coupled control}

$$\bar{I}_g^{-(k)} = -Y_g^- \bar{V}_{pgc}^{-(k)} \quad \textit{(minus sign to have the current from the GSC to the PGC)} \tag{2.104}$$

$$\begin{aligned} I_{dg}^{+\,\prime\prime\prime} &= I_{dg}'^{(k)} \\ I_{qg}^{+\,\prime\prime\prime} &= I_{qg}'^{(k)} \end{aligned} \tag{2.105}$$

IF {decoupled control}

$$V_{dg}^{+} = \left|\bar{V}_{pgc}^{+(k)}\right| \qquad V_{qg}^{+} = 0$$

$$V_{dg}^{-} = \mathrm{Re}\left[\bar{V}_{pgc}^{-(k)} / \exp\left(j\,\mathrm{angle}\left(\bar{V}_{pgc}^{+(k)}\right)\right)\right] \tag{2.106}$$

$$V_{qg}^{-} = -\mathrm{Im}\left[\bar{V}_{pgc}^{-(k)} / \exp\left(j\,\mathrm{angle}\left(\bar{V}_{pgc}^{+(k)}\right)\right)\right]$$

$$P_0 = V_{dg}^{+}\; I_{dg}^{\prime(k)} \qquad\qquad P_{C2} = P_{S2} = 0 \tag{2.107}$$

$$\begin{bmatrix} I_{qg}^{+\prime} \\ I_{dg}^{+\prime} \\ I_{qg}^{-\prime} \\ I_{dg}^{-\prime} \end{bmatrix} = \begin{bmatrix} 1 & 0 & 0 & 0 \\ V_{qg}^{+} & V_{dg}^{+} & V_{qg}^{-} & V_{dg}^{-} \\ V_{qg}^{-} & V_{dg}^{-} & V_{qg}^{+} & V_{dg}^{+} \\ -V_{dg}^{-} & V_{qg}^{-} & V_{dg}^{+} & -V_{qg}^{+} \end{bmatrix}^{-1} \begin{bmatrix} I_{qg}^{\prime(k)} \\ P_0 \\ P_{C2} \\ P_{S2} \end{bmatrix} \tag{2.108}$$

$$\begin{aligned} I_{qg}^{+\prime\prime} &= \mathrm{sign}\left(I_{qg}^{+\prime}\right)\,\min\left(\left|I_{qg}^{+\prime}\right|, I_{qg}^{\lim}\right) \\ I_{dg}^{+\prime\prime} &= \mathrm{sign}\left(I_{dg}^{+\prime}\right)\,\min\left(\left|I_{dg}^{+\prime}\right|, I_{dg}^{\lim}\right) \\ I_{qg}^{-\prime\prime} &= \mathrm{sign}\left(I_{qg}^{-\prime}\right)\,\min\left(\left|I_{qg}^{-\prime}\right|, I_{qg}^{\lim}\right) \\ I_{dg}^{-\prime\prime} &= \mathrm{sign}\left(I_{dg}^{-\prime}\right)\,\min\left(\left|I_{dg}^{-\prime}\right|, I_{dg}^{\lim}\right) \end{aligned} \tag{2.109}$$

$$\begin{aligned} I_{dg}^{+\prime\prime\prime} &= I_{dg}^{+\prime\prime}\;\min\left(\frac{I_{dg}^{\max}}{\left|I_{dg}^{+\prime\prime}\right|+\left|I_{dg}^{-\prime\prime}\right|},1\right) \qquad I_{qg}^{+\prime\prime\prime} = I_{qg}^{+\prime\prime}\;\min\left(\frac{I_{qg}^{\max}}{\left|I_{qg}^{+\prime\prime}\right|+\left|I_{qg}^{-\prime\prime}\right|},1\right) \\ I_{dg}^{-\prime\prime\prime} &= I_{dg}^{-\prime\prime}\;\min\left(\frac{I_{dg}^{\max}}{\left|I_{dg}^{+\prime\prime}\right|+\left|I_{dg}^{-\prime\prime}\right|},1\right) \qquad I_{qg}^{-\prime\prime\prime} = I_{qg}^{-\prime\prime}\;\min\left(\frac{I_{qg}^{\max}}{\left|I_{qg}^{+\prime\prime}\right|+\left|I_{qg}^{-\prime\prime}\right|},1\right) \end{aligned} \tag{2.110}$$

$$\bar{I}_{g}^{-(k)} = \left(I_{dg}^{-\prime\prime\prime} - jI_{qg}^{-\prime\prime\prime}\right)\exp\left[\,j\,\mathrm{angle}\left(\bar{V}_{pgc}^{+(k)}\right)\right] \tag{2.111}$$

END

IF $\left\{\left|\bar{V}_{pgc}^{+(k)} / \bar{I}_{pgc}^{+(k-1)}\right| < Z_{LOS-\lim}\right\}$ *(test for LOS)*

$$\bar{I}_{g}^{+(k)} = \left(I_{dg}^{+\prime\prime\prime} + jI_{qg}^{+\prime\prime\prime}\right)\exp\left[\,j\,\mathrm{angle}\left(\bar{V}_{pgc}^{+(0)}\right)\right] \tag{2.112}$$

ELSE

$$\bar{I}_g^{+(k)} = \left(I_{dg}^{+\,\prime\prime\prime} + jI_{qg}^{+\,\prime\prime\prime} \right) \exp\left[j \,\text{angle}\left(\bar{V}_{pgc}^{+(k)} \right) \right] \tag{2.113}$$

END

The algorithm uses some variation limiters. They tend to increase solution stability and reduce the number of iterations required.

No zero sequence current passes through the GSC as it is connected with 3 wires: $\bar{I}_g^{\,0(k)} = 0$.

2.3.1 List and description of the variables of FSC phasor model algorithm

$\bar{I}_{pgc}^{+}$ the PGC positive sequence current phasor (flowing to the grid),

$\bar{V}_{pgc}^{+}$, $\bar{V}_{pgc}^{-}$ the PGC positive and negative sequence voltage phasor,

$\bar{I}_g^{+}$, $\bar{I}_g^{-}$ the converter positive and negative sequence current phasor (from the GSC to the PGC),

V_{dg}^{+}, V_{qg}^{+} the d- and q-components of $\bar{V}_{pgc}^{+}$,

V_{dg}^{-}, V_{qg}^{-} the d- and q-components of $\bar{V}_{pgc}^{-}$,

$\hat{I}_{dg}$, $\hat{I}_{qg}$ the desired d- and q-components of the GSC current (from the GSC to the grid),

I'_{dg}, I'_{qg} the reference d- and q-components of the GSC current (from the GSC to the grid),

$I_{dg}^{\lim}$, $I_{qg}^{\lim}$ the GSC current limit on d- and q-components,

$I_{dg}^{\max}$, $I_{qg}^{\max}$ the variable current limit of the GSC on d- and q-components depending on P- or Q-priority,

$I_g^{\lim}$ the total current limit of the GSC,

$\bar{V}_{mv}^{+}$ the positive sequence voltage phasor at the medium voltage side of the turbine transformer,

P'_{pgc} the reference active power at the PGC (flowing to the grid),

Z_{filter} the total complex impedance of the shunt filter of the PGC at nominal frequency,

Z_{tt}^{+} the complex positive sequence impedance of the turbine transformer at nominal frequency,

$Z_{LOS-\lim}$ the positive sequence impedance magnitude between the PGC and the farthest node that provokes a LOS during a 3-phase fault,

H_{filter} the complex gain of the measurement filter at nominal frequency,

H_{PI}^{g} the gain of the PI controller at twice the nominal frequency,

R , X the choke resistance and reactance at nominal frequency,

$\bar{Y}_{g}^{-}$ the admittance giving the GSC negative sequence current according to the negative sequence PGC voltage,

K_V the voltage gain of the outer loop (POI control),

K_{FRT} the FRT gain or the FRT slope,

$\Delta U'$ the correction of the WP controller on reactive current,

$I_{dg}^{+}{}'$, $I_{qg}^{+}{}'$, $I_{dg}^{-}{}'$ and $I_{qg}^{-}{}'$ the reference GSC current of the positive and negative sequence, d- and q-components,

$I_{dg}^{+}{}''$, $I_{qg}^{+}{}''$, $I_{dg}^{-}{}''$ and $I_{qg}^{-}{}''$ the reference GSC current of the positive and negative sequence, d- and q-components after a first limiter,

$I_{dg}^{+}{}'''$, $I_{qg}^{+}{}'''$, $I_{dg}^{-}{}'''$ and $I_{qg}^{-}{}'''$ the revised reference GSC current of the positive and negative sequence, d- and q-components.

2.3.2 FSC algorithm: List of inputs

This section presents all of the parameters required to run the algorithm described above. If the fault is balanced, or if there is a decoupled controller, the following parameters are sufficient to calculate the SC current contribution of a FSC:

- Control structure (coupled or decoupled),
- Voltage proportional gain,
- Prefault conditions (at PGC),
- Current limits in dq frame, and P/Q-priority option,
- Availability of FRT function. If available then: FRT slope and FRT activation threshold min and max,
- Total impedance of the shunt filters,
- Series impedance of the turbine transformer at nominal frequency if the MV option is used,
- Impedance limit for LOS, prefault positive sequence voltage angle,
- Power and voltage bases (if the inputs/outputs are not in pu).

When coupled control is in use and the fault is unbalanced the following parameters will be required in addition to the parameters above:

- Gain of measurement filter at nominal frequency,
- Inner loop PI parameters: proportional and integral gains,
- Choke impedance at nominal frequency.

2.4 Conclusion

This chapter describes the FSC/type-IV WTG and its various control possibilities:

- coupled or decoupled sequence control,
- control under normal conditions (reactive power, voltage or power factor), plus the FRT mode,
- P- or Q-priority.

All these control configurations are translated into equations in phasor domain. The negative sequence behavior is also described when it is not controlled, and when it is controlled using a decoupled sequence controller.

A solution is also described for the cases when there is LOS.

Finally, the formulations are summarized in the form of an algorithm which calculates the current contribution of an FSC-type WTG based on the voltage at the PGC.

CHAPTER 3 TYPE-III WIND TURBINE GENERATOR SHORT-CIRCUIT STEADY-STATE MODEL

This chapter presents and details a SC SS model for the type-III WTG. The type-III WTG is more complex than the type-IV because the machine is directly connected to the grid, and has its own behavior. The type-III WTG is also called doubly-fed induction generator (DFIG). The outline of this chapter is similar to that of the previous one.

The first step is to describe in detail in section 3.1 the EMT model of the type-III WTG and to explain the structure of the two controllers. Based on the EMT model, a simple SC phasor model is built in section 3.2 to reproduce the SS behavior of the EMT one. This phasor model employs certain approximations, and gives the global structure of the model by ignoring certain details of the TD model that would have minor impact on the precision of the results in SS. Section 3.3 explains the detailed SS model. The simple and the detailed models give the positive and negative sequence components for a coupled sequence controller, and reproduce the SS behavior of the EMT model. These two phasor models consider all the presented control options, and are presented in the form of an algorithm.

3.1 Controller structure and time-domain model of type-III WTGs

The type-III WTG is composed of an induction machine with a wound rotor excited by the stator through a DC-link (Figure 3.1). This explains why it is also called a DFIG. The principle of this structure is that by varying the frequency of the rotor excitation, the stator can be connected to the grid for different mechanical rotation speeds of the rotor, and manipulation of the rotor voltage permits control of the generator operating conditions. A type-III WTG should cost less than a type-IV WTG because the converters of the former are rated at only 20 to 30% of the nominal machine power, compared to the 100% rating of the converters of the latter.

A type-III WTG has two converters: a grid-side converter (GSC) and a rotor-side converter (RSC). The GSC in a type-III WTG has the same filter as the GSC in a type-IV WTG. The DC-link is also equipped with a chopper to protect it from over-voltages. The rotor may be equipped with a crowbar. A crowbar short-circuits the rotor to protect the RSC against overcurrent. In this

case, the machine becomes a classical wound rotor induction machine and consumes reactive power. As this situation is not desirable during fault conditions, the crowbar is not considered further in this thesis.

As for the type-IV WTG discussed in the previous chapter, the AC terminal of GSC has one series and two shunt filters (Figure 1.7) to prevent harmonics from propagating in the grid (beginning of section 2.1).

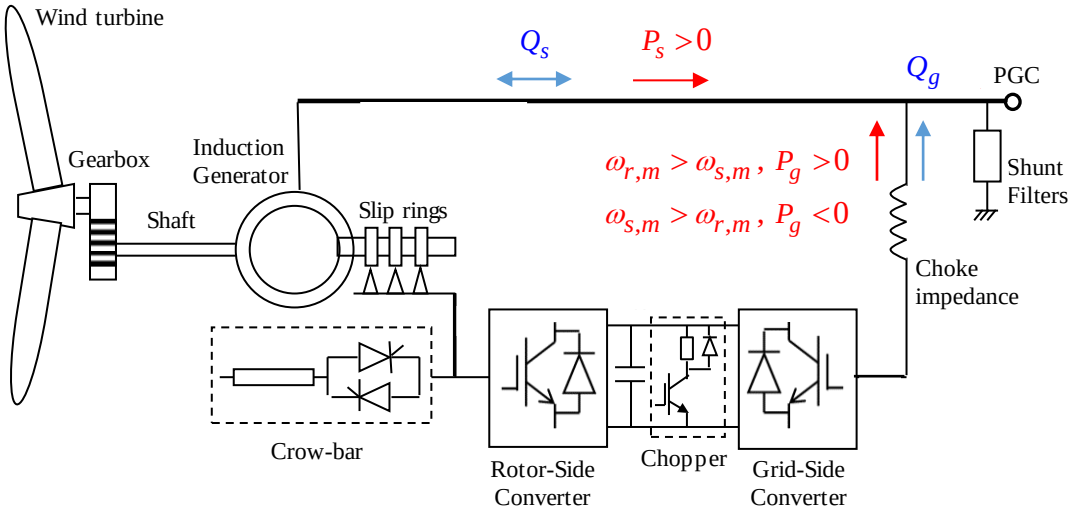

Figure 3.1 Structure of a type-III WTG.

The behavior during faults of a type-III WTG depends on both converters: the GSC by injecting currents directly to the grid, and the RSC by impacting the stator currents. The stator can only produce active power, whereas the active power flow through the two converters depends on the mechanical rotation speed of the rotor $\omega_{r,m}$. If the rotor speed is higher than the mechanical synchronous speed $\omega_{s,m}$, the rotor produces active power. In the opposite case, the rotor consumes active power (Figure 3.1). The stator can produce or consume reactive power. In this thesis, the GSC controller only allows production of reactive power.

The type-III WTG model studied in this thesis has only one coupled sequence controller. Therefore, the negative sequence behavior is not controlled in this model.

Structures of the controllers

The main elements of the controllers of the two converters are presented in Figure 3.2.

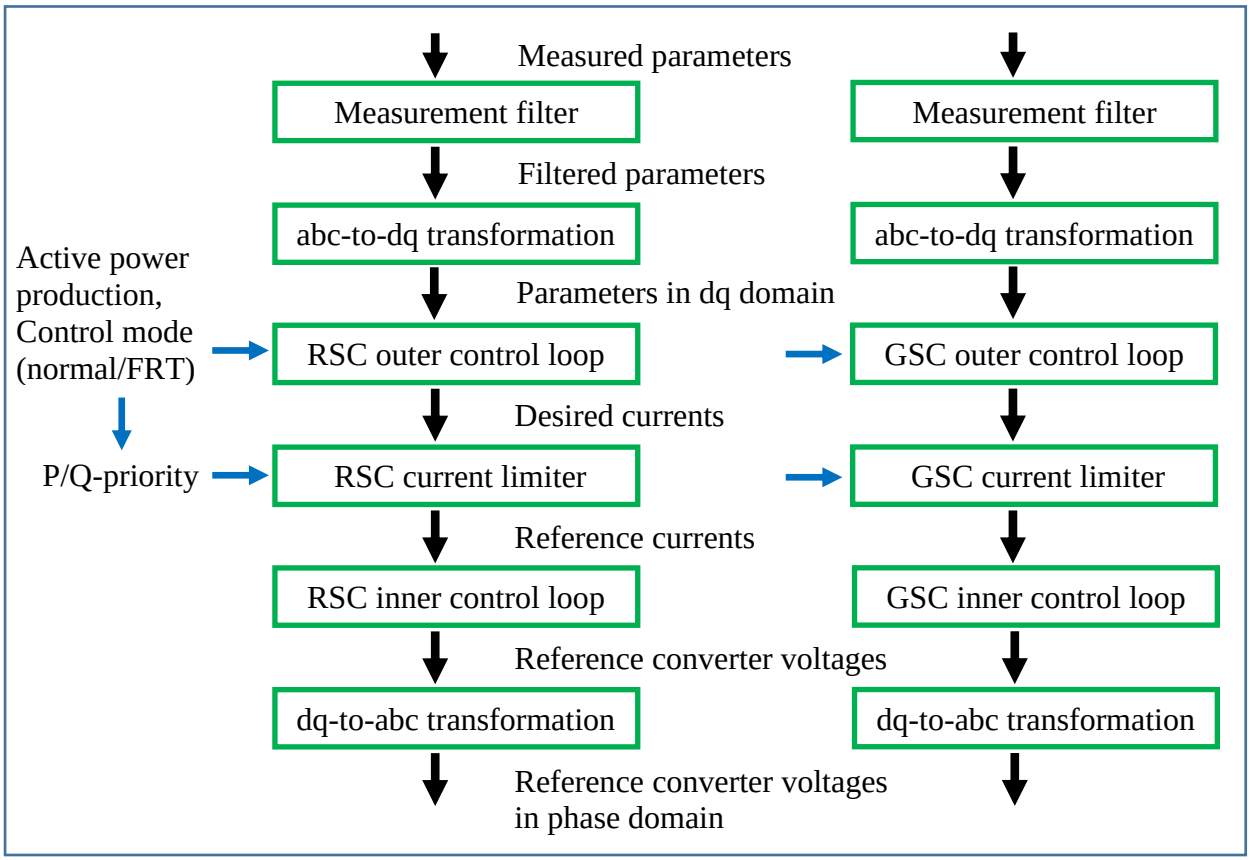

Figure 3.2 Basic structure of a DFIG controller.

The next sections give more details of each block in Figure 3.2. In what follows, all values will be in per-unit.

Variables in this chapter follow the notational rules given as follows:

- the subscript “pgc” refers to the PGC,
- the subscript “g” refers to the AC current of the GSC,
- the subscript “s” refers to the stator current or voltage,
- the subscript “r” refers to the rotor current or voltage,
- the superscript “+” (plus) and “–” (minus) refer, respectively, to the positive and negative sequences,
- the overbar refers to nominal frequency phasors,

- ther upper-case letters refers to the dc component of the signals,
- subscript “d” and “q” refer, respectively, to the d- and q-components of the variable,
- hatted variables indicate the desired values,
- primes (apostrophes) indicate the reference values.

Measurement filter

The first element is a measurement low-pass filter (see section 1.3). Its goal is to remove the harmonics generated by the converters. The two filters are of the same type but with different cut-off frequencies, as their switching frequencies are different.

3.1.1 abc-to-dq transformation

The goal of the abc-to-dq transformation (direct-quadrature transformation) is to convert a given set of three AC signals under steady, balanced conditions into a set of two DC signals. Most converter controllers use this technique because DC signals are easier to manipulate and regulate. Furthermore, the active and reactive components of the current are independently controllable. The zero sequence current does not exist as the GSC and the stator are connected with only 3 wires.

For the type-III WTG, the two converters use different orientations for the abc-to-dq transformation.

The transformation for the GSC controller uses the same principle described for the type-IV WTG (refer to section 2.1.1 for details). The PLL is set to align the d-axis with the positive sequence voltage at the PGC which is also the stator voltage. This orientation is called the stator voltage reference frame (SVR). The PLL calculates the transformation angle θ.

For the RSC, the d-axis is aligned with the positive sequence stator flux, it is called the stator flux reference frame (SFR). This orientation is reached in two steps. The SVR transformation applied to stator currents is the same as the transformation used for the GSC. The rotor currents receive a transformation, using **T** in equation (2.2), but replacing θ with $\theta - \theta_r$ with:

$$\theta_r = \int \omega_s \frac{\omega_{r,m}}{\omega_{r,m}^0} dt \tag{3.1}$$

where ω_s is the grid nominal angular frequency, $\omega_{r,m}$ is the instantaneous mechanical rotation speed of the rotor in rad/s and $\omega_{r,m}^0$ is the synchronous mechanical rotation speed of the rotor in rad/s.

In (3.1) and thereafter, variable names denoted by lower-case letters represent the time-domain variables, and those denoted by upper-case letters represent DC quantities.

The resulting d- and q-components of stator and rotor currents are used to calculate the flux angle [52] for the conversion to the SFR. The calculation is represented in Figure 3.3 where "Lm_pu" is equal to the magnetizing inductance of the machine in pu: L_m. This calculation of the flux angle assumes that $L_m + L_{ls} \approx L_m$ where L_{ls} is the stator leakage inductance in pu.

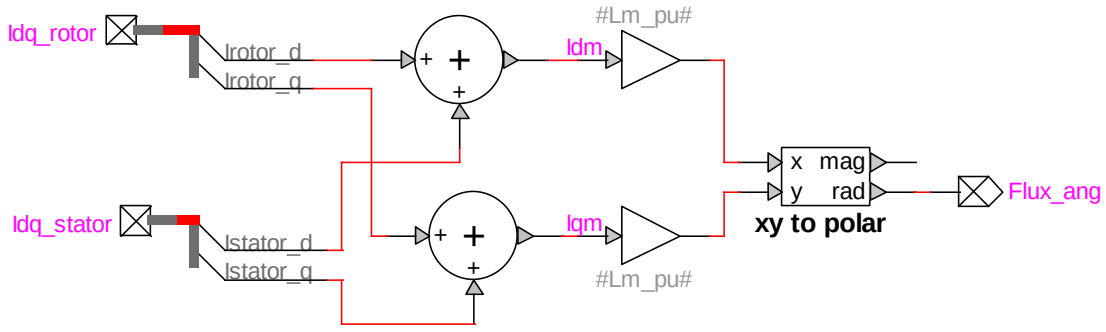

Figure 3.3 Calculation of flux angle for SFR.

The flux angle is denoted by φ_{flux}.

The stator and rotor currents in dq domain are written as: d-component + j·q-component, and rotated of $-\varphi_{flux}$ in the complex plan. The resulting real part becomes the new d-component and the imaginary one becomes the q-components. These new d- and q-components correspond to the value in SFR.

The angle $\theta - \theta_r + \varphi_{flux}$ will be used for the dq-to-abc transformation of the RSC in the section 3.1.6. The frequency of the rotor voltage is controlled so that under SS conditions, the sum of the rotor speed and the rotor-flux speed is equal to the synchronous speed of the grid.

All voltages and currents at the output of the abc-to-dq block will be in dq domain. In SVR, as the d-axis is aligned with the voltage, the d-axis current corresponds to the active current and q-axis current represents the reactive current. In SFR it is the opposite: the d-axis is aligned with the stator flux, then the d-axis current corresponds to the reactive current and the q-axis one represents the active current.

3.1.2 RSC outer control loop

The outer control loop calculates the desired active and reactive currents from the measurements.

An MPPT system calculates the turbine reference active power P'_{tb} through the mechanical rotation speed of the rotor. The turbine power is the sum of the stator and the GSC power. A PI controller on the active power deviation from P'_{tb}, calculates the desired active current $\hat{i}_{qr}^{SFR}$.

The rest of this section describes how the desired reactive current $\hat{i}_{dr}^{SFR}$ is obtained.

The inner control loop and the reactive component of the outer control loop of the RSC are built based on the linear Γ model of an induction machine [53] (Figure 3.4). In this model, the stator/rotor turn ratio is set to eliminate the stator leakage inductance.

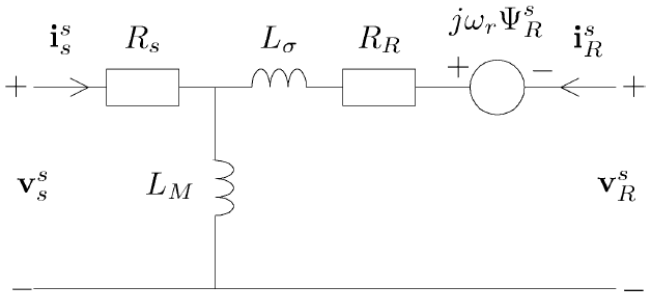

Figure 3.4 Linear Γ model of an induction machine [37].

$$\begin{aligned} \gamma &= L_{ss}/L_m \quad \text{with } L_{ss} = L_{ls} + L_m \\ L_M &= L_{ss} = \gamma L_m \\ L_\sigma &= \gamma L_{ls} + \gamma^2 L_{lr} \\ R_R &= \gamma^2 R_r \end{aligned} \tag{3.2}$$

where R_s and R_r are the stator and rotor resistances respectively, and L_{lr} is the rotor leakage inductance.

In the controller, the stator resistance of the Γ model is neglected, and a direct relation between the stator voltage, the stator current and the rotor current is obtained. Figure 3.5 illustrates this relation.

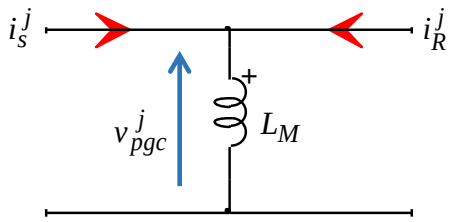

Figure 3.5 Relation between stator and rotor currents with a simplified Γ model.

$$v_{pgc}^j = L\frac{d}{dt}\left(i_s^j + i_R^j\right) \Leftrightarrow i_s^j = -i_R^j + \frac{1}{L}\int v_{pgc}^j\, dt \tag{3.3}$$

where v_{pgc}^j is the AC PGC voltages for phase j (j=a,b,c), i_s^j, i_r^j and i_R^j are, respectively, the AC currents through the stator, the rotor and the rotor in the Γ representation for phase j.

Figure 3.5 also presents the reference directions for currents.

And in dq domain, in SFR:

$$i_{ds}^{SFR} = -\frac{i_{dr}^{SFR}}{\gamma} + \frac{v_{qs}^{SFR}}{\omega_s L_{ss}} \tag{3.4}$$

$$i_{qs}^{SFR} = -\frac{i_{qr}^{SFR}}{\gamma} - \frac{v_{ds}^{SFR}}{\omega_s L_{ss}} \tag{3.5}$$

where i_{ds}^{SFR} and i_{qs}^{SFR} are the d- and q-components of the stator currents in SFR, i_{dr}^{SFR} and i_{qr}^{SFR} are the d- and q-components of the rotor currents in the SFR, and v_{ds}^{SFR} and v_{qs}^{SFR} are the d- and q-components of the stator voltages in the SFR. The stator voltage is also the PGC voltage.

As in SFR, the stator voltage is theorically aligned with the q-axis, (3.4) and (3.5) are simplified as:

$$i_{ds}^{SFR} = -\frac{i_{dr}^{SFR}}{\gamma} + \frac{\left|\bar{V}_{pgc}^{+}\right|}{\omega_s L_{ss}} \tag{3.6}$$

$$i_{qs}^{SFR} = -i_{qr}^{SFR} \Big/ \gamma \tag{3.7}$$

where $\left|\bar{V}_{pgc}^{+}\right|$ is the magnitude of the positive sequence voltage at the PGC.

In (3.4) to (3.7) and thereafter:

- the rotor currents are always given in the SFR and from the RSC to the rotor,
- the stator currents in the SFR follow the direction shown in Figure 3.5, from the grid to the stator,
- the stator currents in the SVR use the generator convention, from the stator to the grid.

Then, considering the theorical relation between the SFR and the SVR, as well as the conventions above:

$$i_{ds}^{SVR} = -\left(i_{qs}^{SFR}\right) \tag{3.8}$$

$$i_{qs}^{SVR} = -\left(-i_{ds}^{SFR}\right) = i_{ds}^{SFR} \tag{3.9}$$

where the minus sign outside the bracket corresponds to the direction change.

The desired reactive stator current (in the SVR) $\hat{i}_{qs}^{SVR}$ is calculated with a proportional gain on voltage deviation, where the reference voltage depends on the WPC (Figure 1.5). $\hat{i}_{qs}^{SVR}$ is calculated in the same way as $\hat{i}_{qg}$ is calculated for a type-IV WTG.

As the WP is represented with an aggregated turbine and collector grid, the circuit becomes:

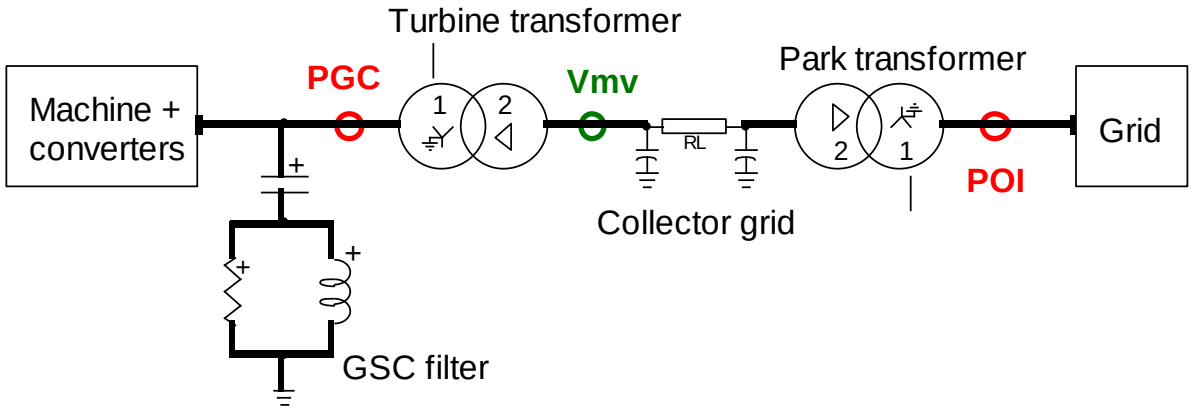

Figure 3.6 Circuit of the aggregated type-III based WP.

To simplify the circuit, only one shunt filter is displayed in Figure 3.6.

In the aggregated model, the output of the WPC, $\Delta U'$ goes directly to the outer loop of the converter controller. Therefore, $\Delta V' = \Delta U'$. The outer loop equation for reactive current is:

$$\hat{i}_{qs}^{SVR} = -K_V \left(1 + \Delta U' - \left|\bar{V}_{ctrl}^{+}\right|\right) \tag{3.10}$$

where K_V is the proportional gain ($K_V > 0$), and $\left|\bar{V}_{ctrl}^{+}\right|$ is the magnitude of the positive sequence controlled voltage. The controlled voltage is either the PGC voltage or the voltage at the MV side of the turbine transformer (Vmv in Figure 3.6). The MV is not measured, but calculated using the turbine transformer series impedance and the voltage and current at the PGC.

The controller also has an FRT mode during low voltage conditions. In this thesis, this mode generates a reactive current component proportional to the voltage deviation from 1pu (Figure 2.5). The FRT mode is essential if the grid code requires voltage support.

The FRT mode is activated only when the controlled positive sequence voltage leaves the deadband. In Figure 2.5, the FRT mode is activated for a voltage deviation greater than 0.1 pu (from 1 pu), and the FRT gain (the slope) is 2.

The outer loop equation in the FRT mode becomes:

$$\hat{i}_{qs}^{SVR} = -K_{FRT} \left(1 - \left|\bar{V}_{ctrl}^{+}\right|\right) \tag{3.11}$$

where K_{FRT} is the proportional gain ($K_{FRT} > 0$).

When the controlled voltage goes slightly below the FRT activation limit, the FRT mode can push the voltage above this activation limit. In the TD, when the FRT mode is activated, the controller stays in this mode for a fixed duration to avoid repetitive mode changing.

The deadband represents the usual or normal conditions (positive sequence voltage between 0.9 and 1.1 pu) where the WPC regulates the reactive power, the voltage or the power factor at the POI.

Calculations of the desired rotor currents

Combining (3.6) and (3.9):

$$i_{qs}^{SVR} = -\frac{i_{dr}^{SFR}}{\gamma} + \frac{\left|\bar{V}_{pgc}^{+}\right|}{\omega_s L_{ss}} \tag{3.12}$$

Then, using (3.10) in (3.12), the desired rotor current $\hat{i}_{dr}^{SFR}$ will be obtained:

$$-K_V\left(1+\Delta U' - \left|\bar{V}_{ctrl}^{+}\right|\right) = -\frac{\hat{i}_{dr}^{SFR}}{\gamma} + \frac{\left|\bar{V}_{pgc}^{+}\right|}{\omega_s L_{ss}} \tag{3.13}$$

$$\begin{aligned} \hat{i}_{dr}^{SFR} &= \gamma K_V\left(1+\Delta U' - \left|\bar{V}_{ctrl}^{+}\right|\right) + \gamma\frac{\left|\bar{V}_{pgc}^{+}\right|}{\omega_s L_{ss}} \\ &= \gamma K_V\left(1+\Delta U' - \left|\bar{V}_{ctrl}^{+}\right|\right) + \frac{\left|\bar{V}_{pgc}^{+}\right|}{\omega_s L_m} \end{aligned} \tag{3.14}$$

And in the FRT mode:

$$\hat{i}_{dr}^{SFR} = \gamma K_{FRT}\left(1-\left|\bar{V}_{ctrl}^{+}\right|\right) + \frac{\left|\bar{V}_{pgc}^{+}\right|}{\omega_s L_m} \tag{3.15}$$

In the EMT model of the type-III WTG, the γ in (3.14) and (3.15) is neglected. The next two equations give the outer control loop equations for the rotor reactive current in the FRT mode, and the normal-condition mode, i.e., V, Q or PF.

In normal-conditions mode:

$$\hat{i}_{dr}^{SFR} = K_V \left(1 + \Delta U' - \left|\bar{V}_{ctrl}^{+}\right|\right) + \frac{\left|\bar{V}_{pgc}^{+}\right|}{\omega_s L_m} \tag{3.16}$$

In the FRT mode:

$$\hat{i}_{dr}^{SFR} = K_{FRT} \left(1 - \left|\bar{V}_{ctrl}^{+}\right|\right) + \frac{\left|\bar{V}_{pgc}^{+}\right|}{\omega_s L_m} \tag{3.17}$$

3.1.3 RSC current limiter

The current limiter of the RSC has the same structure as the current limiter of the GSC of the type-IV WTG, except that, in the case of the RSC, the axes representing the active and reactive currents are reversed. Nonetheless, the complete description is given below.

During voltage sags, $\hat{i}_{dr}^{SFR}$ and $\hat{i}_{qr}^{SFR}$ can be too large and damage the converter. A first bound is set on each component: $I_{dr}^{\lim}$ for the d-axis and $I_{qr}^{\lim}$ for the q-axis. According to those bounds, the total current magnitude can still be too large for the converter. Consequently, a maximum current magnitude $I_r^{\lim}$ that the converter can stand due to thermal constraints is set (usually between 1.1 and 1.4 pu). $I_{dr}^{\lim}$ and $I_{qr}^{\lim}$ are equal to or less than $I_r^{\lim}$. The total current magnitude is maintained within its bound by chopping, if necessary, the active or the reactive component of the current. The component which is not chopped, is the one having the priority.

In normal conditions (no FRT), the priority can be given to the active or reactive component, but usually to the active one (P-priority). In the FRT mode where the goal is to maintain the voltage, priority is always given to the reactive current (Q-priority). The corrected currents are called reference currents and are written with an apostrophe: i'^{SFR}_{dr} and i'^{SFR}_{qr}.

P-priority

The q-component, which represents the active component, respects its limit:

$$i'^{SFR}_{qr} = \text{sign}\left(\hat{i}^{SFR}_{qr}\right) \cdot \min\left(\left|\hat{i}^{SFR}_{qr}\right|, I^{\lim}_{qr}\right) \tag{3.18}$$

The "sign" function gives +1 if the input is positive and –1 if negative.

The d-component also respects its limit, and respects the maximum current magnitude $I_r^{\lim}$:

$$i^{\max}_{dr} = \min\left(I^{\lim}_{dr}, \sqrt{\left(I^{\lim}_{r}\right)^2 - \left(i'^{SFR}_{qr}\right)^2} \right) \tag{3.19}$$

$$i'^{SFR}_{dr} = \text{sign}\left(\hat{i}^{SFR}_{dr}\right) \cdot \min\left(\left|\hat{i}^{SFR}_{dr}\right|, i^{\max}_{dr}\right) \tag{3.20}$$

Q-priority

The d-component, which represents the reactive component, respects its limit:

$$i'^{SFR}_{dr} = \text{sign}\left(\hat{i}^{SFR}_{dr}\right) \cdot \min\left(\left|\hat{i}^{SFR}_{dr}\right|, I^{\lim}_{dr}\right) \tag{3.21}$$

The q-component also respects its limit, and respects the maximum current magnitude $I_r^{\lim}$:

$$i^{\max}_{qr} = \min\left(I^{\lim}_{qr}, \sqrt{\left(I^{\lim}_{r}\right)^2 - \left(i'^{SFR}_{dr}\right)^2} \right) \tag{3.22}$$

$$i'^{SFR}_{qr} = \text{sign}\left(\hat{i}^{SFR}_{qr}\right) \cdot \min\left(\left|\hat{i}^{SFR}_{qr}\right|, i^{\max}_{qr}\right) \tag{3.23}$$

$i^{\max}_{dr}$ and $i^{\max}_{qr}$ are the maximum values which depend on the maximum current magnitude and the prioritized component. These values are consequently fault-dependent.

3.1.4 Total GSC controller

This section develops the outer control loop, the current limiter and the inner control loop of the GSC. The GSC currents are always in the SVR and flowing from the GSC to the PGC.

A PI controller on the DC-link voltage deviation from 1 pu provides the desired active current $\hat{i}^{SVR}_{dg}$, which can be positive or negative as the active power flow depends on the mechanical rotation speed of the rotor.

The reactive component $\hat{i}_{qg}^{SVR}$ is zero in normal conditions. If the FRT is activated, and if the reactive current provided by the stator is not large enough to reach the FRT requirement, $\hat{i}_{qg}^{SVR}$ provides the missing reactive current. The magnetizing inductance of the machine reduces the amount of reactive current that the stator can provide. Then $\hat{i}_{qg}^{SVR}$ is either 0 or negative.

$$\begin{aligned} \hat{i}_{qg}^{SVR} &= \min\left(i'^{SFR}_{dr} - \hat{i}_{dr}^{SFR}, 0\right) \\ &= \min\left(I_{dr}^{\lim} - \left[\frac{\left|\bar{V}_{pgc}^{+}\right|}{\omega_s L_m} + K_{FRT}\left(1 - \left|\bar{V}_{ctrl}^{+}\right|\right)\right], 0\right) \end{aligned} \tag{3.24}$$

The GSC has a limiter to protect against overcurrent, and it always functions with Q-priority:

$$i'^{SVR}_{qg} = \max\left(\hat{i}_{qg}^{SVR}, -I_{qg}^{\lim}\right) \tag{3.25}$$

$$i_{dg}^{\max} = \min\left(\sqrt{\left(I_g^{\lim}\right)^2 - \left(i'^{SVR}_{qg}\right)^2}, I_{dg}^{\lim}\right) \tag{3.26}$$

$$i'^{SVR}_{dg} = \operatorname{sign}\left(\hat{i}_{dg}^{SVR}\right) \cdot \min\left(\left|\hat{i}_{dg}^{SVR}\right|, i_{dg}^{\max}\right) \tag{3.27}$$

The limits are chosen according to the rating of the GSC which is around 30% of the nominal power of the WTG.

The inner control loop of the GSC of a type-III WTG is the same as the coupled control loop of the GSC of a type-IV WTG. Refer to section 2.1.4 for details. The inner control loop calculates the converter reference voltages v'_{dcv} and v'_{qcv} for the GSC. The output of the two PI controllers of the inner loop (d- and q-axis) are limited to 1 pu (as for the type-IV WTG) to avoid over-correction, and an anti-windup system prevents the integral part from growing when the PI output is limited.

3.1.5 RSC inner control loop

The inner control loop calculates the converter reference voltages (in dq domain) to reach the desired currents. This section presents how the RSC inner control loop equations are obtained.

The electrical equations of the machine in the Laplace domain are [54]:

$$\begin{aligned}\tilde{V}_{dr}^{SFR} &= R_r \tilde{I}_{dr}^{SFR} - s\omega_s \tilde{\lambda}_{qr}^{SFR} + p\tilde{\lambda}_{dr}^{SFR} \\ \tilde{V}_{qr}^{SFR} &= R_r \tilde{I}_{qr}^{SFR} + s\,\omega_s \tilde{\lambda}_{dr}^{SFR} + p\tilde{\lambda}_{qr}^{SFR}\end{aligned} \tag{3.28}$$

$$\begin{aligned}\tilde{V}_{ds}^{SFR} &= R_s \tilde{I}_{ds}^{SFR} - \omega_s \tilde{\lambda}_{qs}^{SFR} + p\tilde{\lambda}_{ds}^{SFR} \\ \tilde{V}_{qs}^{SFR} &= R_s \tilde{I}_{qs}^{SFR} + \omega_s \tilde{\lambda}_{ds}^{SFR} + p\tilde{\lambda}_{qs}^{SFR}\end{aligned} \tag{3.29}$$

with:

$$\begin{aligned}\tilde{\lambda}_{ds}^{SFR} &= L_{ss}\tilde{I}_{ds}^{SFR} + L_m \tilde{I}_{dr}^{SFR} \\ \tilde{\lambda}_{qs}^{SFR} &= L_{ss}\tilde{I}_{qs}^{SFR} + L_m \tilde{I}_{qr}^{SFR}\end{aligned} \tag{3.30}$$

$$\begin{aligned}\tilde{\lambda}_{dr}^{SFR} &= L_{rr}\tilde{I}_{dr}^{SFR} + L_m \tilde{I}_{ds}^{SFR} \\ \tilde{\lambda}_{qr}^{SFR} &= L_{rr}\tilde{I}_{qr}^{SFR} + L_m \tilde{I}_{qs}^{SFR}\end{aligned} \tag{3.31}$$

- "~" indicates the signals in the Laplace domain,
- p is the Laplace complex variable,
- $L_{rr} = L_{lr} + L_m$,
- ω_s is the stator angular frequency.

The current convention for the SFR is the same as in section 3.1.2: stator current flowing from the PGC to the stator, and rotor current flowing from the RSC to the rotor.

Substituting (3.31) into (3.28):

$$\tilde{V}_{dr}^{SFR} = R_r \tilde{I}_{dr}^{SFR} - s\omega_s \left(L_{rr}\tilde{I}_{qr}^{SFR} + L_m \tilde{I}_{qs}^{SFR} \right) + p\left(L_{rr}\tilde{I}_{dr}^{SFR} + L_m \tilde{I}_{ds}^{SFR} \right) \tag{3.32}$$

$$\tilde{V}_{qr}^{SFR} = R_r \tilde{I}_{qr}^{SFR} + s\,\omega_s \left(L_{rr}\tilde{I}_{dr}^{SFR} + L_m \tilde{I}_{ds}^{SFR} \right) + p\left(L_{rr}\tilde{I}_{qr}^{SFR} + L_m \tilde{I}_{qs}^{SFR} \right) \tag{3.33}$$

We set the derivatives of the stator fluxes equal to zero:

$$\begin{aligned}p\tilde{\lambda}_{ds}^{SFR} &= 0 = L_{ss}\, p\tilde{I}_{ds}^{SFR} + L_m\, p\tilde{I}_{dr}^{SFR} \\ p\tilde{\lambda}_{qs}^{SFR} &= 0 = L_{ss}\, p\tilde{I}_{qs}^{SFR} + L_m\, p\tilde{I}_{qr}^{SFR}\end{aligned} \tag{3.34}$$

$$p\tilde{I}_{ds}^{SFR} = -\frac{L_m}{L_{ss}}\, p\tilde{I}_{dr}^{SFR}$$
$$p\tilde{I}_{qs}^{SFR} = -\frac{L_m}{L_{ss}}\, p\tilde{I}_{qr}^{SFR} \tag{3.35}$$

And considering that the $\tilde{\lambda}_{qs}^{SFR}$ is zero (as the flux is aligned with the d-axis):

$$\tilde{\lambda}_{qs}^{SFR} = 0 = L_{ss}\tilde{I}_{qs}^{SFR} + L_m\tilde{I}_{qr}^{SFR}$$
$$\tilde{I}_{qs}^{SFR} = -\frac{L_m}{L_{ss}}\,\tilde{I}_{qr}^{SFR} \tag{3.36}$$

Using (3.35) and (3.36) into (3.32) and (3.33):

$$\tilde{V}_{dr}^{SFR} = R_r\tilde{I}_{dr}^{SFR} - s\omega_s\, L_X\,\tilde{I}_{qr}^{SFR} + pL_X\,\tilde{I}_{dr}^{SFR} \tag{3.37}$$

$$\tilde{V}_{qr}^{SFR} = R_r\tilde{I}_{qr}^{SFR} + s\,\omega_s\left(L_{rr}\tilde{I}_{dr}^{SFR} + L_m\tilde{I}_{ds}^{SFR}\right) + pL_X\,\tilde{I}_{qr}^{SFR} \tag{3.38}$$

with

$$\begin{aligned} L_X &= L_{rr} - \frac{{L_m}^2}{L_{ss}} = L_{lr} + L_m - \frac{{L_m}^2}{L_{ls}+L_m} = L_{lr} + \frac{L_m\left(L_{ls}+L_m\right) - {L_m}^2}{L_{ls}+L_m} \\ &= L_{lr} + \frac{L_{ls}L_m}{L_{ls}+L_m} = L_{lr} + \frac{L_{ls}}{\gamma} \end{aligned} \tag{3.39}$$

where: $\gamma = \left(L_{ls}+L_m\right)/L_m$.

The inner loop of the RSC controller is based on (3.37) and (3.38). Rewritten in TD:

$$v_{dr}^{SFR} = R_r\; i_{dr}^{SFR} + L_X\,\frac{d\; i_{dr}^{SFR}}{dt} - \omega_r\; L_X\; i_{qr}^{SFR} \tag{3.40}$$

$$v_{qr}^{SFR} = R_r\; i_{qr}^{SFR} + L_X\,\frac{d\; i_{qr}^{SFR}}{dt} + \omega_r\left[L_{rr}\; i_{dr}^{SFR} + L_m i_{ds}^{SFR}\right] \tag{3.41}$$

with ω_r the electrical angular frequency of the rotor ($\omega_r = s\,\omega_s$).

In the Γ representation (see section 3.1.2):

$$v_{dR}^{SFR} = R_R\; i_{dR}^{SFR} + L_\sigma\,\frac{d\; i_{dR}^{SFR}}{dt} - \omega_r\; L_\sigma\; i_{qR}^{SFR} \tag{3.42}$$

$$v_{qR}^{SFR} = R_R\, i_{qR}^{SFR} + L_\sigma \frac{d\, i_{qR}^{SFR}}{dt} - \omega_r \left[\left(L_M + L_\sigma \right) i_{dR}^{SFR} + L_M i_{ds}^{SFR} \right] \tag{3.43}$$

$$\begin{aligned} L_\sigma &= \gamma^2\, L_X \qquad\qquad R_R = \gamma^2 R_r \\ L_M &= \gamma L_m \end{aligned} \tag{3.44}$$

The i_{dR}^{SFR} and i_{qR}^{SFR} errors are processed by the PI controller (inner loop) to give v_{dR}^{SFR} and v_{qR}^{SFR}, respectively. To ensure good tracking, the feedforward compensating terms $-\omega_r\, L_\sigma\, i_{qR}^{SFR}$ in (3.42) and $-\omega_r \left[\left(L_M + L_\sigma \right) i_{dR}^{SFR} + L_M i_{ds}^{SFR} \right]$ in (3.43) are retained. Due to the very low values of R_R compared to the inductances, R_R is neglected.

$$v'^{SFR}_{dR} = K_P^r \left(i'^{SFR}_{dR} - i_{dR}^{SFR} \right) + K_I^r \int \left(i'^{SFR}_{dR} - i_{dR}^{SFR} \right) dt - \omega_r\, L_\sigma\, i_{qR}^{SFR} \tag{3.45}$$

$$v'^{SFR}_{qR} = K_P^r \left(i'^{SFR}_{qR} - i_{qR}^{SFR} \right) + K_I^r \int \left(i'^{SFR}_{qR} - i_{qR}^{SFR} \right) dt + \omega_r \left[\left(L_M + L_\sigma \right) i_{dR}^{SFR} + L_M i_{ds}^{SFR} \right] \tag{3.46}$$

K_P^r and K_I^r are, respectively, the proportional and the integral gains. Their values are calculated based on R_R, L_σ and the desired time response of the rotor inner loop [37]. The K_P^r and K_I^r are calculated for variables in Γ representation.

The outputs of the PI controllers (in the Γ representation) are limited to 0.2γ pu to avoid over-correction, and an anti-windup system prevents the integral parts from growing when the PI output is limited. In other words, the amplitude of the terms: $K_P^r \left(i'^{SFR}_{dR} - i_{dR}^{SFR} \right) + K_I^r \int \left(i'^{SFR}_{dR} - i_{dR}^{SFR} \right) dt$ in (3.45), and $K_P^r \left(i'^{SFR}_{qR} - i_{qR}^{SFR} \right) + K_I^r \int \left(i'^{SFR}_{qR} - i_{qR}^{SFR} \right)$ in (3.46) are limited to 0.2γ pu.

Equations (3.45) and (3.46) can be written using the normal variables to give:

$$v'^{SFR}_{dr} = \frac{K_P^r}{\gamma^2} \left(i'^{SFR}_{dr} - i_{dr}^{SFR} \right) + \frac{K_I^r}{\gamma^2} \int \left(i'^{SFR}_{dr} - i_{dr}^{SFR} \right) dt - \omega_r\, L_X\, i_{qr}^{SFR} \tag{3.47}$$

$$v'^{SFR}_{qr} = \frac{K_P^r}{\gamma^2} \left(i'^{SFR}_{qr} - i_{qr}^{SFR} \right) + \frac{K_I^r}{\gamma^2} \int \left(i'^{SFR}_{qr} - i_{qr}^{SFR} \right) dt + \omega_r \left[L_{rr}\, i_{dr}^{SFR} + L_m i_{ds}^{SFR} \right] \tag{3.48}$$

Equations (3.45) and (3.46) represent the inner control loop of the RSC. The bounds on the PI outputs $\frac{K_P^r}{\gamma^2}\left(i'^{SFR}_{dr} - i^{SFR}_{dr}\right) + \frac{K_I^r}{\gamma^2}\int\left(i'^{SFR}_{dr} - i^{SFR}_{dr}\right)dt$ and $\frac{K_P^r}{\gamma^2}\left(i'^{SFR}_{qr} - i^{SFR}_{qr}\right) + \frac{K_I^r}{\gamma^2}\int\left(i'^{SFR}_{qr} - i^{SFR}_{qr}\right)dt$ become 0.2 pu.

Figure 3.7 shows the outer and the inner control loops with the limiters of the RSC and the GSC. In Figure 3.7, v_{dc} is the measured and filtered DC-link voltage, V'_{dc} is the reference value for the DC voltage (= 1pu), P_{tb} is the measured positive sequence active power of the turbine (the stator and the GSC), P'_{tb} is the reference active power calculated by the MPPT system, and m is the modulation pattern for the switches of the converters.

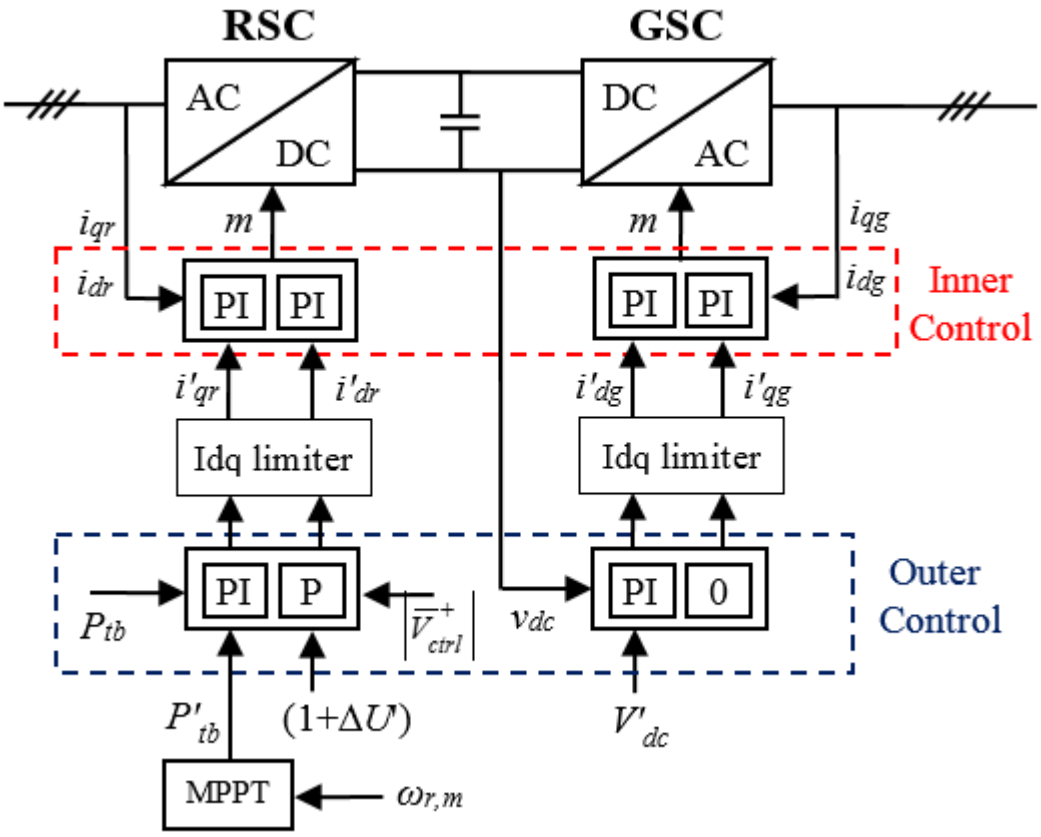

Figure 3.7 A schematic diagram of the converter controllers of a type-III WTG in normal conditions.

3.1.6 dq-to-abc transformation

The last step is the transformation of the reference converter voltages in phase domain. These reference voltages are used by the PWM system to control the switching of the semiconductor switches of the converter.

To avoid overvoltages on the converter, the reference voltages used by the PWM system are limited in dq domain. The magnitude of the dq converter voltage is limited to 1.5 times the DC-link voltage:

For the RSC:

$$v''^{SFR}_{dr} + jv''^{SFR}_{qr} = \frac{\left(v'^{SFR}_{dr} + jv'^{SFR}_{qr}\right)}{v_{dc}\sqrt{2/3}} \min\left(\frac{1.5v_{dc}\sqrt{2/3}}{\sqrt{\left(v'^{SFR}_{dr}\right)^2 + \left(v'^{SFR}_{qr}\right)^2}}, 1\right) \tag{3.49}$$

For the GSC:

$$v''_{dcv} + jv''_{qcv} = \frac{\left(v'_{dcv} + jv'_{qcv}\right)}{v_{dc}\sqrt{2/3}} \min\left(\frac{1.5v_{dc}\sqrt{2/3}}{\sqrt{\left(v'_{dcv}\right)^2 + \left(v'_{qcv}\right)^2}}, 1\right) \tag{3.50}$$

where v''^{SFR}_{dr} and v''^{SFR}_{qr} are the corrected d- and q-components of the RSC reference voltage, and v''_{dcv} and v''_{qcv} are the corrected d- and q-components of the GSC reference voltage.

Finally, the corrected converter reference voltages are transformed into phase domain using the inverse of the matrix **T**.

For the GSC we have:

$$\begin{bmatrix} v'_{a,cv} \\ v'_{b,cv} \\ v'_{c,cv} \end{bmatrix} = \mathbf{T}^{-1}(\theta) \begin{bmatrix} v''_{dcv} \\ v''_{qcv} \\ 0 \end{bmatrix} \tag{3.51}$$

$$\mathbf{T}^{-1}(\theta) = \begin{bmatrix} \cos(\theta) & -\sin(\theta) & 1 \\ \cos(\theta - 2\pi/3) & -\sin(\theta - 2\pi/3) & 1 \\ \cos(\theta + 2\pi/3t) & -\sin(\theta + 2\pi/3) & 1 \end{bmatrix} \tag{3.52}$$

where $v'_{a,cv}$, $v'_{b,cv}$ and $v'_{c,cv}$ are the voltage references of the a, b, c phases for the PWM system of the GSC.

For the RSC, the inverse transformation uses $\theta - \theta_r + \varphi_{flux}$ as mentioned in section 3.1.1.

$$\begin{bmatrix} v'_{a,r} \\ v'_{b,r} \\ v'_{c,r} \end{bmatrix} = \mathbf{T}^{-1}(\theta - \theta_r + \varphi_{flux}) \begin{bmatrix} v''^{SFR}_{dr} \\ v''^{SFR}_{qr} \\ 0 \end{bmatrix} \tag{3.53}$$

where $v'_{a,r}$, $v'_{b,r}$ and $v'_{c,r}$ are the voltage references of the a, b, c phases for the PWM system of the RSC.

3.2 Simple steady-state model of the type-III WTG

This simple SS model provides the SC current of type-III WTGs without requiring control paramaters of the RSC and GSC. It is less accurate than the detailed model of section 3.3 but easier to implement.

For the DFIGs, the stator currents depend on the rotor currents. As the RSC is equipped with a limiter to protect the semiconductor devices of the power electronics circuitry, the rotor current limits will have an impact on the stator currents. In other words, to know the actual stator currents, the rotor currents must be calculated first to check if the current limits have been respected.

The desired stator currents are calculated using the reference active power output and the control mode. Then the rotor currents are calculated and checked to see if their limits are respected. If the limits are respected, the actual stator currents will be equal to the desired stator currents. If not, the stator currents are corrected according to the corrected rotor currents.

For the GSC, the active power flow depends on the active power flow on the RSC. As the DC-link is not consuming or storing any active power in SS, the active power flows on the RSC and on the GSC are equal to each other. For the reactive current output of the GSC, it is 0 except if the desired reactive current of the stator is not reached.

As presented in the section 3.1, for the RSC controller the d and q voltages and currents are in the SFR. In other word, the d axis is aligned with the stator flux. In the SFR the d-axis is at an angle of -90° with respect to the stator voltage. The stator currents in SVR and SFR are defined in the opposite direction. For the sake of comparison of the SFR and SVR, Figure 3.8 illustrates the two frames in the complex plane with currents in the same direction. In Figure 3.8, an arrow in the SFR subscript is added to distinguish them from the conventional ones.

As in the previous section:

- the rotor currents are always given in the SFR, and they circulate from the RSC to the rotor,
- the stator currents in the SFR follow the direction given in Figure 3.5, from the grid to the stator,
- the stator currents in the SVR use the generator convention, from the stator to the grid.

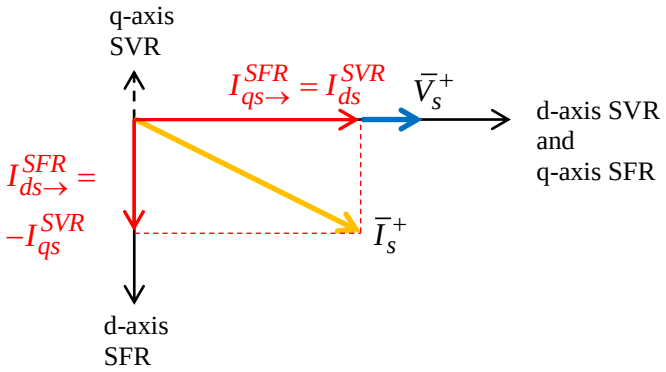

Figure 3.8 Stator dq axes in SFR and SVR.

Then:

$$I_{ds}^{SFR} = -\left(-I_{qs}^{SVR}\right) = I_{qs}^{SVR} \tag{3.54}$$

$$I_{qs}^{SFR} = -\left(I_{ds}^{SVR}\right) \tag{3.55}$$

where the minus signs outside the parentheses represent the change of convention.

For the DFIG, the stator voltage and the PGC voltage are the same:

$$\bar{V}_s^+ = \bar{V}_{pgc}^+ \tag{3.56}$$

Equations (3.4) and (3.5) give the relations between the stator and rotor currents. Rewriten with phasor variables:

$$I_{ds}^{SFR} = -\frac{I_{dr}^{SFR}}{\gamma} + \frac{V_{qs}^{SFR}}{X_{ss}} \tag{3.57}$$

$$I_{qs}^{SFR} = -\frac{I_{qr}^{SFR}}{\gamma} - \frac{V_{ds}^{SFR}}{X_{ss}} \tag{3.58}$$

where $X_{ss} = \omega_s L_{ss}$.

As this section is concerned with a phasor represention, and as the controller structure is built for the fundamental frequency, the machine inductances of section 3.1 are replaced by reactances at the nominal grid frequency. The subscript used for a reactance is the same as that used for the corresponding inductance. For example, we write $X_{ls} = \omega_s L_{ls}$.

As in the SFR, the stator voltage is aligned on the q-axis:

$$\begin{aligned} V_{ds}^{SFR} &= 0 \\ V_{qs}^{SFR} &= \left|\bar{V}_{pgc}^+\right| \end{aligned} \tag{3.59}$$

Therefore, (3.57) and (3.58) are simplified as:

$$I_{ds}^{SFR} = -\frac{I_{dr}^{SFR}}{\gamma} + \frac{\left|\bar{V}_{pgc}^+\right|}{X_{ss}} \tag{3.60}$$

$$I_{qs}^{SFR} = -I_{qr}^{SFR} \Big/ \gamma \tag{3.61}$$

These two equations give the relation between the stator and the rotor currents. They are used to calculate the rotor currents from the desired stator currents, and to correct the stator currents according to the limited rotor currents as explained below.

3.2.1 Desired stator and rotor currents

The control mode and the reference active power together determine the desired stator current. This is also the case in type-IV WTG.

Active power behavior

For all control modes, the controller always tries to transmit the active power coming from the wind. We assume that there is no wind speed variation between SS and fault. Consequently, the active power production is constant.

In the event of voltage sag, the active part of the current will increase to maintain the active power output. This will continue until either the WTG active power output reaches its prefault value $\left(i.e.\, P_{pgc} = P'_{pgc}\right)$ or the rotor active current component reaches its own limit.

$$\hat{I}_{ds}^{SVR} = \frac{P'_{pgc}}{\left|\bar{V}_{pgc}^{+}\right|} + \text{real}\left(\frac{\left|\bar{V}_{pgc}^{+}\right|}{Z_{filter}}\right) - I_{dg}^{SVR-old} \tag{3.62}$$

where Z_{filter} is the total impedance of the GSC shunt filters at grid frequency. Its resistive part is usually negligible, but the general formula is given here for the sake of completeness. $I_{dg}^{SVR-old}$ is the active part of the current coming from the GSC obtained at the previous iteration. The previous iteration value is used because the new value needs the rotor currents to be calculated. For the first iteration, $I_{dg}^{SVR-old}$ is estimated by:

$$I_{dg}^{SVR-old} = -s\frac{P'_{pgc}}{\left|\bar{V}_{pgc}^{+}\right|} \tag{3.63}$$

where *s* is the slip of the machine.

Slip calculation

If the slip is unknown, it can be estimated. For a type-III WTG, the slip follows the relation:

$$P_{tb} = P_0(1-s)^3 \tag{3.64}$$

where P_{tb} is the active power output of the WTG (from the stator and the GSC), and P_0 is a constant depending of the size and the structure of the WTG.

This constant is obtained from the nominal conditions:

$$P_0 = \frac{P_{rated}}{(1 - s_{rated})^3} \tag{3.65}$$

where P_{rated} is the rated active power of the WTG, and s_{rated} is the slip of the machine corresponding to this rated power.

$$s = 1 - \sqrt[3]{\frac{P'_{tb}}{P_0}} \tag{3.66}$$

$$P'_{tb} = P'_{pgc} - \text{real}\left(\frac{\left| \bar{V}^{+}_{pgc} \right|^2}{Z_{filter}} \right) \tag{3.67}$$

If the resistive part of the filter is negligible, then (3.66) is rewritten as:

$$s = 1 - \sqrt[3]{\frac{P'_{pgc}}{P_0}} \tag{3.68}$$

Combining (3.55) and (3.61), the desired active component of the rotor current $\hat{I}^{SFR}_{qr}$ is obtained:

$$\hat{I}^{SFR}_{qr} = \gamma \hat{I}^{SVR}_{ds} \tag{3.69}$$

Reactive power behavior

Recall that control is performed at the POI, the point where the wind park is connected to the host grid. The WPC can have three control modes under normal conditions: V-control, Q-control and PF-control. For any control mode, the WPC provides the outer control loop of the RSC controller with a correction $\Delta U'$. As an aggregated turbine model is used, $\Delta U'$ is directly used in the RSC controller.

As the WPC has a very slow response (second scale), its output variation during faults lasting for less than half a second is neglected. Consequently, the $\Delta U'$ during the fault is equal to the $\Delta U'$ before the fault, and it is calculated on the basis of prefault conditions which depend on the control mode (details in section 3.2.4).

The controlled voltage V_{ctrl}^{+} can be either the PGC voltage or the voltage at the MV side of turbine transformer ("Vmv" on Figure 3.6). In the first case, $V_{ctrl}^{+} = \left|\bar{V}_{pgc}^{+}\right|$ and in the second case $V_{ctrl}^{+} = \left|\bar{V}_{mv}^{+}\right|$. $\bar{V}_{mv}^{+}$ is obtained by using the series impedance of the turbine transformer and the positive sequence voltage and current at the PGC:

$$\bar{V}_{mv}^{+} = \bar{V}_{pgc}^{+} - \bar{I}_{pgc}^{+} Z_{tt}^{+} \tag{3.70}$$

where Z_{tt}^{+} is the positive sequence series complex impedance at the nominal frequency of the turbine transformer.

During the fault, the desired reactive current $\hat{I}_{qs}^{SVR}$ is obtained with V-control, Q-control or PF-control from the following equation:

$$\hat{I}_{qs}^{SVR} = -K_V \left(1 - V_{ctrl}^{+} + \Delta U'\right) \tag{3.71}$$

where K_V is the proportional gain of the outer loop ($K_V > 0$).

The control mode does not directly affect the outer control loop, however, it does affect the prefault conditions which in turn determine $\Delta U'$. Consequently, the outer control loop responses will be identical for different control modes yielding the same prefault conditions.

All control modes associated with the normal conditions can have an FRT function. If the WP has an FRT function, this function is activated when V_{ctrl}^{+} leaves the deadband (see Figure 2.5). With an FRT function, the desired reactive current $\hat{I}_{qs}^{SVR}$ becomes:

$$\hat{I}_{qs}^{SVR} = -K_{FRT} \left(1 - V_{ctrl}^{+}\right) \tag{3.72}$$

where K_{FRT} is the proportional voltage regulator gain defined by the FRT requirement ($K_{FRT} > 0$).

Combining $\hat{I}_{qs}^{SFR}$ with (3.54) and (3.60), the desired reactive component of the rotor current $\hat{I}_{dr}^{SFR}$ is obtained:

$$\hat{I}_{dr}^{SFR} = \gamma \left(V_{pgc}^{+} \big/ X_{ss} - \hat{I}_{qs}^{SVR} \right) \tag{3.73}$$

3.2.2 Current limiter & calculation of stator reference currents

The current limiter protects the RSC against overcurrent by cutting the active and/or the reactive component of the desired current. This section uses the same equations as those of section 3.1.3, except that the variables are DC signals (uppercase letters instead of lowercase).

P-priority

The q-component, which represents the active component, respects its limit:

$$I'^{SFR}_{qr} = \text{sign}\left(\hat{I}_{qr}^{SFR} \right) \cdot \min\left(\left| \hat{I}_{qr}^{SFR} \right|, I_{qr}^{\lim} \right) \tag{3.74}$$

The d-component also respects its limit, and respects the maximum current magnitude $I_r^{\lim}$:

$$I_{dr}^{\max} = \sqrt{\left(I_r^{\lim} \right)^2 - \left(I'^{SFR}_{qr} \right)^2} \tag{3.75}$$

$$I'^{SFR}_{dr} = \text{sign}\left(\hat{I}_{dr}^{SFR} \right) \cdot \min\left(\left| \hat{I}_{dr}^{SFR} \right|, I_{dr}^{\max}, I_{dr}^{\lim} \right) \tag{3.76}$$

Q-priority

The d-component, which represents the reactive component, respects its limit:

$$I'^{SFR}_{dr} = \text{sign}\left(\hat{I}_{dr}^{SFR} \right) \cdot \min\left(\left| \hat{I}_{dr}^{SFR} \right|, I_{dr}^{\lim} \right) \tag{3.77}$$

The q-component also respects its limit, and respects the maximum current magnitude $I_r^{\lim}$:

$$I_{qr}^{\max} = \sqrt{\left(I_r^{\lim} \right)^2 - \left(I'^{SFR}_{dr} \right)^2} \tag{3.78}$$

$$I'^{SFR}_{qr} = \text{sign}\left(\hat{I}^{SFR}_{qr}\right) \cdot \min\left(\left|\hat{I}^{SFR}_{qr}\right|, I^{\max}_{qr}\right) \tag{3.79}$$

$I^{\max}_{dr}$ and $I^{\max}_{qr}$ are the maximum values which depend on the maximum current magnitude and the prioritized component. These values are consequently fault-dependent.

Conversion to stator currents

The reference rotor current I'^{SFR}_{dr} is converted to the stator current through (3.73) where the desired values are replaced by the reference ones:

$$I'^{SVR}_{qs} = V^{+}_{pgc} \big/ X_{ss} - I'^{SFR}_{dr} / \gamma \tag{3.80}$$

The reference rotor current I'^{SFR}_{qr} is converted to the stator current through (3.69) where the desired values are replaced by the reference ones:

$$I'^{SVR}_{ds} = I'^{SFR}_{qr} / \gamma \tag{3.81}$$

3.2.3 GSC currents and negative sequence behavior

To calculate the desired active current of the GSC, $\hat{I}^{SVR}_{dg}$, the active power flowing through the DC-link must be known. The active power flowing through the GSC is the same as the one flowing through the RSC in order to keep the DC voltage constant.

The negative sequence current flowing through the GSC is very low (like coupled sequence FSC WTG, see section 2.2.4) and is neglected here: $\bar{I}^{-}_{g} = 0$. Consequently, there is no negative sequence active power circulating in the GSC.

On the RSC, there is active power flow due to two reasons:

1. the currents calculated by the controller in the previous section,
2. the negative sequence power coming from the stator.

For the first point above, the rotor currents are already known. To obtain the active power flowing through the RSC, the output voltages of this converter are calculated. By neglecting the resistance and the derivative elements in (3.28), and applying (3.31), the electrical equations of the rotor voltages are obtained:

$$V_{qr}^{SFR} = s\left(\left(X_{lr} + X_m\right) I'^{SFR}_{dr} + X_m I_{ds}^{SFR}\right) \tag{3.82}$$

$$V_{dr}^{SFR} = -s\left(\left(X_{lr} + X_m\right) I'^{SFR}_{qr} + X_m I_{qs}^{SFR}\right) \tag{3.83}$$

Using (3.61), (3.83) is simplified as:

$$V_{dr}^{SFR} = -s\left(X_{lr} + X_{ls}/\gamma\right) I'^{SFR}_{qr} \tag{3.84}$$

Therefore, the active power flow from the RSC to the rotor is:

$$P_{RSC}^{+} = V_{dr}^{SFR} I'^{SFR}_{dr} + V_{qr}^{SFR} I'^{SFR}_{qr} \tag{3.85}$$

In the left-hand side of this equation the superscript + (plus) is used because the power computed corresponds only to the DC component of the dq signals. Here we may not use the term “positive sequence” because the order of the phases depends on the slip of the machine.

For the second point in the list above, the negative sequence current in the stator is approximated by:

$$\bar{I}_s^{-} = \frac{-\bar{V}_s^{-}}{R_s + R_r + j\left(X_{ls} + X_{lr}\right)} \tag{3.86}$$

where R_s is the stator resistance and R_r is the rotor resistance. This approximation is done by assuming that $X_m \gg X_{lr}$ and $X_m \gg X_{ls}$, that the measurement filters have no impact, and that the complex gain of the PI controller of the rotor inner loop is zero. The origin of this formula is explained in section 3.4.

The reason for the minus sign is that $\bar{I}_s^{-}$ is the current flowing from the stator to the grid (generator convention).

The negative sequence current and voltage on the stator also create an active power flow which is transferred to the RSC via the rotor. Due to the low values in the denominator of (3.86) this power cannot be neglected. Its expression is approximated by (3.87), where the machine resistances are neglected.

$$P_{RSC}^{-} = \text{real}\left(\bar{V}_s^{-} \left(\bar{I}_s^{-} \right)^* \right) \tag{3.87}$$

Finally, the active component of the GSC current (from the GSC to the PGC) is:

$$\hat{I}_{dg}^{SVR} = -\left(P_{RSC}^{+} + P_{RSC}^{-} \right) / \left| \bar{V}_{pgc}^{+} \right| \tag{3.88}$$

The reactive component of the current from the GSC to the PGC depends on the activation of the FRT mode.

If the FRT mode is not activated:

$$\begin{aligned} I_{dg}'^{SVR} &= \text{sign}\left(\hat{I}_{dg}^{SVR} \right) \min\left(\left| \hat{I}_{dg}^{SVR} \right|, I_{dg}^{\lim} \right) \\ I_{qg}'^{SVR} &= 0 \end{aligned} \tag{3.89}$$

If the FRT mode is activated, then the role of the GSC is to supply the reactive current that cannot be supplied by the RSC (due to thermal limit) in order to respect the FRT requirement. The GSC only supplies the extra reactive power during low voltage conditions but does not consume reactive power during overvoltage.

$$\begin{aligned} \hat{I}_{qg}^{SVR} &= \min\left(I_{dr}'^{SFR} - \hat{I}_{dr}^{SFR}, 0 \right) \\ &= \min\left(I_{dr}^{\lim} - \left[\left| \bar{V}_{pgc}^{+} \right| / X_m + K_{FRT} \left(1 - \left| \bar{V}_{ctrl}^{+} \right| \right) \right], 0 \right) \end{aligned} \tag{3.90}$$

$$I_{qg}'^{SVR} = \max\left(\hat{I}_{qg}^{SVR}, -I_{qg}^{\lim} \right) \tag{3.91}$$

$$I_{dg}^{\max} = \sqrt{\left(I_g^{\lim} \right)^2 - \left(I_{qg}'^{SVR} \right)^2} \tag{3.92}$$

$$I_{dg}'^{SVR} = \text{sign}\left(\hat{I}_{dg}^{SVR} \right) \cdot \min\left(\left| \hat{I}_{dg}^{SVR} \right|, I_{dg}^{\max}, I_{dg}^{\lim} \right) \tag{3.93}$$

Finally, the total current of the turbine is calculated by adding the GSC and the stator currents:

$$\bar{I}_{tb}^{+} = \left[I_{ds}'^{SVR} + I_{dg}'^{SVR} + j\left(I_{qs}'^{SVR} + I_{qg}'^{SVR} \right) \right] \exp\left[j \,\text{angle}\left(\bar{V}_{pgc}^{+} \right) \right] \tag{3.94}$$

$$\bar{I}_{tb}^{-} = \bar{I}_{s}^{-} \tag{3.95}$$

where the subscript *tb* means turbine (i.e. stator + GSC).

3.2.4 DFIG simple model algorithm

The following algorithm summarizes the calculation of the current contribution of a DFIG-type WP.

The algorithm is divided into two parts: the prefault calculations and the iterative algorithm. The prefault calculations provide the reference values and perform the necessary initialization for the iterative algorithm.

Due to the non-linear behavior of the current limiter, the solution requires an iterative algorithm. The iterative algorithm will calculate the current contribution of the DFIG according to the control mode and the voltage at the PGC. The algorithm below gives the procedure for a single iteration, namely, iteration number *k*. The iteration number will appear inside a pair of parentheses and as a superscript. The superscript (0) will refer to prefault values, and $k-1$ will refer to the previous iteration.

Figure 3.9 presents in a visual way the main steps of the DFIG algorithm.

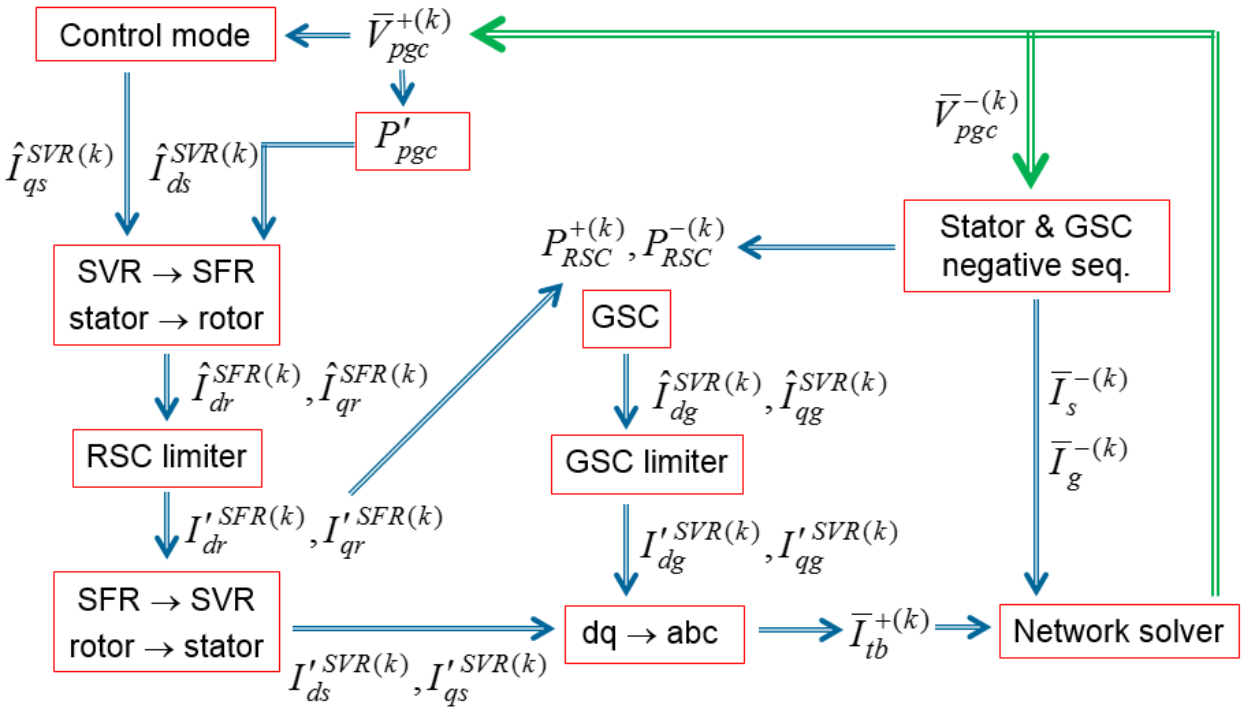

Figure 3.9 Block diagram of the simple DFIG algorithm.

The complete solver which considers several WTGs with both type-III and type-IV WTG is given in CHAPTER 4.

Prefault calculations

$$P'_{pgc} + jQ'_{pgc} = \bar{V}_{pgc}^{+(0)} \left(\bar{I}_{pgc}^{+(0)} \right)^{*} \tag{3.96}$$

$$\bar{I}_{tb}^{+(0)} = \bar{I}_{pgc}^{+(0)} + \frac{\bar{V}_{pgc}^{+(0)}}{Z_{filter}} \tag{3.97}$$

$$P_0 = \frac{P_{rated}}{(1 - s_{rated})^3} \tag{3.98}$$

$$P'_{tb} = P'_{pgc} - \text{real}\left(\frac{\left| \bar{V}_{pgc}^{+(0)} \right|^2}{Z_{filter}} \right) \tag{3.99}$$

$$s = 1 - \sqrt[3]{\frac{P'_{tb}}{P_0}} \tag{3.100}$$

$$I_{dtb}^{SVR(0)} + j\, I_{qtb}^{SVR(0)} = \frac{\bar{I}_{tb}^{+(0)}}{\exp\left(j \operatorname{angle}\left(\bar{V}_{pgc}^{+(0)} \right) \right)} \tag{3.101}$$

$$\begin{aligned} I_{ds}^{SFR(0)} &= I_{qs}^{SVR(0)} = I_{qtb}^{SVR(0)} \\ I_{dr}^{SFR(0)} &= \gamma \left(\left| \bar{V}_{pgc}^{+(0)} \right| \Big/ X_{ss} - \hat{I}_{ds}^{SFR(0)} \right) \end{aligned} \tag{3.102}$$

$$I_{dg}^{SVR(0)} = s I_{dtb}^{SVR(0)} \tag{3.103}$$

$$\begin{aligned} I_{ds}^{SVR(0)} &= (1-s)\, I_{dtb}^{SVR(0)} \\ I_{qs}^{SFR(0)} &= -I_{ds}^{SVR(0)} \\ I_{qr}^{SFR(0)} &= -\gamma I_{qs}^{SFR(0)} = \gamma (1-s)\, I_{dtb}^{SVR(0)} \end{aligned} \tag{3.104}$$

IF {control at MV side of turbine transformer}

$$\bar{V}_{ctrl}^{+(0)} = \bar{V}_{mv}^{+(0)} = \bar{V}_{pgc}^{+(0)} - \bar{I}_{pgc}^{+(0)} \bar{Z}_{tt}^{+} \tag{3.105}$$

ELSE

$$\bar{V}_{ctrl}^{+(0)} = \bar{V}_{pgc}^{+(0)} \tag{3.106}$$

END

$$\Delta U' = \left(\hat{I}_{dr}^{SFR(0)} - \left| \bar{V}_{pgc}^{+(0)} \right| / X_m \right) / K_V + \left| \bar{V}_{ctrl}^{+(0)} \right| - 1 \tag{3.107}$$

DFIG iterative algorithm

$$V_{pgc}^{+(k)} = \left| \bar{V}_{pgc}^{+(k)} \right| \tag{3.108}$$

$$\hat{I}_{ds}^{SVR(k)} = \frac{P'_{pgc}}{V_{pgc}^{+(k)}} + \operatorname{real}\left(\frac{V_{pgc}^{+(k)}}{Z_{filter}} \right) - I_{dg}^{SVR(k-1)} \tag{3.109}$$

$$\hat{I}_{qr}^{SFR(k)} = \gamma \hat{I}_{ds}^{SVR(k)} \tag{3.110}$$

$$\hat{I}_{qr}^{SFR(k)} = 0.5\left(\hat{I}_{qr}^{SFR(k)} + I'^{SFR(k-1)}_{qr}\right) \qquad \textit{(variation limiter)} \tag{3.111}$$

Calculation of the desired reactive component of the stator current:

IF {controlled voltage is $\bar{V}_{mv}^{+}$ }

$$\begin{aligned} \bar{V}_{mv}^{+(k)} &= \bar{V}_{pgc}^{+(k)} - \bar{I}_{pgc}^{+(k-1)} Z_{tt}^{+} \\ V_{ctrl}^{+(k)} &= \left|\bar{V}_{mv}^{+(k)}\right| \end{aligned} \tag{3.112}$$

ELSE

$$V_{ctrl}^{+(k)} = \left|\bar{V}_{pgc}^{+(k)}\right| \tag{3.113}$$

END

IF {Q-control **OR** PF-control **OR** V-control}

$$\hat{I}_{dr}^{SFR(\mathrm{k})} = K_V \left(1 - V_{ctrl}^{+(k)} + \Delta U'\right) + V_{pgc}^{+(k)} / X_m \tag{3.114}$$

IF {FRT-function}

$$\hat{I}_{dr}^{SFR(\mathrm{k})} = K_{FRT} \left(1 - V_{ctrl}^{+(k)}\right) + V_{pgc}^{+(k)} / X_m \tag{3.115}$$

END

RSC limitation according to the priority:

IF {P-priority}

$$I'^{SFR(k)}_{qr} = \mathrm{sign}\left(\hat{I}_{qr}^{SFR(k)}\right) \min\left(\left|\hat{I}_{qr}^{SFR(k)}\right|, I_{qr}^{\lim}\right) \tag{3.116}$$

$$\begin{aligned} I_{dr}^{\max} &= \min\left(\sqrt{\left(I_r^{\lim}\right)^2 - \left(I'^{SFR(k)}_{qr}\right)^2},\ I_{dr}^{\lim}\right) \\ I'^{SFR(k)}_{dr} &= \mathrm{sign}\left(\hat{I}_{dr}^{SFR(k)}\right) \min\left(\left|\hat{I}_{dr}^{SFR(k)}\right|, I_{dr}^{\max}\right) \end{aligned} \tag{3.117}$$

IF {Q-priority **OR** FRT-function}

$$\hat{I}_{dr}^{SFR(k)} = 0.5\left(\hat{I}_{dr}^{SFR(k)} + I'^{SFR(k-1)}_{dr}\right) \quad \textit{(variation limier)} \tag{3.118}$$

$$I'^{SFR(k)}_{dr} = \mathrm{sign}\left(\hat{I}_{dr}^{SFR(k)}\right) \min\left(\left|\hat{I}_{dr}^{SFR(k)}\right|, I_{dr}^{\lim}\right) \tag{3.119}$$

$$I_{qr}^{\max} = \min\left(\sqrt{\left(I_r^{\lim}\right)^2 - \left(I_{dr}'^{SFR(k)}\right)^2}, I_{qr}^{\lim}\right)$$
$$I_{qr}'^{SFR(k)} = \text{sign}\left(\hat{I}_{qr}^{SFR(k)}\right)\min\left(\left|\hat{I}_{qr}^{SFR(k)}\right|, I_{qr}^{\max}\right) \quad (3.120)$$

END

Conversion from rotor currents to stator currents:

$$I_{ds}'^{SVR(k)} = I_{qr}'^{SFR(k)} / \gamma$$
$$I_{qs}'^{SVR(k)} = V_{pgc}^{+(k)} \Big/ X_{ss} - I_{dr}'^{SFR(k)} / \gamma \quad (3.121)$$

GSC calculations:

$$V_{dr}^{SFR(k)} = -s\left(X_{lr} + X_{ls}/\gamma\right) I_{qr}'^{SFR(k)}$$
$$V_{qr}^{SFR(k)} = s\left(\left(X_{lr} + X_m\right) I_{dr}'^{SFR(k)} + X_m I_{ds}^{SFR(k)}\right) \quad (3.122)$$

$$P_{RSC}^{+(k)} = V_{dr}^{SFR(k)} I_{dr}'^{SFR(k)} + V_{qr}^{SFR(k)} I_{qr}'^{SFR(k)} \quad (3.123)$$

$$\bar{I}_s^{-(k)} = \frac{-\bar{V}_s^{-(k)}}{R_s + R_r + j\left(X_{ls} + X_{lr}\right)} \quad (3.124)$$

$$P_{RSC}^{-(k)} = \text{real}\left(\bar{V}_s^{-(k)}\left(\bar{I}_s^{-(k)}\right)^*\right) \quad (3.125)$$

$$\hat{I}_{dg}^{SVR(k)} = -\left(P_{RSC}^{+(k)} + P_{RSC}^{-(k)}\right) / V_{pgc}^{+(k)} \quad (3.126)$$

$$\bar{I}_s^{-(k)} = 0.5\left(\bar{I}_s^{-(k)} + \bar{I}_s^{-(k-1)}\right) \qquad \textit{(variation limiter)} \quad (3.127)$$

IF {FRT-control}

$$\hat{I}_{qg}^{SVR(k)} = -\left[\gamma K_{FRT}\left(1 - V_{ctrl}^{+(k)}\right) + V_{pgc}^{+(k)} \Big/ X_m - I_{dr}^{\lim}\right] \quad (3.128)$$

$$I_{qg}'^{SVR(k)} = \max\left(\min\left(\hat{I}_{qg}^{SVR(k)}, 0\right), -I_{qg}^{\lim}\right) \quad (3.129)$$

$$I_{dg}^{\max} = \min\left(\sqrt{\left(I_g^{\lim}\right)^2 - \left(I_{qg}'^{SVR(k)}\right)^2}, I_{dg}^{\lim}\right) \quad (3.130)$$

$$I'^{SVR(k)}_{dg} = \text{sign}\left(\hat{I}^{SVR(k)}_{dg}\right) \min\left(\left|\hat{I}^{SVR(k)}_{dg}\right|, I^{\max}_{dg}\right) \tag{3.131}$$

ELSE

$$\begin{aligned} I'^{SVR(k)}_{dg} &= \text{sign}\left(\hat{I}^{SVR(k)}_{dg}\right) \min\left(\left|\hat{I}^{SVR(k)}_{dg}\right|, I^{\lim}_{dg}\right) \\ I'^{SVR(k)}_{qg} &= 0 \end{aligned} \tag{3.132}$$

END

$$\begin{aligned} \bar{I}^{+(k)}_{tb} &= \left(I'^{SVR(k)}_{dg} + j\, I'^{SVR(k)}_{qg} + I'^{SVR(k)}_{ds} + j\, I'^{SVR(k)}_{qs}\right) \exp\left(j\, \text{angle}\left(\bar{V}^{+(k)}_{pgc}\right)\right) \\ \bar{I}^{-(k)}_{tb} &= \bar{I}^{-(k)}_{s} \end{aligned} \tag{3.133}$$

The algorithm uses some variation limiters. They tend to increase solution stability and reduce the number of iterations required of the solver.

No zero sequence current passes through the GSC or the stator as each is connected with 3 wires: $\bar{I}^{0\,(k)}_{tb} = 0$.

3.2.5 List and descriptions of the variables of the DFIG phasor model algorithm

$\bar{I}^{+}_{pgc}$	the PGC positive sequence current phasor (flowing to the grid)
$\bar{V}^{+}_{pgc}$, $\bar{V}^{-}_{pgc}$	the PGC positive and negative sequence voltage phasor
$\hat{I}^{SFR}_{dr}$, $\hat{I}^{SFR}_{qr}$	the desired d- and q-components of the RSC current (from the rotor to the RSC)
I'^{SFR}_{dr}, I'^{SFR}_{qr}	the reference d- and q-components of the RSC current (from the rotor to the RSC)
$\hat{I}^{SVR}_{ds}$, $\hat{I}^{SVR}_{qs}$	the desired d- and q-components of the stator current in the SVR (from the stator to the PGC)

I'^{SVR}_{ds}, I'^{SVR}_{qs} the reference d- and q-components of the stator current in the SVR (from the stator to the PGC)

V^{SFR}_{dr}, V^{SFR}_{qr} the d- and q-components of the rotor voltage.

$\hat{I}^{SVR}_{dg}$, $\hat{I}^{SVR}_{qg}$ the desired d- and q-components of the GSC current (from the GSC to the grid)

I'^{SVR}_{dg}, I'^{SVR}_{qg} the reference d- and q-components of the GSC current (from the GSC to the grid)

$\bar{I}^{+}_{tb}$, $\bar{I}^{-}_{tb}$, $\bar{I}^{0}_{tb}$ the positive, negative and zero sequence current phasorw produced by the turbine (stator + GSC) (from the turbine to the PGC)

$I^{\lim}_{dr}$, $I^{\lim}_{qr}$ the RSC current limits on d- and q-components

$I^{\max}_{dr}$, $I^{\max}_{qr}$ the variable current limits of the RSC on d- and q-components depending on P- or Q-priority

$I^{\lim}_{r}$ the total current limit of the RSC

$I^{\lim}_{dg}$, $I^{\lim}_{qg}$ the GSC current limits on d- and q-components

$I^{\max}_{dg}$ the variable current limit of the GSC on d-components

$I^{\lim}_{g}$ the total current limit of the GSC

$\bar{I}^{-}_{s}$ the stator negative sequence current phasor (from the stator to the PGC)

$\bar{V}^{+}_{mv}$ the positive sequence voltage phasor at the medium voltage side of the turbine transformer

P'_{pgc} the reference active power at the PGC

Z_{filter} the complex total impedance of the shunt filters of the PGC at nominal frequency

Z_{tt}^{+} the complex positive sequence impedance of the turbine transformer at nominal frequency

K_V the voltage gain of the outer loop (POI control)

K_{FRT} the FRT gain or the FRT slope

$\Delta U'$ the correction of the WP controller on reactive current

s the slip of the machine under prefault conditions

P_{tb}' the active power produced by the turbine (stator + GSC) under prefault conditions

P_0 a constant parameter for the calculation of the slip

P_{rated} the nominal active power of the turbine

s_{rated} the slip when the turbine produces its nominal power

R_s, R_r the stator and rotor resistances

X_{ls}, X_{lr} the stator and rotor leakage reactances at the nominal grid frequency

X_m the magnetizing reactance at the nominal grid frequency

X_{ss} the stator self-inductance at the nominal grid frequency ($= X_{ls} + X_m$)

γ a coefficient ($= X_{ss} / X_m = L_{ss} / L_m$)

P_{RSC}^{+} the active power transfer on the RSC due to the DC components in dq domain (from the RSC to the rotor)

P_{RSC}^{-} the active power transfer on the RSC due to twice the grid frequency oscillations in dq domain (from the RSC to the rotor)

3.2.6 DFIG algorithm: list of inputs

Below is the information required to run the above algorithm.

- Voltage proportional gain,
- Prefault conditions (at PGC),
- Current limits in dq domain for the RSC and GSC, P/Q-priority for the RSC
- Availability of FRT function. If available: FRT slope and FRT activation threshold min and max,
- Total impedance of the shunt filters,
- Series impedance of the turbine transformer at nominal frequency if the MV option is used,
- Machine parameters: stator and rotor resistances, stator and rotor leakage inductances, magnetizing inductance,
- Prefault slip OR Nominal active power at the PGC, actual active power at the PGC, rated slip,
- Power and voltage bases (if the inputs/outputs are not in pu).

3.3 Complete steady-state model of the type-III WTG

This section gives a more detailed and precise SS model of the type-III WTG. The model to be presented also involves more details about the control system than the simple model does.

The two main differences between the detailed model and the simple model presented in section 3.2 are as follows:

- the flux angle used for the SVR and SFR conversion is calculated,
- the negative sequence of the stator current is calculated in a precise manner.

As a reminder, “SFR” stands for stator flux reference frame, and “SVR” for stator voltage reference frame.

3.3.1 Flux angle, SFR and SVR conversions

In the simple model, the flux angle is always equal to – 90°. In practice, the flux angle is calculated with the stator flux (3.30) in dq domain (section 3.1.1). It is obtained from the rotor and the stator currents by assuming $L_{ss} \approx L_m$ (Figure 3.3).

Consequently, the flux angle is not always –90°, and it must be calculated and considered in the calculation of flux frame components. Figure 3.10 illustrates the SFR for a flux angle $\varphi_{flux} = -79°$.

Because the SVR and SFR currents are defined in opposite directions, in Figure 3.10 an arrow in the SFR subscript is added to distinguish them from the conventional ones.

The dq components of the stator current in the SFR no longer represent the active and reactive components separately. The q-component represents mostly the active part, but it has also a reactive part. The d-component represents mostly the reactive part, but it has also an active part.

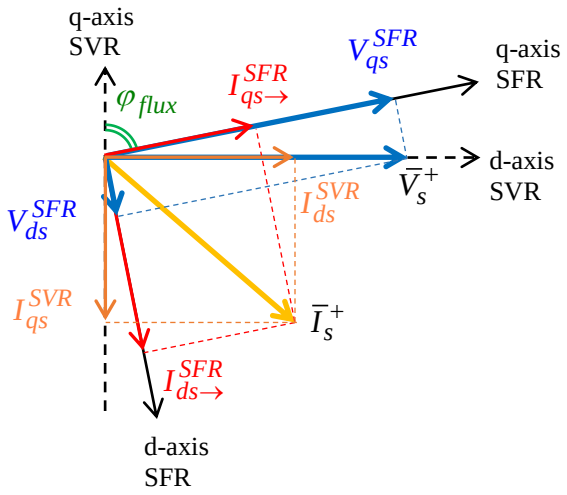

Figure 3.10 Stator flux (SFR) and stator voltage (SVR) reference frames.

As the PLL calculates the transformation angle with respect to the voltage reference frame, the d- and q-components need to be rotated to obtain them in the flux reference frame. By definition of the PLL, in voltage reference frame, the q-component of voltage is zero in SS.

$$V_{ds}^{SVR} = \left|\bar{V}_s^+\right| = \left|\bar{V}_{pgc}^+\right|$$
$$V_{qs}^{SVR} = 0 \tag{3.134}$$

Consequently, we obtain:

$$V_{ds}^{SFR} = \left|\bar{V}_{pgc}^+\right| \cos\left(-\varphi_{flux}\right) \tag{3.135}$$

$$V_{qs}^{SFR} = \left|\bar{V}_{pgc}^+\right| \sin\left(-\varphi_{flux}\right) \tag{3.136}$$

V_{ds}^{SFR} and V_{qs}^{SFR} are the d- and q-components of voltage in the flux reference frame.

For the stator currents, the relations between the SFR and the SVR are:

$$I_{ds}^{SVR} = -\left[I_{ds}^{SFR} \cos(-\varphi_{flux}) + I_{qs}^{SFR} \sin(-\varphi_{flux}) \right] \tag{3.137}$$

$$I_{qs}^{SVR} = -\left[I_{qs}^{SFR} \cos(-\varphi_{flux}) - I_{ds}^{SFR} \sin(-\varphi_{flux}) \right] \tag{3.138}$$

The minus sign in front of the bracket is present because the direction is reversed. In the SVR the current direction is from the stator to the grid, and in the SFR, it is from the grid to the stator.

Here again the linear Γ model of an induction machine gives the relation between stator and rotor currents. Recall equations (3.57), (3.58) and (3.2):

$$I_{ds}^{SFR} = -\frac{I_{dr}^{SFR}}{\gamma} + \frac{V_{qs}^{SFR}}{X_{ss}}$$

$$I_{qs}^{SFR} = -\frac{I_{qr}^{SFR}}{\gamma} - \frac{V_{ds}^{SFR}}{X_{ss}}$$

$$X_{ss} = X_{ls} + X_m \quad \text{and} \quad \gamma = \frac{X_{ss}}{X_m} = \frac{L_{ss}}{L_m}$$

where X_{ls} and X_m are, respectively, the stator leakage reactance and the magnetizing reactance at the nominal grid frequency.

The convention for rotor currents is from the RSC to the rotor.

Here, as in section 3.2, the machine inductances are replaced by reactances at the nominal grid frequency.

3.3.2 Positive sequence stator currents

For the calculation of the q-component of the rotor current (mainly active part), we need the active current of the turbine:

$$I_{ds}^{SVR} + I_{dg}^{SVR} = \frac{P'_{tb}}{\left|\bar{V}_{pgc}^{+}\right|} \tag{3.139}$$

where P'_{tb} is the reference active power output of the turbine (stator plus GSC).

I_{dg}^{SVR} and I_{ds}^{SVR} are flowing to the grid.

As a reminder, I_{ds}^{SVR} and I_{dg}^{SVR} are positive when active power is flowing from the stator or the GSC to the grid. I_{qs}^{SVR} and I_{qg}^{SVR} are negative when reactive power is flowing from the stator or the GSC to the grid.

Combining (3.139) and (3.137) and applying (3.58), we obtain:

$$\frac{P'_{tb}}{\left|\bar{V}_{pgc}^{+}\right|} = \left(\frac{I_{qr}^{SFR}}{\gamma} + \frac{V_{ds}^{SFR}}{X_{ss}}\right)\sin(-\varphi_{flux}) - I_{ds}^{SFR}\cos(-\varphi_{flux}) + I_{dg}^{SVR(old)} \tag{3.140}$$

$$\hat{I}_{qr}^{SFR} = \gamma\left[\frac{\dfrac{P'_{tb}}{\left|\bar{V}_{pgc}^{+}\right|} + I_{ds}^{SFR}\cos(-\varphi_{flux}) - I_{dg}^{SVR(old)}}{\sin(-\varphi_{flux})} - \frac{V_{ds}^{SFR}}{X_{ss}}\right] \tag{3.141}$$

The superscript "*old*" refers to values corresponding to the previous iteration. The previous iteration value is taken because I_{dg}^{SVR} is obtained later in the calculation process. More details are given in the algorithm part later.

For the d-axis component of the rotor current, the equations are the same as those for the simple model because it only depends on the positive sequence voltage magnitude (section 3.2.1).

$$\begin{aligned} \hat{I}_{dr}^{SFR} &= K_{FRT}\left(1 - \left|\bar{V}_{ctrl}^{+}\right|\right) + \left|\bar{V}_{pgc}^{+}\right| / X_m \qquad \text{for FRT mode} \\ \hat{I}_{dr}^{SFR} &= K_V\left(1 - \left|\bar{V}_{ctrl}^{+}\right| + \Delta U'\right) + \left|\bar{V}_{pgc}^{+}\right| / X_m \qquad \text{for other control mode} \end{aligned} \tag{3.142}$$

Once both the d- and q-components of the rotor current are calculated, the current limiter is applied. The rules are the same as those for Type-III simple model (see section 3.2.2).

Then the reference stator currents are calculated using the reference rotor currents and using equations (3.57) and (3.58):

$$I'^{SFR}_{ds} = \frac{V^{SFR}_{qs}}{X_{ss}} - \frac{I'^{SFR}_{dr}}{\gamma}$$
$$I'^{SFR}_{qs} = -\frac{V^{SFR}_{ds}}{X_{ss}} - \frac{I'^{SFR}_{qr}}{\gamma} \tag{3.143}$$

3.3.3 Negative sequence stator currents

The negative sequence behavior of a type-III WTG depends on both the control system and the machine. In a similar way to what happens in the FSC WTG (section 2.2.4), the negative sequence becomes twice the grid frequency oscillations in dq domain. The negative sequence behavior is dictated by the way these double-frequency oscillations circulate in the control system, and how the machine reacts to the negative sequence.

The inner loop equations of the RSC are presented in section 3.1.5. In the Laplace domain, those equations take the following form:

$$\tilde{V}'^{SFR}_{dr-ct} = \frac{\tilde{I}'^{SFR}_{dr} - \tilde{I}^{SFR}_{dr}}{\gamma^2}\left(K^r_P + \frac{K^r_I}{p}\right) - s\, X_X \tilde{I}^{SFR}_{qr} \tag{3.144}$$

$$\tilde{V}'^{SFR}_{qr-ct} = \frac{\tilde{I}'^{SFR}_{qr} - \tilde{I}^{SFR}_{qr}}{\gamma^2}\left(K^r_P + \frac{K^r_I}{p}\right) + s\left(X_{rr}\tilde{I}^{SFR}_{dr} + X_m \tilde{I}^{SFR}_{ds-ct}\right) \tag{3.145}$$

where $X_X = X_{lr} + X_{ls}/\gamma$, $X_{rr} = X_{lr} + X_m$, and the subscript "ct" means in the control system, the reason of this notation is given below. "~" indicates the signals in the Laplace domain, and p is the complex Laplace variable.

In (3.144) and (3.145), the current differences are divided by γ^2 because K^r_P and K^r_I are calculated in the Γ representation.

As in the case of the negative sequence model of type-IV WTG, the voltages and currents in the above equations are taken at the frequency of the oscillations, i.e., at twice the grid frequency due to the negative sequence. In the following equations, the double bar indicates the second harmonic phasors in dq domain. The reactances retain their values corresponding to the nominal frequency because the controller equations are based on the positive sequence. The reference currents are removed as they do not have these oscillations:

$$\bar{\bar{V}}_{dr-ct}^{SFR} = \frac{-H_{PI}^{rd}}{\gamma^2}\bar{\bar{I}}_{dr}^{SFR} - sX_X\bar{\bar{I}}_{qr}^{SFR} \tag{3.146}$$

$$\bar{\bar{V}}_{qr-ct}^{SFR} = \frac{-H_{PI}^{rq}}{\gamma^2}\bar{\bar{I}}_{dr}^{SFR} + s\left(X_{rr}\bar{\bar{I}}_{dr}^{SFR} + X_m\bar{\bar{I}}_{ds-ct}^{SFR}\right) \tag{3.147}$$

where H_{PI}^{rd} and H_{PI}^{rq} are the complex gains of the PI controllers at twice the grid frequency.

The measured currents and voltages undergo a phase shift because of the control filter. Consequently, the flux angle is also shifted. As the rotor current frequency is equal to the grid frequency multiplied by the slip, its frequency is low. In this thesis, the phase shift of the rotor current is neglected. The flux angle is shifted by approximately as much as the phase shift of the stator current. This flux angle is then used to change the stator and rotor currents from the voltage reference frame to the flux reference frame in dq domain. This angle is also used for the dq-to-abc transformation for the rotor voltage. Consequently, the phase shift on rotor voltage is:

$$\bar{\bar{V}}_{dr-ct}^{SFR} = \frac{\bar{\bar{V}}_{dr}^{SFR}}{H_{filter}} \qquad \bar{\bar{V}}_{qr-ct}^{SFR} = \frac{\bar{\bar{V}}_{qr}^{SFR}}{H_{filter}} \tag{3.148}$$

where H_{filter} is the complex gain of the measurement filter at the network frequency.

The stator currents in the control system are also delayed compared to the true values:

$$\bar{\bar{I}}_{ds}^{SFR} = \frac{\bar{\bar{I}}_{ds-ct}^{SFR}}{H_{filter}} \qquad \bar{\bar{I}}_{qs}^{SFR} = \frac{\bar{\bar{I}}_{qs-ct}^{SFR}}{H_{filter}} \tag{3.149}$$

Equations (3.146) and (3.147) become:

$$\bar{\bar{V}}_{dr}^{SFR} = \left[\frac{-H_{PI}^{rd}}{\gamma^2}\bar{\bar{I}}_{dr}^{SFR} - sX_X\bar{\bar{I}}_{qr}^{SFR}\right]H_{filter} \tag{3.150}$$

$$\bar{\bar{V}}_{qr}^{SFR} = \left[\frac{-H_{PI}^{rq}}{\gamma^2} \bar{\bar{I}}_{qr}^{SFR} + s\left(X_{rr} \bar{\bar{I}}_{dr}^{SFR} + X_m \bar{\bar{I}}_{ds}^{SFR} H_{filter} \right) \right] H_{filter} \tag{3.151}$$

The electrical equations between the rotor voltages and the machine currents, i.e., the rotor plus the stator currents, (3.32) and (3.33) are converted to twice the grid frequency phasors:

$$\bar{\bar{V}}_{dr}^{SFR} = \left(R_r + 2jX_{rr}\right)\bar{\bar{I}}_{dr}^{SFR} - sX_{rr}\bar{\bar{I}}_{qr}^{SFR} - sX_m\bar{\bar{I}}_{qs}^{SFR} + 2jX_m\bar{\bar{I}}_{ds}^{SFR} \tag{3.152}$$

$$\bar{\bar{V}}_{qr}^{SFR} = \left(R_r + 2jX_{rr}\right)\bar{\bar{I}}_{qr}^{SFR} + sX_{rr}\bar{\bar{I}}_{dr}^{SFR} + sX_m\bar{\bar{I}}_{ds}^{SFR} + 2jX_m\bar{\bar{I}}_{qs}^{SFR} \tag{3.153}$$

The electrical equations between the stator voltages and the machine currents, i.e., the combination of (3.29) and (3.30) are converted to twice the grid frequency phasors:

$$\bar{\bar{V}}_{ds}^{SFR} = \left(R_s + 2jX_{ss}\right)\bar{\bar{I}}_{ds}^{SFR} - X_{ss}\bar{\bar{I}}_{qs}^{SFR} - X_m\bar{\bar{I}}_{qr}^{SFR} + 2jX_m\bar{\bar{I}}_{dr}^{SFR} \tag{3.154}$$

$$\bar{\bar{V}}_{qs}^{SFR} = \left(R_s + 2jX_{ss}\right)\bar{\bar{I}}_{qs}^{SFR} + X_{ss}\bar{\bar{I}}_{ds}^{SFR} + X_m\bar{\bar{I}}_{dr}^{SFR} + 2jX_m\bar{\bar{I}}_{qr}^{SFR} \tag{3.155}$$

In (3.154) and (3.155), the voltages $\bar{\bar{V}}_{ds}^{SFR}$ and $\bar{\bar{V}}_{qs}^{SFR}$ are known , because the stator voltages are the inputs to the phasor model. Consequently equations (3.150) to (3.155) form a system of six equations and six unknowns: $\bar{\bar{V}}_{dr}^{SFR}$, $\bar{\bar{V}}_{qr}^{SFR}$, $\bar{\bar{I}}_{dr}^{SFR}$, $\bar{\bar{I}}_{qr}^{SFR}$, $\bar{\bar{I}}_{ds}^{SFR}$, $\bar{\bar{I}}_{qs}^{SFR}$.

The double the frequency voltage phasors in the SVR, $\bar{\bar{V}}_{ds}^{SVR}$ and $\bar{\bar{V}}_{qs}^{SVR}$, are obtained from the negative sequence voltage at the stator terminals in the same manner as described in section 2.2.4:

$$\bar{\bar{V}}_{ds}^{SVR} = -j\bar{V}_s^- \tag{3.156}$$

$$\bar{\bar{V}}_{qs}^{SVR} = \bar{V}_s^- \tag{3.157}$$

Then these voltages are transformed into the SFR with the flux angle:

$$\bar{\bar{V}}_{ds}^{SFR} = \bar{\bar{V}}_{ds}^{SVR}\cos(-\varphi_{flux}) - \bar{\bar{V}}_{qs}^{SVR}\sin(-\varphi_{flux}) \tag{3.158}$$

$$\bar{\bar{V}}_{qs}^{SFR} = \bar{\bar{V}}_{qs}^{SVR}\cos(-\varphi_{flux}) + \bar{\bar{V}}_{ds}^{SVR}\sin(-\varphi_{flux}) \tag{3.159}$$

From the system of equations (3.150) to (3.155), the stator currents $\bar{\bar{I}}_{ds}^{SFR}$ and $\bar{\bar{I}}_{qs}^{SFR}$ can be determined. However, there is another element in the inner control loop that affects the system.

The outputs of the two inner loop PI controllers of the rotor have a limiter to avoid over-reaction of the integral (section 3.1.5). The double frequency oscillations can be cut if their amplitudes are too large, as shown in Figure 3.11.

Because of this limiter, rotor currents $\bar{\bar{I}}_{dr}^{SFR}$ and $\bar{\bar{I}}_{qr}^{SFR}$ must be calculated first to check if the limiter will modify the signal. To study the impact of this limiter, the DC component at the outputs of the PI controllers is neglected. In SS (prefault or fault SS) the output of a PI controller is very close to zero.

Double grid frequency rotor currents

The peak value V_1 of the fundamental component (at twice the grid frequency) of the limited output (in green in Figure 3.11) is calculated by using the Fourier series expansion.

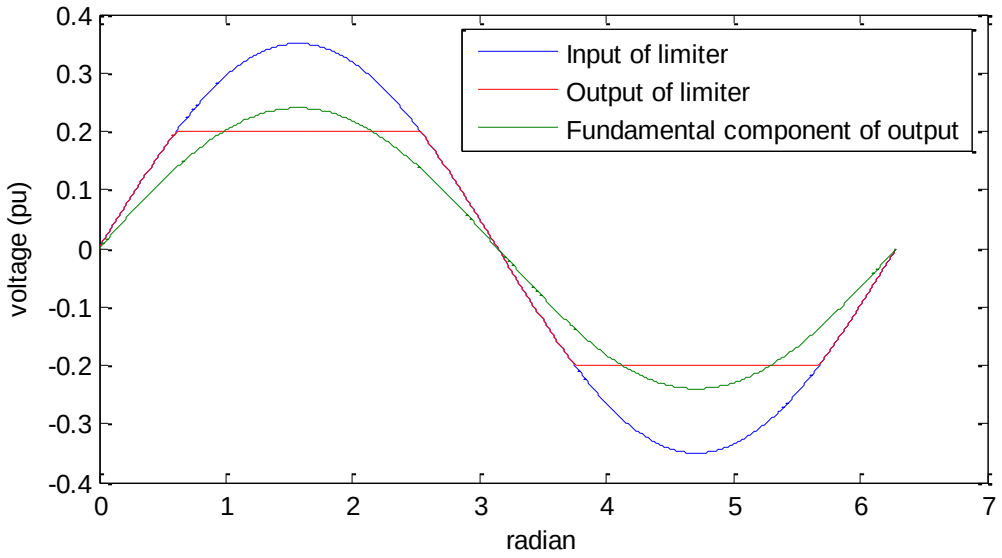

Figure 3.11 How the RSC inner loop PI limiter cuts oscillations.

With the variables as defined in Figure 3.12, the fundamental component is:

$$V_1 = \frac{2}{\pi}\left[V\alpha + V_{\text{lim}}\cos(\alpha)\right] \tag{3.160}$$

where V_{lim} is the limit of the limiter, V is the peak value of the input signal, and α is angle for which the input signal equals the limit (see Figure 3.12).

The procedure to obtain (3.160) is detailed in Appendix A.1.

If one or both signals (d and/or q) is corrected, the previous system of equations (3.150) to (3.155) must be modified accordingly.

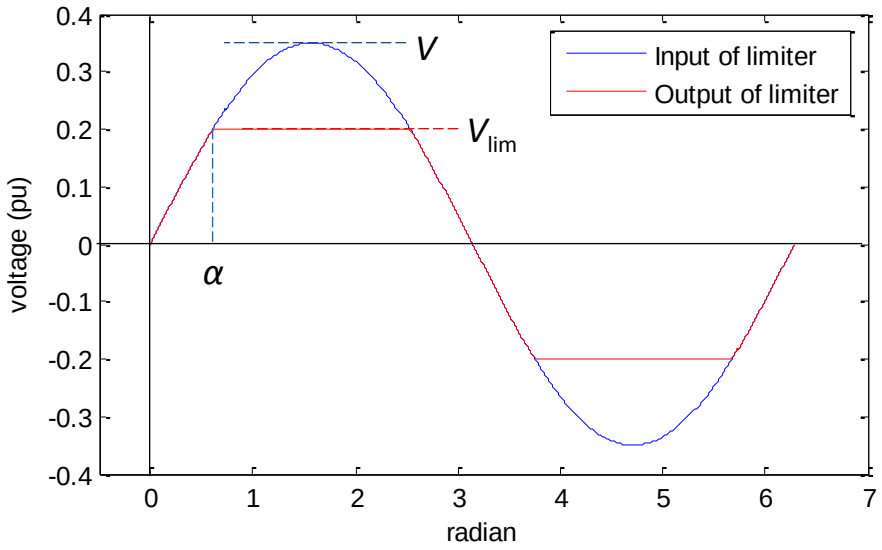

Figure 3.12 Inner loop PI limiter: α and $V_{\lim}$ definitions.

Here, the rotor currents are obtained from equations (3.150) to (3.155) by substitution. The details are given in Appendix A.2, and the results are as follows:

$$\bar{\bar{I}}_{dr}^{SFR} = K_{r1}\bar{\bar{V}}_{ds}^{SFR} + K_{r2}\bar{\bar{V}}_{qs}^{SFR} \tag{3.161}$$

$$\bar{\bar{I}}_{qr}^{SFR} = K_{r3}\bar{\bar{V}}_{ds}^{SFR} + K_{r4}\bar{\bar{V}}_{qs}^{SFR} \tag{3.162}$$

where K_{r1}, K_{r2}, K_{r3} and K_{r4} are complex coefficients depending only on machine resistances and inductances, slip, and control constant coefficients.

The input of the limiter is the output of the PI controller: $H_{PI}^{rd}\,\bar{\bar{I}}_{dr}^{SFR}$ for the d-axis, and $H_{PI}^{rq}\,\bar{\bar{I}}_{qr}^{SFR}$ for the q-axis. If $\left|H_{PI}^{rd}\,\bar{\bar{I}}_{dr}^{SFR}\right| > V_{\lim}$ and/or $\left|H_{PI}^{rq}\,\bar{\bar{I}}_{qr}^{SFR}\right| > V_{\lim}$, H_{PI}^{rd} and/or H_{PI}^{rq} are modified to force their outputs to match the limited signal. In this thesis, $V_{\lim} = 0.2$ pu. In other words, the goal is to have:

$$V_{out-d} = \left| H_{PI}^{rd-\lim} \bar{\bar{I}}_{dr}^{SFR} \right| \tag{3.163}$$

where V_{out-d} is the peak value of the fundamental component of the limiter output of the d-component. V_{out-d} is obtained with (3.160), and $H_{PI}^{rd-\lim}$ is the corrected gain of the d-axis PI controller.

Equations (3.163) to (3.166) concern the d-axis, however, the same principles apply to the q-axis as well. If $\left| H_{PI}^{rd} \bar{\bar{I}}_{dr}^{SFR} \right| > V_{\lim}$, then, by using (3.160), we get the following:

$$\left| H_{PI}^{rd-\lim} \bar{\bar{I}}_{dr}^{SFR} \right| = \frac{2}{\pi} \left[\left| H_{PI}^{rd} \bar{\bar{I}}_{dr}^{SFR} \right| \alpha + V_{\lim} \cos(\alpha) \right] \tag{3.164}$$

$$\left| H_{PI}^{rd-\lim} \right| = \frac{2}{\left| \bar{\bar{I}}_{dr}^{SFR} \right| \pi} \left[\left| H_{PI}^{rd} \bar{\bar{I}}_{dr}^{SFR} \right| \alpha + V_{\lim} \cos(\alpha) \right] \tag{3.165}$$

As the limiter does not induce any phase shift:

$$\begin{aligned} H_{PI}^{rd-\lim} &= \left| H_{PI-d}^{rot-\lim} \right| \exp\left(\mathrm{j} \cdot \mathrm{angle}\left(H_{PI}^{rd} \right) \right) \\ &= \frac{2}{\left| \bar{\bar{I}}_{dr}^{SFR} \right| \pi} \left[\left| H_{PI}^{rd} \bar{\bar{I}}_{dr}^{SFR} \right| \alpha + V_{\lim} \cos(\alpha) \right] \exp\left(\mathrm{j}\ \mathrm{angle}\left(H_{PI}^{rd} \right) \right) \end{aligned} \tag{3.166}$$

Similarly, for the q-axis:

$$H_{PI}^{rq-\lim} = \frac{2}{\left| \bar{\bar{I}}_{qr}^{SFR} \right| \pi} \left[\left| H_{PI}^{rq} \bar{\bar{I}}_{qr}^{SFR} \right| \alpha + V_{\lim} \cos(\alpha) \right] \exp\left(\mathrm{j}\ \mathrm{angle}\left(H_{PI}^{rq} \right) \right) \tag{3.167}$$

As a modification of the PI gains of the rotor inner loop impacts the coefficients K_{r1}, K_{r2}, K_{r3} and K_{r4}, equations (3.161) and (3.162) will give new AC components of rotor currents $\bar{\bar{I}}_{dr}^{SFR}$ and $\bar{\bar{I}}_{qr}^{SFR}$. Then an internal iterative loop is required, until the PI gains $H_{PI}^{rd-\lim}$ and $H_{PI}^{rq-\lim}$ converge, and therefore, $\bar{\bar{I}}_{dr}^{SFR}$ and $\bar{\bar{I}}_{qr}^{SFR}$.

If the limit is not reached, $H_{PI}^{rd-\lim}$ and $H_{PI}^{rq-\lim}$ are defined as the original gains:

$$H_{PI}^{rd-\lim} = H_{PI}^{rd}$$
$$H_{PI}^{rq-\lim} = H_{PI}^{rq} \tag{3.168}$$

Then (3.150) and (3.151) are replaced with:

$$\bar{\bar{V}}_{dr}^{SFR} = \left[\frac{-H_{PI}^{rd-\lim}}{\gamma^2} \bar{\bar{I}}_{dr}^{SFR} - sX_X \bar{\bar{I}}_{qr}^{SFR} \right] H_{filter}^{60} \tag{3.169}$$

$$\bar{\bar{V}}_{qr}^{SFR} = \left[\frac{-H_{PI}^{rq-\lim}}{\gamma^2} \bar{\bar{I}}_{qr}^{SFR} + s\left(X_{rr} \bar{\bar{I}}_{dr}^{SFR} + X_m \bar{\bar{I}}_{ds}^{SFR} H_{filter}^{60} \right) \right] H_{filter}^{60} \tag{3.170}$$

The next step is to calculate the stator currents from equations (3.152) to (3.155) and by using (3.169) and (3.170):

$$\bar{\bar{I}}_{ds}^{SFR} = K_{s1} \bar{\bar{V}}_{ds}^{SFR} + K_{s2} \bar{\bar{V}}_{qs}^{SFR} \tag{3.171}$$

$$\bar{\bar{I}}_{qs}^{SFR} = K_{s3} \bar{\bar{V}}_{ds}^{SFR} + K_{s4} \bar{\bar{V}}_{qs}^{SFR} \tag{3.172}$$

The substitution method is also used to obtain K_{s1}, K_{s2}, K_{s3} and K_{s4}. The details are given in Appendix A.3. The coefficients K_{s1}, K_{s2}, K_{s3} and K_{s4} depend only on machine resistances and inductances, slip, and control constant coefficients and the corrected PI gains.

The twice the grid frequency phasors of d and q stator currents in the flux reference frame have been defined. The last step is to express those currents in the voltage reference frame using the flux angle and then to convert these dq domain phasors into the negative sequence phasor at grid frequency.

$$\bar{\bar{I}}_{ds}^{SVR} = -\left[\bar{\bar{I}}_{ds}^{SFR} \cos(-\varphi_{flux}) + \bar{\bar{I}}_{qs}^{SFR} \sin(-\varphi_{flux}) \right] \tag{3.173}$$

$$\bar{\bar{I}}_{qs}^{SVR} = -\left[\bar{\bar{I}}_{qs}^{SFR} \cos(-\varphi_{flux}) - \bar{\bar{I}}_{ds}^{SFR} \sin(-\varphi_{flux}) \right] \tag{3.174}$$

It is reminded that the current direction in the SVR is from the stator to the grid and that φ_{flux} should be negative. The theoretical value of φ_{flux} is –90°.

The negative sequence stator current phasor at grid frequency is:

$$\bar{I}_s^- = \left|\bar{I}_s^-\right| \angle \varphi_{Is}^- \tag{3.175}$$

with

$$\left|\bar{I}_s^-\right| = \frac{1}{2}\sqrt{\left|\bar{\bar{I}}_{ds}^{SVR}\right|^2 + \left|\bar{\bar{I}}_{qs}^{SVR}\right|^2 - 2\left|\bar{\bar{I}}_{ds}^{SVR}\right|\left|\bar{\bar{I}}_{qs}^{SVR}\right|\sin\left(\varphi_{Ids}^{SVR} - \varphi_{Iqs}^{SVR}\right)} \tag{3.176}$$

$$\varphi_{Is}^- = \arctan\left(\frac{\left|\bar{\bar{I}}_{ds}^{SVR}\right|\sin\left(\varphi_{Ids}^{SVR}\right) - \left|\bar{\bar{I}}_{qs}^{SVR}\right|\cos\left(\varphi_{Iqs}^{SVR}\right)}{\left|\bar{\bar{I}}_{ds}^{SVR}\right|\cos\left(\varphi_{Ids}^{SVR}\right) + \left|\bar{\bar{I}}_{qs}^{SVR}\right|\sin\left(\varphi_{Iqs}^{SVR}\right)}\right) \tag{3.177}$$

where

$$\begin{aligned} \varphi_{Ids}^{SVR} &= \text{angle}\left(\bar{\bar{I}}_{ds}^{SVR}\right) \\ \varphi_{Iqs}^{SVR} &= \text{angle}\left(\bar{\bar{I}}_{qs}^{SVR}\right) \end{aligned} \tag{3.178}$$

The details of this result are presented in Appendix A.4.

3.3.4 GSC currents

The active part of the positive sequence GSC current depends on all other active power transfers to the DC-link. The goal of the GSC is to keep the voltage of the DC-link constant. Those other active power transfers come from the negative sequence active power on the GSC, and the active power on the RSC related to the DC and AC components in dq domain. These three elements are described in the following bulleted list.

- To obtain the negative sequence active power flow in the GSC we use the equation:

$$\bar{I}_g^- = Y_g^- \bar{V}_{pgc}^- \tag{3.179}$$

where Y_g^- is the constant of proportionality between the negative sequence GSC current and the PGC voltage. The negative sequence behavior of the GSC of a type-III WTG is similar to that of a type-IV WTG with coupled control. The calculations of Y_g^- was carried out in section 2.2.4.

It follows that the negative sequence active power flow at the GSC is given by:

$$P_{GSC}^- = \text{real}\left(\bar{V}_{conv}^-\left(\bar{I}_g^-\right)^*\right) = \text{real}\left(\left[\bar{V}_{pgc}^- + \left(R + jX\right)\bar{I}_g^-\right]\left(\bar{I}_g^-\right)^*\right) \tag{3.180}$$

where $R + jX$ is the choke impedance at the nominal frequency of the GSC, $\bar{V}_{conv}^{-}$ is the negative sequence voltage at the terminal of the GSC.

- The DC components of the rotor currents were determined in the previous section. The rotor voltages are calculated based on the equations of the inner loop. This calculation is the same as the one in the simple model, with (3.82), (3.84) and (3.85):

$$V_{dr}^{SFR} = -s\left(X_{lr} + X_{ls}/\gamma\right) I'^{SFR}_{qr}$$

$$V_{qr}^{SFR} = s\left(\left(X_{lr} + X_m\right) I'^{SFR}_{dr} + X_m I'^{SFR}_{ds}\right)$$

The active power transferred from the RSC to the rotor is:

$$P_{RSC}^{+} = V_{dr}^{SFR} I'^{SFR}_{dr} + V_{qr}^{SFR} I'^{SFR}_{qr}$$

The symbol "+" is used because this only corresponds to the DC component of the dq signals. Here we cannot say "positive sequence" because the order of the phases depends on the slip of the machine.

- The oscillations in rotor voltage and rotor current create also an active power transfer between the rotor and the RSC: P_{RSC}^{-}. The instantaneous power transferred through the RSC is:

$$\begin{aligned} P_{RSC}(t) &= v_{dr}^{SFR}(t) i_{dr}^{SFR}(t) + v_{qr}^{SFR}(t) i_{qr}^{SFR}(t) \\ &= \left[V_{dr}^{SFR} + \left|\bar{\bar{V}}_{dr}^{SFR}\right| \cos\left(2\omega t + \varphi_{Vdr}^{SFR}\right)\right]\left[I'^{SFR}_{dr} + \left|\bar{\bar{I}}_{dr}^{SFR}\right| \cos\left(2\omega t + \varphi_{Idr}^{SFR}\right)\right] + \\ &\left[V_{qr}^{SFR} + \left|\bar{\bar{V}}_{qr}^{SFR}\right| \cos\left(2\omega t + \varphi_{Vqr}^{SFR}\right)\right]\left[I'^{SFR}_{qr} + \left|\bar{\bar{I}}_{qr}^{SFR}\right| \cos\left(2\omega t + \varphi_{Iqr}^{SFR}\right)\right] \end{aligned} \quad (3.181)$$

where

$$\begin{aligned} \varphi_{Idr}^{SVR} &= \text{angle}\left(\bar{\bar{I}}_{dr}^{SVR}\right) & \varphi_{Vdr}^{SVR} &= \text{angle}\left(\bar{\bar{V}}_{dr}^{SVR}\right) \\ \varphi_{Iqr}^{SVR} &= \text{angle}\left(\bar{\bar{I}}_{qr}^{SVR}\right) & \varphi_{Vqr}^{SVR} &= \text{angle}\left(\bar{\bar{V}}_{qr}^{SVR}\right) \end{aligned} \quad (3.182)$$

The active power is the average value or the DC component of (3.181). After simplification, it becomes:

$$P_{RSC} = V_{dr}^{SFR} I_{dr}'^{SFR} + V_{qr}^{SFR} I_{qr}'^{SFR} + \left|\bar{\bar{V}}_{dr}^{SFR}\right|\left|\bar{\bar{I}}_{dr}^{SFR}\right| \frac{\cos\left(\varphi_{Vdr}^{SFR} - \varphi_{Idr}^{SFR}\right)}{2} + \left|\bar{\bar{V}}_{qr}^{SFR}\right|\left|\bar{\bar{I}}_{qr}^{SFR}\right| \frac{\cos\left(\varphi_{Vqr}^{SFR} - \varphi_{Iqr}^{SFR}\right)}{2} \quad (3.183)$$

where the first part corresponds to the active power from the DC parts: P_{RSC}^{+} (see (3.85)), and the second part corresponds to the active power from the AC parts of the dq components:

$$P_{RSC}^{-} = \left|\bar{\bar{V}}_{dr}^{SFR}\right|\left|\bar{\bar{I}}_{dr}^{SFR}\right| \frac{\cos\left(\varphi_{Vdr}^{SFR} - \varphi_{Idr}^{SFR}\right)}{2} + \left|\bar{\bar{V}}_{qr}^{SFR}\right|\left|\bar{\bar{I}}_{qr}^{SFR}\right| \frac{\cos\left(\varphi_{Vqr}^{SFR} - \varphi_{Iqr}^{SFR}\right)}{2} \quad (3.184)$$

This active power is transferred from the RSC to the rotor.

Finally, using (3.180), (3.85) and (3.184), the active part of the current flowing from the GSC to the grid is obtained as:

$$\hat{I}_{dg}^{SVR} = \left(P_{GSC}^{-} - P_{RSC}^{+} - P_{RSC}^{-}\right) / \left|\bar{V}_{pgc}^{+}\right| \quad (3.185)$$

The GSC reactive current calculation and the GSC current limiter are the same as those for the DFIG simple model. Please refer to equations (3.89) to (3.93).

3.3.5 Flux angle and turbine currents

Once all rotor and stator currents have been determined, φ_{flux} can be updated. Using (3.186) and (3.187), the stator currents before the flux angle shift can be calculated. The same is done for rotor currents. Then the equation corresponding to Figure 3.3 is applied to calculate the new φ_{flux}.

$$I_{ds}'^{SVR} = -\left[I_{ds}'^{SFR}\cos\left(-\varphi_{flux}\right) + I_{qs}'^{SFR}\sin\left(-\varphi_{flux}\right)\right] \quad (3.186)$$

$$I_{qs}'^{SVR} = -\left[I_{qs}'^{SFR}\cos\left(-\varphi_{flux}\right) - I_{ds}'^{SFR}\sin\left(-\varphi_{flux}\right)\right] \quad (3.187)$$

$$I_{dr}'^{SVR} = I_{dr}'^{SFR}\cos\left(-\varphi_{flux}\right) + I_{qr}'^{SFR}\sin\left(-\varphi_{flux}\right) \quad (3.188)$$

$$I_{qr}'^{SVR} = I_{qr}'^{SFR}\cos\left(-\varphi_{flux}\right) - I_{dr}'^{SFR}\sin\left(-\varphi_{flux}\right) \quad (3.189)$$

$$\varphi_{flux} = \text{angle}\left[-I'^{SVR}_{ds} + I'^{SVR}_{dr} + j\left(-I'^{SVR}_{qs} + I'^{SVR}_{qr} \right) \right] \tag{3.190}$$

As this flux angle will affect the earlier calculations of this detailed model (see (3.135) and (3.136)), all of the calculations performed thus far will have to be repeated. Such repetitions will be continued until the flux angle converges. This requires an iterative loop.

Once the convergence of this flux angle has been achieved, the current contribution of the type-III WTG can be obtained. The current of the turbine is calculated as the sum of the GSC and the stator currents:

$$\bar{I}^{+}_{tb} = \left[I'^{SVR}_{ds} + I'^{SVR}_{dg} + j\left(I'^{SVR}_{qs} + I'^{SVR}_{qg} \right) \right] \exp\left[j\,\text{angle}\left(\bar{V}^{+}_{pgc} \right) \right] \tag{3.191}$$

$$\bar{I}^{-}_{tb} = \bar{I}^{-}_{s} + \bar{I}^{-}_{g} \tag{3.192}$$

Appendix B presents the algorithm reproducing this complete DFIG model.

3.4 Negative sequence gain to obtain $\bar{I}^{-}_{s}$

The previous section considers the impact of the limiter at the output of the PI controllers of the RSC inner control loops. If there is no limiter or the limit is high or the negative sequence voltage at the PGC is low, then this limiter will have no impact on the negative sequence response of the machine.

Then the system of six equations and six unknowns (equations (3.150) to (3.155)) is solved directly to obtain the AC components of the dq components of the stator current: $\bar{\bar{I}}^{SFR}_{ds}$ and $\bar{\bar{I}}^{SFR}_{qs}$. Equations (3.156) to (3.159) give the relations among the stator negative sequence voltage phasor $\bar{V}^{-}_{s}$ and the voltages $\bar{\bar{V}}^{SFR}_{ds}$ and $\bar{\bar{V}}^{SFR}_{qs}$. To solve the system and to obtain $\bar{\bar{V}}^{SFR}_{ds}$ and $\bar{\bar{V}}^{SFR}_{qs}$, the flux angle is required. The theoretical value of this angle is –90° and can be used. Alternatively, the flux angle can be estimated by running the solver in section 4.1.2 with prefault conditions.

After solving the previous system, the rotor currents $\bar{\bar{I}}_{ds}^{SFR}$ and $\bar{\bar{I}}_{qs}^{SFR}$ can be written as:

$$\bar{\bar{I}}_{ds}^{SFR} = \bar{V}_s^- Y_{ds}^{SFR} \tag{3.193}$$

$$\bar{\bar{I}}_{qs}^{SFR} = \bar{V}_s^- Y_{qs}^{SFR} \tag{3.194}$$

where Y_{ds}^{SFR} and Y_{qs}^{SFR} are complex constants which only depends on resistances and inductances of the machine, the complex gains of the RSC inner loop controllers, the slip and the measurement filter complex gain.

Equations (3.193) and (3.194) imply the equations below for the angles of the variables involved. The angles are denoted by φ, and the sub- and super-scripts indicate the corresponding variables:

$$\varphi_{Ids}^{SFR} = \varphi_{Vs}^- + \varphi_{Yds}^{SFR} \tag{3.195}$$

$$\varphi_{Iqs}^{SFR} = \varphi_{Vs}^- + \varphi_{Yqs}^{SFR} \tag{3.196}$$

From $\bar{\bar{I}}_{ds}^{SFR}$ and $\bar{\bar{I}}_{qs}^{SFR}$, the negative sequence stator current is calculated using the dq-to-abc transformation (Appendix A.4):

$$\left|\bar{I}_s^-\right| = \frac{1}{2}\sqrt{\left|\bar{\bar{I}}_{ds}^{SFR}\right|^2 + \left|\bar{\bar{I}}_{qs}^{SFR}\right|^2 - 2\left|\bar{\bar{I}}_{ds}^{SFR}\right|\left|\bar{\bar{I}}_{qs}^{SFR}\right|\sin\left(\varphi_{Ids}^{SFR} - \varphi_{Iqs}^{SFR}\right)} \tag{3.197}$$

$$\varphi_{Is}^- = \arctan\left(\frac{\left|\bar{\bar{I}}_{qs}^{SFR}\right|\sin\left(\varphi_{Iqs}^{SFR}\right) + \left|\bar{\bar{I}}_{ds}^{SFR}\right|\cos\left(\varphi_{Ids}^{SFR}\right)}{\left|\bar{\bar{I}}_{qs}^{SFR}\right|\cos\left(\varphi_{Iqs}^{SFR}\right) - \left|\bar{\bar{I}}_{ds}^{SFR}\right|\sin\left(\varphi_{Ids}^{SFR}\right)}\right) \tag{3.198}$$

where φ_{Is}^- is the phase angle of the negative sequence current flowing from the stator to the grid.

By substituting equation (3.193) into equation (3.196):

$$\left|\bar{I}_s^-\right| = \frac{\left|\bar{V}_s^-\right|}{2}\sqrt{\left|Y_{ds}^{SFR}\right|^2 + \left|Y_{qs}^{SFR}\right|^2 - 2\left|Y_{ds}^{SFR}\right|\left|Y_{qs}^{SFR}\right|\sin\left(\varphi_{Yds}^{SFR} - \varphi_{Yqs}^{SFR}\right)} \tag{3.199}$$

$$\varphi_{Is}^- = \varphi_{Vs}^- + \arctan\left(\frac{\left|Y_{qs}^{SFR}\right|\sin\left(\varphi_{Yqs}^{SFR}\right) + \left|Y_{ds}^{SFR}\right|\cos\left(\varphi_{Yds}^{SFR}\right)}{\left|Y_{qs}^{SFR}\right|\cos\left(\varphi_{Yqs}^{SFR}\right) - \left|Y_{ds}^{SFR}\right|\sin\left(\varphi_{Yds}^{SFR}\right)}\right) \tag{3.200}$$

From equations (3.199) and (3.200), we obtain an admittance relating the negative sequence voltage to the negative sequence current:

$$\bar{I}_s^- = \bar{V}_s^- Y_s^- \quad \text{with} \quad Y_s^- = \left|Y_s^-\right| \angle \varphi_{Ys}^- \tag{3.201}$$

$$\left|Y_s^-\right| = \frac{1}{2}\sqrt{\left|Y_{ds}^{SFR}\right|^2 + \left|Y_{qs}^{SFR}\right|^2 - 2\left|Y_{ds}^{SFR}\right|\left|Y_{qs}^{SFR}\right|\sin\left(\varphi_{Yds}^{SFR} - \varphi_{Yqs}^{SFR}\right)} \tag{3.202}$$

$$\varphi_{Ys}^- = \arctan\left(\frac{\left|Y_{qs}^{SFR}\right|\sin\left(\varphi_{Yqs}^{SFR}\right) + \left|Y_{ds}^{SFR}\right|\cos\left(\varphi_{Yds}^{SFR}\right)}{\left|Y_{qs}^{SFR}\right|\cos\left(\varphi_{Yqs}^{SFR}\right) - \left|Y_{ds}^{SFR}\right|\sin\left(\varphi_{Yds}^{SFR}\right)}\right) \tag{3.203}$$

The coefficient Y_s^- gives a direct relation between the negative sequence stator current and voltage. If there is no PI limiter, Y_s^- replaces the complex procedure of 3.2.3. A LF solver can use this coefficient to calculate the negative sequence current of a type-III WTG in an unbalanced network.

Impact of machine and control parameters on Y_s^-

To observe the impact of the input parameters on Y_s^-, variations are applied around the default parameters taken from CHAPTER 4.

Table 3.1 presents the impact of the measurement filter and the PI controllers of the RSC inner loop on Y_s^-. To fill this table, the slip is equal to –0.2 (slip for nominal active power production), and the machine parameters are:

$R_s = 0.033\,pu$ $\quad X_{ls} = 0.18\,pu$ $\quad X_m = 2.9\,pu$

$R_r = 0.026\,pu$ $\quad X_{lr} = 0.16\,pu$

The proportional and the integral gains of the RSC inner loop PI controllers are calculated on the basis of the time response of the inner loop [37]:

$$\alpha_c = \frac{\ln(9)}{t_{rise}^{RSC}\,\omega_s} \tag{3.204}$$

where ω_s is the nominal angular frequency of the grid (in rad/s), and t_{rise}^{RSC} is the response time of the RSC inner loop.

$$\begin{aligned} K_I^r &= \alpha_c X_\sigma \\ K_P^r &= \alpha_c R_R \omega_s \end{aligned} \tag{3.205}$$

We also remind equation (3.2) as follows: $R_R = \gamma^2 R_r$ and $X_\sigma = \gamma X_{ls} + \gamma^2 X_{lr}$.

Table 3.1 shows that the gain of the measurement filter H_{filter} has little impact on Y_s^-, and that $H_{PI}^{rd} \left(= H_{PI}^{rq}\right)$ has little impact on the magnitude of Y_s^- but more on the angle.

Table 3.1 Impact of control parameters on Y_s^-.

Y_s^-	t_{rise}^{RSC} = 10 ms	15 ms	40 ms
angle(H_{filter}) = –1°	2.929 (112.3)	3.013 (107.9)	3.089 (102.0)
= –4°	2.952 (113.6)	3.031 (109.1)	3.098 (103.1)

Table 3.2 presents the impact of the machine parameters using t_{rise}^{RSC} = 15ms and angle(H_{filter}) = –1°. Each column gives a different X_m, and each row gives a different magnitude of the total series impedance $Z_{series} = R_s + R_r + j\left(X_{ls} + X_{lr}\right)$ of the machine. The angle of this impedance Z_{series} and the ratio between the stator and rotor values are kept constant based on the ones used in Table 3.1.

Table 3.2 shows that X_m also has a little impact on Y_s^-. From Table 3.1 and Table 3.2, we see that the magnitude of the series impedance (winding resistances and leakage inductances) has the highest impact on Y_s^-. The higher is the series impedance of machine, the lower is Y_s^- and the negative sequence current.

Table 3.2 Impact of machine parameters on Y_s^-.

Y_s^-	X_m = 2 pu	2.9 pu	5 pu
$\lvert Z_{series} \rvert$ = 0.2 pu	5.180 (108.1)	5.147 (108.6)	5.108 (109.4)
0.345 pu	3.042 (107.3)	3.013 (107.9)	2.983 (108.6)
0.6 pu	1.787 (106.2)	1.760 (106.9)	1.733 (107.8)

Simple model

To have a simpler model, some approximations are applied to the coefficients Y_{ds}^{SFR} and Y_{qs}^{SFR}. The phase shift of the measurement filter is neglected, as well as the resistances of the machine. The inner loop PI gain is low and considered as zero. And the stator and rotor leaking reactances are much smaller than the magnetizing one:

$$\begin{aligned} &H_{PI}^{rq} = H_{PI}^{rd} \approx 0 && H_{filter} \approx 1 \\ &R_s \approx 0 && R_r \approx 0 \\ &X_m >> X_{ls} && X_m >> X_{lr} \end{aligned} \tag{3.206}$$

After these approximations, Y_s^- becomes:

$$\frac{-1}{Y_s^-} \approx j\left(X_{ls} + X_{lr}\right) \tag{3.207}$$

The minus sign appears because $\bar{I}_s^-$ in (3.201) is the current flowing from the stator to the grid. This means that the stator behaves like a passive inductance for negative sequence.

After several EMT simulations, and calculations of the Y_s^- using TD results, it appears that the real part of Y_s^- is nonzero. The proposed approximation is updated empirically to add a real part:

$$\frac{-1}{Y_s^-} \approx R_s + R_r + j\left(X_{ls} + X_{lr}\right) \tag{3.208}$$

This justifies the expression (3.86) in the section 3.2.3.

3.5 Conclusion

This chapter described the type-III WTG by using the EMT model. This model has various control possibilities:

- control under normal conditions (reactive power, voltage or power factor), plus the FRT mode,
- P- or Q-priority.

The above control configurations, and the behavior of the WTG are translated into two phasor models to calculate the current contribution of the WTG. The first model is a simplified one and gives the structure of the control system and how the current contribution is calculated. The second model considers all details of the controller, and removes the approximations done in the simple one. The complete model is more complex and requires more details about the controller, but it is also more precise (section 4.5.1 in the next chapter). These two models are summarized as two algorithms which calculate the current contribution of the type-III WTG based on the voltage at the PGC.

Finally, an intermediate model for the stator negative sequence current is proposed. This last one can be implemented in an unbalanced LF solver to represent the negative sequence behavior of type-III WTGs.

CHAPTER 4 STEADY-STATE SOLVER, SIMULATIONS AND VALIDATIONS

In CHAPTER 2 and CHAPTER 3, the SS response of WPs in terms of current injection as a function of terminal voltages is developed in phasor domain. In this chapter, the behavioral models developed in phasor domain are used to perform system level SS SC studies.

The first section proposes an iterative method to carry out SC studies using the previously proposed WTG models. Sections 4.2 and 4.3 present the two test cases used for simulation studies of this chapter. Finally, this chapter cross-examines the proposed SS models against detailed TD models and simulations within EMTP-RV.

4.1 Development of a functional short-circuit solver

The goal of the solver is to give the SS fault behavior of FSC- and DFIG-type ECGs in a network. The solver should be able to accomodate different control schemes and the possible change of control mode under fault conditions such as switching to FRT mode.

4.1.1 Solver structure

The main steps of the SC solver are shown in Table 4.1 and described afterwards.

Table 4.1 List of the four main steps of the SC solver.

Step	Desciption
1	Run the LF solver
2	Linearize the network from the LF results to build the SS system
3	Apply fault
4	Run the SS solver and update the current contributions of the ECGs iteratively until convergence

The LF solver and the SS solver are built using the modified-augmented-nodal-analysis (MANA) approach [24] which augments the classical nodal equations with supplementary component equations, i.e., switches and transformers. It should be noted that both solvers function in phase domain. The LF and SS solvers are implemented in MATLAB. The LF solver is not mandatory for SC studies but it is applied in this thesis to specify initial conditions.

The LF solver uses Newton's method to find the network states respecting all the predefined constraints. The non-linear constraints are mainly the active and reactive powers (PQ), the active power and voltage magnitude (PV), and the voltage magnitude and angle (slack bus). The LF solver performs a multiphase LF where the ECGs are represented with PQ constraints at the PGC (Figure 4.1). The LF solution is the prefault state of the network. This solution provides the inputs to the prefault calculations of the type-III and type-IV WTG SS models.

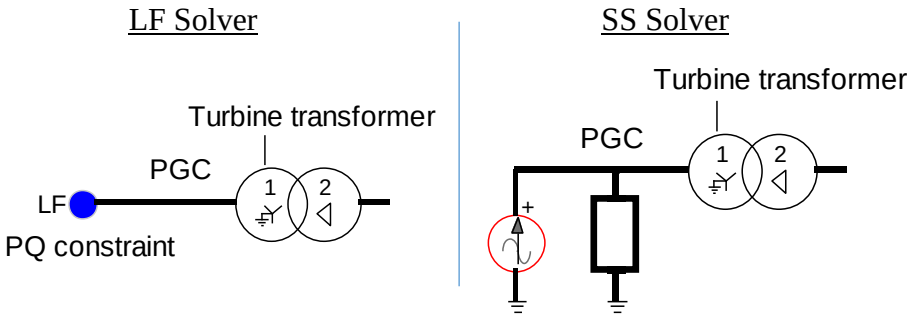

Figure 4.1 ECG representation in the LF and the SS solver.

The SS solver consists of a linear representation of the network. This system is written under the form $\mathbf{A}\,\mathbf{x} = \mathbf{b}$ where $\mathbf{A}$ is the MANA matrix, $\mathbf{b}$ is the vector containing the currents of the current sources and the voltages of the voltage sources, and $\mathbf{x}$ is the vector of unknowns ,i.e., the voltage of each node, the currents of voltage sources and the currents of switches. The SS system is built by linearizing all the non-linear elements using the LF solution:

- The loads are replaced with constant impedances using the LF voltage.
- The slack bus, generators with PV and PQ constraints are replaced with Thevenin equivalents.
- The ECGs are replaced with a current source in parallel with shunt filters (Figure 4.1). This equivalent circuit is used for both type-III and and type-IV WTGs.

The currents of the current source in Figure 4.1 are calculated as:

$$\bar{I}_{cs}^{j} = \bar{I}_{pgc,LF}^{j} - \bar{V}_{pgc,LF}^{j} \Big/ Z_{filter} \tag{4.1}$$

where $\bar{I}_{cs}^{j}$ is the current of the current source with the convention indicated on Figure 4.1, $\bar{I}_{pgc,LF}^{j}$ is the current obtained from the LF, flowing from the PGC into the turbine transformer, and $\bar{V}_{pgc,LF}^{j}$ is the PGC voltage obtained from the LF for phase j ($j = a,b,c$).

In this SS system, the SC conditions are added with switches for any type and number of simultaneous shunt or series faults [55] [56].

Because of the current limiters and other limiters inside the controllers, the behaviors of type-III and type-IV WTGs are not linear. To solve this non-linear system, an iterative approach is used. At each iteration, the current sources representing the WTGs are updated ($\bar{I}_{ecg}^{+}$ and $\bar{I}_{ecg}^{-}$ in Figure 4.2) according to the PGC voltage phasors ($\bar{V}_{pgc}^{+}$ and $\bar{V}_{pgc}^{-}$) using the algorithms of CHAPTER 2 and CHAPTER 3. Then, the network system is solved to obtain the new voltages. Consequently, at each iteration, only the **b** vector is updated and the **A** matrix does not need refactorization (fixed point method).

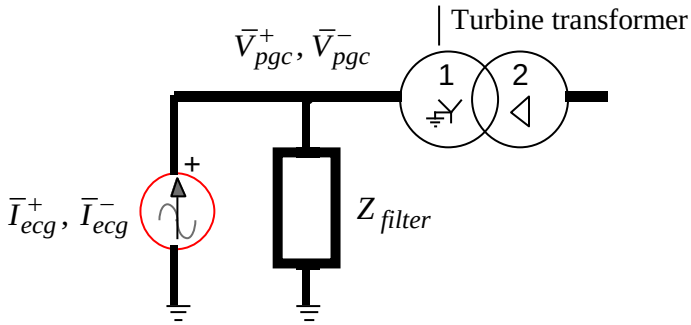

Figure 4.2 Currents and voltages exchanged during the SC iterative process.

In Figure 4.2, $\bar{I}_{ecg}^{+}$ and $\bar{I}_{ecg}^{-}$ correspond, respectively, to $\bar{I}_{g}^{+}$ and $\bar{I}_{g}^{-}$ for a type-IV WTG, and to $\bar{I}_{tb}^{+}$ and $\bar{I}_{tb}^{-}$ for a type-III WTG.

The ECGs were also modeled using a voltage source behind the choke impedance. But this resulted in a significantly larger number of iterations for most cases tested; therefore, the current source model was retained.

An arbitrary solver built in sequence domain can also be used since the WTGs are modeled with controlled current sources, and the currents computed using the SS models are composed of sequence components. The sequence and the phase approaches are equivalent if the network is balanced. In this thesis, the solver is implemented in phase domain together with a multiphase LF solver to provide a generic platform that can be also used for unbalanced systems such as distribution networks.

4.1.2 Functional solver for current contribution of type-III and -IV WTGs

The solver algorithm computes the current contributions of all WPs present in the network during fault in the network. The solver uses the SS solution of the previous section and the algorithms detailed in the two previous chapters: section 2.3 for the type-IV model, section 3.2.4 for the simple type-III model, and Appendix B for the detailed type-III model. In this section, the expression “WTG algorithm” refers to one of these algorithms.

Figure 4.3 illustrates with a flowchart the different steps of the solver. In the following description, the expressions in curly brackets {} refer to the blocks of Figure 4.3.

The solver starts with the initialization step, the top left block in Figure 4.3. The initial conditions of the network can be either determined by running LF or simply from nominal state. Then, using the initial state of the network, the ECG currents are initialized, and the network is transformed into its linear equivalent. Afterwards, the linearized network is subjected to a fault {Apply Fault}, and solved for voltages in the presence of the fault {SC Network Solution (prefault currents)}.

The new network voltages are used to update the ECG currents {Update Wind/Solar SC Model Current Injection}. The network is resolved for voltages using the updated ECG currents {SC Network Solution}.

At this step, the positive and negative sequence voltage magnitudes at the PGC of each WP are compared with previous iteration. If the magnitude variation is above a threshold ε for either the positive or the negative sequence voltage, the current contributions of all ECGs are updated, and the new network voltages are calculated. This procedure is repeated until the voltage magnitudes converge, i.e., the variation compared to the previous iteration is below ε for all WPs. Under this condition, convergence is reached{Convergence?}. This procedure is called the first iterative loop.

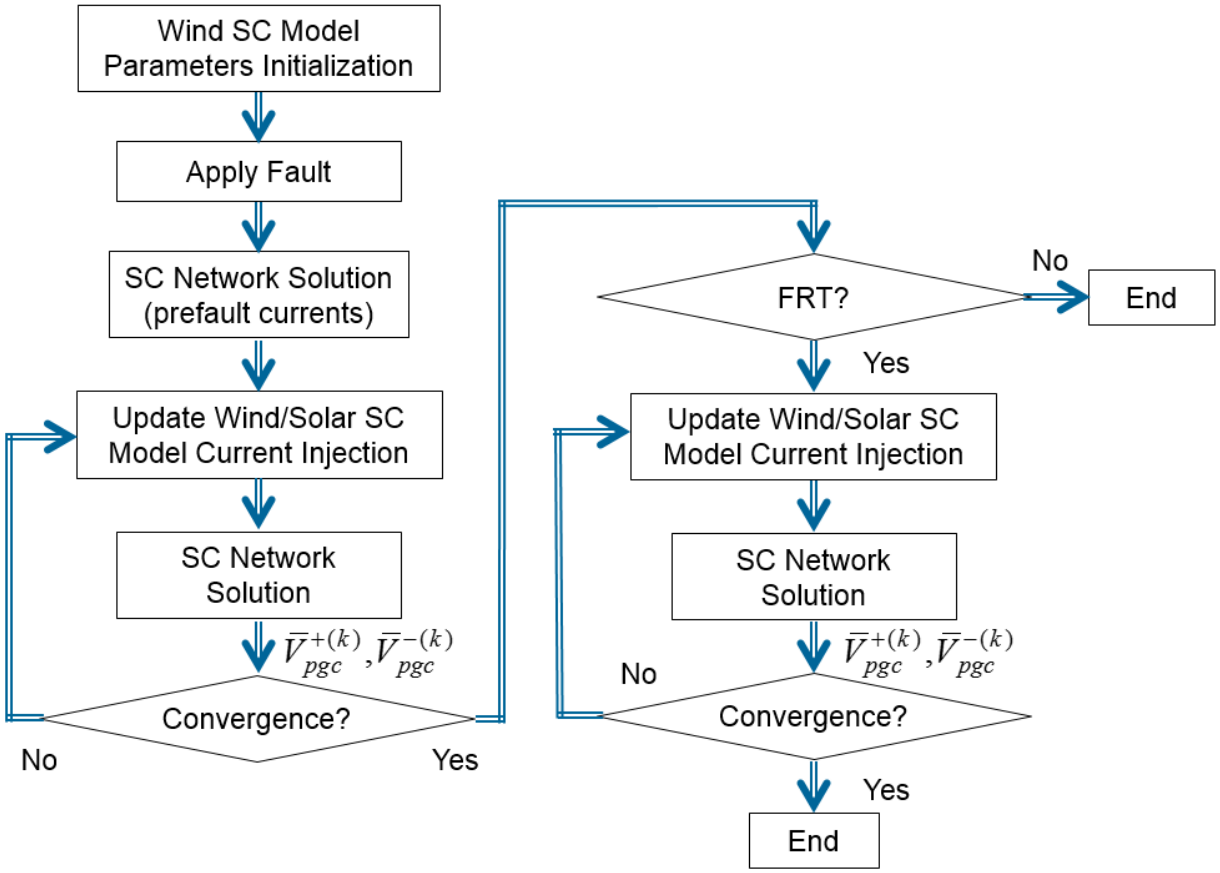

Figure 4.3 Block diagram of the solver.

This is a fixed-point approach and it is useful to apply a decelerator to assure convergence and avoid brusque variations in WTG currents. In this thesis, the moving average is applied when updating WTG currents: variation limiters in the WTG algorithms.

During this first loop, all WPs function under their prefault control modes. If one or several WPs have an FRT mode available and the FRT conditions are fulfilled, those WPs change their control

to FRT {FRT?}. If no WPs change modes, the last calculated variables correspond to the final results of the solver.

If one of the WPs changes to FRT mode, a second loop starts. The current contributions of all WPs are updated {Update Wind/Solar SC Model Current Injection} and the SS solver calculates the new network voltages {SC Network Solution}. The same convergence criteria are applied for the second loop. After the convergence of this second loop, the final solution is obtained.

The solver variables not defined yet are described below:

ε	the tolerance for the convergence of iterative loops,
V_{FRT-ON}	the voltage deviation from 1pu which activates the FRT mode (if available). For example, in Figure 2.5, $V_{FRT-ON} = 0.1\text{pu}$,
n	the maximum number of iterations, to avoid infinite loops,
k	index k denotes the value of a variable in the k-th iteration,
loop	loop counter,
control	control mode of one WP,
Δ	refers to the magnitude difference between two phasors,
convergence	= 0 at the beginning of a loop, =1 when convergence is reached.

SOLVER

Solve the network with prefault conditions (SS solution with or without LF)

FOR all WPs

Run the prefault calculations (see the FSC and DFIG algorithms)

END

The fault conditions are applied: the switches representing faults in the MANA matrix **A** are switched.

$k = 0$

loop = 0

convergence = 0

LOOP

$k = k + 1$

Perform network calculation using $\bar{I}_{ecg}^{+(k-1)}$ and $\bar{I}_{ecg}^{-(k-1)}$ for each WP. Thus $\bar{V}_{pgc}^{+(k)}$ and $\bar{V}_{pgc}^{-(k)}$ for each WP are obtained.

FOR each WP

Calculate the magnitude difference with the previous iteration PGC sequence voltages,

$$\Delta V_{pgc}^{+(k)} = \left|\bar{V}_{pgc}^{+(k)}\right| - \left|\bar{V}_{pgc}^{+(k-1)}\right|, \quad \Delta V_{pgc}^{-(k)} = \left|\bar{V}_{pgc}^{-(k)}\right| - \left|\bar{V}_{pgc}^{-(k-1)}\right| \tag{4.2}$$

IF $\{\left|\Delta V_{pgc}^{+(k)}\right| < \varepsilon$ **AND** $\left|\Delta V_{pgc}^{-(k)}\right| < \varepsilon\ \}$

$$\bar{I}_{ecg}^{+(k)} = \bar{I}_{ecg}^{+(k-1)} \text{ and } \bar{I}_{ecg}^{-(k)} = \bar{I}_{ecg}^{-(k-1)} \tag{4.3}$$

convergence = 1

ELSE

IF {DFIG-type ECG}

Run the DFIG algorithm in section 3.2.4 (simple) or B.1 (complete)

$$\bar{I}_{ecg}^{+(k)} = \bar{I}_{tb}^{+(k)} \text{ and } \bar{I}_{ecg}^{-(k)} = \bar{I}_{tb}^{-(k)} \tag{4.4}$$

ELSE {FSC-type ECG}

Run the FSC algorithm in section 2.3

$$\bar{I}_{ecg}^{+(k)} = \bar{I}_{g}^{+(k)} \text{ and } \bar{I}_{ecg}^{-(k)} = \bar{I}_{g}^{-(k)} \tag{4.5}$$

END

END

END

IF {convergence = 1 for all WPs}

EXIT LOOP

IF {k > n}

EXIT LOOP *(the algorithm does not converge)*

END

END LOOP

loop = loop + 1

IF {loop = 1}

FOR each WP

IF {FRT available **AND** $\left|1-\left|\bar{V}_{ctrl}^{+(k)}\right|\right| > V_{FRT-ON}$ }

convergence = 0

Control = FRT

END

END

IF {at least one WP has: convergence = 0} *(at least one WP changes control)*

GO TO "**LOOP**" *(the second loop starts)*

END

END

Sections 4.2 and 4.3 introduce two test cases. Then, sections 4.4 to 4.6 test the effectiveness of the proposed solver algorithm by applying it to the test cases including type-III and type-IV WPs and comparing the solutions against the TD solution of EMTP-RV.

4.2 Test case 1: single WP

Figure 4.4 shows a schematic diagram of the first test case; this schematic comes from the EMTP-RV interface.

Test case 1 is composed of 9 buses: one slack bus (BUS2), 2 loads (BUS 5 and 6), one WP connected at BUS1 and 5 lines. The WP can be either a type-IV or type-III one. The red section has a nominal line-to-line voltage of 120kV, the black one 25kV, the blue one 34.5kV and the orange one 575V.

Table 4.2 gives the WP electrical parameters. The configuration of the turbine transformer and the park transformer are as shown in Figure 4.4, and repeated here with their nominal voltages:

- Park transformer 34.5kV/120kV Dyg +30°
- Turbine transformer 575V/34.5kV Ygd –30°

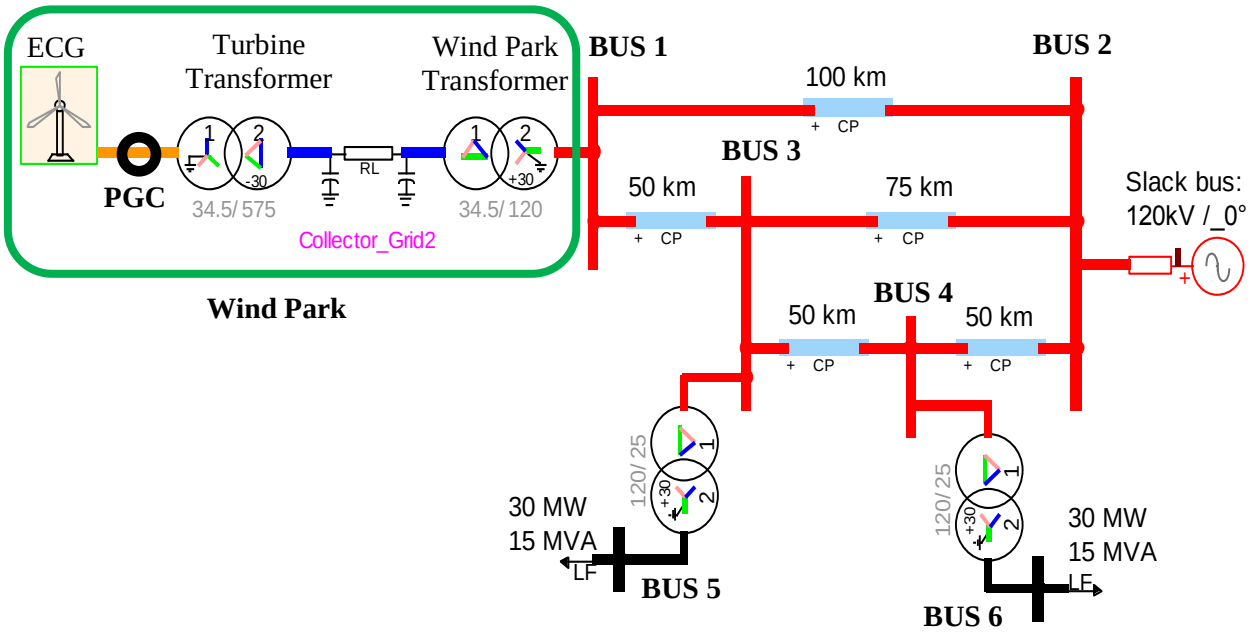

Figure 4.4 Test case 1: 120 kV system.

Recall that each turbine has two shunt filters to give a low impedance path for the harmonics of the GSC. One filter has its cut-off frequency at the switching frequency of the converter, and the second one twice this frequency. In Table 4.2, only the lowest cut-off frequency is given. The other electrical parameters of this circuit are available in Appendix C.

In the LF solver, the slack constraint imposes the nominal voltage with 0° on phase A at BUS2. The loads are represented with PQ constraints. The loads at BUS 5 and BUS 6 are identical with 10 + 5j MVA of power per phase. Both the EMTP-RV simulation and the SC solver are initialized from LF solution.

In TD simulations, all lines are represented by a CP model. In the SS solver, pi-equivalents are used. In EMTP-RV, the turbine and the park transformers have a non-linear magnetizing inductance. The relation between the voltage and current of this inductance is given in Table 4.3. Intermediate voltages and currents are obtained by linear interpolation. The SS solver represents the magnetizing inductance with a fixed reactance of 500 pu (equivalent to the second numerical row of Table 4.3). All other circuit parameters in EMTP-RV are equal to their corresponding parameters in the SS solver.

Table 4.2 Test case 1, electrical parameters of the WP.

Nominal active power	67.5 MW (45 turbines of 1.5 MW)
Nominal apparent power (= power base)	75.015 MVA (45 times 1.667 MVA)
Turbine transformer	
Nominal power	78.75 MVA
Series Impedance	0.002 + 0.05j pu
Park transformer	
Nominal power	75 MVA
Series Impedance	0.003 + 0.12j pu
PGC filter	
Reactive power Q_{filter}	75 kVAR
Cut-off frequency f_c	2.5 kHz
Quality factor Q_f	1000
Collector grid	
Series resistance	0.1265 Ω
Series inductance	0.3831 mH
Total shunt capacitance	7 µF

Table 4.3 Current vs voltage relation of the non-linear magnetizing inductance of transformers.

Voltage (pu)	Current (pu)
0.000	0.000
1.000	0.002
1.075	0.010
1.150	0.025
1.200	0.050
1.230	0.100
1.720	2.000

The control mode and the controller parameters are given in sections 4.4 to 4.6. Different settings are used for different simulation cases for testing purposes.

4.3 Test case 2: multiple WPs

This second test case is based on the IEEE 39bus system. The EMTP-RV data of the original IEEE 39 bus system are available in [57]. In test case 2, two synchronous generators are replaced by WPs (see Figure 4.5). The generators replaced are unit 8 on bus 25, and unit 10 on bus 2.

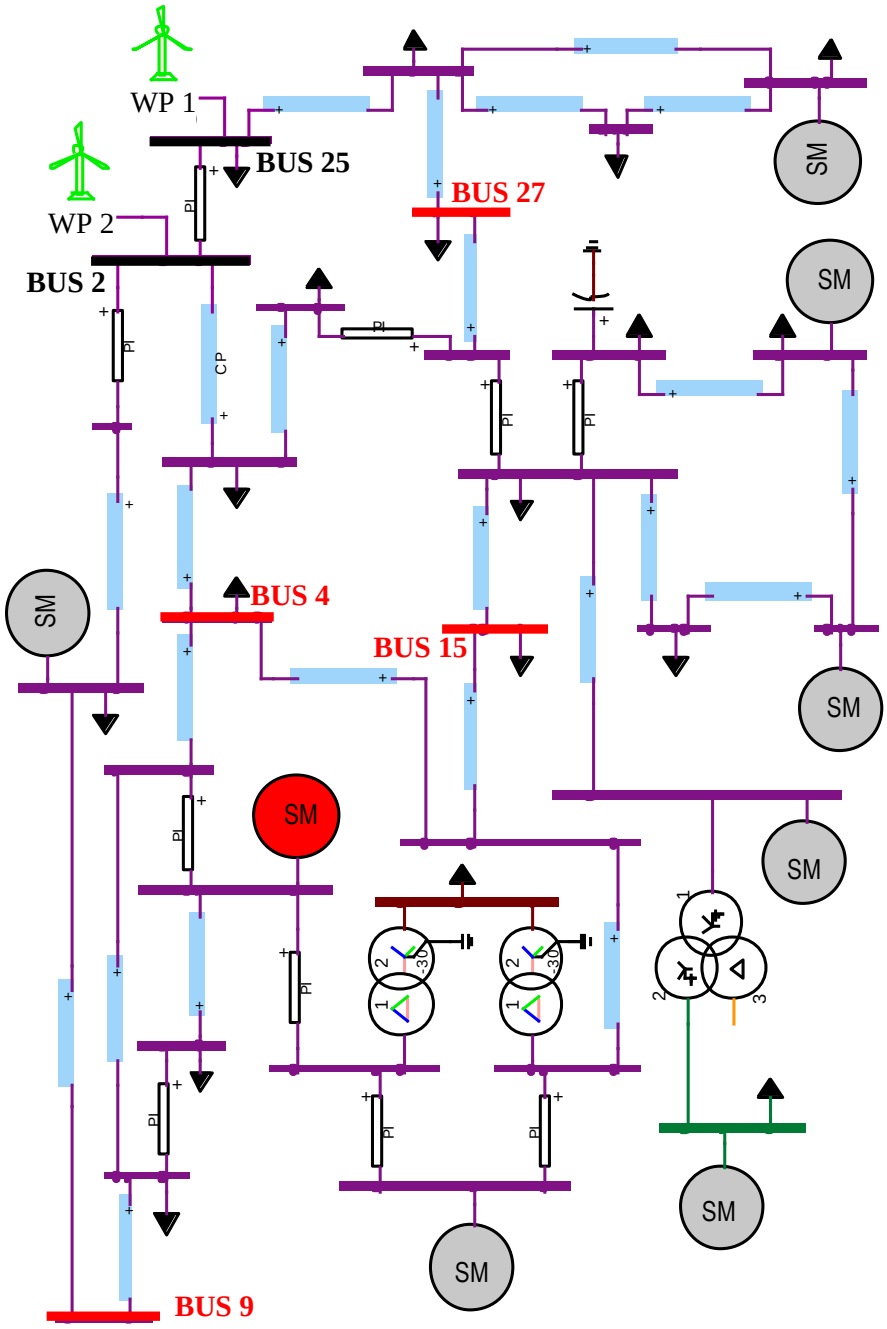

Figure 4.5 Test case 2: IEEE 39bus system with two WPs.

Here again, each WP can be either a type-IV or type-III one. In the same figure, each grey disk with "SM" represents a transformer which decreases the voltage to 20 kV and a generator represented with a PV constraint in the LF solver. The red disk has the transformer but with a slack constraint. The LF is run in EMTP-RV and in the proposed phasor solver. To only observe the behavior of WPs and not the slow mechanical response of SMs, all SMs are replaced by a Thevenin equivalent in EMTP-RV, similar to the model in SS solver. The impedances in all Thevenin equivalents are obtained from the armature resistance and armature leakage reactance of the synchronous machines.

In Figure 4.5, the green bus has a nominal line-to-line voltage of 300 kV, the brown 25 kV, and all other visible buses 500 kV. The black triangles represent the loads. The two WPs in this test case have the same structure as the WP of Figure 4.4. The park transformer connects the POI to the collector grid, and the turbine transformer connects the collector grid to the PGC. The transformer configurations are also the same as in Figure 4.4. The only difference is that the nominal high voltage of the park transformer is 512.5 kV. The other electrical parameters of the two WPs are presented in Table 4.4.

Recall that each turbine has two shunt filters to give a low impedance path for the harmonics of the GSC. One filter has its cut-off frequency at the switching frequency of the converter, and the second one twice this frequency. In Table 4.4, only the lowest cut-off frequency is given.

In TD simulations in EMTP-RV, the lines represented by light blue rectangle (in Figure 4.5) are modeled with CP model, and the ones represented by a white rectangle are modeled with a pi-model. In the SS solver, each line is reproduced by a pi-model.

In EMTP-RV, all transformers have a non-linear magnetizing inductance similar to that of test case 1 (see Table 4.3). The SS solver represents them with a fixed reactance of 500 pu. All other circuit parameters in EMTP-RV are equal to their corresponding parameters in the SS solver.

The control mode and the controller parameters are given in sections 4.4 to 4.6. Different settings are used for different simulation cases for testing purposes. The simulation results of this thesis present faults at the buses depicted in red color in Figure 4.5.

Table 4.4 Test case 2, electrical parameters of the two WPs.

	WP1	**WP2**
Nominal active power	540 MW (360 turbines of 1.5 MW)	270 MW (180 turbines of 1.5 MW)
Nominal apparent power (= power base)	600.12 MVA (360 times 1.667 MVA)	300.06 MVA (180 times 1.667 MVA)
Turbine transformer		
Nominal power	630 MVA	315 MVA
Series Impedance	0.002 + 0.05j pu	0.002 + 0.05j pu
Park transformer		
Nominal power	600 MVA	300 MVA
Series Impedance	0.003 + 0.12j pu	0.003 + 0.12j pu
PGC filter		
Reactive power Q_{filter}	75 kVAR	75 kVAR
Cut-off frequency f_c	2.5 kHz	2.5 kHz
Quality factor Q_f	1000	1000
Collector grid		
Series resistance	15.8 mΩ	31.6 mΩ
Series inductance	47.9 µH	95.8 µH
Total shunt capacitance	56 µF	28 µF

4.4 FSC generator: simulation and cross-examination with EMTP-RV

This section presents comparisons between the TD model in EMTP-RV and the proposed SS model and solver, for the type-IV based WP. The objective is to test the precision of the SS model through cross-examination against EMTP-RV.

The case studies consider a variety of balanced and unbalanced faults including line-to-line (LL), line-to-ground (LG) and line-to-line-to-ground (LLG). They also consider various operating conditions such as different wind speeds and different reactive power exchanges with the grid in prefault conditions.

In the EMTP-RV simulations, the faults are not cleared, so that the faulted SS is observable. For FSC-type WTGs, SS is reached after the fast transient of the fault. The EMTP-RV values given in this section are the asymptotic values measured during the faulted SS.

The TD simulations are run with a time step of 50 µs. This value is the largest time step that the TD model can use to function properly. For all SS simulations, the convergence criterion ε is equal to 0.0001. This value was chosen to have enough accuracy to observe variables with a small magnitude.

The comparison tables present the positive and negative sequence phasors of the PGC voltage and converter current. They are presented under the form: "Magnitude in pu (angle in degree)".

The parentheses in the title of each table indicate what the faulted phases are.

4.4.1 FSC generator in test case 1

Table 4.6 to Table 4.12 present comparisons of a type-IV based WP in test case 1. The tables also compare the coupled and decoupled control. Under normal conditions, the current limiter applies P-priority. The FRT mode is available, and works with Q-priority. Table 4.5 shows the controller parameters of the FSC-type WP.

For

Table 4.6 to Table 4.8:

- the WP produces its nominal active power (nominal wind speed = 11.24 m/s)
- the controlled voltage is the PGC one: $\bar{V}^{+}_{ctrl} = \bar{V}^{+}_{pgc}$
- the control mode gives: $Q'_{POI} = 0\,\text{pu} \;\Leftrightarrow\; PF'_{POI} = 1 \;\Leftrightarrow\; V'_{POI} = 1\,\text{pu}$

Table 4.5 Test case 1, WTG-IV: Controller parameters.

Outer loop	
K_V	2
K_{FRT}	2
V_{FRT-ON}	0.125 pu
Measurements filter: 2nd order Butterworth type	
Cut-off frequency	2.5 kHz
Phase shift at 60Hz: angle(H_{filter}^{60})	–1.95°
Choke impedance	
R	0.005 pu
X	0.5 pu
Current limiter	
$I_g^{\lim}$	1.1 pu
$I_{dg}^{\lim} = I_{qg}^{\lim}$	1 pu
Inner loop parameters	
K_P	0.413
K_I	38.57
Complex gain at 120 Hz: H_{PI}^{g}	0.417 / –7.1°

Table 4.6 Test case 1, comparison between TD and SS solution: WTG-IV with LLG (ABG) fault at Bus 1.

	Coupled Control		Decoupled Control	
WTG variable	**EMTP-RV Solution**	**Phasor Domain Solution**	**EMTP-RV Solution**	**Phasor Domain Solution**
$\bar{V}_{pgc}^{+}$	0.513 (17.5)	0.517 (17.7)	0.482 (7.2)	0.484 (7.8)
$\bar{V}_{pgc}^{-}$	0.319 (–114.9)	0.331 (–114.7)	0.269 (–120.9)	0.270 (–121.0)
$\bar{I}_g^{+}$	1.125 (–48.7)	1.100 (–47.7)	0.980 (–69.4)	0.983 (–68.1)
$\bar{I}_g^{-}$	0.010 (151.1)	0.013 (149.7)	0.234 (–4.2)	0.239 (–3.3)

Table 4.7 Test case 1, comparison between TD and SS solution: WTG-IV with LLG (ABG) fault at Bus 4.

	Coupled Control		Decoupled Control	
WTG variable	**EMTP-RV Solution**	**Phasor Domain Solution**	**EMTP-RV Solution**	**Phasor Domain Solution**
$\bar{V}_{pgc}^{+}$	0.804 (22.0)	0.804 (22.1)	0.812 (16.3)	0.812 (16.4)
$\bar{V}_{pgc}^{-}$	0.243 (–119.6)	0.244 (–119.6)	0.201 (–136.0)	0.201 (–136.0)
$\bar{I}_{g}^{+}$	1.074 (0.6)	1.074 (0.7)	0.893 (–8.6)	0.893 (–8.5)
$\bar{I}_{g}^{-}$	0.009 (57.4)	0.008 (84.3)	0.228 (26.5)	0.228 (26.5)

Table 4.8 Test case 1, comparison between TD and SS solution: WTG-IV with LLG (ABG) fault at Bus 6.

	Coupled Control		Decoupled Control	
WTG variable	**EMTP-RV Solution**	**Phasor Domain Solution**	**EMTP-RV Solution**	**Phasor Domain Solution**
$\bar{V}_{pgc}^{+}$	0.927 (19.7)	0.936 (19.5)	0.930 (19.4)	0.936 (19.3)
$\bar{V}_{pgc}^{-}$	0.055 (-71.3)	0.055 (-71.7)	0.047 (-88.8)	0.047 (-88.5)
$\bar{I}_{g}^{+}$	1.003 (11.0)	0.999 (9.5)	0.990 (10.3)	0.992 (9.3)
$\bar{I}_{g}^{-}$	0.001 (158.4)	0.002 (132.2)	0.051 (82.9)	0.050 (81.8)

Figure 4.6 to Figure 4.8 illustrate the difference between coupled and decoupled sequence controller. Figure 4.6 and Figure 4.7 present the GSC output power for a line-to-line-to-ground (LLG) fault at the POI. To reduce active power oscillations, decoupled control reduces its average active power.

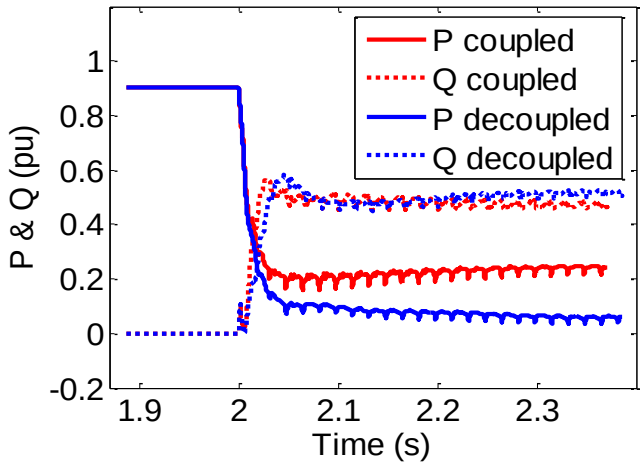

Figure 4.6 The sequence control has no impact on the reactive power output.

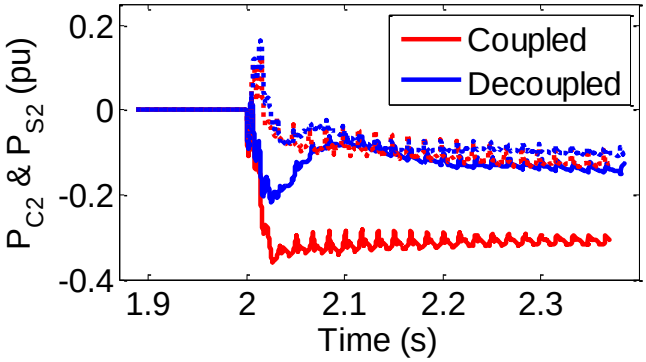

Figure 4.7 The decoupled control reduces magnitude of active power oscillations.

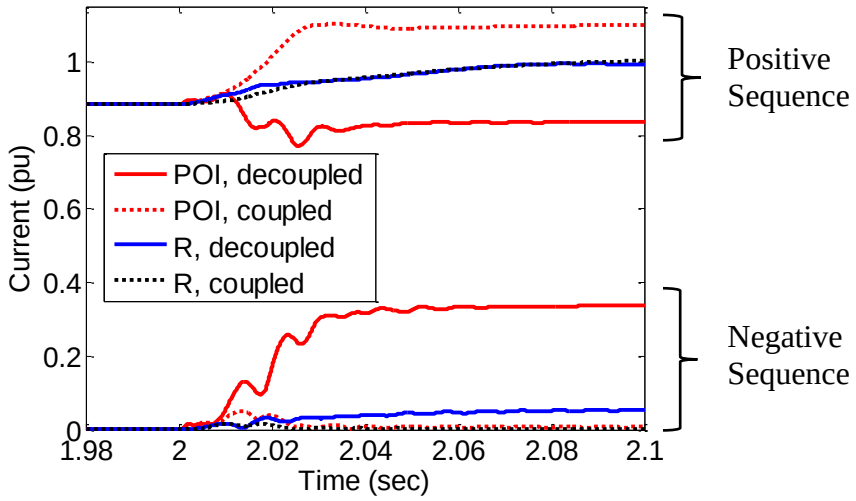

Figure 4.8 GSC current contribution for LLG fault on 2 locations.

Figure 4.8 presents sequence current magnitudes for an LLG fault at the POI and a remote fault (R). For the remote fault, the difference appears only on the negative sequence current as the thermic limits of the GSC are not reached. However, for the POI fault, the GSC with decoupled control carries less positive sequence current and much more negative sequence current compared to coupled control. With decoupled control, the negative sequence current reduces the power oscillations, but due to the current limit, the positive sequence must decrease.

For Table 4.9:

- the WP produces about 40% of its nominal active power (wind speed = 8 m/s)
- the controlled voltage is the PGC one: $\bar{V}^{+}_{ctrl} = \bar{V}^{+}_{pgc}$
- the control mode gives: $Q'_{POI} = 0\,\text{pu} \;\Leftrightarrow\; PF'_{POI} = 1 \;\Leftrightarrow\; V'_{POI} = 0.988\,\text{pu}$

Table 4.9 Test case 1, comparison between TD and SS solution: WTG-IV with LLG (ABG) fault at Bus 4, and low wind speed.

	Coupled Control		Decoupled Control	
WTG variable	**EMTP-RV Solution**	**Phasor Domain Solution**	**EMTP-RV Solution**	**Phasor Domain Solution**
$\bar{V}^{+}_{pgc}$	0.822 (8.1)	0.823 (8.2)	0.821 (8.9)	0.821 (9.0)
$\bar{V}^{-}_{pgc}$	0.247 (–121.0)	0.247 (–121.0)	0.207 (–128.6)	0.207 (–128.7)
$\bar{I}^{+}_{g}$	0.582 (–29.6)	0.583 (–29.3)	0.609 (–27.2)	0.611 (–26.9)
$\bar{I}^{-}_{g}$	0.010 (93.7)	0.008 (82.9)	0.153 (15.4)	0.154 (15.5)

For Table 4.10 and Table 4.11:

- the WP produces its nominal active power
- the controlled voltage is the medium voltage one: $\bar{V}^{+}_{ctrl} = \bar{V}^{+}_{mv}$
- the control mode gives: $Q'_{POI} = +0.2\,\text{pu} \;\Leftrightarrow\; PF'_{POI} = 0.975 \;\Leftrightarrow\; V'_{POI} = 1.026\,\text{pu}$,
  and $Q'_{POI} = -0.2\,\text{pu} \;\Leftrightarrow\; PF'_{POI} = -0.975 \;\Leftrightarrow\; V'_{POI} = 0.976\,\text{pu}$

Such difference of reactive power exchange at the POI induces variation of the voltage at the MV side of the park transformer. The park transformer is equipped with taps to maintain the voltage at its MV terminal at 1 pu. The nominal transformation ratio is the ratio of the nominal voltages at each side of the transformer: 120/34.5 = 3.478. For $Q'_{POI} = -0.2\,\text{pu}$, the transformation ratio of the WP transformer is divided by 1.04. For $Q'_{POI} = 0.2\,\text{pu}$, the transformation ratio of the WP transformer is divided by 0.95.

Table 4.10 Test case 1, comparison between TD and SS solution: WTG-IV with **coupled** control and two reactive power references for LLG (ABG) fault at Bus 6.

	$Q'_{POI} = -0.2\,\text{pu}$		$Q'_{POI} = +0.2\,\text{pu}$	
WTG variable	**EMTP-RV Solution**	**Phasor Domain Solution**	**EMTP-RV Solution**	**Phasor Domain Solution**
$\bar{V}^{+}_{pgc}$	0.914 (20.1)	0.918 (20.6)	0.953 (18.5)	0.954 (17.7)
$\bar{V}^{-}_{pgc}$	0.057 (–69.5)	0.057 (–72.0)	0.053 (–69.0)	0.053 (–71.7)
$\bar{I}^{+}_{g}$	1.001 (20.5)	0.997 (20.6)	1.037 (–3.4)	1.041 (–4.4)
$\bar{I}^{-}_{g}$	0.001 (138.0)	0.002 (131.9)	0.001 (-165.0)	0.002 (132.2)

Table 4.11 Test case 1, comparison between TD and SS solution: WTG-IV with **decoupled** control for LLG (ABG) fault at Bus 6.

	$Q'_{POI} = -0.2\,\text{pu}$		$Q'_{POI} = +0.2\,\text{pu}$	
WTG variable	**EMTP-RV Solution**	**Phasor Domain Solution**	**EMTP-RV Solution**	**Phasor Domain Solution**
$\bar{V}^{+}_{pgc}$	0.916 (19.7)	0.918 (20.2)	0.951 (18.8)	0.954 (17.8)
$\bar{V}^{-}_{pgc}$	0.051 (–89.5)	0.050 (–92.0)	0.043 (–83.9)	0.043 (–85.3)
$\bar{I}^{+}_{g}$	0.984 (20.1)	0.980 (20.3)	1.045 (–2.9)	1.043 (–4.3)
$\bar{I}^{-}_{g}$	0.055 (91.9)	0.054 (88.5)	0.048 (74.9)	0.047 (72.7)

Table 4.6 to Table 4.11 illustrate the accuracy of the proposed SS model for various fault conditions, two different levels of active power production, various prefault reactive power, the

two control structures (coupled and decoupled) and the two controlled voltages. For decoupled control, the highest magnitude difference between EMTP-RV and the SS model is lower than 0.01 pu, and the highest phase angle difference is lower than 3.5°. Those two values take into account the differences among the positive and negative sequence voltage and current. In the same way for coupled control, the magnitude difference between EMTP-RV and the SS model is equal or lower than 0.025 pu. For the two voltages and the positive sequence current, the highest phase angle difference is lower than 3.0°. The difference on the phase angle of the negative sequence current $\bar{I}_g^-$ reaches 62.8° in Table 4.10, but its magnitude is very low. The reason for this large error will be explained in section 5.1.1.

The other differences between the TD and the SS model stem in part from the non-linear magnetizing inductances of the transformers. In addition, the impact of the fault on the PMSG and the MSC are neglected.

The accuracy level is high enough for protection studies. The protection equipement has a safety margin higher than the worst-case error which is around 0.025 pu.

The previous tables of this section illustrate fault conditions where the GSC stays synchronised with the Thevenin equivalent of the slack bus. The following paragraph presents simulations where the GSC undergoes a LOS.

Loss of synchronism

This paragraph tests the type-IV algorithm in LOS conditions, i.e., when $\left|\bar{V}_{pgc}^{+(k)} / \bar{I}_{pgc}^{+(k-1)}\right| < Z_{LOS-\lim}$. The LOS equation is tested with a 3-phase fault at the POI of the WP, i.e., in Bus 1. Under such conditions, the WP produces more active power than what is dissipated by the collector grid, the WP and the turbine transformers. The frequency in the WP increases and the GSC loses synchronisation with the grid. Because of this frequency variation, the TD variables do not converge. For the sake of comparison, the EMTP-RV values are taken three cycles after the beginning of the fault:

Table 4.12 Control mode impacts the LOS behavior of FSCs.

Control mode ($I_{dg}^{+\prime\prime\prime} + jI_{qg}^{+\prime\prime\prime}$)	FSC Variables	EMTP-RV Solution	Phasor Domain Solution
$Q_g = 0$ (1 + 0j)	$\bar{I}_g^+$	0.993 (15.3)	1.000 (12.7)
	$\bar{V}_{pgc}^+$	0.180 (100.3)	0.181 (98.4)
no FRT, P-priority (1 – 0.458j)	$\bar{I}_g^+$	1.103 (–11.7)	1.100 (–11.9)
	$\bar{V}_{pgc}^+$	0.201 (74.3)	0.199 (73.8)
with FRT, Q-priority (0.458 – 1j)	$\bar{I}_g^+$	1.126 (–52.5)	1.102 (–50.9)
	$\bar{V}_{pgc}^+$	0.207 (34.1)	0.201 (34.8)

Table 4.12 shows that the LOS response of the type-IV WTG depends on the control mode. It verifies the precision of the LOS model. For the positive sequence current $\bar{I}_g^+$, the magnitude difference between the TD and the SS model is less than 0.025 pu and the angle difference is less than 3.0°. The LOS model stays valid for only a few cycles as the frequency varies.

4.4.2 FSC generator in test case 2

Table 4.14 to Table 4.16 present comparisons of type-IV based WPs in test case 2. The tables show coupled and decoupled control simulations. For both WPs, under normal conditions, the current limiter applies P-priority. The FRT mode is available, and works with Q-priority. The controller details of the two WPs are the same as in Table 4.5, except for the gains of the inner loop PI controller (Table 4.13).

Table 4.13 Test case 2, WTG-IV: inner loop parameters.

	WP1	**WP2**
K_P	0.422	0.407
K_I	25.21	13.91
Complex gain at 120 Hz: H_{PI}^{g}	0.423 /–4.5°	0.407 /–2.6°

For Table 4.14 to Table 4.16:

- the two WPs produce their nominal active power
- for both WPs, the controlled voltage is the PGC one: $\bar{V}^{+}_{ctrl} = \bar{V}^{+}_{pgc}$
- the control mode gives:

$$\text{WP1} \quad Q'_{POI} = 0\,\text{pu} \;\Leftrightarrow\; PF'_{POI} = 1 \;\Leftrightarrow\; V'_{POI} = 1.008\,\text{pu}$$

$$\text{WP2} \quad Q'_{POI} = 0\,\text{pu} \;\Leftrightarrow\; PF'_{POI} = 1 \;\Leftrightarrow\; V'_{POI} = 0.994\,\text{pu}$$

Table 4.14 Test case 2, comparison between TD and SS solution: WTG-IV with LL (AB) fault at Bus 27, with decoupled control.

	WP1		WP2	
WTG variable	**EMTP-RV Solution**	**Phasor Domain Solution**	**EMTP-RV Solution**	**Phasor Domain Solution**
$\bar{V}^{+}_{pgc}$	0.854 (9.9)	0.852 (9.9)	0.825 (9.1)	0.823 (9.1)
$\bar{V}^{-}_{pgc}$	0.142 (–157.5)	0.142 (–157.8)	0.157 (–155.9)	0.157 (–156.1)
$\bar{I}^{+}_{g}$	0.945 (–8.5)	0.947 (–8.3)	0.930 (–13.7)	0.931 (–13.2)
$\bar{I}^{-}_{g}$	0.159 (5.9)	0.161 (5.7)	0.180 (4.4)	0.181 (4.4)

Table 4.15 Test case 2, comparison between TD and SS solution: WTG-IV with LG (BG) fault at Bus 4, with decoupled control.

	WP1		WP2	
WTG variable	**EMTP-RV Solution**	**Phasor Domain Solution**	**EMTP-RV Solution**	**Phasor Domain Solution**
$\bar{V}^{+}_{pgc}$	0.949 (6.9)	0.953 (6.5)	0.929 (6.0)	0.933 (5.8)
$\bar{V}^{-}_{pgc}$	0.096 (–100.9)	0.097 (–100.5)	0.106 (–99.8)	0.107 (–99.3)
$\bar{I}^{+}_{g}$	0.959 (–1.1)	0.952 (–1.8)	0.966 (–3.6)	0.968 (–4.2)
$\bar{I}^{-}_{g}$	0.098 (72.0)	0.097 (71.2)	0.117 (72.2)	0.113 (71.5)

Table 4.16 Test case 2, comparison between TD and SS solution: WTG-IV with LG (BG) fault at Bus 25, with coupled control.

	WP1		WP2	
WTG variable	**EMTP-RV Solution**	**Phasor Domain Solution**	**EMTP-RV Solution**	**Phasor Domain Solution**
$\bar{V}_{pgc}^{+}$	0.752 (10.6)	0.764 (10.2)	0.823 (4.3)	0.828 (4.1)
$\bar{V}_{pgc}^{-}$	0.396 (–68.4)	0.411 (–69.1)	0.295 (–60.8)	0.301 (–61.5)
$\bar{I}_{g}^{+}$	1.101 (–15.8)	1.100 (–15.2)	1.061 (–15.0)	1.058 (–14.9)
$\bar{I}_{g}^{-}$	0.021 (129.9)	0.037 (135.0)	0.018 (137.9)	0.024 (141.6)

For test case 2, the magnitude and the phase angle differences have the same order of magnitude as test case 1. For decoupled control (Table 4.14 and Table 4.15), the highest magnitude difference between EMTP-RV and the SS model is less than 0.01 pu, and the highest phase angle difference is less than 1.0°. Those two values take into account the difference among the positive and negative sequence voltage and current. In the same way for coupled control (Table 4.16), the highest magnitude difference between EMTP-RV and the SS model is lower than 0.02 pu. For the two voltages and the positive sequence current, the highest phase angle difference is lower than 1.0°. For the phase angle of the negative sequence current, the difference is 5.1°.

The explanations for the differences between the TD and the SS models are similar to those for test case 1.

4.5 DFIG generator: simulation and cross-examination with EMTP-RV

This section presents comparisons between the TD model in EMTP-RV and the proposed SS model and solver, for the type-III based WP. The objective is to test the precision of the SS model through cross-examination against EMTP-RV.

The case studies consider a variety of unbalanced faults including line-to-line (LL), line-to-ground (LG) and line-to-line-to-ground (LLG). They also consider various operating conditions as different wind speeds and different reactive power exchanges with the grid.

In the EMTP-RV simulations, the faults are not cleared, so that the faulted SS is observable. For DFIG-type WTGs, a faulted SS is not always reached because of the slow mechanical response of the machine does not necessarly converge. If the mechanical model induces variations of the phasor magnitude or angle, an average value is taken over 200 ms to 500 ms after the fast transient of the fault.

The TD simulations are run with a time step of 50 µs. This value is the largest time step that the TD model can use to function properly. For all SS simulations, the convergence criterion ε is equal to 0.0001. This value was chosen to have enough accuracy to compare the complete and simple SS models.

The comparison tables present the positive and negative sequence phasors of the PGC voltage and the turbine current. They are presented under the form: “Magnitude in pu (angle in degree)”.

The parentheses in the title of each table indicate what the faulted phases are.

4.5.1 DFIG generator in test case 1

Table 4.18 to Table 4.24 present comparisons of a type-III based WP in test case 1. Under normal conditions, the RSC current limiter applies P-priority. The FRT mode is available, and works with Q-priority. In this section, the results of the simple and complete SS models are compared to the EMTP-RV results. The WP electrical parameters are equal to those shown in Table 4.2 except that:

- The series impedance of the park transformer is: 0.005 + 0.125j pu
- The cut-off frequency f_c of the PGC filter is: 4.5 kHz

Table 4.17 shows the controller and machine parameters of the DFIG-type WP.

Table 4.17 Test case 1, WTG-III: Controller and machine parameters.

Outer loop			
K_V		2	
K_{FRT}		2	
V_{FRT-ON}		0.100 pu	
Measurements filter: 2nd order Bessel type			
		RSC	GSC
Cut-off frequency		4.5 kHz	9 kHz
Phase shift at 60Hz: angle(H_{filter}^{60})		–1.0°	–0.5°
Choke impedance			
R		0.015 pu	
X		1.5 pu	
Machine parameters			
X_m		2.9 pu	
stator		**rotor**	
R_s	0.033 pu	R_r	0.026 pu
X_{ls}	0.18 pu	X_{lr}	0.16 pu
Current limiter			
GSC		**RSC**	
$I_g^{\lim} = I_{dg}^{\lim}$	0.35 pu	$I_r^{\lim}$	1.1 pu
$I_{qg}^{\lim}$	0.3 pu	$I_{dr}^{\lim} = I_{qr}^{\lim}$	1 pu
Inner loop parameters			
GSC		**RSC**	
K_P	0.975	K_P^r	0.144
K_I	4.813	K_I^r	4.296
Complex gain at 120 Hz: H_{PI}^g	0.975 /–0.4°	Complex gain at 120 Hz: H_{PI}^r	0.144 /–2.3°

In Table 4.18 to Table 4.20, the last column gives the absolute difference of magnitudes, and the absolute difference of angle (not the complex difference). Its goal is to observe the difference between the complete and the simple models.

- the WP produces its nominal active power (nominal wind speed = 11.24 m/s)
- the controlled voltage is the PGC one: $\bar{V}^{+}_{ctrl} = \bar{V}^{+}_{pgc}$
- the control mode gives: $Q'_{POI} = 0\,\text{pu} \;\Leftrightarrow\; PF'_{POI} = 1 \;\Leftrightarrow\; V'_{POI} = 1\,\text{pu}$

Table 4.18 Test case 1, comparison between TD and SS solution (simple and complete): WTG-III with LL (AB) fault at Bus 4.

WTG variable	EMTP-RV Solution	Phasor Domain Solution (Complete model)	Phasor Domain Solution (Simple model)	Absolute difference (phasor models)
$\bar{V}^{+}_{pgc}$	0.792 (21.8)	0.794 (21.7)	0.824 (21.3)	0.030 (0.4)
$\bar{V}^{-}_{pgc}$	0.140 (–125.6)	0.140 (–124.3)	0.143 (–120.2)	0.003 (4.1)
$\bar{I}^{+}_{tb}$	1.036 (8.0)	1.031 (7.6)	1.054 (2.9)	0.023 (4.7)
$\bar{I}^{-}_{tb}$	0.421 (–15.0)	0.421 (–16.4)	0.415 (–20.3)	0.006 (3.9)

Table 4.19 Test case 1, comparison between TD and SS solution (simple and complete): WTG-III with LG (AG) fault at Bus 4.

WTG variable	EMTP-RV Solution	Phasor Domain Solution (Complete model)	Phasor Domain Solution (Simple model)	Absolute difference (phasor models)
$\bar{V}^{+}_{pgc}$	0.932 (17.5)	0.935 (17.6)	0.939 (17.4)	0.004 (0.2)
$\bar{V}^{-}_{pgc}$	0.065 (171.3)	0.064 (172.5)	0.065 (176.7)	0.001 (4.2)
$\bar{I}^{+}_{tb}$	0.978 (8.5)	0.982 (8.2)	0.979 (7.5)	0.003 (0.7)
$\bar{I}^{-}_{tb}$	0.193 (–78.3)	0.193 (–79.5)	0.189 (–83.4)	0.004 (3.9)

Table 4.20 Test case 1, comparison between TD and SS solution (simple and complete): WTG-III with LL (AB) fault at Bus 1.

WTG variable	EMTP-RV Solution	Phasor Domain Solution (Complete model)	Phasor Domain Solution (Simple model)	Absolute difference (phasor models)
$\bar{V}_{pgc}^{+}$	0.597 (23.5)	0.598 (21.6)	0.620 (15.9)	0.022 (5.7)
$\bar{V}_{pgc}^{-}$	0.309 (–121.1)	0.308 (–120.4)	0.318 (–118.9)	0.010 (1.5)
$\bar{I}_{tb}^{+}$	1.135 (–15.1)	1.076 (–18.1)	0.972 (–31.5)	0.104 (13.4)
$\bar{I}_{tb}^{-}$	0.929 (–9.9)	0.930 (–12.5)	0.921 (–19.0)	0.009 (6.5)

The last case is the one with the highest negative sequence voltage at the PGC. This case shows the limit of the simple model. The error on positive sequence current comes from the calculation of negative sequence active power transferred from the stator to the RSC (P_{RSC}^{-}).

For Table 4.21 and Table 4.22, the wind speed is smaller:

- the WP produces about 40% of its nominal active power (wind speed = 8 m/s)
- the controlled voltage is the PGC one: $\bar{V}_{ctrl}^{+} = \bar{V}_{mv}^{+}$
- the control mode gives: $Q'_{POI} = 0\,\text{pu} \;\Leftrightarrow\; PF'_{POI} = 1 \;\Leftrightarrow\; V'_{POI} = 0.987\,\text{pu}$

Table 4.21 Test case 1, comparison between TD and SS solution (simple and complete): WTG-III for LL (AB) fault at Bus 4.

WTG variable	EMTP-RV Solution	Phasor Domain Solution (Complete model)	Phasor Domain Solution (Simple model)
$\bar{V}_{pgc}^{+}$	0.843 (6.0)	0.842 (6.0)	0.849 (5.7)
$\bar{V}_{pgc}^{-}$	0.149 (–126.9)	0.147 (–125.2)	0.145 (–121.8)
$\bar{I}_{tb}^{+}$	0.499 (–31.4)	0.492 (–31.4)	0.501 (–34.0)
$\bar{I}_{tb}^{-}$	0.413 (–16.4)	0.414 (–18.3)	0.421 (–21.9)

Table 4.22 Test case 1, comparison between TD and SS solution (simple and complete): WTG-III for LLG (ABG) fault at Bus 1.

WTG variable	EMTP-RV Solution	Phasor Domain Solution (Complete model)	Phasor Domain Solution (Simple model)
$\bar{V}_{pgc}^{+}$	0.474 (24.2)	0.454 (28.9)	0.477 (18.3)
$\bar{V}_{pgc}^{-}$	0.193 (–117.9)	0.188 (–114.9)	0.190 (–115.3)
$\bar{I}_{tb}^{+}$	1.141 (–38.1)	1.122 (–28.8)	1.076 (–49.5)
$\bar{I}_{tb}^{-}$	0.538 (–6.4)	0.528 (–8.1)	0.551 (–15.4)

For Table 4.23 and Table 4.24, the prefault conditions are different:

- the WP produces its nominal active power (nominal wind speed)
- the controlled voltage is the medium voltage one: $\bar{V}_{ctrl}^{+} = \bar{V}_{mv}^{+}$
- the control mode gives: $Q'_{POI} = +0.2\,\text{pu} \Leftrightarrow PF'_{POI} = 0.975 \Leftrightarrow V'_{POI} = 1.025\,\text{pu}$,
  and $Q'_{POI} = -0.2\,\text{pu} \Leftrightarrow PF'_{POI} = -0.975 \Leftrightarrow V'_{POI} = 0.976\,\text{pu}$

Such difference of reactive power exchange at the POI induces variation of the voltage at the MV side of the park transformer. The park transformer is equipped with taps to maintain the voltage at its MV terminal at 1 pu. The nominal transformation ratio is the ratio of the nominal voltages at each side of the transformer: 120/34.5 = 3.478. For $Q'_{POI} = -0.2\,\text{pu}$, the transformation ratio of the WP transformer is divided by 1.04. For $Q'_{POI} = 0.2\,\text{pu}$, the transformation ratio of the WP transformer is divided by 0.95.

Table 4.23 Test case 1, comparison between TD and SS solution (simple and complete): WTG-III for LLG (ABG) fault at Bus 6, with $Q'_{POI} = -0.2\,\text{pu}$.

WTG variable	EMTP-RV Solution	Phasor Domain Solution (Complete model)	Phasor Domain Solution (Simple model)
$\bar{V}^{+}_{pgc}$	0.907 (20.4)	0.901 (21.6)	0.936 (20.3)
$\bar{V}^{-}_{pgc}$	0.027 (–76.8)	0.026 (–75.5)	0.027 (–71.4)
$\bar{I}^{+}_{tb}$	0.995 (22.3)	1.006 (22.6)	0.970 (16.6)
$\bar{I}^{-}_{tb}$	0.081 (33.5)	0.079 (32.4)	0.078 (28.5)

Table 4.24 Test case 1, comparison between TD and SS solution (simple and complete): WTG-III for LLG (ABG) fault at Bus 6, with $Q'_{POI} = 0.2\,\text{pu}$.

WTG variable	EMTP-RV Solution	Phasor Domain Solution (Complete model)	Phasor Domain Solution (Simple model)
$\bar{V}^{+}_{pgc}$	0.931 (19.2)	0.945 (17.7)	0.956 (17.3)
$\bar{V}^{-}_{pgc}$	0.026 (–76.8)	0.027 (–75.7)	0.027 (–71.7)
$\bar{I}^{+}_{tb}$	1.013 (1.3)	1.012 (-1.4)	1.012 (-3.6)
$\bar{I}^{-}_{tb}$	0.078 (33.9)	0.081 (32.3)	0.079 (28.1)

Table 4.18 to Table 4.24 illustrate the accuracy of the proposed DFIG SS models for various fault conditions, two different levels of active power productions, various prefault reactive powers, and the two options of controlled voltage.

The largest difference between EMTP-RV and the SS models appears on the positive sequence current. It reaches 0.059 pu for the magnitude and 9.3° for the phase angle with the complete model. For the simple model, the difference on the positive sequence current reaches 0.163 pu for the magnitude and 16.4° for the phase angle. The larger error on the positive sequence current stems in part from the fact that the impact of the fault on the mechanical behavior of the machine are neglected. More details will be given in section 5.1.2.

Considering the two voltages and the negative sequence current, the magnitude difference between EMTP-RV and the complete SS model is equal to or lower than 0.01 pu, and the highest phase angle difference is lower than 5.0°. The largest magnitude difference between EMTP-RV and the simple SS model is less than 0.035 pu, and the largest phase angle difference is less than 9.5°.

Those differences between the SS models and the TD model highlight the higher accuracy of the complete SS model compared to the simple model. The errors with the complete type-III SS model are larger than the errors of type-IV ones, but stay acceptable for protection studies. The accuracy of the simple type-III SS model is acceptable for remote faults, then it gives a simple alternative to the complete model. But the error of the simple model can reach the protection margin for nearby faults.

The other differences between the TD model and the SS one comes partly from the non-linear magnetizing inductances of transformers.

4.5.2 DFIG generator in test case 2

Table 4.25 to Table 4.27 present comparisons of type-III based WPs for test case 2. The DFIG SS model used is the complete one. For both WPs, under normal conditions the RSC current limiter applies P-priority. The FRT mode is available, and works with Q-priority. The controller details and machine details of the two WPs are the same as in Table 4.17. The WP electrical parameters are the one shown in Table 4.4 except that:

- The series impedance of the park transformer is: 0.005 + 0.125j pu
- The cut-off frequency f_c of the PGC filter is: 4.5 kHz

Those modifications apply to both WPs.

For Table 4.25 to Table 4.27:

- the two WPs produce their nominal active power
- for both WPs, the controlled voltage is the PGC one: $\bar{V}^{+}_{ctrl} = \bar{V}^{+}_{pgc}$
- the control mode gives:

$$\text{WP1} \quad Q'_{POI} = 0\,\text{pu} \;\Leftrightarrow\; PF'_{POI} = 1 \;\Leftrightarrow\; V'_{POI} = 0.999\,\text{pu}$$

$$\text{WP2} \quad Q'_{POI} = 0\,\text{pu} \;\Leftrightarrow\; PF'_{POI} = 1 \;\Leftrightarrow\; V'_{POI} = 0.987\,\text{pu}$$

Table 4.25 Test case 2, comparison between TD and SS solution: WTG-III with LL (AB) fault at Bus 27.

	Wind Park 1 (bus 25)		Wind Park 2 (bus 2)	
WTG variable	**EMTP-RV Solution**	**Phasor Domain Solution**	**EMTP-RV Solution**	**Phasor Domain Solution**
$\bar{V}^{+}_{pgc}$	0.805 (13.8)	0.808 (13.7)	0.817 (9.7)	0.820 (9.8)
$\bar{V}^{-}_{pgc}$	0.128 (–145.1)	0.127 (–143.1)	0.110 (–141.2)	0.110 (–139.6)
$\bar{I}^{+}_{tb}$	1.025 (1.6)	1.025 (1.1)	1.018 (–1.3)	1.020 (–1.6)
$\bar{I}^{-}_{tb}$	0.381 (–33.3)	0.384 (–35.2)	0.329 (–30.2)	0.331 (–31.6)

Table 4.26 Test case 2, comparison between TD and SS solution: WTG-III with LG (AG) fault at Bus 15.

	Wind Park 1 (bus 25)		Wind Park 2 (bus 2)	
WTG variable	**EMTP-RV Solution**	**Phasor Domain Solution**	**EMTP-RV Solution**	**Phasor Domain Solution**
$\bar{V}^{+}_{pgc}$	0.965 (6.0)	0.948 (6.8)	0.950 (5.0)	0.934 (5.7)
$\bar{V}^{-}_{pgc}$	0.041 (151.5)	0.040 (153.5)	0.044 (152.0)	0.043 (153.6)
$\bar{I}^{+}_{tb}$	0.937 (0.1)	0.954 (3.3)	0.954 (–1.5)	0.970 (1.6)
$\bar{I}^{-}_{tb}$	0.121 (–96.9)	0.122 (–98.5)	0.129 (–97.0)	0.130 (–98.4)

Table 4.27 Test case 2, comparison between TD and SS solution: WTG-III with LLG (BCG) fault at Bus 9.

	Wind Park 1 (bus 25)		Wind Park 2 (bus 2)	
WTG variable	**EMTP-RV Solution**	**Phasor Domain Solution**	**EMTP-RV Solution**	**Phasor Domain Solution**
$\bar{V}_{pgc}^{+}$	0.975 (6.1)	0.962 (6.7)	0.957 (5.5)	0.944 (6.0)
$\bar{V}_{pgc}^{-}$	0.025 (–37.9)	0.025 (–36.0)	0.029 (–39.2)	0.029 (–37.6)
$\bar{I}_{tb}^{+}$	0.927 (1.1)	0.940 (3.7)	0.948 (–0.3)	0.960 (2.3)
$\bar{I}_{tb}^{-}$	0.074 (73.7)	0.074 (72.0)	0.087 (71.8)	0.087 (70.3)

For test case 2, the magnitude and phase angle differences have the same order of magnitude as for test case 1. Considering the two voltages and the two currents, the largest magnitude difference between EMTP-RV and the SS model is less than 0.02 pu, and the largest phase angle difference is less than 3.5°.

The explanations for the differences between the TD and the SS models are similar to those for test case 1.

4.6 FSC and DFIG generators: simulation and cross-examination with EMTP-RV

In this section, the two types of WTGs (FSC and DFIG) are tested in a single network with test case 2. WP1 (at bus 25) is a type-III based WP and WP2 (at bus 2) is a type-IV based WP with coupled control. Under normal conditions, the RSC current limiter of WP1, and the GSC current limiter of WP2 applies P-priority. The FRT mode is available for both WPs, and works with Q-priority.

As in the previous two sections, the convergence criterion of the SS solver is $\varepsilon = 1e-4$, and the EMTP-RV simulations run with a time step of 50μs.

Other details, for example, how the EMTP-RV values are obtained, are identical to those given in sections 4.4 and 4.5.

The electrical parameters of the two WPs are the same as in Table 4.4 except that:

- The series impedance of the two park transformers is: 0.005 + 0.125j pu
- The cut-off frequency f_c of the PGC filter of WP1 (DFIG-type) is: 4.5 kHz

The controller and machine details of WP1 are the same as in Table 4.17. The controller details of WP2 are the same as the WP2 in section 4.4.2.

For Table 4.28 to Table 4.30:

- the two WPs produce their nominal active power
- for both WPs, the MV side voltage is controlled: $\bar{V}^{+}_{ctrl} = \bar{V}^{+}_{mv}$
- the control mode gives:

$$\text{WP1} \quad Q'_{POI} = 0\,\text{pu} \;\Leftrightarrow\; PF'_{POI} = 1 \;\Leftrightarrow\; V'_{POI} = 1.001\,\text{pu}$$

$$\text{WP2} \quad Q'_{POI} = 0\,\text{pu} \;\Leftrightarrow\; PF'_{POI} = 1 \;\Leftrightarrow\; V'_{POI} = 0.989\,\text{pu}$$

In those tables, the currents of WP1 correspond to $\bar{I}^{+}_{tb}$ and the currents of WP2 correspond to $\bar{I}^{+}_{g}$.

Table 4.28 Test case 2, comparison between TD and SS solution: WTG-III and IV with LLG (ABG) fault at Bus 27.

	Wind Park 1 (bus 25)		Wind Park 2 (bus 2)	
WTG variable	**EMTP-RV Solution**	**Phasor Domain Solution**	**EMTP-RV Solution**	**Phasor Domain Solution**
$\bar{V}^{+}_{pgc}$	0.787 (15.3)	0.785 (16.7)	0.826 (10.6)	0.829 (10.9)
$\bar{V}^{-}_{pgc}$	0.113 (–144.6)	0.112 (–142.5)	0.153 (–135.7)	0.155 (–135.2)
$\bar{I}^{+}_{tb}$, $\bar{I}^{+}_{g}$	1.038 (–0.4)	1.092 (1.8)	1.075 (–10.1)	1.076 (–10.7)
$\bar{I}^{-}_{tb}$, $\bar{I}^{-}_{g}$	0.335 (–32.7)	0.338 (–34.6)	0.006 (36.5)	0.005 (67.7)

Table 4.29 Test case 2, comparison between TD and SS solution: WTG-III and IV with LG (BG) fault at Bus 15.

	Wind Park 1 (bus 25)		Wind Park 2 (bus 2)	
WTG variable	**EMTP-RV Solution**	**Phasor Domain Solution**	**EMTP-RV Solution**	**Phasor Domain Solution**
$\bar{V}_{pgc}^{+}$	0.968 (5.7)	0.971 (5.7)	0.959 (4.9)	0.959 (4.7)
$\bar{V}_{pgc}^{-}$	0.044 (–88.1)	0.044 (–86.4)	0.074 (–81.9)	0.075 (–82.3)
$\bar{I}_{tb}^{+}$, $\bar{I}_{g}^{+}$	0.924 (–0.6)	0.930 (–0.5)	0.960 (–3.9)	0.950 (–2.9)
$\bar{I}_{tb}^{-}$, $\bar{I}_{g}^{-}$	0.131 (23.6)	0.134 (21.5)	0.001 (–150.1)	0.002 (120.6)

Table 4.30 Test case 2, comparison between TD and SS solution: WTG-III and IV with LL (AB) fault at Bus 25.

	Wind Park 1 (bus 25)		Wind Park 2 (bus 2)	
WTG variable	**EMTP-RV Solution**	**Phasor Domain Solution**	**EMTP-RV Solution**	**Phasor Domain Solution**
$\bar{V}_{pgc}^{+}$	0.637 (9.9)	0.615 (10.5)	0.747 (1.6)	0.747 (1.6)
$\bar{V}_{pgc}^{-}$	0.326 (–132.9)	0.321 (–130.9)	0.365 (–119.1)	0.365 (–118.9)
$\bar{I}_{tb}^{+}$, $\bar{I}_{g}^{+}$	1.136 (–32.7)	1.072 (–28.5)	1.100 (–29.7)	1.100 (–30.0)
$\bar{I}_{tb}^{-}$, $\bar{I}_{g}^{-}$	0.970 (–20.4)	0.967 (–23.0)	0.008 (47.6)	0.012 (84.0)

Table 4.31 Test case 2 with WTG-III and IV, maximum difference between the TD and SS solution.

	Wind Park 1 (bus 25)		Wind Park 2 (bus 2)	
WTG variable	**Magnitude difference (pu)**	**Angle difference (deg.)**	**Magnitude difference (pu)**	**Angle difference (deg.)**
$\bar{V}_{pgc}^{+}$	0.022	1.4	0.003	0.3
$\bar{V}_{pgc}^{-}$	0.005	2.1	0.002	0.5
$\bar{I}_{tb}^{+}$, $\bar{I}_{g}^{+}$	0.064	4.2	0.010	1.0
$\bar{I}_{tb}^{-}$, $\bar{I}_{g}^{-}$	0.003	2.6	0.004	89.3

These results show that the solver can work with the same precision, with different WTG types in the same network. Table 4.31 summarize the largest difference between EMTP-RV and the SS model for the results shown in Table 4.28 to Table 4.30.

4.7 Conclusion

This chapter has proposed a solver package which allows the simulation of the fault response of the proposed WP SS models of CHAPTER 2 and CHAPTER 3 in two test systems under a variety of fault conditions. The objective is to verify the accuracy of the proposed SS models of CHAPTER 2 and CHAPTER 3 through cross-examination against TD results of EMTP-RV. The solver achieves this objective by solving the WPs and the rest of the network in phase domain using an iterative process to account for non-linear control schemes. The iterative process functions with a fixed-point method, and one iterative loop requires between 5 and 15 iterations to converge.

The chapter has illustrated the accuracy of the solver by comparing the results against those of the TD solver of EMTP-RV. The comparisons have shown the effectiveness of the proposed SS model for both type-III and type-IV based WPs under different operating conditions including different wind generation levels and various prefault conditions, various fault types and locations, and different WP control modes. The proposed solver package gives accurate results for all electrical parameters for magnitude and angle. In most cases, the difference between the TD and SS models is less than 0.03 pu for the magnitude and less than 5.0° for the phase angle. This accuracy is acceptable for protection studies. The chapter has further tested the simple and complete SS models and concluded that the complete model provides a higher precision.

Small differences between the TD and SS models exist because of the non-linear inductances of transformers in EMTP-RV. The main differences are detailed in the next chapter.

CHAPTER 5 ACCURACY LIMITATIONS OF THE STEADY-STATE MODELS

The previous chapter shows that the proposed SS models produce results that are very close to the results of EMTP-RV models. However, there are certain limitations inherent in phasor models.

Given that the models are phasor domain equivalents, it is not possible to encapsulate all of the details of the TD models. The phasor models are integrated into a linear SS solver, and naturally they cannot reproduce the dynamic behaviour of the converters. Finally, a few words have been added in section 5.3 regarding the power system phenomena that cannot be studied in phasor frame in general.

5.1 Limitations of the ECG models

5.1.1 FSC negative sequence behavior with coupled sequence control

In the proposed SS model, the desired active current $\hat{i}_{dg}$ is considered constant. In practice, it comes from a PI controller based on the deviation of the DC-link voltage. Therefore, the oscillations on the DC-link voltage will appear on $\hat{i}_{dg}$ after being processed by the PI controller.

When $\hat{i}_{dg}$ is larger than the limit $I_{dg}^{\max}$ of the current limiter, the limiter sets back i'_{dg} which then becomes a constant signal. However, when $\hat{i}_{dg}$ is not reduced, oscillations remain on i'_{dg}. The presence of negative sequence on the AC side of the GSC induces oscillations in the active power, causing the DC-link voltage to have oscillations at the same frequency of the oscillations on the active power (twice the grid frequency). In addition, the operation of the DC-chopper also results in oscillations on the DC-link voltage. If the frequency of activation of the chopper is close to twice the grid frequency, the chopper also impacts the negative sequence response of the GSC.

In the process of dq-to-abc transformation (section 2.1.7), the magnitude of converter voltage before the choke impedance is divided by the filtered DC-link voltage (2.42). As the filter cannot

remove all oscillations, the oscillations due to the presence of negative sequence or the operation of chopper impact the converter voltage signals.

5.1.2 DFIG positive sequence behavior

This section discusses the limitations of the complete SS model. Limitations due to the simplification of the SS model have been already presented in sections 3.2 and 3.3.

The slip is taken as constant in the model. The slip is related to the mechanical behavior of the machine. However, during a fault, it still varies. The larger the voltage drop and the longer the faults, the larger the magnitude of the oscillations in slip (Figure 5.1). The capital letters indicate the faulted phases.

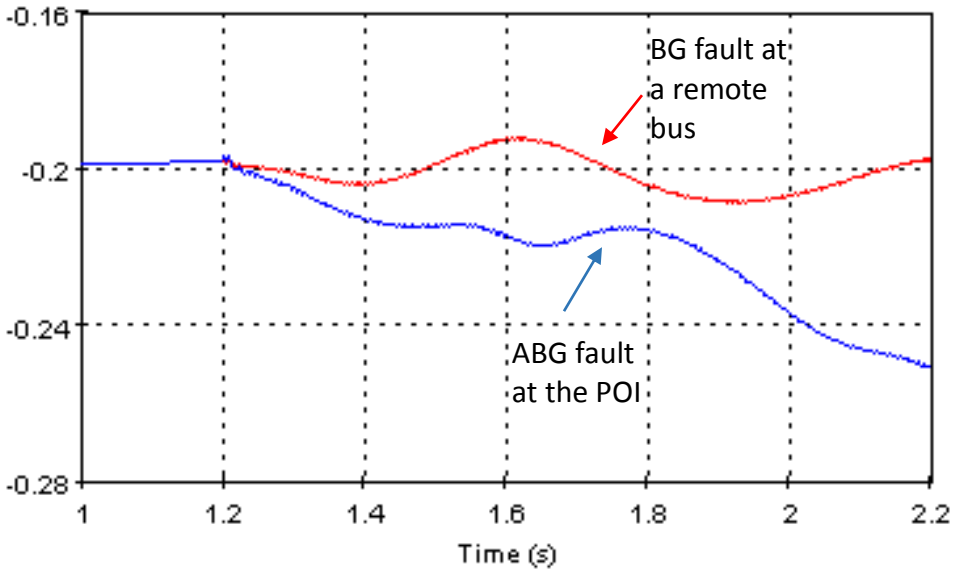

Figure 5.1 Slip variation during uninterrupted faults.

In the complete model, the controller calculates the flux angle, and the calculated value can differ from its theoretical value of –90°. If it is not –90°, the dq components of rotor currents in SFR $I_{qr}^{\prime SFR}$ and $I_{dr}^{\prime SFR}$ will not correspond exclusively to the active and reactive currents. The same observation is true for $I_{qs}^{\prime SFR}$ and $I_{ds}^{\prime SFR}$ as it is seen in Figure 3.10. Consequently, the reactive current dictated by the control mode is not always respected during a fault. This becomes important when the calculated flux angle deviates significantly from its theoretical value.

To calculate the flux angle, the TD model assumes that $L_{ss} \approx L_m$ (Figure 3.3). The deviation from –90° is reduced without making this assumption. In theory, the rotor currents are multiplied by L_m and the stator currents by L_{ss}. In EMT models, under prefault conditions the flux angle is –82.4° with the assumption ($L_{ss} \approx L_m$) and –89.8° without that assumption.

5.1.3 DFIG negative sequence behavior

It is recalled that, the negative sequence parameters appear as oscillations at twice the grid frequency in dq domain.

The phase shift introduced by the measuring filter has an impact on the rotor AC current components, but it is neglected in the SS model as the rotor currents have a low frequency and accordingly the phase shift is negligible. However, the phase shift introduced by the measuring filter has a more important impact on the stator AC current components. The flux angle is corrected by adding this phase shift (3.148).

The next point is the limiter at the output of the inner loop PI controller. It is assumed that the DC component of these two outputs (dq components) is zero. In EMT simulations, the DC component is not always zero because of the correction required to compensate for the phase shift introduced by the measurement filter. The measurement filter shifts the parameters used for the calculation of the abc-to-dq transformation. Therefore, for dq-to-abc transformation, the calculated reference voltages for the PWM system are also shifted. The integral controller of the inner loops corrects this with a DC-offset.

With a DC component present, the output of the limiter will be deformed and the proposed calculations which involve the limiter, will not be valid.

By cutting the PI output, the inner loop limiter creates a non-sinusoidal signal, which contains then harmonics. This signal is then used to obtain the reference voltages for the PWM system. During the dq-to-abc transformation, the harmonics in dq domain becomes other harmonics in phase domain. As the proposed model considers only the nominal frequency phasor, it is not affected by this effect, but it must be highlighted that harmonics are present on the RSC.

5.2 Limitations due to phasor domain solver

The phasor solver does not capture transients and is designed to solve SS conditions iteratively until the network solution and WP control output agree. The adjustment of the reactive current throughout iterations may result in either false or missed transitions to the FRT mode. It is conceivable that the SS model switches to the FRT mode while the EMT model does not.

For example, consider test case 1 with a type-III based WP. The conditions are the same as the conditions provided in section 4.5.1, with $Q'_{POI} = -0.2\,\text{pu}$.

For a line-to-line fault at bus 6 with a fault resistance of 0.5 Ω, the controlled voltage ($\left|\bar{V}^{+}_{mv}\right|$) stays slightly above the FRT activation limit in the EMT model (Figure 5.2). But the SS model switches to the FRT mode.

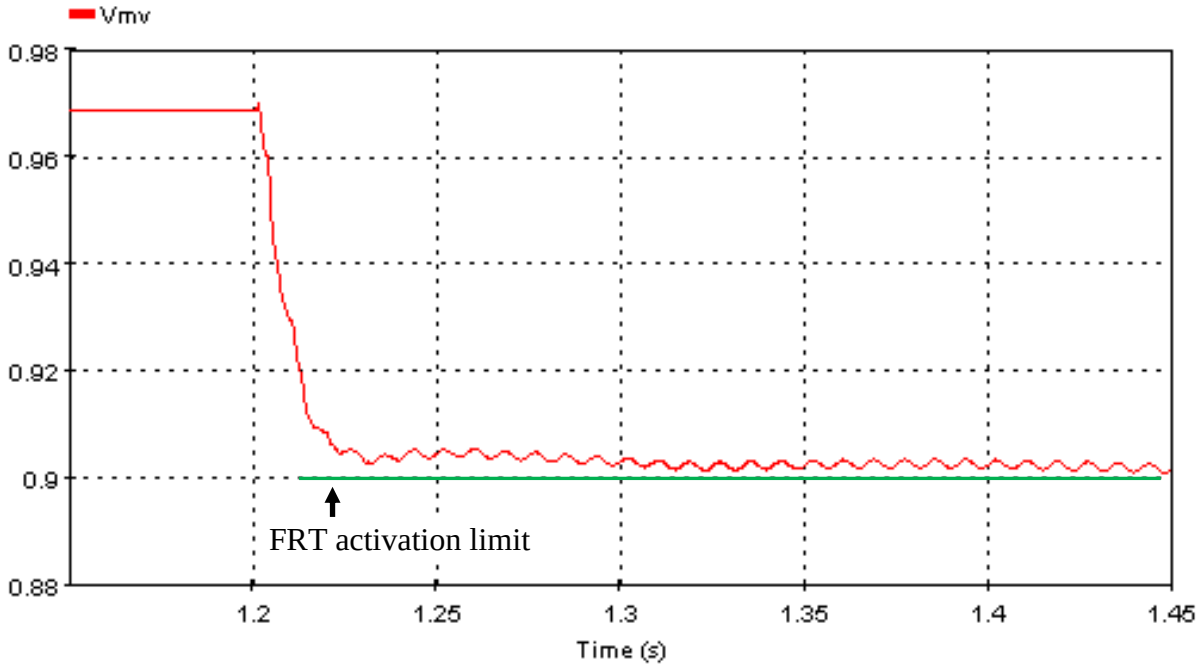

Figure 5.2 FRT mode is not activated in EMT model.

Table 5.1 Test case 1, comparison between TD and SS solution in case of false FRT activation.

WTG variable	EMTP-RV Solution (Q control)	Phasor Domain Solution (FRT mode)
$\bar{V}_{pgc}^{+}$	0.904 (17.8)	0.935 (16.9)
$\bar{V}_{pgc}^{-}$	0.043 (–70.1)	0.043 (–69.1)
$\bar{I}_{tb}^{+}$	0.997 (21.7)	0.968 (16.3)
$\bar{I}_{tb}^{-}$	0.129 (40.1)	0.131 (38.8)

This situation is typically expected for a remote fault as in this example, and the differences between the EMT and SS results are not supposed to be significant.

Table 5.1 compares the results of different solvers for the case under study, and the magnitude difference on the positive sequence voltage and current is 0.03 pu.

5.3 Limitations due to fundamental frequency representation

The proposed SS models provide the current phasor of an ECG during a fault.

For FSC type ECGs, the fault transient is very quick (in the order of 1 to 3 cycles) and the GSC maintains in most cases the output current constant afterwards. Figure 5.3 and Figure 5.4 show, respectively, the TD current and voltage magnitudes of the type-IV WTG for an uninterrupted fault in the test case 1. In those conditions, the activation of the DC chopper induces oscillations of the current magnitudes around an asymptot. In case of loss of synchronism (LOS), i.e. bolted three-phase fault near the ECG, the solution becomes temporary, and is only valid during the first cycles of the fault.

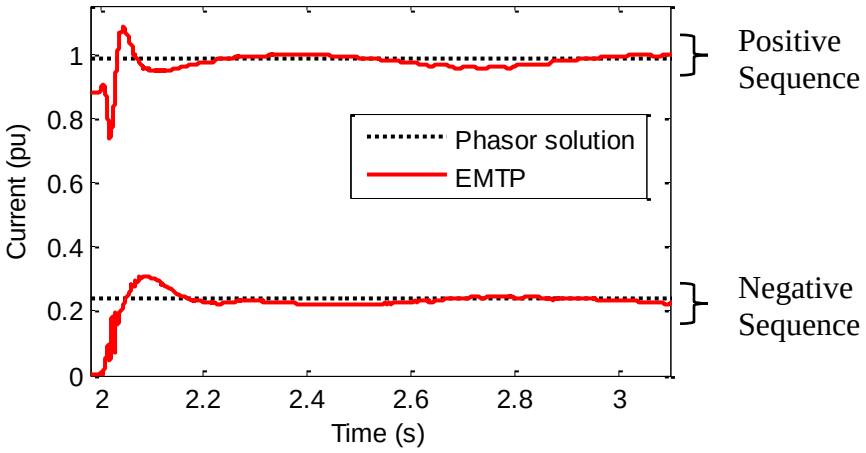

Figure 5.3 Test case 1, EMTP-RV current magnitude waveforms and SS solution: WTG-IV with decoupled control, with LLG (ABG) fault at Bus 1.

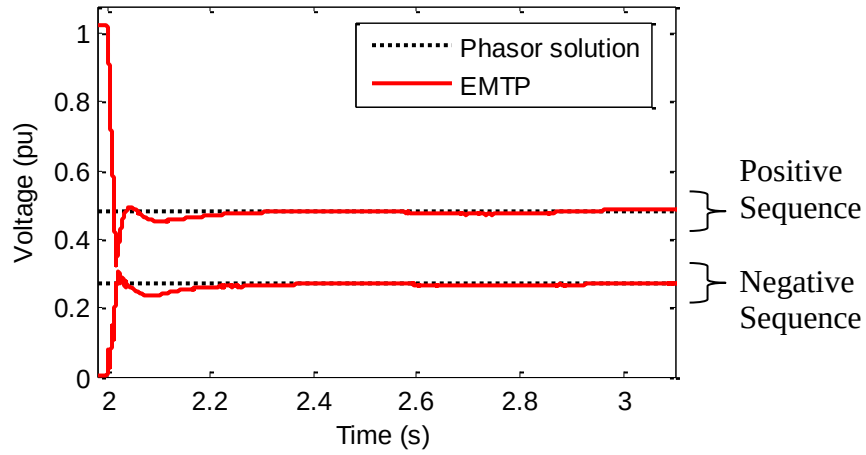

Figure 5.4 Test case 1, EMTP-RV voltage magnitude waveforms and SS solution: WTG-IV with decoupled control, with LLG (ABG) fault at Bus 1.

The type-III WTGs, even when there is no LOS, cannot be fully modeled in phasor domain due to the absence of full SS conditions during a fault. Since the machine is directly connected to the grid through its stator windings, a voltage drop induces an active power drop and a variation in the mechanical rotational speed of the rotor. The slip variation also impacts the RSC inner control loop. Due to these factors, the current output of the WTG will not always stabilize.

Figure 5.5 and Figure 5.6 show, respectively, the TD current and voltage magnitudes of the type-III WTG for an uninterrupted fault at the POI in the test case 1. The magnitudes do not converge to a SS. Figure 5.7 and Figure 5.8 show, respectively, the TD current and voltage magnitudes of the type-III WTG for an uninterrupted remote fault in the test case 1. The magnitudes converge after 250ms.

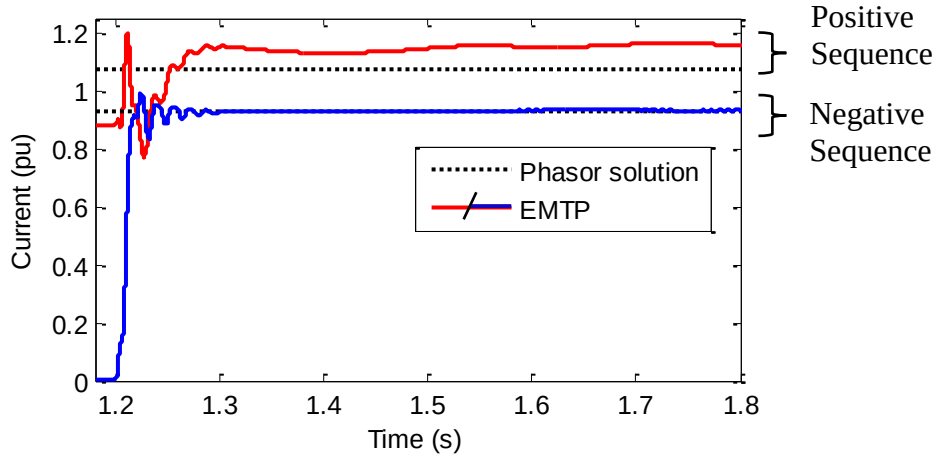

Figure 5.5 Test case 1, EMTP-RV current magnitude waveforms and complete SS solution: WTG-III with LL (AB) fault at Bus 1.

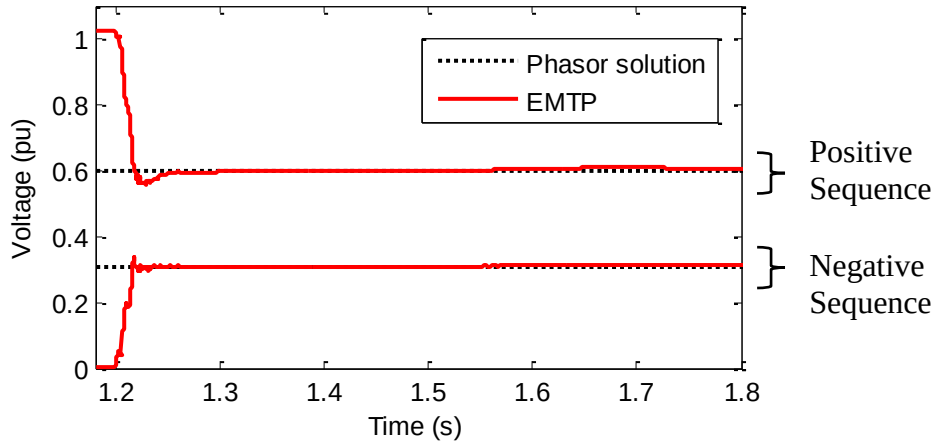

Figure 5.6 Test case 1, EMTP-RV voltage magnitude waveforms and complete SS solution: WTG-III with LL (AB) fault at Bus 1.

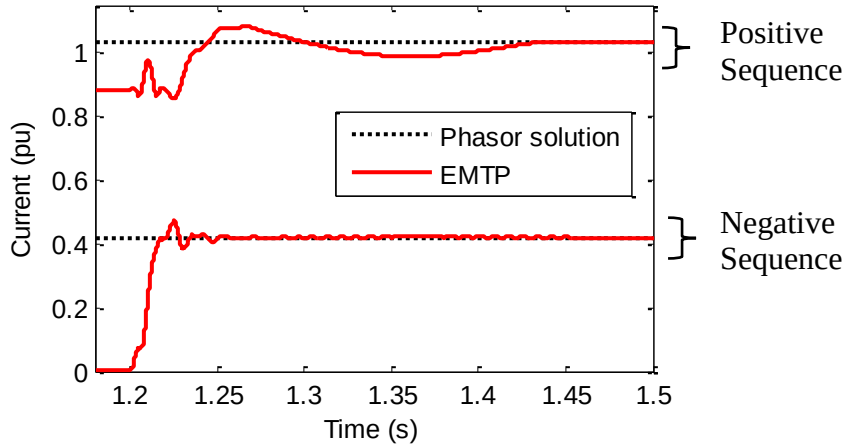

Figure 5.7 Test case 1, EMTP-RV current magnitude waveforms and complete SS solution: WTG-III with LL (AB) fault at Bus 4.

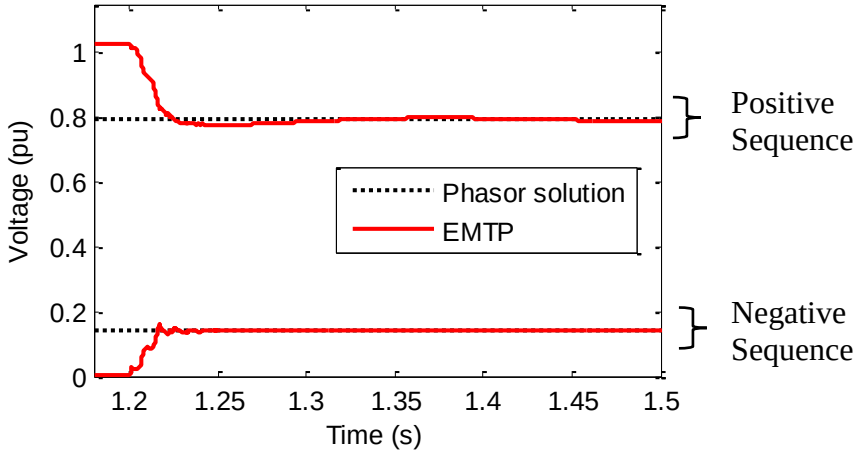

Figure 5.8 Test case 1, EMTP-RV voltage magnitude waveforms and complete SS solution: WTG-III with LL (AB) fault at Bus 4.

For both types of WTGs, the SS model does not calculate the frequency. Therefore, it is unable to detect frequency stability problems.

For example, in an FSC type WP with coupled control, an open phase at the medium voltage side of the park transformer can incite a LOS. The open phase is also represented in the MANA matrix as a switch. It is reminded that the collector grid, on each end, sees the delta side of transformers that are connecting it to the grid or WTGs. Due to open phase, the GSC loses the frequency reference of the grid. As it is an open phase fault, the LOS may be overlooked but when the open phase is closed again, the GSC can become unstable. The stability depends on the

duration of open phase condition and the design of the PLL, in other words, its dynamic behavior.

Figure 5.9 gives an example of an open phase fault in the collector grid of the type-IV based WP of test case 1. In Figure 5.9, the voltage protection system of the GSC is disabled.

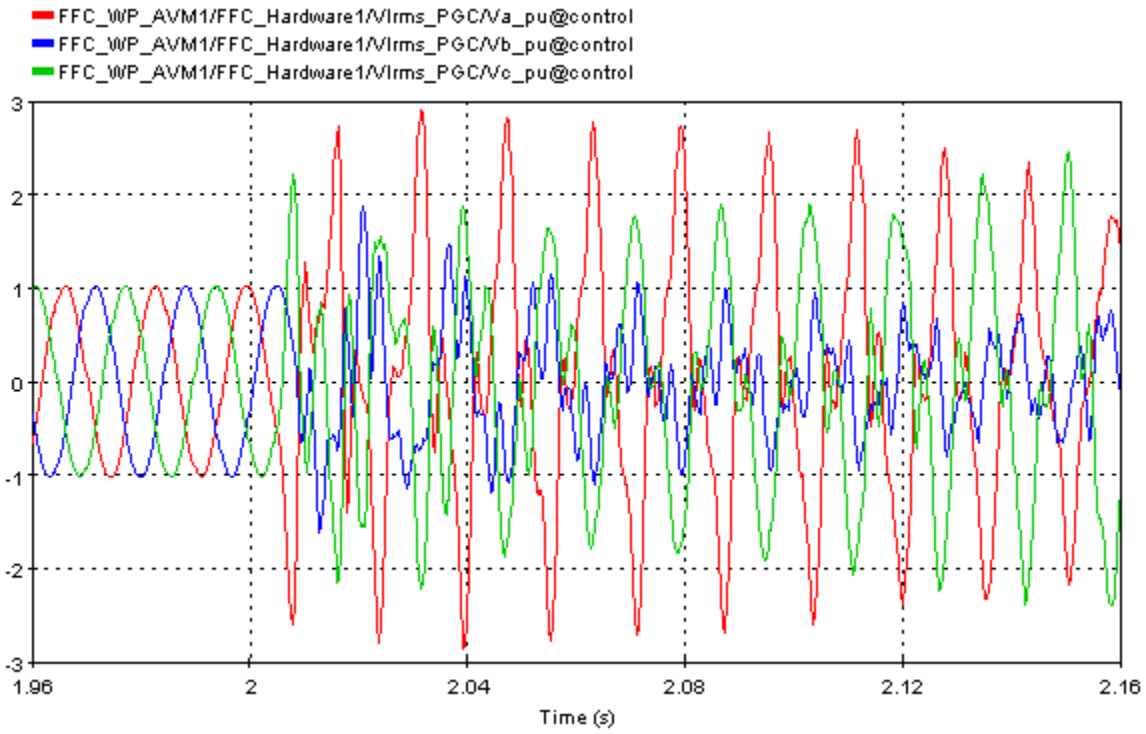

Figure 5.9 PGC phase voltages when a phase opens at MV level.

In this example, the stability of frequency depends on the duration of the open phase. As can be observed from the following figures, an upper bound on open phase duration to ensure stability is between 6 and 7 cycles:

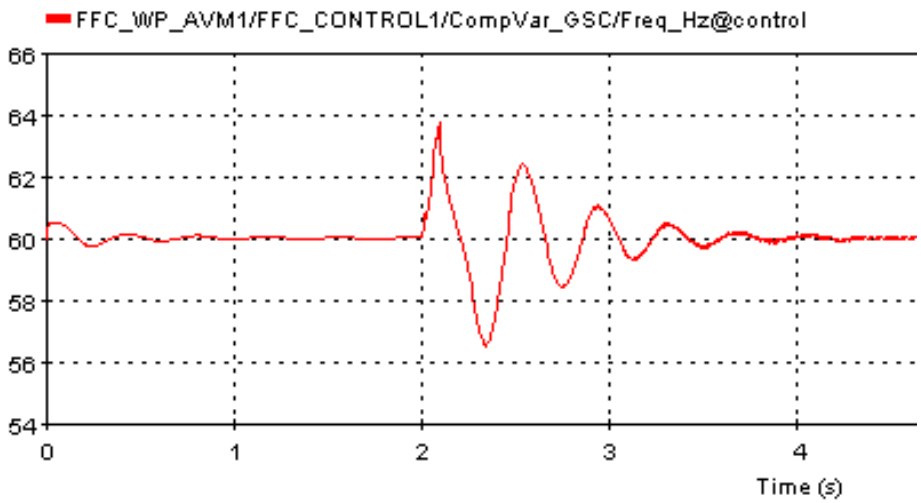

Figure 5.10 GSC recovers after an open phase lasting 6 cycles.

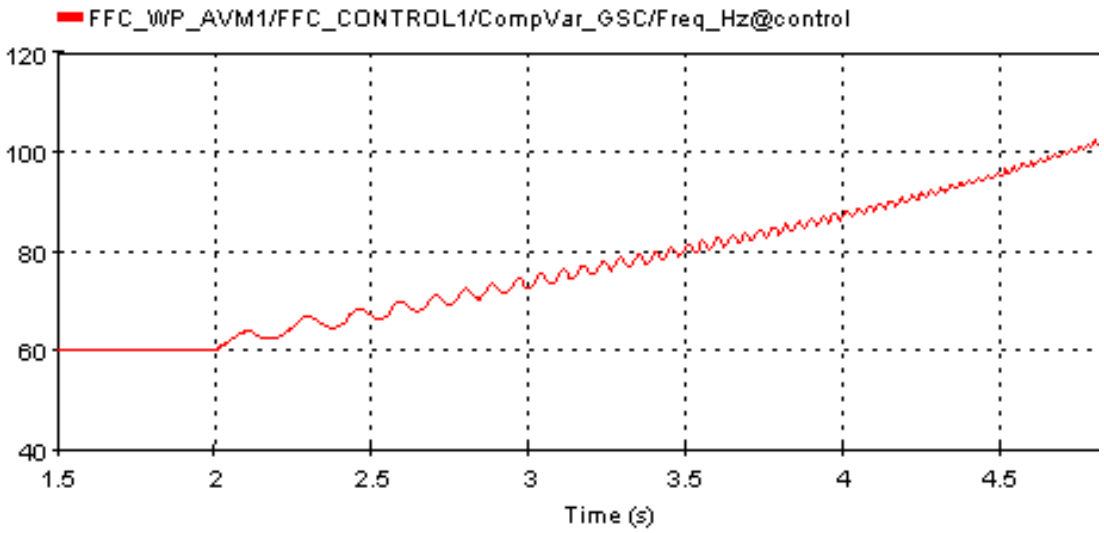

Figure 5.11 GSC becomes unstable after an open phase lasting 7 cycles.

In the SS solver, this open phase condition results in an unstable system. The SS solver will be unable to converge and will reach its maximum iteration number. In the case the maximum number of iteration is reached, the WTGs which are unable to converge must disconnect, i.e., $\bar{I}_{ecg}^{+} = \bar{I}_{ecg}^{-} = 0$.

The WTG SS models cannot be used in the identification of other power system phenomena associated with the dynamic behaviour of controllers and power electronic converters. These phenomena include power swing, ferroresonance, stability and subsynchronous resonance.

5.4 Conclusion

This chapter presents the limitations of the proposed SC models of FSC and DFIG type generators. As the models are in phasor domain, they cannot capture the dynamic behaviour of WTGs. In addition to limitations in modeling, the fundemantal frequency approach prevents us from observing certain phenomena such as the loss of frequency stability.

As the transient behaviour cannot be reproduced, and as the steps in the iterative solution do not really represent the actual operating conditions but only the numerical steps between the prefault conditions and the final SS solution under faulted conditions, the FRT activation in SS models may not always match the activation in detailed TD simulations.

Nevertheless, the proposed SS models give a quick and realistic solution regarding the current contributions of FSC and DFIG type generators under SC conditions.

CHAPTER 6 CONCLUSION AND RECOMMENDATIONS

6.1 Thesis summary

This thesis is about the modeling in phasor domain of electronically coupled renewables, for SS SC and protection studies. To study the impact of renewables on system protection, it is first necessary to characterize the complex fault response characteristics of these generators with reasonable accuracy. Most renewables, such as utility-scale solar/photovoltaic power plants and WPs employing type-IV and type-III WTGs, are integrated into networks by means of electronic power converters. The type-IV WTGs transfer all their power through a DC-link and a GSC. The type-III WTGs are induction machines with a rotor excited by the grid through a DC-link. The type-III WTGs transfer their power through the stator and the GSC. Therefore, they produce current waveform signatures significantly different from traditional synchronous or asynchronous generators. The SC behavior of these ECGs can be analyzed with high precision using circuit-based TD simulation methods and tools such as EMT-type programs. However, due to concerns about engineering time and modeling efforts, it is a common practice to perform SC analysis in phasor domain, and avoid TD methods. TD simulations require more detailed line and control parameters, and require more time with the same computational capacity. Therefore, there is a need to include precise phasor models of renewable powered generating plants in the existing engineering tools of protection and SC studies that rely on phasor solvers.

This thesis describes a SS phasor domain models for renewable power generating plants coupled to the grid by means of power converters, namely type-III and type-IV WTGs. Utility-scale solar plants can be modeled in a manner similar to what is done for type-IV WTGs. The presented models have been developed with the sponsorship of EPRI. Additionally, they have been transferred to the industry and are being implemented in well known protection packages. The SC current contributions of WTGs to faults are controlled by their controllers and must be evaluated by considering the reaction of controls (including various reactive power control schemes) during faults. This thesis developed a SS model for coupled and decoupled sequence controllers for the type-IV WTGs. The coupled controller almost behaves like an open circuit for the negative sequence current. On the other hand, the decoupled controller injects negative sequence current to reduce the active power oscillations during unbalanced faults. For the type-III WTGs, only a

coupled controller is developed but with two levels of accuracy. The complete model requires many controller parameters but is more precise than the simple one.

The presented SS models are control-based equivalent circuits (or simply controlled current sources) that can be integrated into an arbitrary network solver or SC package. The models consist of algorithms that compute the current contributions from WTGs given the terminal voltages, control settings and electrical parameters. The interrelation between network conditions and current contributions is handled by performing iterations as the behavior of converter controllers is non-linear. The non-linearity comes from the current limiter which protects the converters against overcurrents. As the control mode can change during fault conditions, two iterative loops are required. Without any change in control mode, a single iterative loop would be sufficient. The reason that a current source model is used is because the power converter controllers modulate reactive and active power components of the WTGs using current reference in dq frame of reference. The algorithms are implemented in MATLAB and validated with EMTP-RV simulations for various fault conditions using various realistic test systems. The accuracy level of the SS model is sufficient for protection studies. The EMTP-RV models have been developed and improved with the feedback from manufacturers and have been validated against field tests and manufacturer's black box models.

It should be underlined that phasor models provide the SS SC current behavior. For stability or resonance analysis, detailed TD models are required.

6.2 Future work

Under the general scope of the SC SS models of ECGs, future work may be divided into two categories: (1) Improvements on WP models, and (2) Development of models for other applications of grid-connected converters.

Improvements on WP models

The proposed SS models are inspired by the WP behavior of a specific manufacturer. One area of improvement could be the addition of new manufacturer-based models or other types of control.

For example, the FRT mode presented in this thesis is independent of the prefault conditions. Other FRT configurations give an additional reactive current to the prefault one, or set the voltage deviation from prefault conditions [12].

During unbalanced faults, the high injection of positive sequence reactive current can induce overvoltages on the healthy phases [58]. One German grid code indicates that the reactive current requirement during unbalanced fault is only 0.4 pu (compared to 1 pu during balanced faults).

For type-III WTGs, the decoupled control was not developed, but it can be implemented with different purposes: to limit the negative sequence in stator currents or in rotor currents, to limit torque oscillations with the RSC, to limit negative sequence current of the GSC, or to limit the DC-link voltage oscillations with the GSC [59]. [60]–[64] present different control strategies for DFIG under unbalanced conditions.

Other grid applications of converters

Several other equipments require converters connected to the grid, and have specific behavior during fault conditions.

- High Voltage Direct Current (HVDC) terminals,
- Static synchronous compensator (Statcom),
- Grid-scale energy storage.

Each one of them has specific control systems, and bi-directional active power flow.

In the case of multi-terminal HVDC system, the SS model must consider the behavior of each terminal in order to maintain the balance of active power. HVDC model in hybrid configuration (DC and AC lines in parallel) may also bring stability problems as at least two terminals are connected to the same AC network.

With the evolving battery technologies, utility-scale energy storage will become more prevalent in power networks in the coming years. With converters at the scale of HVDC system, the behavior of battery converters during fault conditions must be represented with accuracy for SC and protection studies.

REFERENCES

[1] Global Wind Energy Council (GWEC), "Global Statistics," *gwec.net/global-figures/graphs/* .

[2] Global Wind Energy Council (GWEC), "Market Forecast for 2018-2022," *gwec.net/global-figures/market-forecast-2012-2016/* .

[3] Global Wind Energy Council (GWEC), "Wind in Numbers," *gwec.net/global-figures/wind-in-numbers/* .

[4] P. Barker and R. W. DeMello, "Determining the impact of DG on power systems, radial distribution," *IEEE Power Eng. Soc. Summer Meet.*, pp. 1645–1656, 2000.

[5] M. T. Doyle, "Reviewing the impacts of distributed generation on distribution system protection," *IEEE Power Eng. Soc. Summer Meet.*, pp. 103–105, 2002.

[6] International Std. IEC 909, "Short circuit current calculation in three phase AC systems," 1988.

[7] ANSI/IEEE Std. 141, "IEEE Recommended practice for electric power distribution for industrial plants (Red Book)," 1993.

[8] IEEE Std. 551, "Recommended practice for calculating short circuit currents in industrial and commercial power systems (Violet Book)," 2006.

[9] IEEE Application Guide for IEEE Std. 1547, "IEEE Standard for Interconnecting Distributed Resources with Electric Power Systems," 2008.

[10] A. G. Endegnanew, S. D'Arco, R. E. Torres-Olguin, J. I. Marvik, and E. Tedeschi, "Collation of European grid codes," *Mar. Rep.*, pp. 1–39, 2013.

[11] Hydro-Québec TransÉnergie, "Démonstration du respect des exigences technique d'Hydro-Québec Transénergie visant les centrales éoliennes de producteurs privés," 2013.

[12] "Grid code - high and extra high voltage," E.ON Netz GmbH, Bayreuth, Germany, 2006.

[13] Hydro-Québec TransÉnergie, "Exigences Techniques du Transporteur Relatives au Raccordement des Centrales Électrique au Réseau d'Hydro-Québec," 2009.

[14] E. Farantatos, U. Karaagac, H. Saad, and J. Mahseredjian, "Short-Circuit Current

Contribution of Converter Interfaced Wind Turbines and the Impact on System Protection," *Bulk Power Syst. Dyn. Control – IX*, p. Rethymnon, Greece, 2013.

[15] M. Prodanovic and T. C. Green, "High-quality power generation through distributed control and power park microgrid," *IEEE Trans. Ind. Electron.*, vol. 53, no. 5, pp. 1471–1482, 2006.

[16] A. V. Timbus, P. Rodríguez, R. Teodorescu, M. Liserre, and F. Blaabjerg, "Control strategies for distributed power generation systems operating on faulty grid," *IEEE Int. Symp. Ind. Electron.*, 2006.

[17] M. Brucoli, T. C. Green, and J. D. F. McDonald, "Modelling and analysis of fault behaviour of inverter microgrids to aid future fault detection," *IEEE Int. Conf. Syst. Syst. Eng.*, 2007.

[18] E. Muljadi, N. Samaan, V. Gevorgian, J. Li, and S. Pasupulati, "Short circuit current contribution for different wind turbine generator types," *IEEE PES Gen. Meet.*, 2010.

[19] J. F. Conroy and R. Watson, "Low-voltage ride-through of a full converter wind turbine with permanent magnet generator," *IET Renew. Power Gener.*, vol. 1, no. 3, pp. 182–189, 2007.

[20] C. A. Plet, M. Graovac, T. C. Green, and R. Iravani, "Fault response of grid-connected inverter dominated networks," *IEEE PES Gen. Meet.*, 2010.

[21] J. Martinez, P. C. Kjar, P. Rodríguez, and R. Teodorescu, "Short Circuit Signatures from Different Wind Turbine Generator Types," *IEEE Power Syst. Conf. Expo.*, 2011.

[22] IEEE PES Joint Working Group, "Fault Current Contributions from Wind Plants," 2013.

[23] R. A. Walling, E. Gursoy, and B. English, "Current Contribution from Type III and Type IV Wind Turbine Generators During Faults," *IEEE Transm. Distrib. Conf. Expo.*, p. Orlando, FL, 2012.

[24] I. Kocar, J. Mahseredjian, U. Karaagac, G. Soykan, and O. Saad, "Multiphase load-flow solution for large-scale distribution systems using MANA," *IEEE Trans. Power Deliv.*, vol. 29, no. 2, pp. 908–915, 2014.

[25] M. Z. Kamh and R. Iravani, "Three-phase steady-state model of Type-3 wind generation

unit - Part I: Mathematical models," *IEEE Trans. Sustain. Energy*, vol. 2, no. 4, pp. 477–486, 2011.

[26] M. Z. Kamh and R. Iravani, "A Unified Three-Phase Power-Flow Analysis Model For Electronically Coupled Distributed Energy Resources," *IEEE Trans. Power Deliv.*, vol. 26, no. 2, pp. 899–909, 2011.

[27] H. Hooshyar and M. E. Baran, "Fault Analysis on Distribution Feeders With High Penetration of PV Systems," *IEEE Trans. Power Syst.*, vol. 28, no. 3, pp. 2890–2896, 2013.

[28] M. Fischer and Â. Mendonça, "Representation Of Variable Speed Full Conversion Wind Energy Converters For Steady State Short-Circuit Calculations," *IEEE PES Tansmission Distrib.*, 2012.

[29] M. Valentini, V. Akhmatov, F. Iov, and J. Thisted, "Fault Current Contribution from VSC-based Wind Turbines to the Grid," *2nd Int. Symp. Electr. Electron. Eng.*, 2008.

[30] D. F. Howard, "Short-Circuit Currents in Wind-Turbine Generator Networks," 2013.

[31] D. F. Howard, J. Liang, and R. G. Harley, "Short-circuit modeling of DFIGs with uninterrupted control," *IEEE J. Emerg. Sel. Top. Power Electron.*, vol. 2, no. 1, pp. 47–57, 2014.

[32] A. D. Hansen, G. Michalke, P. Srensen, T. Lund, and F. Iov, "Co-ordinated voltage control of DFIG wind turbines in uninterrupted operation during grid faults," *Wind Energy*, vol. 6, pp. 22–26, 2006.

[33] Q. Wang, N. Zhou, and L. Ye, "Fault Analysis for Distribution Networks With Current-Controlled Three-Phase Inverter-Interfaced Distributed Generators," *IEEE Trans. Power Deliv.*, vol. 30, no. 3, pp. 1532–1542, 2015.

[34] Ö. Göksu, R. Teodorescu, B. Bak-Jensen, F. Iov, and P. C. Kjar, "An iterative approach for symmetrical and asymmetrical Short-circuit calculations with converter-based connected renewable energy sources. Application to wind power," *IEEE Power Energy Soc. Gen. Meet.*, pp. 1–8, 2012.

[35] J. Mahseredjian, S. Dennetière, L. Dubé, B. Khodabakhchian, and L. Gérin-Lajoie, "On a

New Approach for the Simulation of Transients in Power Systems," *Electr. Power Syst. Res.*, vol. 77, no. 11, pp. 1514–1520, 2007.

[36] O. Anaya-Lara, N. Jenkins, J. Ekanayake, P. Cartwright, and M. Hughes, *Wind energy generation : modelling and control*. 2009.

[37] U. Karaagac, H. Saad, J. Peralta, and J. Mahseredjian, "Simulation models for wind parks with variable speed wind turbines in EMTP-RV," Polytechnique Montreal, 2016.

[38] Jorge Martinez Garcia, "Voltage Control in Wind Power Plants with Doybly Fed Generators," 2010.

[39] E. Muljadi *et al.*, "Equivalencing the collector system of a large wind power plant," *IEEE PES Gen. Meet.*, 2006.

[40] S. R. Sanders, J. M. Noworolski, X. Z. Liu, and G. C. Verghese, "Generalized averaging method for power conversion circuits," *IEEE Trans. Power Electron.*, vol. 6, no. 2, pp. 251–259, 1991.

[41] J. Morren, S. W. H. de Haan, P. Bauer, J. Pierik, and J. Bozelie, "Comparison of complete and reduced models of a wind turbine with Doubly-fed Induction Generator," *Proc. 10th Eur. Conf. Power Electron. Appl.*, 2003.

[42] J. G. Slootweg, H. Polinder, and W. L. Kling, "Representing wind turbine electrical generating systems in fundamental frequency simulations," *IEEE Trans. Energy Convers.*, vol. 18, no. 4, pp. 516–524, 2003.

[43] J. Peralta, S. Member, H. Saad, and S. Dennetière, "Dynamic Performance of Average-Value Models for Multi-terminal VSC-HVDC Systems," *IEEE PES Gen. Meet.*, pp. 1–8, 2012.

[44] "Impact of Renewables on System Protection: Wind/PV Short-Circuit Phasor Model Library and Guidelines for System Protection Studies," EPRI 3002008367, Palo Alto, CA, 2016.

[45] Electrocon International Incoporated, "www.electrocon.com" .

[46] APSEN, "www.aspeninc.com" .

[47] B. Cetindag, T. Kauffmann, and I. Kocar, "Modeling of wind parks in multiphase load

flow solver with augmented Jacobian matrix formulation," *IEEE PES Gen. Meet.*, 2016.

[48] EPRI, "Renewable Energy Systems Modeling Considerations for Weak Grid Studies - Limitations of Positive Sequence Models in Comparison with Three-Phase Models," no. 3002010928, 2017.

[49] P. Rodriguez, J. Pou, J. Bergas, I. Candela, R. Burgos, and D. Boroyevich, "Double synchronous reference frame PLL for power converters," *Proc. IEEE PESC*, pp. 1415–1421, 2005.

[50] I. Erlich and U. Bachmann, "Grid code requirements concerning connection and operation of wind turbines in Germany," *IEEE Power Eng. Soc. Gen. Meet. 2005*, pp. 1–5, 2005.

[51] R. Teodorescu, M. Liserre, and P. Rodríguez, *Grid Converters for Photovoltaic and Wind Power Systems*. IEEE/Wiley, 2011.

[52] R. Pena, J. C. Clare, and G. M. Asher, "Doubly fed induction generator using back-to-back PWM converters and its application to variable-speed wind-energy generation," *IEE Proc. - Electr. Power Appl.*, vol. 143, no. 3, p. 231, 1996.

[53] G. R. Slemon, "Modelling of induction machines for electric drives," vol. 25, no. 6, pp. 1126–1131, 1989.

[54] J. B. Ekanayake, L. Holdsworth, and N. Jenkins, "Comparison of 5th order and 3rd order machine models for doubly fed induction generator (DFIG) wind turbines," *Electr. Power Syst. Res.*, vol. 67, no. 3, pp. 207–215, 2003.

[55] I. Kocar, J. S. Lacroix, and F. Therrien, "General and simplified computation of fault flow and contribution of distributed sources in unbalanced distribution networks," *IEEE Power Energy Soc. Gen. Meet.*, pp. 1–8, 2012.

[56] J. S. Lacroix, I. Kocar, and M. Belletête, "Accelerated computation of multiphase short circuit summary for unbalanced distribution systems using the concept of selected inversion," *IEEE Trans. Power Syst.*, vol. 28, no. 2, pp. 1515–1522, 2013.

[57] "http://sites.ieee.org/pes-psdp/benchmark-systems-2/." .

[58] Ö. Göksu, R. Teodorescu, C. L. Bak, F. Iov, and P. Carne Kjær, "Impact of wind power plant reactive current injection during asymmetrical grid faults," *IET Renew. Power*

Gener., vol. 7, no. 5, pp. 484–492, 2013.

[59] S. Engelhardt, J. Kretschmann, J. Fortmann, F. Shewarega, I. Erlich, and C. Feltes, "Negative sequence control of DFG based wind turbines," *IEEE Power Energy Soc. Gen. Meet.*, pp. 1–8, 2011.

[60] T. K. A. Brekken and N. Mohan, "Control of a doubly fed induction wind generator under unbalanced grid voltage conditions," *IEEE Trans. Energy Convers.*, vol. 22, no. 1, pp. 129–135, 2007.

[61] L. Xu and Y. Wang, "Dynamic modeling and control of DFIG-based wind turbines under unbalanced network conditions," *IEEE Trans. Power Syst.*, vol. 22, no. 1, pp. 314–323, 2007.

[62] R. Pena, R. Cardenas, and E. Escobar, "Control system for unbalanced operation of stand-alone doubly fed induction generators," *IEEE Trans. Energy Convers.*, vol. 22, no. 2, pp. 544–545, 2007.

[63] H. Yin, L. Fan, and R. Kavasseri, "Negative sequence compensation techniques of dfig-based wind energy systems under unbalanced grid conditions," in *IEEE Power Electronics and Machines in Wind Applications (PEMWA)*, 2009, p. Lincoln, NE.

[64] L. Fan, H. Yin, and Z. Miao, "A novel control scheme for DFIG-based wind energy systems under unbalanced grid conditions," *Electr. Power Syst. Res.*, vol. 81, no. 2, pp. 254–262, 2011.

APPENDIX A – DETAILED CALCULATIONS OF COMPLETE DFIG MODEL

A.1 RSC inner loop PI limiter

Based on Figure 3.12, the input signal is defined as:

$$v_{in}(\theta) = V\sin(\theta) \tag{A.1}$$

Output signal is defined as:

$$v_{out}(\theta) = \min\left(\left|V\sin(\theta)\right|, V_{\lim}\right)\cdot \operatorname{sign}\left(\sin(\theta)\right) \tag{A.2}$$

Parameter α is defined as:

$$\begin{aligned} V\sin(\alpha) &= V_{lim} \\ \alpha &= \sin^{-1}\left(\frac{V_{lim}}{V}\right) \end{aligned} \tag{A.3}$$

As both v_{in} and v_{out} are odd functions, the fundamental component is only a sine. Consequently, the fundamental component can be calculated with:

$$V_1 = \frac{2}{\pi/2}\int_0^{\pi/2} v_{out}(\theta)\sin(\theta)\,d\theta \tag{A.4}$$

$$V_1 = \frac{4}{\pi}\left(\int_0^{\alpha} V\sin(\theta)\sin(\theta)\,d\theta + \int_{\alpha}^{\pi/2} V_{\lim}\sin(\theta)\,d\theta\right) \tag{A.5}$$

$$V_1 = \frac{4}{\pi}\left(\int_0^{\alpha} V\frac{1-\cos(2\theta)}{2}\,d\theta + \int_{\alpha}^{\pi/2} V_{\lim}\sin(\theta)\,d\theta\right)$$

$$V_1 = \frac{4}{\pi}\left(\frac{V}{2}\left[\theta - \frac{\sin(2\theta)}{2}\right]_0^{\alpha} + V_{\lim}\left[-\cos(\theta)\right]_{\alpha}^{\pi/2}\right)$$

$$V_1 = \frac{4}{\pi}\left(\frac{V}{2}\left[\alpha - \frac{\sin(2\alpha)}{2}\right] + V_{\lim}\cos(\alpha)\right)$$

It holds that: $\sin(2\alpha) = 2\cos(\alpha)\sin(\alpha)$

$$V_1 = \frac{4}{\pi}\left(\frac{V}{2}\left[\alpha - \frac{2\cos(\alpha)\sin(\alpha)}{2}\right] + V_{\lim}\cos(\alpha)\right)$$

$$V_1 = \frac{4}{\pi}\left(\frac{V\alpha}{2} - \frac{V\cos(\alpha)\sin(\alpha)}{2} + V_{\lim}\cos(\alpha)\right)$$

By using (A.3):

$$V_1 = \frac{4}{\pi}\left(\frac{V\alpha}{2} - \frac{V_{\lim}\cos(\alpha)}{2} + V_{\lim}\cos(\alpha)\right)$$

$$V_1 = \frac{4}{\pi}\left(\frac{V\alpha}{2} + \frac{V_{\lim}\cos(\alpha)}{2}\right) = \frac{2}{\pi}\left[V\alpha + V_{\lim}\cos(\alpha)\right] \qquad \text{(A.6)}$$

A.2 Substitution to calculate rotor currents

Equations (3.150) to (3.155) form a system of 6 equations with 6 unknowns: $\underline{\underline{\bar{V}}}_{dr}^{SFR}$, $\underline{\underline{\bar{V}}}_{qr}^{SFR}$, $\underline{\underline{\bar{I}}}_{dr}^{SFR}$, $\underline{\underline{\bar{I}}}_{qr}^{SFR}$, $\underline{\underline{\bar{I}}}_{ds}^{SFR}$, $\underline{\underline{\bar{I}}}_{qs}^{SFR}$. The expressions of rotor currents are calculated here by substitution.

By canceling $\underline{\underline{\bar{V}}}_{dr}^{SFR}$ with the combination of (3.150) and (3.152) we obtain:

$$\begin{aligned} 0 = {} & \underline{\underline{\bar{I}}}_{dr}^{SFR}\left[\frac{-H_{PI}^{rd}}{\gamma^2}H_{filter} - R_r - 2jX_{rr}\right] + \underline{\underline{\bar{I}}}_{qr}^{SFR}s\left[X_{rr} - X_X H_{filter}\right] \\ & -2jX_m\underline{\underline{\bar{I}}}_{ds}^{SFR} + sX_m\underline{\underline{\bar{I}}}_{qs}^{SFR} \end{aligned} \qquad \text{(A.7)}$$

It is rewritten as:

$$0 = A_{rd}\underline{\underline{\bar{I}}}_{dr}^{SFR} + A_{rq}\underline{\underline{\bar{I}}}_{qr}^{SFR} + A_{sd}\underline{\underline{\bar{I}}}_{ds}^{SFR} + A_{sq}\underline{\underline{\bar{I}}}_{qs}^{SFR} \qquad \text{(A.8)}$$

with:

$$\begin{aligned} A_{rd} &= \frac{-H_{PI}^{rd}}{\gamma^2} H_{filter} - R_r - 2jX_{rr} \\ A_{rq} &= s\left[X_{rr} - X_X H_{filter} \right] \\ A_{sd} &= -2jX_m \\ A_{sq} &= sX_m \end{aligned} \tag{A.9}$$

The same is done for $\underline{\underline{V}}_{qr}^{SFR}$ with (3.151) and (3.153):

$$\begin{aligned} 0 = {} & \underline{\underline{I}}_{dr}^{SFR} sX_{rr}\left(H_{filter} - 1\right) + \underline{\underline{I}}_{qr}^{SFR}\left[\frac{-H_{PI}^{rq}}{\gamma^2} H_{filter} - R_r - 2jX_{rr} \right] \\ & + \underline{\underline{I}}_{ds}^{SFR} sX_m\left[\left(H_{filter}\right)^2 - 1 \right] - 2jX_m \underline{\underline{I}}_{qs}^{SFR} \end{aligned} \tag{A.10}$$

It is rewritten as:

$$0 = B_{rd}\underline{\underline{I}}_{dr}^{SFR} + B_{rq}\underline{\underline{I}}_{qr}^{SFR} + B_{sd}\underline{\underline{I}}_{ds}^{SFR} + B_{sq}\underline{\underline{I}}_{qs}^{SFR} \tag{A.11}$$

with:

$$\begin{aligned} B_{rd} &= sX_{rr}\left(H_{filter} - 1\right) \\ B_{rq} &= \frac{-H_{PI}^{rq}}{\gamma^2} H_{filter} - R_r - 2jX_{rr} \\ B_{sd} &= sX_m\left[\left(H_{filter}\right)^2 - 1 \right] \\ B_{sq} &= -2jX_m \end{aligned} \tag{A.12}$$

To calculate the two rotor currents from (3.154) and (3.155), the two stator currents need to be replaced by two expressions containing only rotor currents. These two expressions are obtained from (A.8) and (A.11).

$\underline{\underline{I}}_{qs}^{SFR}$ is isolated in (A.8), and then injected in (A.11). Then $\underline{\underline{I}}_{ds}^{SFR}$ can be expressed as a function of rotor currents:

$$\underline{\underline{I}}_{ds}^{SFR} = E_{rd}\underline{\underline{I}}_{dr}^{SFR} + E_{rq}\underline{\underline{I}}_{qr}^{SFR} \tag{A.13}$$

with

$$E_{rd} = \frac{-B_{rd}A_{sq} + B_{sq}A_{rd}}{B_{sd}A_{sq} - B_{sq}A_{sd}}$$
$$E_{rq} = \frac{-B_{rq}A_{sq} + B_{sq}A_{rq}}{B_{sd}A_{sq} - B_{sq}A_{sd}} \quad \text{(A.14)}$$

The same principle is applied to have an expression of $\bar{\bar{I}}_{qs}^{SFR}$. For that purpose, (A.13) is injected in (A.8):

$$\bar{\bar{I}}_{qs}^{SFR} = F_{rd}\bar{\bar{I}}_{dr}^{SFR} + F_{rq}\bar{\bar{I}}_{qr}^{SFR} \quad \text{(A.15)}$$

with

$$F_{rd} = \frac{-A_{sd}E_{rd} - A_{rd}}{A_{sq}}$$
$$F_{rq} = \frac{-A_{sd}E_{rq} - A_{rq}}{A_{sq}} \quad \text{(A.16)}$$

(A.13) and (A.15) give expressions of stator currents as a function of rotor currents. These two relations are now injected in the electrical equations of stator voltages (3.154) and (3.155).

$$\bar{\bar{V}}_{ds}^{SFR} = H_{rd}\bar{\bar{I}}_{dr}^{SFR} + H_{rq}\bar{\bar{I}}_{qr}^{SFR} \quad \text{(A.17)}$$

with

$$H_{rd} = E_{rd}\left(R_s + 2jX_{ss}\right) + 2jX_m - X_{ss}F_{rd}$$
$$H_{rq} = E_{rq}\left(R_s + 2jX_{ss}\right) - X_m - X_{ss}F_{rq} \quad \text{(A.18)}$$

and

$$\bar{\bar{V}}_{qs}^{SFR} = K_{rd}\bar{\bar{I}}_{dr}^{SFR} + K_{rq}\bar{\bar{I}}_{qr}^{SFR} \quad \text{(A.19)}$$

with

$$K_{rd} = F_{rd}\left(R_s + 2jX_{ss}\right) + X_m + X_{ss}E_{rd}$$
$$K_{rq} = F_{rq}\left(R_s + 2jX_{ss}\right) + 2jX_m + X_{ss}E_{rq} \quad \text{(A.20)}$$

With (A.17) and (A.19) there is a basic system of two equations with two unknowns: the rotor currents.

$$\underline{\underline{I}}_{dr}^{SFR} = \frac{H_{rq}\underline{\underline{V}}_{qs}^{SFR} - K_{rq}\underline{\underline{V}}_{ds}^{SFR}}{K_{rd}H_{rq} - K_{rq}H_{rd}} \tag{A.21}$$

$$\underline{\underline{I}}_{qr}^{SFR} = \frac{\underline{\underline{V}}_{ds}^{SFR} - H_{rd}\underline{\underline{I}}_{dr}^{SFR}}{H_{rq}} \tag{A.22}$$

Changing (A.21) and (A.22) to fit (3.161) and (3.162):

$$K_{r1} = \frac{-K_{rq}}{K_{rd}H_{rq} - K_{rq}H_{rd}} \qquad K_{r2} = \frac{H_{rq}}{K_{rd}H_{rq} - K_{rq}H_{rd}} \tag{A.23}$$

$$K_{r3} = \frac{K_{rd}}{K_{rd}H_{rq} - K_{rq}H_{rd}} \qquad K_{r4} = \frac{-H_{rd}}{K_{rd}H_{rq} - K_{rq}H_{rd}} \tag{A.24}$$

A.3 Substitution to calculate stator currents

To calculate the stator currents, the electrical equations of stator voltages (3.154) and (3.155) are combined with (A.8) and (A.11). Here, the rotor currents are replaced by expression only containing stator currents.

$\underline{\underline{I}}_{dr}^{SFR}$ is isolated in (A.8), and then injected in (A.11):

$$\underline{\underline{I}}_{qr}^{SFR} = D_{sd}\underline{\underline{I}}_{ds}^{SFR} + D_{sq}\underline{\underline{I}}_{qs}^{SFR} \tag{A.25}$$

with

$$\begin{aligned} D_{sd} &= \frac{B_{rd}A_{sd} - B_{sd}A_{rd}}{B_{rq}A_{rd} - B_{rd}A_{rq}} \\ D_{sq} &= \frac{B_{rd}A_{sq} - B_{sq}A_{rd}}{B_{rq}A_{rd} - B_{rd}A_{rq}} \end{aligned} \tag{A.26}$$

The same principle is applied to obtain an expression of $\underline{\underline{I}}_{dr}^{SFR}$. For that purpose, (A.25) is injected in (A.8):

$$\underline{\underline{I}}_{dr}^{SFR} = C_{sd}\underline{\underline{I}}_{ds}^{SFR} + C_{sq}\underline{\underline{I}}_{qs}^{SFR} \tag{A.27}$$

with

$$C_{sd} = \frac{-A_{sd} - A_{rq}D_{sd}}{A_{rd}}$$
$$C_{sq} = \frac{-A_{rq}D_{sq} - A_{sq}}{A_{rd}} \tag{A.28}$$

Now expressions (A.25) and (A.27) can be injected in (3.154) and (3.155):

$$\bar{\bar{V}}_{ds}^{SFR} = H_{sd}\bar{\bar{I}}_{ds}^{SFR} + H_{sq}\bar{\bar{I}}_{qs}^{SFR} \tag{A.29}$$

with

$$H_{sd} = R_s + 2jX_{ss} - X_m D_{sd} + 2jX_m C_{sd}$$
$$H_{sq} = -X_{ss} - X_m D_{sq} + 2jX_m C_{sq} \tag{A.30}$$

and for $\bar{\bar{V}}_{qs}^{SFR}$:

$$\bar{\bar{V}}_{qs}^{SFR} = K_{sd}\bar{\bar{I}}_{ds}^{SFR} + K_{sq}\bar{\bar{I}}_{qs}^{SFR} \tag{A.31}$$

with

$$K_{sd} = X_{ss} + X_m C_{sd} + 2jX_m D_{sd}$$
$$K_{sq} = R_s + 2jX_{ss} + X_m C_{sq} + 2jX_m D_{sq} \tag{A.32}$$

Expressions (A.29) and (A.31) give a system with the two unknown stator currents. This system is solved by substitution in the same way as rotor currents (see (3.161) and (A.22)):

$$\bar{\bar{I}}_{ds}^{SFR} = \frac{H_{sq}\bar{\bar{V}}_{qs}^{SFR} - K_{sq}\bar{\bar{V}}_{ds}^{SFR}}{K_{sd}H_{sq} - K_{sq}H_{sd}} \tag{A.33}$$

$$\bar{\bar{I}}_{qs}^{SFR} = \frac{\bar{\bar{V}}_{ds}^{SFR} - H_{sd}\bar{\bar{I}}_{ds}^{SFR}}{H_{sq}} \tag{A.34}$$

Changing (A.33) and (A.34) to fit (3.171) and (3.172):

$$K_{s1} = \frac{-K_{sq}}{K_{sd}H_{sq} - K_{sq}H_{sd}} \qquad K_{s2} = \frac{H_{sq}}{K_{sd}H_{sq} - K_{sq}H_{sd}} \tag{A.35}$$

$$K_{s3} = \frac{K_{sd}}{K_{sd}H_{sq} - K_{sq}H_{sd}} \qquad K_{s4} = \frac{-H_{sd}}{K_{sd}H_{sq} - K_{sq}H_{sd}} \tag{A.36}$$

A.4 Reverse dq0 transformation: from dq0 to abc

Let us define d and q signals as:

$$x_d = X_d + A_d \cos\left(2\omega_s t + \varphi_d\right) \tag{A.37}$$

$$x_q = X_q + A_q \cos\left(2\omega_s t + \varphi_q\right) \tag{A.38}$$

where

- X_d and X_q are the DC components of the d and q signals respectively
- A_d and A_q are the magnitudes of AC component of the d and q signals respectively
- φ_d and φ_q are the angles of AC component of the d and q signals respectively

The reverse transformation matrix gives the relations to obtain phase signals:

$$x_a = x_d \cos\left(\theta_{park}\right) - x_q \sin\left(\theta_{park}\right) + x_0 \tag{A.39}$$

$$x_b = x_d \cos\left(\theta_{park} - \frac{2\pi}{3}\right) - x_q \sin\left(\theta_{park} - \frac{2\pi}{3}\right) + x_0 \tag{A.40}$$

$$x_c = x_d \cos\left(\theta_{park} + \frac{2\pi}{3}\right) - x_q \sin\left(\theta_{park} + \frac{2\pi}{3}\right) + x_0 \tag{A.41}$$

with

$$\theta_{park} = \omega_s t + \varphi_{park} \tag{A.42}$$

Here zero sequence is equal to zero:

$$x_0 = 0 \tag{A.43}$$

As example, the calculation details are given for x_a. So (A.37) and (A.38) are injected in (A.39):

$$\begin{aligned} x_a = {} & X_d \cos\left(\theta_{park}\right) + A_d \cos\left(2\omega_s t + \varphi_d\right)\cos\left(\theta_{park}\right) \\ & - X_q \sin\left(\theta_{park}\right) - A_q \cos\left(2\omega_s t + \varphi_q\right)\sin\left(\theta_{park}\right) \end{aligned} \tag{A.44}$$

By applying several trigonometric equations, we obtain:

$$\begin{aligned} x_a = {} & \sqrt{{X_d}^2 + {X_q}^2}\cos\left(\omega_s t + \varphi_{park} + \tan^{-1}\left(\frac{X_q}{X_d}\right)\right) \\ & + \frac{A_d}{2}\left[\cos\left(\omega_s t + \varphi_d - \varphi_{park}\right) + \cos\left(3\omega_s t + \varphi_d + \varphi_{park}\right)\right] \\ & \frac{-A_q}{2}\left[-\sin\left(\omega_s t + \varphi_q - \varphi_{park}\right) + \sin\left(3\omega_s t + \varphi_q + \varphi_{park}\right)\right] \end{aligned} \tag{A.45}$$

Here, as we are focused on negative sequence, the components with $3\omega_s t$ are removed to make the equations less heavy:

$$\begin{aligned} x_a = {} & \sqrt{{X_d}^2 + {X_q}^2}\cos\left(\omega_s t + \varphi_{park} + \tan^{-1}\left(\frac{X_q}{X_d}\right)\right) \\ & + \frac{A_d}{2}\cos\left(\omega_s t - \varphi_{park} + \varphi_d\right) + \frac{A_q}{2}\sin\left(\omega_s t - \varphi_{park} + \varphi_q\right) \end{aligned} \tag{A.46}$$

By applying another trigonometric conversion on the second line of (A.46), we obtain:

$$\begin{aligned} x_a = {} & \sqrt{{X_d}^2 + {X_q}^2}\cos\left(\omega_s t + \varphi_{park} + \tan^{-1}\left(\frac{X_q}{X_d}\right)\right) \\ & + A_2\cos\left(\omega_s t - \varphi_{park} + \theta_2\right) \end{aligned} \tag{A.47}$$

with

$$A_2 = \frac{1}{2}\sqrt{{A_d}^2 + {A_q}^2 - 2A_d A_q \sin\left(\varphi_d - \varphi_q\right)} \tag{A.48}$$

$$\theta_2 = \tan^{-1}\left(\frac{A_d \sin\left(\varphi_d\right) - A_q \cos\left(\varphi_q\right)}{A_d \cos\left(\varphi_d\right) + A_q \sin\left(\varphi_q\right)}\right) \tag{A.49}$$

The same development is done with b and c:

$$\begin{aligned} x_b = {} & \sqrt{{X_d}^2 + {X_q}^2}\cos\left(\omega_s t + \varphi_{park} + \tan^{-1}\left(\frac{X_q}{X_d}\right) - \frac{2\pi}{3}\right) \\ & + A_2\cos\left(\omega_s t - \varphi_{park} + \theta_2 + \frac{2\pi}{3}\right) \end{aligned} \tag{A.50}$$

$$x_c = \sqrt{X_d{}^2 + X_q{}^2}\cos\left(\omega_s t + \varphi_{park} + \tan^{-1}\left(\frac{X_q}{X_d}\right) + \frac{2\pi}{3}\right) + A_2\cos\left(\omega_s t - \varphi_{park} + \theta_2 - \frac{2\pi}{3}\right) \tag{A.51}$$

From the three phase expressions, the positive and negative sequences can be easily identified:

$$x_{pos} = \sqrt{X_d{}^2 + X_q{}^2}\cos\left(\omega_s t + \varphi_{park} + \tan^{-1}\left(\frac{X_q}{X_d}\right)\right) \tag{A.52}$$

$$x_{neg} = A_2\cos\left(\omega_s t - \varphi_{park} + \theta_2\right) \tag{A.53}$$

where A_2 and θ_2 are defined in (A.48) and (A.49).

APPENDIX B – DFIG COMPLETE MODEL ALGORITHM

B.1 Main algorithm

This algorithm is similar to the one in section 3.2.4 but with the complete model described in section 3.3. As for the other algorithm, there are initialization calculations.

Initialization

$$P'_{pgc} + j\,Q'_{pgc} = \bar{V}^{+(0)}_{pgc}\left(\bar{I}^{+(0)}_{pgc}\right)^{*} \tag{B.1}$$

$$\bar{I}^{+(0)}_{tb} = \bar{I}^{+(0)}_{pgc} + \frac{\bar{V}^{+(0)}_{pgc}}{\bar{Z}_{filter}} \tag{B.2}$$

$$P_0 = \frac{P_{rated}}{(1-s_{rated})^3} \tag{B.3}$$

$$P'_{tb} = P'_{pgc} - \text{real}\left(\frac{\left|\bar{V}^{+}_{pgc}\right|^2}{\bar{Z}_{filter}}\right) \tag{B.4}$$

$$s = 1 - \sqrt[3]{\frac{P'_{tb}}{P_0}} \tag{B.5}$$

$$I^{SVR(0)}_{dtb} + j\,I^{SVR(0)}_{qtb} = \frac{\bar{I}^{+(0)}_{tb}}{\exp\left(j\ \text{angle}\left(\bar{V}^{+(0)}_{pgc}\right)\right)} \tag{B.6}$$

$$\begin{aligned} I^{SFR(0)}_{ds} &= I^{SVR(0)}_{qs} = I^{SVR(0)}_{qtb} \\ I^{SFR(0)}_{dr} &= \gamma\left(\left|\bar{V}^{+(0)}_{pgc}\right| \Big/ X_{ss} - \hat{I}^{SFR(0)}_{ds}\right) \end{aligned} \tag{B.7}$$

$$I^{SVR(0)}_{dg} = sI^{SVR(0)}_{dtb} \tag{B.8}$$

$$
\begin{aligned}
I_{ds}^{SVR(0)} &= \left(1-s\right) I_{dtb}^{SVR(0)} \\
I_{qs}^{SFR(0)} &= -I_{ds}^{SVR(0)} \\
I_{qr}^{SFR(0)} &= -\gamma I_{qs}^{SFR(0)} = \gamma\left(1-s\right) I_{dtb}^{SVR(0)}
\end{aligned}
\tag{B.9}
$$

IF {control at MV side of turbine transformer}

$$V_{ctrl}^{+(0)} = \left|\bar{V}_{mv}^{+(0)}\right| = \left|\bar{V}_{pgc}^{+(0)} - \bar{I}_{pgc}^{+(0)}\bar{Z}_{tt}^{+}\right| \tag{B.10}$$

ELSE

$$V_{ctrl}^{+(0)} = \left|\bar{V}_{pgc}^{+(0)}\right| \tag{B.11}$$

END

$$dU' = \left(\hat{I}_{dr}^{SFR(0)} - \left|\bar{V}_{pgc}^{+(0)}\right| / X_m\right) / K_V + V_{ctrl}^{+(0)} - 1 \tag{B.12}$$

$$
\begin{aligned}
\varphi_{flux}^{(0)} &= -80° \\
\bar{I}_s^{-(0)} &= 0
\end{aligned}
\tag{B.13}
$$

Algorithm

$$V_{pgc}^{+(k)} = \left|\bar{V}_{pgc}^{+(k)}\right| \tag{B.14}$$

LOOP 2

$$
\begin{aligned}
V_{ds}^{SFR(k)} &= V_{pgc}^{+(k)} \cos\left(-\varphi_{flux}^{(k-1)}\right) \\
V_{qs}^{SFR(k)} &= V_{pgc}^{+(k)} \sin\left(-\varphi_{flux}^{(k-1)}\right)
\end{aligned}
\tag{B.15}
$$

Calculation of $\hat{I}_{dr}^{SFR(k)}$:

IF {controlled voltage is $\bar{V}_{mv}^{+}$}

$$V_{ctrl}^{+(k)} = \left|\bar{V}_{mv}^{+(k)}\right| = \left|\bar{V}_{pgc}^{+(k)} - \bar{I}_{pgc}^{+(k)}\bar{Z}_{tt}^{+}\right| \tag{B.16}$$

ELSE

$$V_{ctrl}^{+(k)} = V_{pgc}^{+(k)} \tag{B.17}$$

END

IF {Q-control **OR** PF-control **OR** V-control}

$$\hat{I}_{dr}^{SFR(\mathrm{k})} = K_V \left(1 - \bar{V}_{ctrl}^{+(k)} + \Delta U'\right) + V_{pgc}^{+(k)} / X_m \tag{B.18}$$

IF {FRT-function}

$$\hat{I}_{dr}^{SFR(\mathrm{k})} = K_{FRT} \left(1 - V_{ctrl}^{+(k)}\right) + V_{pgc}^{+(k)} / X_m \tag{B.19}$$

END

$$\hat{I}_{dr}^{SFR(k)} = \mathrm{sign}\left(\hat{I}_{dr}^{SFR(k)}\right) \min\left(\left|\hat{I}_{dr}^{SFR(k)}\right|, I_{dr}^{\lim}\right) \tag{B.20}$$

Calculation of $\hat{I}_{qr}^{SFR(k)}$:

$$P_{tb}' = P_{pgc}' + \mathrm{real}\left(\frac{\left(V_{pgc}^{+(k)}\right)^2}{Z_{filter}^{\ *}}\right) \tag{B.21}$$

$$\hat{I}_{qr}^{SFR(k)} = \gamma \left[\frac{\frac{P_{tb}'}{V_{pgc}^{+(k)}} - I_{dg}'^{SVR(k-1)} + I_{ds}'^{SFR(k-1)} \cos\left(-\varphi_{flux}^{(k-1)}\right)}{\sin\left(-\varphi_{flux}^{(k-1)}\right)} - \frac{V_{ds}^{SFR(k)}}{X_{ss}}\right] \tag{B.22}$$

Note: $I_{ds}'^{SFR(k-1)}$ *is used, instead of the new one, because it is not limited.*

$$\hat{I}_{qr}^{SFR(k)} = 0.5\left(\hat{I}_{qr}^{SFR(k)} + I_{qr}'^{SFR(k-1)}\right) \tag{B.23}$$

$$\hat{I}_{qr}^{SFR(k)} = \min\left(\hat{I}_{qr}^{SFR(k)}, I_{qr}^{\lim}\right), \qquad I_{qr}^{\lim} = 1pu \tag{B.24}$$

RSC limits according to the priority:

IF {P-priority}

$$I'^{SFR}_{qr} = \hat{I}^{SFR(k)}_{qr} \tag{B.25}$$

$$\begin{aligned} I^{\max}_{dr} &= \sqrt{\left(I^{\lim}_{r}\right)^2 - \left(I'^{SFR(k)}_{qr}\right)^2} \\ I'^{SFR}_{dr} &= \operatorname{sign}\left(\hat{I}^{SFR(k)}_{dr}\right) \min\left(\left|\hat{I}^{SFR(k)}_{dr}\right|, I^{\max}_{dr}\right) \end{aligned} \tag{B.26}$$

IF {Q-priority **OR** FRT-function}

$$\hat{I}^{SFR(k)}_{dr} = 0.5\left(\hat{I}^{SFR(k)}_{dr} + I'^{SFR(k-1)}_{dr}\right) \tag{B.27}$$

$$I'^{SFR}_{dr} = \hat{I}^{SFR(k)}_{dr} \tag{B.28}$$

$$\begin{aligned} I^{\max}_{qr} &= \sqrt{\left(I^{\lim}_{r}\right)^2 - \left(I'^{SFR(k)}_{dr}\right)^2} \\ I'^{SFR}_{qr} &= \operatorname{sign}\left(\hat{I}^{SFR(k)}_{qr}\right) \min\left(\left|\hat{I}^{SFR(k)}_{qr}\right|, I^{\max}_{qr}\right) \end{aligned} \tag{B.29}$$

END

Conversion from rotor to stator currents:

$$\begin{aligned} I'^{SFR}_{ds} &= \frac{V^{SFR(k)}_{qs}}{X_{ss}} - \frac{I'^{SFR(k)}_{dr}}{\gamma} \\ I'^{SFR(k)}_{qs} &= -\frac{V^{SFR(k)}_{ds}}{X_{ss}} - \frac{I'^{SFR(k)}_{qr}}{\gamma} \end{aligned} \tag{B.30}$$

GSC calculations:

$$\begin{aligned} V^{SFR(k)}_{dr} &= -s\left(X_{lr} + X_{ls}/\gamma\right) I'^{SFR(k)}_{qr} \\ V^{SFR(k)}_{qr} &= s\left(\left(X_{lr} + X_{m}\right) I'^{SFR(k)}_{dr} + X_{m} I'^{SFR(k)}_{ds}\right) \end{aligned} \tag{B.31}$$

$$P^{+(k)}_{RSC} = V^{SFR(k)}_{dr} I'^{SFR(k)}_{dr} + V^{SFR(k)}_{qr} I'^{SFR(k)}_{qr} \tag{B.32}$$

NEGATIVE SEQUENCE CALCULATIONS give $\bar{I}^{-(k)}_{s}$ and $P^{-(k)}_{RSC}$ (see algorithm in Apppendix B.2)

$$\bar{I}_s^- = 0.5\left(\bar{I}_s^{-(k)} + \bar{I}_s^{-(k-1)}\right) \tag{B.33}$$

$$\bar{I}_g^{-(k)} = \bar{Y}_g^- \bar{V}_{pgc}^{-(k)} \tag{B.34}$$

$$P_{GSC}^{-(k)} = \text{real}\left(\left[\bar{V}_{pgc}^{-(k)} + \left(R + jX\right)\bar{I}_g^{-(k)}\right]\left(\bar{I}_g^{-(k)}\right)^*\right) \tag{B.35}$$

$$\hat{I}_{dg}^{SVR(k)} = \left(P_{GSC}^{-(k)} - P_{RSC}^{+(k)} - P_{RSC}^{-(k)}\right) / \left|\bar{V}_{pgc}^{+(k)}\right| \tag{B.36}$$

IF {FRT-control}

$$\begin{aligned} \hat{I}_{qg}^{SVR(k)} &= -\left[K_{FRT}\left(1 - V_{ctrl}^{+(k)}\right) + V_{pgc}^{+(k)} \Big/ X_m - I_{dr}^{\lim}\right] \\ I'^{SVR(k)}_{qg} &= \max\left(\min\left(\hat{I}_{qg}^{SVR(k)}, 0\right), -I_{qg}^{\lim}\right) \end{aligned} \tag{B.37}$$

$$\begin{aligned} I_{dg}^{\max} &= \min\left(\sqrt{\left(I_g^{\lim}\right)^2 - \left(I'^{SVR(k)}_{qg}\right)^2}, I_{dg}^{\lim}\right) \\ I'^{SVR}_{dg} &= \text{sign}\left(\hat{I}_{dg}^{SVR(k)}\right) \min\left(\left|\hat{I}_{dg}^{SVR(k)}\right|, I_{dg}^{\max}\right) \end{aligned} \tag{B.38}$$

ELSE

$$I'^{SVR(k)}_{qg} = 0 \tag{B.39}$$

$$I'^{SVR}_{dg} = \text{sign}\left(\hat{I}_{dg}^{SVR(k)}\right) \min\left(\left|\hat{I}_{dg}^{SVR(k)}\right|, I_{dg}^{\lim}\right) \tag{B.40}$$

END

Flux angle calculations:

$$\begin{aligned} I'^{SVR\,(k)}_{ds} &= -\left[I'^{SFR\,(k)}_{ds} \cos\left(-\varphi_{flux}^{(k-1)}\right) + I'^{SFR\,(k)}_{qs} \sin\left(-\varphi_{flux}^{(k-1)}\right)\right] \\ I'^{SVR\,(k)}_{qs} &= -\left[I'^{SFR\,(k)}_{qs} \cos\left(-\varphi_{flux}^{(k-1)}\right) - I'^{SFR\,(k)}_{ds} \sin\left(-\varphi_{flux}^{(k-1)}\right)\right] \end{aligned} \tag{B.41}$$

$$\begin{aligned} I_{dr}^{SVR\,(k)} &= I'^{SFR\,(k)}_{dr} \cos\left(-\varphi_{flux}^{(k-1)}\right) + I'^{SFR\,(k)}_{qr} \sin\left(-\varphi_{flux}^{(k-1)}\right) \\ I_{qr}^{SVR\,(k)} &= I'^{SFR\,(k)}_{qr} \cos\left(-\varphi_{flux}^{(k-1)}\right) - I'^{SFR\,(k)}_{dr} \sin\left(-\varphi_{flux}^{(k-1)}\right) \end{aligned} \tag{B.42}$$

$$\varphi_{flux} = \text{angle}\left[-I_{ds}^{SVR\,(k)} + I_{dr}^{SVR\,(k)} + j\left(-I_{qs}^{SVR\,(k)} + I_{qr}^{SVR\,(k)} \right) \right] \tag{B.43}$$

$$\Delta\varphi_{flux} = \left| \varphi_{flux} - \varphi_{flux}^{old} \right| \tag{B.44}$$

$$\begin{aligned} I'^{SFR\,old}_{dr} &= I'^{SFR}_{dr} & \varphi_{flux}^{old} &= \varphi_{flux} \\ I'^{SFR\,old}_{qr} &= I'^{SFR}_{qr} & \bar{I}_s^{-\,old} &= \bar{I}_s^{-} \\ I'^{SFR\,old}_{ds} &= I'^{SFR}_{ds} & I'^{SVR\,old}_{dg} &= I'^{SVR}_{dg} \end{aligned} \tag{B.45}$$

WHILE $\{ \Delta\varphi_{flux} > \varepsilon_{flux} \}$ **GO TO** "**LOOP 2**"

$$\begin{aligned} I'^{SFR(k)}_{dr} &= I'^{SFR}_{dr} & \varphi_{flux}^{(k)} &= \varphi_{flux} \\ I'^{SFR(k)}_{qr} &= I'^{SFR}_{qr} & \bar{I}_s^{-(k)} &= \bar{I}_s^{-} \\ I'^{SFR(k)}_{ds} &= I'^{SFR}_{ds} & I'^{SVR(k)}_{dg} &= I'^{SVR}_{dg} \end{aligned} \tag{B.46}$$

Total currents:

$$\begin{aligned} \bar{I}_{tb}^{+(k)} &= \left(I'^{SVR(k)}_{dg} + j\, I'^{SVR(k)}_{qg} + I'^{SVR(k)}_{ds} + j\, I'^{SVR(k)}_{qs} \right) \exp\left(j\ \text{angle}\left(\bar{V}_{pgc}^{+(k)} \right) \right) \\ \bar{I}_{tb}^{-(k)} &= \bar{I}_s^{-(k)} + \bar{I}_g^{-(k)} \end{aligned} \tag{B.47}$$

B.2 Negative sequence algorithm

This algorithm is a sub-fonction of the one above. It is separated from the one above because it contains its own iterative loop.

Initialization

$$X_X = \frac{X_{ls} X_m}{X_m + X_{ls}} + X_{lr} \tag{B.48}$$

$$\begin{aligned} H_{PI}^{rd\,(0)} &= H_{PI}^{r} \\ H_{PI}^{rq\,(0)} &= H_{PI}^{r} \end{aligned} \tag{B.49}$$

Algorithm

DO

$$A_{rd}^{(j)} = \frac{-H_{PI}^{rd(j)}}{\gamma^2} H_{filter} - R_r - 2jX_{rr}$$
$$A_{rq} = s\left[X_{rr} - X_X H_{filter}\right]$$
$$A_{sd} = -2jX_m$$
$$A_{sq} = sX_m \tag{B.50}$$

$$B_{rd} = sX_{rr}\left(H_{filter} - 1\right)$$
$$B_{rq}^{(j)} = -\frac{H_{PI}^{rq(j)}}{\gamma^2} H_{filter} - R_r - 2jX_{rr}$$
$$B_{sd} = sX_m\left[\left(H_{filter}\right)^2 - 1\right]$$
$$B_{sq} = -2jX_m \tag{B.51}$$

$$E_{rd}^{(j)} = \frac{-B_{rd}A_{sq} + B_{sq}A_{rd}^{(j)}}{B_{sd}A_{sq} - B_{sq}A_{sd}}$$
$$E_{rq}^{(j)} = \frac{-B_{rq}^{(j)}A_{sq} + B_{sq}A_{rq}}{B_{sd}A_{sq} - B_{sq}A_{sd}} \tag{B.52}$$

$$F_{rd}^{(j)} = \frac{-A_{sd}E_{rd}^{(j)} - A_{rd}^{(j)}}{A_{sq}}$$
$$F_{rq}^{(j)} = \frac{-A_{sd}E_{rq}^{(j)} - A_{rq}}{A_{sq}} \tag{B.53}$$

$$H_{rd}^{(j)} = E_{rd}^{(j)}\left(R_s + 2jX_{ss}\right) + 2jX_m - X_{ss}F_{rd}^{(j)}$$
$$H_{rq}^{(j)} = E_{rq}^{(j)}\left(R_s + 2jX_{ss}\right) - X_m - X_{ss}F_{rq}^{(j)} \tag{B.54}$$

$$K_{rd}^{(j)} = F_{rd}^{(j)}\left(R_s + 2jX_{ss}\right) + X_m + X_{ss}E_{rd}^{(j)}$$
$$K_{rq}^{(j)} = F_{rq}^{(j)}\left(R_s + 2jX_{ss}\right) + 2jX_m + X_{ss}E_{rq}^{(j)} \tag{B.55}$$

$$\bar{\bar{I}}_{dr}^{SFR(j)} = \frac{H_{rq}^{(j)}\bar{\bar{V}}_{qs}^{SFR} - K_{rq}^{(j)}\bar{\bar{V}}_{ds}^{SFR}}{K_{rd}^{(j)}H_{rq}^{(j)} - K_{rq}^{(j)}H_{rd}^{(j)}}$$
$$\bar{\bar{I}}_{qr}^{SFR(j)} = \frac{\bar{\bar{V}}_{ds}^{SFR} - H_{rd}^{(j)}\bar{\bar{I}}_{dr}^{SFR}}{H_{rq}^{(j)}} \quad \text{(B.56)}$$

The outputs of the rotor inner loops are:

$$\bar{\bar{V}}_{PI}^{rd(j)} = \bar{\bar{I}}_{dr}^{SFR(j)}H_{PI}^{rd(j)}$$
$$\bar{\bar{V}}_{PI}^{rq(j)} = \bar{\bar{I}}_{qr}^{SFR(j)}H_{PI}^{rq(j)} \quad \text{(B.57)}$$

IF $\{V_{PI}^{\lim} < \bar{\bar{V}}_{PI}^{rd(j)}\}$

$$\alpha_d^{(j)} = \operatorname{asin}\left(V_{PI}^{\lim} / \bar{\bar{V}}_{PI}^{rd(j)}\right) \quad \text{(B.58)}$$

$$H_{PI}^{rd(j+1)} = \frac{2}{\left|\bar{\bar{I}}_{dr}^{SFR(j)}\right|\pi}\left[\left|H_{PI}^{rd(j)}\bar{\bar{I}}_{dr}^{SFR(j)}\right|\alpha_d^{(j)} + V_{PI}^{\lim}\cos\left(\alpha_d^{(j)}\right)\right] \cdot \exp\left(\mathrm{j}\cdot\operatorname{angle}\left(H_{PI}^{rd(j)}\right)\right) \quad \text{(B.59)}$$

END

WHILE $\{V_{PI}^{\lim} < \bar{\bar{V}}_{PI}^{rd}$ **OR** $V_{PI}^{\lim} < \bar{\bar{V}}_{PI}^{rq}\}$

With the last $A_{rd}^{(j)}$ and $B_{rq}^{(j)}$:

$$A_{rd} = A_{rd}^{(\text{end})}$$
$$B_{rq} = B_{rq}^{(\text{end})} \quad \text{(B.60)}$$

$$D_{sd} = \frac{B_{rd}A_{sd} - B_{sd}A_{rd}}{B_{rq}A_{rd} - B_{rd}A_{rq}}$$
$$D_{sq} = \frac{B_{rd}A_{sq} - B_{sq}A_{rd}}{B_{rq}A_{rd} - B_{rd}A_{rq}} \quad \text{(B.61)}$$

$$C_{sd} = \frac{-A_{sd} - A_{rq}D_{sd}}{A_{rd}}$$
$$C_{sq} = \frac{-A_{rq}D_{sq} - A_{sq}}{A_{rd}} \quad \text{(B.62)}$$

$$H_{sd} = R_s + 2jX_{ss} - X_m D_{sd} + 2jX_m C_{sd}$$
$$H_{sq} = -X_{ss} - X_m D_{sq} + 2jX_m C_{sq} \tag{B.63}$$

$$K_{sd} = X_{ss} + LX_m C_{sd} + 2jX_m D_{sd}$$
$$K_{sq} = R_s + 2jX_{ss} + X_m C_{sq} + 2jX_m D_{sq} \tag{B.64}$$

$$\bar{\bar{I}}_{ds}^{SFR} = \frac{H_{sq}\bar{\bar{V}}_{qs}^{SFR} - K_{sq}\bar{\bar{V}}_{ds}^{SFR}}{K_{sd}H_{sq} - K_{sq}H_{sd}}$$
$$\bar{\bar{I}}_{qs}^{SFR} = \frac{\bar{\bar{V}}_{ds}^{SFR} - H_{sd}\bar{\bar{I}}_{ds}^{SFR}}{H_{sq}} \tag{B.65}$$

$$\bar{\bar{I}}_{ds}^{SVR} = -\left[\bar{\bar{I}}_{ds}^{SFR}\cos(-\varphi_{flux}) + \bar{\bar{I}}_{qs}^{SFR}\sin(-\varphi_{flux})\right]$$
$$\bar{\bar{I}}_{qs}^{SVR} = -\left[\bar{\bar{I}}_{qs}^{SFR}\cos(-\varphi_{flux}) - \bar{\bar{I}}_{ds}^{SFR}\sin(-\varphi_{flux})\right] \tag{B.66}$$

Current in SVR are from the stator to the grid.

$$\varphi_{Ids}^{SVR} = \text{angle}\left(\bar{\bar{I}}_{ds}^{SVR}\right)$$
$$\varphi_{Iqs}^{SVR} = \text{angle}\left(\bar{\bar{I}}_{qs}^{SVR}\right) \tag{B.67}$$

$$\left|\bar{I}_s^-\right| = \frac{1}{2}\sqrt{\left|\bar{\bar{I}}_{ds}^{SVR}\right|^2 + \left|\bar{\bar{I}}_{qs}^{SVR}\right|^2 - 2\left|\bar{\bar{I}}_{ds}^{SVR}\right|\left|\bar{\bar{I}}_{qs}^{SVR}\right|\sin\left(\varphi_{Ids}^{SVR} - \varphi_{Iqs}^{SVR}\right)}$$
$$\varphi_{Is}^- = \arctan\left(\frac{\left|\bar{\bar{I}}_{ds}^{SVR}\right|\sin\left(\varphi_{Ids}^{SVR}\right) - \left|\bar{\bar{I}}_{qs}^{SVR}\right|\cos\left(\varphi_{Iqs}^{SVR}\right)}{\left|\bar{\bar{I}}_{ds}^{SVR}\right|\cos\left(\varphi_{Ids}^{SVR}\right) + \left|\bar{\bar{I}}_{qs}^{SVR}\right|\sin\left(\varphi_{Iqs}^{SVR}\right)}\right) \tag{B.68}$$

Active power flow on RSC due to 120Hz oscillations:

$$\bar{\bar{I}}_{dr}^{SFR} = \bar{\bar{I}}_{dr}^{SFR(\text{end})}$$
$$\bar{\bar{I}}_{qr}^{SFR} = \bar{\bar{I}}_{qr}^{SFR(\text{end})} \tag{B.69}$$

$$\bar{\bar{V}}_{dr}^{SFR} = \left(R_r + 2jX_{rr}\right)\bar{\bar{I}}_{dr}^{SFR} - sX_{rr}\bar{\bar{I}}_{qr}^{SFR} - sX_m\bar{\bar{I}}_{qs}^{SFR} + 2jX_m\bar{\bar{I}}_{ds}^{SFR}$$
$$\bar{\bar{V}}_{qr}^{SFR} = \left(R_r + 2jX_{rr}\right)\bar{\bar{I}}_{qr}^{SFR} + sX_{rr}\bar{\bar{I}}_{dr}^{SFR} + sX_m\bar{\bar{I}}_{ds}^{SFR} + 2jX_m\bar{\bar{I}}_{qs}^{SFR} \tag{B.70}$$

$$P_{RSC}^{-} = \left|\bar{\bar{V}}_{dr}^{SFR}\right|\left|\bar{\bar{I}}_{dr}^{SFR}\right|\frac{\cos\left(\varphi_{Vdr}^{SFR} - \varphi_{Idr}^{SFR}\right)}{2} + \left|\bar{\bar{V}}_{qr}^{SFR}\right|\left|\bar{\bar{I}}_{qr}^{SFR}\right|\frac{\cos\left(\varphi_{Vqr}^{SFR} - \varphi_{Iqr}^{SFR}\right)}{2} \quad \text{(B.71)}$$

B.3 Additional variables for complete model

φ_{flux} the flux angle

ε_{flux} the tolerance for the convergence of the flux angle

$\bar{\bar{V}}_{dr}^{SFR}$, $\bar{\bar{V}}_{qr}^{SFR}$ the twice the grid frequency phasor of the rotor voltage d- and q-components in SFR

$\bar{\bar{V}}_{ds}^{SFR}$, $\bar{\bar{V}}_{qs}^{SFR}$ the twice the grid frequency phasor of the stator voltage d- and q-components in SFR

$\bar{\bar{I}}_{dr}^{SFR}$, $\bar{\bar{I}}_{qr}^{SFR}$ the twice the grid frequency phasor of the rotor current d- and q-components in SFR

$\bar{\bar{I}}_{ds}^{SFR}$, $\bar{\bar{I}}_{qs}^{SFR}$ the twice the grid frequency phasor of the stator current d- and q-components in SFR

φ_{Vdr}^{SFR}, φ_{Vqr}^{SFR} the angle of the phasor $\bar{\bar{V}}_{dr}^{SFR}$ and $\bar{\bar{V}}_{qr}^{SFR}$

φ_{Ids}^{SVR}, φ_{Iqs}^{SVR} the angle of the phasor $\bar{\bar{I}}_{ds}^{SFR}$ and $\bar{\bar{I}}_{qs}^{SFR}$

φ_{Idr}^{SFR}, φ_{Iqr}^{SFR} the angle of the phasor $\bar{\bar{I}}_{dr}^{SFR}$ and $\bar{\bar{I}}_{qr}^{SFR}$

$V_{PI}^{\lim}$ the limit of the rotor inner loop proportional-integral output

H_{filter} the complex gain of the measurement filter at nominal frequency

H_{PI}^{r} the complex gain at twice the grid frequency of the rotor inner loop proportional-integral controller

$H_{PI}^{rd(k)}$, $H_{PI}^{rq(k)}$ the complex gain at twice the grid frequency of the rotor inner loop proportional-integral controller on d- and q-axis when the gain is corrected

$A_x, B_x, C_x, D_x, E_x, F_x, H_x, K_x$ the constants used to solve the system of equations of twice the grid frequency phasors (where *x* can be: *rd, rq, ds, sq*)

APPENDIX C – TEST CASE 1 DATA: 120 kV SYSTEM

The circuit of test case 1 is presented in Figure 4.4.

Slack bus: Line voltage: 120 kV Phase A voltage at 0°

Z0 = 3 + 30j Ω Z1 = 1 + 9j Ω Z2 = Z1

Lines (the lengths are in Figure 4.4):

R0 = 0.3125 Ω/km R1 = 0.127 Ω/km R2 = R1

L0 = 1.6621 Ω/km L1 = 0.4794 Ω/km L2 = L1

C0 = 1.8166 µS/km C1 = 3.4788 µS/km C2 = C1

The loads and their transformers on the bus 5 and 6 are identical.

Constant power load, 3 phase power = 30 + 15j MVA Nominal line voltage: 25 kV

Load transformers:

S = 50 MVA, 120kV/25kV Dyg+30° connection

Z = 0.00375 + 0.1578j pu (in transformer base)

90% of the series impedance on the 120kV side

No shunt impedance